THE HII REGIONS AND OB STARS OF M33 AND NGC 6822

By

KANAN PATEL

A Thesis

Submitted to the School of Graduate Studies

in Partial Fulfilment of the Requirements for the Degree

Doctor of Philosophy

McMaster University

THE HII REGIONS AND OB STARS OF

M33 AND NGC 6822

DOCTOR OF PHILOSOPHY (1995)

Department of Physics and Astronomy

McMaster University

Hamilton, Ontario

TITLE: The HII Regions and OB Stars of M33 and NGC 6822

AUTHOR: Kanan Patel, B. Sc. (University of Windsor), M.Sc. (Queen's University)

SUPERVISOR: Dr. Christine Wilson

NUMBER OF PAGES: xx, 198

ACKNOWLEDGEMENTS

I would like to extend my sincere and heartfelt thanks to Dr. Christine Wilson for introducing me to this project and by thus doing, allowing me to experience the many marvels of observational astronomy. The guidance and support she has extented to me in the past two years will always remain with me. I would like also to thank Dr. Ralph Pudritz for his encouragement and support as well for providing me with an opportunity to conduct research in an exciting area of theoretical astrophysics, that of star formation. My sincere thanks to Drs. Peter Sutherland, Bill Harris and Doug Welch of the Department of Physics and Astronomy. It has been an privilege to have been able to learn from and work with persons who have so much command of and love for their work.

I would not like to image what life for the past few years would have been like without my extraordinary office mates- Patrick Cote, Dean McLaughlin, Jeff Secker, Pat Durell and most recently, Denise Kaiser. Their humour, boundless helpfulness, council and indulgence of the 4:00 hour made even the dullest days so much brighter. My thanks and gratitude to the lively lunchtime group that provided entertaining, enlightening and non-astronomical food for thought.

There is no doubt that this would not have been possible without the constant love, understanding and blessing of my family, both immediate and extended: R.C, Mukta, Om, Rahul, Sangita, Nirav, Raju, Puni, Annie, Rick, Maggie, Joanne, Enrique, Shirley, Hugo and dear Peter. My deepest thanks to them for continuously reminding me of the many other forms of art within the universe.

For Mukta and R.C.

ABSTRACT

We have used $H\alpha$ and photometric data for two morphologically distinct Local Group galaxies, the spiral M33 and dwarf irregular NGC 6822, to study the distribution of the luminous blue O and B (OB) stars and HII regions in the galaxies as well as to determine whether individual regions of the galaxies are separately and/or collectively in a state of ionization balance. In the case of M33, we have concentrated on the inner 1 kpc region of the galaxy. Using the $H\alpha$ data, three distinct ionized gas environments (bright, halo and field) defined by the surface brightness of the $H\alpha$ emission have been identified. We find that $\sim$50% of the OB stars are located in the field, so that 1/2 of the lifetime of OB stars must be spent outside recognizable HII regions. This result suggests that if OB stars escape from bright HII regions by destroying their parent molecular clouds, then molecular cloud lifetimes after forming OB stars could be as low as $\sim 5 \times 10^6$ yrs or 1/2 the typical lifetime of OB stars. We show that a possible origin for the large field OB population is that they were born in and subsequently percolated out of the $\sim 10^3$ giant molecular clouds with masses $\gtrsim 10^3 M_\odot$ predicted to exist within the inner kpc of the galaxy. Using UBV photometry and stellar ionization models, we predict $H\alpha$ fluxes in the bright, halo and field regions and compare them to those observed to find that predicted fluxes are a factor of $\sim$3-7 greater than observed so that the three ionized gas environments, separately as well as collectively, are not in ionization balance. Furthermore, the most substantial loss of ionizing photons appears to be taking place in the field. We find that observed

and predicted $H\alpha$ luminosities are in best agreement when Case A recombination is assumed in the field. Our findings suggest that star formation rates obtained from $H\alpha$ luminosities must underestimate the true star formation rate within the inner region of M33. A similar analysis of an individual, isolated region with bright and halo $H\alpha$ emission has produced results that are comparable to those found on the larger scale: the isolated region, as a whole, is also not in ionization balance.

In the case of NGC 6822, four distinct components of the $H\alpha$ emission (bright, halo, diffuse and field) differentiated by their surface brightnesses have been identified. We find that only 1/4 of the OB stars are found in the combined bright and halo regions, suggesting that OB stars spend roughly 3/4 of their lifetimes outside "classical" HII regions. Molecular cloud lifetimes after forming OB stars could be as low as $\sim$1-3$\times10^6$ yrs or 1/4 the typical main sequence lifetimes of OB stars if OB stars escape from bright HII regions by destroying their parent clouds. Additionally, the field population of OB stars cannot have originated in and percolated out of existing HII regions. Comparing the observed $H\alpha$ emission with that predicted from BV photometry and stellar ionizing flux models, we find that although the bright, halo and diffuse regions are probably in a state of ionization balance, the field region, which is producing at least 6 times as much ionizing flux as is observed, is clearly not. The ionization balance results suggest that star formation rates obtained from $H\alpha$ luminosities must underestimate the true star formation rate in NGC 6822 by about 50%. Comparing the results for NGC 6822 and M33 reveals that the inner kiloparsec region of M33 is in a more serious state of ionization imbalance, perhaps due to its higher surface density of blue stars. Thus the morphological class or surface density of a galaxy may be important factors in how accurately we can determine star formation rates from $H\alpha$ luminosities.

Finally, we have performed optical spectroscopy of luminous blue stars in both NGC 6822 and M33 using respectively, the 4-m CTIO telescope plus ARGUS spectrograph and the 4-m Mayall telescope at KPNO plus HYDRA spectrograph. Due to the limited S/N ratio of the data, we have been able to classify only ~50% of the stars observed in NGC 6822 and ~40% of the stars observed in M33. Out of the 37 NGC 6822 and 15 M33 stars with classifiable spectra respectively 28 and 11 potential OB stars have been identified. We have used the NGC 6822 spectra to gauge the reliability of the principle stellar ionization model used for the ionization balance calculations in both galaxies.

Contents

List of Figures

List of Tables

LIST OF ACRONYMS

ADU	Analog-to-Digital Conversion Units
BC	Bolometric Correction
CCD	Charge Coupled Device
CFHT	Canada-France-Hawaii Telescope
CTIO	Cerro Tololo Inter-American Observatory
DIG	Diffuse Interstellar Gas
H I	Neutral Hydrogen Gas
H II	Ionized Hydrogen
HST	Hubble Space Telescope
IAU	International Astronomical Union
IMF	Initial Mass Function
IRAF	Image Reduction and Analysis Facility
KPNO	Kitt Peak National Observatories
LMC	Large Magellanic Cloud
LTE	Local Thermodynamic Equilibrium
NGC	New General Catalogue
NLTE	Non-Local Thermodynamic Equilibrium
OVRO	Owens Valley Radio Observatory

OB	O and B type Stars
QE	Quantum Efficiency
SFE	Star Formation Efficiency
SFR	Star Formation Rate
SMC	Small Magellanic Cloud
S/N	Signal-to-Noise Ratio
TAMS	Terminal Age Main Sequence
ZAMS	Zero Age Main Sequence

JOURAL ACRONYMS

A&A	Astronomy and Astrophysics
AA&AS	Astronomy and Astrophysics Suppliment Series
ARA&A	Annual Review of Astronomy and Astrophysics
AJ	Astronomical Journal
ApJ	Astrophysical Journal
ApJL	Astrophysical Journal Letters
ApJS	Astrophysical Journal Suppliment
AZh	Astronomicheskij Zhurnal
BAAS	Bulletin of the American Astronomical Society
MNRAS	Monthly Notices of the Royal Astronomical Society
MmRAS	Memoirs of the Royal Astronomical Society
PASP	Publications of the Physical Society of the Pacific
PASJ	Publications of the Astronomical Society of Japan

LIST OF SYMBOLS

A_V	Visual Extinction
$A_{H\alpha}$	Extinction at λ=6563Å
B,V,U	Broadband Photometric Magnitudes in Johnson-Morgan System
(B-V)	Colour Index in Johnson-Morgan System
$(B-V)_o$	Intrinsic (unreddened) (B-V)
E(B-V)	Colour Excess in (B-V)
$F_{H\alpha}$	Flux in Hα
g	Stellar Surface Gravity
Hα	Hydrogen Balmer Line at λ=6563Å
L	Luminosity
M_V	Visual Absolute Magnitude
Q	Reddening-Free Index [Q≡(U-B)-0.72(B-V)]
R_*	Radius of Star
Σ	Surface Density
σ_B	Stefan-Boltzmann Constant
T_{eff}	Effective Temperature
Z	Fractional Abundance by Weight of Elements Other than Hydrogen and Helium

Chapter 1

INTRODUCTION

1.1 THE ISSUES

Amongst the qualities that make the Local Group galaxies so attractive to astronomers is the fact that a wide range of different types of galaxies, from giant spirals to dwarf ellipticals, all at a fairly uniform distance from the Milky Way (from d=50 kpc for our nearest galaxy neighbour, the Large Magellanic Cloud, to d=800 kpc for the spiral galaxy M33) are available for investigation. This makes the Local Group an excellent laboratory in which to study a number of important issues in astrophysics including the structure, evolution and dynamics of individual galaxies as well as differences and similarities within individual galaxies and between different morphological galaxy types. Investigations of Local Group galaxies located above and below the plane of the Milky Way have the added advantage of not suffering from variable absorption (or extinction) that is often such a serious problem in studies of objects in our own Galactic plane.

One area in which Local Group galaxies have proven to be extremely useful is in the study of extragalactic star formation. As low mass stars, because of their faint

luminosities, cannot be resolved in these extragalactic systems, studies concentrate on the luminous high mass stars. Since it is not easy to resolve individual stars in galaxies beyond the Local Group (using ground based telescopes), these galaxies are even more valuable in the area of extragalactic star formation. The relative proximity of the Local Group galaxies permits a direct investigation of the gaseous and stellar components involved in high mass star formation including individual stars as well as stellar associations (through the optical, infrared and/or ultraviolet windows), the molecular clouds, which are the birth places of stars (at radio wavelengths), and the tracers of recent high mass star formation such as ionized atomic hydrogen gas (or HII) regions (observed in the optical hydrogen Balmer line, $H\alpha$=6563Å). These studies can, in turn, be used to determine important characteristics of the galaxy, such as the initial mass function for massive stars and star formation rates and efficiencies. The initial mass function is a relation which gives the number of stars formed per unit mass interval in a unit volume as a function of the stellar mass, the star formation rate measures the mass of material that is converted into stars per unit time interval (usually measured in $M_\odot$ yr^{-1}) and the star formation efficiency is defined as the fraction of the total mass of a region (gas plus stars) that is locked up in stars.

In particular, HII regions are very important tools for studies of ionized gas and massive star formation as they provide fundamental information on the mass and luminosity function of the star forming environments and can also be used to determine star formation rates, stellar initial mass functions and chemical abundances in galaxies. While luminous massive young stars (spectral class O and B or hereafter, OB) have long been recognized as the source of the ionizing radiation that defines the optically luminous HII regions, only recently has it become clear that two are not always spatially coincident. Extragalactic examples of individual and/or groups

of OB stars that are not associated with any bright HII regions include our closest galactic neighbours, the Large and Small Magellanic Clouds (respectively, LMC and SMC) (Massey *et al.* 1994) as well as the spiral galaxy M33 (Wilson 1990). Examples of the opposite, of filamentary $H\alpha$ structures with no obvious ionizing sources, are found in the LMC and SMC (Wilcots & Hodge 1991) and the more distant edge-on spiral galaxy NGC 891 (Rand *et al.* 1990). These observations which suggest that massive stars must spend some portion of their lives in the "field", far from dense gas clouds and hence outside bright H II regions. have important implications for a number of key issues in star formation and the interstellar medium. including the evolution of molecular clouds. the ionization of diffuse interstellar gas and the calculation of extragalactic star formation rates.

The length of time that massive stars spend in the H II region phase, and thus at least partially embedded in their natal atomic and molecular environments, is important for estimating molecular cloud lifetimes after the formation of OB stars and, therefore, understanding the evolution of the interstellar medium. Estimates of short cloud lifetimes of $\sim 10^7$ yrs (Blitz & Shu 1980) assume that a large fraction of the total lifetime of the star is spent embedded in the parental molecular cloud and that the clouds are destroyed by the first generation of O stars formed within them. Longer lifetime estimates ($\geq 10^8$ yrs, Solomon & Sanders 1980) do not consider the length of time OB stars spend in their parental clouds but rather assume the clouds are formed within a stable environment where the overall star formation rate is low. Alternatively, molecular clouds undergoing periods of intense followed by quiescent star formation would also produce long-lived clouds (lifetimes $\sim 4 \times 10^7$yrs, Elmegreen 1991). If O stars destroy their natal environments, then the fraction of O stars observed in the field or outside of bright H II regions (which is proportional to

the length of time a typical O star spends outside a bright H II region) determines the time required to destroy the cloud. However, if these field OB stars have simply moved out of their parent clouds, then cloud lifetimes after the formation of OB stars could be considerably longer.

Field OB stars may be an important factor in understanding the origin of the diffuse ionized gas observed in our own Galaxy as well as extragalactic systems. Characterized by its low density (electron density $n_e \sim 0.2$ cm^{-3}), cool temperatures (<10,000 K) and high intensities of forbidden ionized sulfur ([SII]) emission relative to $H\alpha$ (Walterbos 1991), the diffuse ionized gas is believed to constitute a substantial fraction of the total $H\alpha$ emission within a galaxy (20-30% in the LMC, Kennicutt & Hodge 1986; 20-40% in M31, Walterbos & Braun 1994) and plays a vital role in the interface between the disk and halo components of spiral galaxies. Galactic and extragalactic observations reveal filaments, shells and bubbles (Davies *et al.* 1976; Courtes *et al.* 1987; Hodge & Kennicutt 1983) as well as extended diffuse structures which extend a few kpc above the galactic plane (Rand *et al.* 1990). Although OB stars are currently believed to be the most likely candidate sources of ionizing photons powering the diffuse ionized gas, understanding how these photons can reach such large heights above the plane of the galaxy has been one of the glaring problems with the theory. One possible solution may be the presence of OB stars in the field: if significant numbers of these stars are located in regions of low gas density and/or optical depth (as is likely to be the case in the field) then a potentially enormous reservoir of ionizing photons would be available to ionize gas at high latitudes.

The importance of estimating the star formation rate (SFR) in galaxies cannot be over-stated. Correlations between properties of the interstellar medium (which consists of atomic and molecular gas in the neutral and ionized phases as well as dust

particles) and the SFR are useful diagnostics of the star formation mechanism, including the triggering and regulation of the star forming process, as well as determining the star formation efficiency and studying the past and predicting the future history of star formation in the galaxy. In fact, the relationship between the SFR and the properties of the interstellar medium is an important tool in understanding the evolution of galaxies as virtually all contemporary models of the galactic evolution parameterize the SFR by a function of the density or some other property of the gas (Schmidt 1959; Kennicutt 1989).

Vital to many of the issues mentioned above, and others such as the mode of star formation (*i.e.*, are star forming regions made up of predominantly high, intermediate or low mass stars?), models of chemical evolution of galaxies, stellar population synthesis, and evolutionary models used in predicting the appearance of primeval galaxies, is the initial mass function (IMF) which together with the star formation rate constitute two of the fundamental relations of star formation. While these two functions can be independently determined through observations, it is possible to constrain one given the other if it can be assumed that the IMF of newly formed stars is independent of time (Miller & Scalo 1979). Estimates of the SFR are extremely important in systems where the IMF cannot be easily measured. Example of such systems include distant galaxies in which it is not possible to resolve individual stars and/or the range of masses that can be resolved is not sufficiently wide. Certain methods of estimating the total SFR (*i.e.*, including high and low mass stars) in extragalactic systems have the further complication of being particularly sensitive to the adopted IMF. This is due to the fact that in distant systems, the SFR tracers sample only the massive end of the stellar population ($M \gtrsim 10 M_{\odot}$) so that up to 80-90% of the total stellar mass is not reflected in the observations and therefore the total SFR

requires a large extrapolation of the IMF.

Until about 1980, there was only one way to estimate the star formation rate in a galaxy and that was by modeling its broadband visible colours (a measure the ratio of the flux in two different wavelength bands) and magnitudes (Roberts 1963; Larson & Tinsley 1978; Tinsley and Danly 1980). Since that time, a number of other techniques have been developed. These include observations of the ultraviolet continuum flux, far infrared continuum, resolved stars and Lyman continuum emission (Huchra *et al.* 1983, Hunter *et al.* 1986; Thronson *et al.* 1989; Kennicutt 1983).

The most widely used method of obtaining SFRs is by counting the ionizing flux (λ<912Å) emitted by the massive young stars in a galaxy. The theory requires that the galaxy (or region thereof) is ionization bounded: *i.e.*, the number of ionizing Lyman continuum photons emitted by the exciting stars is proportional to the number of photons emitted in a recombination line or in the nebular continuum. Although the thermal radio continuum or the Brackett or Paschen lines are sometimes used, the most common tracer of the SFR in external galaxies is the $H\alpha$ emission line at $\lambda 6563\mathring{A}$. We will direct the remainder of this discussion to using $H\alpha$ emission to estimate SFRs. The details of the technique are from Kennicutt (1983) who, using a large sample of field spiral and irregular galaxies, calibrated the extensively used relation,

$$SFR(\geq 10M_{\odot}) = \frac{L(H\alpha)}{7.02 \times 10^{41} erg\, s^{-1}} M_{\odot} yr^{-1}$$

$$SFR(Total) = \frac{L(H\alpha)}{1.12 \times 10^{41} erg\, s^{-1}} M_{\odot} yr^{-1}. \qquad (1\text{-}1)$$

where L($H\alpha$) is the total $H\alpha$ luminosity of the galaxy. Intrinsic to this relationship is an initial mass function $\phi(m) \propto m^{-1.4}$ (for $0.1 \leq m \leq 1$ $M_\odot$) and $\phi(m) \propto m^{-2.5}$ (for $1 \leq m \leq 100$ $M_\odot$) and a steady-state SFR. We briefly outline the steps involved in deriving this relation.

The first step is to convert the observed $H\alpha$ fluxes into Lyman continuum luminosities using recombination theory. In deriving equation 1-1, Kennicutt (1983) used Case B recombination for optically thick gas at ~10,000 K and densities of 10^2-10^4 cm^{-3} for which N(LyC)/N($H\alpha$)=2.22 (Osterbrock 1989). (Case B recombination assumes that all photons in the Lyman series, emitted when an electron drops down to the n=1 level, are reabsorbed. There are no reabsorptions for photons at longer wavelengths for Case B.) However, Case A may be more appropriate for gas that is optically thin in all Lyman transitions for which N(LyC)/N($H\alpha$)=5.36 (Brockelhurst 1971). (Case A recombination assumes all photons in the Lyman series escape with no reabsorption taking place.) Next, stellar atmosphere models and evolutionary tracks are used together to determine the Lyman continuum luminosity as a function of time for various stellar masses. (Stellar evolution tracks trace the different stages of a star's evolution along the Hertzsprung-Russell diagram which plots T_{eff} as a function of M_V, where T_{eff} is the effective temperature of the star, defined as the temperature of a blackbody that would emit the same total energy as the star, and M_V is the absolute visual magnitude of the star.) The results for each mass are integrated to obtain the total number of Lyman continuum photons emitted by that star over its lifetime (typically $<10^7$ yrs for young, massive OB stars that are the primary source of ionizing photons).

The final step is to select an appropriate initial mass function to determine the constant of proportionality in equation 1-1. (Note that the total number of Lyman

continuum photons observed in a galaxy is proportional to the IMF and, therefore, the star formation rate.) While the SFR for massive (OB) stars is only mildly sensitive to the adopted IMF, this is not at all the case for the total SFR, which is obtained by extrapolating the high mass SFR via an assumed IMF. To constrain the range of IMF slopes possible, Kennicutt (1983) used model galaxy colours (determined in the fashion of Tinsley 1972; Searle *et al.* 1973), to predict the $H\alpha$ equivalent widths which in addition to representing the strengths of absorption lines, are tightly correlated with the broad-band colours and proportional to the number of Lyman continuum photons. The best fitting IMF was used in combination with the photoionization models to determine the SFR relationships given above.

The principle attraction of using $H\alpha$ to determine star formation rates is in its sensitivity and the relative ease with which observations can be obtained. While sub-arcsec resolution is easily attainable in nearby galaxies, sensitivity is not a limiting consideration for using this SFR tracer even in distant galaxies. What does limit its use is extinction internal to the galaxy which can act to either underestimate or overestimate the SFR. A large source of uncertainty in this technique, as in many others mentioned above, is in the slope and upper mass cutoff of the adopted initial mass function. Systematic uncertainties due to this effect can be reduced by factors of a few to $\sim$50% using constraints on low mass SFRs obtained from optical continuum as well as galaxy colours (Kennicutt 1983; 1990). But before one can worry about the above mentioned sources of uncertainty using $H\alpha$ to determine SFRs, it is crucial that the underlying assumption of the theory, that the galaxy is ionization balanced, be realized. If ionizing flux is being lost from the system, then SFRs will be underestimated: the extent of the uncertainty in the deduced SFR will depend on the amount of flux that is lost.

Global star formation rates estimated from observed broadband (often U (λ=3500Å), B (λ=4500Å) and V (λ=5500Å)) photometric data are based on a comparison of the observed integrated colours of a galaxy with those computed for synthetic galaxies of a given age, initial mass function, chemical composition and SFR: the model that best matches the observed galaxy colours determines its SFR, initial mass function, age and chemical composition. The synthetic galaxies are generated using evolutionary models, in particular the isochrones (constant time evolutionary tracks) on the theoretical Hertzsprung-Russell diagram (Log(T_{eff}) versus M_V). Standard synthetic models include those proposed by Roberts (1963), Searle *et al.* (1973), Huchra (1977), Larson & Tinsley (1978), Tinsley and Danly (1980), Rocca-Volmerange *et al.* (1981) and Mochkovitch *et al.* (1987). An excellent review of the models and applications is given by Tinsley (1980). Although this technique yields only very rough estimates of the SFR and is not recommended for quantitative results, it can be used with other tracers of star formation to constrain the average IMF in the galaxy (Kennicutt 1990).

Of all the techniques used to obtain the star formation rate in a galaxy, photometry and spectroscopy of the individual resolved stars is most direct. This approach uses star counts along with the mass and main sequence lifetime of the stars to determine the SFR as:

$$SFR = \sum \frac{n_k m_k}{t_k} \tag{1-2}$$

where n_k is the number of stars of mass m_k and main sequence lifetime t_k (Wilson 1990). One of the largest sources of error in this technique is in estimating the mass of the star. Without spectroscopy, the mass is determined by comparing the position of

the star on the colour-magnitude ((B-V) versus V) diagram with stellar evolutionary tracks. The problem with this technique is that along the main sequence, the optical colours are degenerate: massive main sequence stars evolve along lines of constant colour and increasing luminosity (or effective temperature, T_{eff}) so that the stellar evolutionary tracks are almost vertical. Massive stars with Log(T_{eff})>4.4 have degenerate colours because at these characteristic high temperatures, the optical continuum distributions are far out on the tail of the Rayleigh-Jeans distribution of the black-body curve and therefore, the ratio of the flux at two separate bandpasses for stars of different T_{eff}s is the same. Photometric mass determinations carry uncertainties of ~50% (Wilson 1990). This error is considerably reduced if spectral classifications (from optical spectroscopy) are available as calibrated mass-spectral class relations can be used to directly determine the stellar masses. The added advantage in working with spectroscopic data is that a mass-limited sample is obtained. This is not certain to be the case in photometric studies as the most massive stars are not necessarily the visually brightest stars (Massey 1994).

The correlation between the blue luminosity and far-infrared emission (20-400 μm) in galaxies has been interpreted as a correlation between long- and short-term star formation rates (Thronson & Telesco 1986). Far-infrared luminosities determine the current rate of formation of OB stars as only these stars can cause the surrounding dust to re-radiate significant amounts of such radiation. This approach is especially useful wherever dust opacities are large and/or where most of the radiation from young stars is absorbed by dust, for example in compact H II regions (observed in the radio wavelengths as compact, intense sources of thermal emission) and starburst galaxies (galaxies which have undergone a vigorous episode of star formation). A serious problem with this technique is that a large component of the far-infrared

emission may be due to cool dust that is heated by the general interstellar radiation field (which is composed of radiation from galactic and extragalactic objects such as supernova remnants, globular clusters, active galaxies as well as cosmic rays) and not the hot, young stars associated with recent star formation (Walterbos & Schwering 1987; Thronson *et al.* 1989). Therefore the total far-infrared luminosity of a galaxy may not necessarily be proportional to its SFR. Within regions where the ultraviolet radiation field is dominated by young stars, SFRs obtained using far-infrared fluxes are generally consistent with those estimated using other techniques (Hunter *et al.* 1986; Thronson *et al.* 1987, 1988). This is not the case in normal spiral galaxies (Lonsdale & Helou 1987), where far-infrared fluxes predict SFRs that are much higher than expected.

1.2 RELEVANT RESULTS FOR LOCAL GROUP GALAXIES

To date, our closest galactic neighbours, the Large and Small Magellanic Clouds, have been at the prime focus of attention. Numerous investigations of the young stellar content and star forming regions of these irregular galaxies appear in the literature. The proximity of the Clouds makes them the only systems for which a complete survey of current and/or very recent star forming H II regions, from the smallest compact regions to the giant complexes (such as 30 Dor) is possible (Kennicutt 1991). Catalogs of H II regions in the Magellanic Clouds have been compiled by Henize (1956), Davies *et al.* (1976) and Kennicutt & Hodge (1986). The initial mass function and massive star content of the Clouds have been extensively studied by Heydari-Melayeri *et al.* (1987), Loret & Testor (1984), 1988, Massey *et al.* (1989a, 1989b) and Parker *et al.* (1992). A recent investigation of OB stars in both the LMC and SMC finds that an entire population of these stars originate

in the "field", far from neighbouring OB associations (Massey *et al.* 1994). Studies of ionization balance in a number of individual regions have revealed a range of conditions. Comparison of the predicted $H\alpha$ fluxes from stellar ionization models with that observed show that neither NGC 2122 nor LH 118 (both OB associations in the LMC) are ionization bounded (Massey *et al.* 1989a) but that LH 9 and LH 10 (also in the LMC) are at the limit of ionization balance (Parker *et al.* 1992). Finally, NGC 346 in the SMC appears to be ionization bounded as predicted $H\alpha$ fluxes are less than what is observed (Massey *et al.* 1989b). The star formation rate estimated using the Kennicutt (1983) formula is 0.14 $M_{\odot}yr^{-1}$ for the LMC and 0.038 $M_{\odot}yr^{-1}$ for the SMC (Hodge 1995).

The Local Group galaxies M33 and NGC 6822 are the next natural choices for our investigation. At a distance of 790 kpc (van den Bergh 1991), M33 (or NGC 598 as it is also known) is the third spiral galaxy, after M31 and the Milky Way, in the Local Group. This small galaxy is undergoing vigorous high mass star formation throughout the disk and spiral arm regions (Sandage & Humphreys 1980, Bothun 1992, Kent 1987). The distribution of atomic hydrogen has been extensively studied in M33 starting with Volders (1959) and most recently by Deul & van der Hulst (1987). The latest study revealed that small H I holes correlate well with OB associations and high-contrast H I holes coincide with giant H II regions. Large H I holes are anticorrelated in the sense that the H II regions and OB associations are found to lie along their edges (Deul & van der Hulst 1987, Deul & den Hartog 1990). The H II regions of M33 have been mapped through the photometric $H\alpha$ survey of Courtes *et al.* (1987). A subsequent radio continuum survey of sources associated with $H\alpha$ emission showed that radio H II regions suffered from significant levels of internal extinction (Viallefond *et al.* 1986). In such case, star formation rates based on optical

observations may be underestimated.

The inner 1 kpc region of M33 has recently been the focus of a wide range of investigations: a map in the CO J=1-0 transition (Wilson & Scoville 1989) and a radio-interferometric study (Wilson & Scoville 1990) have identified individual molecular clouds with properties similar to those found in the Galaxy. The studies also indicate that a significant fraction of the molecular gas is in either a smooth diffuse component or low mass ($M \lesssim 0.5 \times 10^5 M_\odot$) structures (Wilson & Scoville 1990). Wilson *et al.* (1991) have used H I, CO, and $H\alpha$ data to study high mass star formation in this region of M33. The authors find that 2/3 of the molecular clouds are undergoing star formation. Based on the $H\alpha$ luminosities and assuming a modified Miller-Scalo initial mass function, the authors find high mass and total star formation rates of 0.007 and 0.04 $M_\odot yr^{-1}$ (Wilson & Scoville 1991). Although SFRs inferred from 60 μm and 100 μm emission were found to be roughly twice those calculated using $H\alpha$ fluxes, the authors attribute the higher SFR estimate to a cool dust component that contributes 1/2 the total observed far-infrared luminosity. The spiral arm regions are found to have high SFRs but not unusually high star formation efficiencies (Wilson *et al.* 1991). OB associations in M33 have been identified by eye from photographic plates (Humphrey & Sandage 1980) and most recently by applying an automated grouping algorithm to three colour (B, V and U) CCD images by Wilson (1991). Differences in the ages and masses of OB associations in the northern and southern spiral arms suggest that perhaps high mass star formation has ceased in the northern arm of the galaxy. Diffuse ionized gas has been detected by Courtes *et al.* (1987) and Hester & Kulkarni (1990). The distribution of the diffuse ionized gas in M33 is similar to that observed in the LMC: extensive and filamentary (Courtes *et al.* 1987).

Local Group dwarf irregular galaxies provide invaluable information on the

interstellar medium and star formation. General characteristics of these galaxies include a conspicuous population of young stars, high gas content, simple structures and low metallicities (*i.e.*, abundance of all elements *except* hydrogen and helium), all of which indicate that they are in an early stage of evolution. These galaxies are especially interesting for star formation studies as, unlike spiral systems, there is as yet no clear connection between the star formation rate and global properties of the galaxies. Despite the difficulties incurred by its low Galactic latitude, including a high level of extinction and contamination due to foreground stars in our own Galaxy, NGC 6822 is one of the best studied dwarf irregular galaxies in the Local Group.

Contributing to its popularity is its proximity to the Milky Way (estimated at 510 kpc from infrared observations of the regularly pulsating Cepheid variable stars, McAlary *et al.* 1983). The first photometric investigation of the galaxy was due to Kayser (1967) who used UBV data to find and study Cepheid variables in the galaxy. The structure of the galaxy has been studied through photometric surveys by Hodge (1977) and Hodge *et al.* (1991). OB associations in the galaxy have been identified by Hodge (1977) and, most recently, through CCD imaging in the B and V filters by Wilson (1992a). Other surveys of the stellar population of NGC 6822 include photoelectric UBV photometry of stars (van den Bergh & Humphreys 1979) and spectroscopic and photometric investigations of luminous blue stars (Humphreys 1980) and Wolf-Rayet stars (Armandroff & Massey 1991, 1985). The H II regions of NGC 6822 have been catalogued and studied by Hodge *et al.* (1989,1988). At Z=0.0045, the fractional abundance by weight of "metals" (all elements except hydrogen and helium) in NGC 6822 is slightly smaller than that in the LMC (Hodge 1989). The recent evolutionary history, including determinations of the star formation rate within NGC 6822, have been discussed by Hodge (1980) and Hodge *et al.* (1991).

Based on $H\alpha$ fluxes, the current star formation rate in NGC 6822 is estimated to be 0.021 $M_{\odot}yr^{-1}$. Finally, the molecular gas content of the galaxy has recently received some attention with the CO surveys by Wilson (1992b), Ohta *et al.* (1993) and Wilson (1994).

By choosing M33 and NGC 6822 as the objects for our study, we will not only be able to compare the results of our investigation of the H II region and OB star populations in these two morphologically distinct galaxies, but also contribute towards a better understanding of the processes that are important in our own spiral system as well as the nearby irregular galaxies, the LMC and SMC.

1.3 OUTLINE OF THE THESIS

In light of the importance of knowing the star formation rate of galaxies, the wide spread use of $H\alpha$ as a star formation rate tracer, as well as the proven connection between ionized gas regions and massive star formation, we undertook an investigation of the H II regions and OB star populations of two Local Group galaxies, NGC 6822 and M33. The questions we hope to address include: How does the OB star distribution compare with that of the ionized gas? What fraction of the main sequence lifetime of an O star is spent within a luminous ("classical") H II region? Are the two galaxies in a state of ionization balance? How reliable are ionization fluxes determined from photometric data of the ionizing stars and how do results from photometric data compare with those from optical spectroscopy? The relevance of these questions extends to estimating the lifetimes of molecular clouds (after the formation of OB stars) in these galaxies, addressing problems posed by observations of the diffuse ionized gas in galaxies (*i.e.*, what is the mechanism powering it), testing the

underlying assumption of the most popular method of obtaining star formation rates in extragalactic systems (by means of the $H\alpha$ luminosity *i.e.*, using the Kennicutt (1983) formula) as well as allowing us to gauge the accuracy of optical photometry in these types of studies. We chose to conduct the investigation in two morphologically different galaxies, a late-type spiral and dwarf irregular, so that the effect of galaxy type could also be studied.

The outline of the thesis is as follows. Chapter 2 describes the investigation of the OB stars and H II regions within the inner kpc region of M33. An $H\alpha$ image of the galaxy is used to identify three distinct ionized gas environments and stellar U, B, and V photometry is used to identify OB stars in the galaxy as well as to calculate the theoretical ionizing flux from these stars using stellar ionizing flux models. Issues addressed include the fraction of an OB star's lifetime that is spent outside a classical HII region and the effect of this on molecular cloud lifetimes, after the formation of O stars, ionization balance, and the implications for the calculation of star formation rates and powering the diffuse ionized gas. This chapter has been submitted for publication to The Astrophysical Journal.

The details of a similar investigation of the H II regions and OB stars of NGC 6822 are given in Chapter 3. The data consist of BV photometry of luminous stars and CCD images of the galaxy in the red-continuum and $H\alpha$ filters. The $H\alpha$ image is used to define four distinct ionized gas environments in NGC 6822. The fractional lifetime of an OB star that is spent outside a classical H II region is determined and the implications of this to post OB star formation lifetimes of molecular clouds are considered. The photometric data are used in stellar ionization models to determine whether individual regions are separately and/or collectively in a state of ionization balance. Optical spectra of luminous blue stars in NGC 6822 are used to gauge

the performance of the principal ionization model used in the investigation. The implications of the state of ionization balance for the star formation rates estimated from $H\alpha$ luminosities are also discussed. The results found in NGC 6822 are compared with those determined from Chapter 3 for M33. This chapter has also been submitted to The Astrophysical Journal for publication.

Chapter 4 describes the observations, reduction and classification of optical spectra of luminous blue stars in M33 and NGC 6822 obtained using, respectively, the Kitt Peak National Observatories (KPNO) Mayall 4-m telescope+HYDRA multi-object spectrograph and the Cerro Tololo Inter-American Observatories (CTIO) 4-m telescope+ARGUS spectrograph. Although these spectra were originally intended to be used to obtain accurate effective temperatures, masses and ionizing fluxes of OB stars as well as to enable a direct determination of the initial mass function at the high mass end in the two galaxies, small number statistics due to unfavourable observing conditions prevented this. Instead, the individual stars studied here will add to the existing bank of information on the massive star content of nearby galaxies and the NGC 6822 spectra are used to gauge the performance of the stellar ionizing flux models applied in the ionization balance calculations (Chapter 3).

We summarize, in Chapter 5, the results from the previous chapters and discuss areas of future investigation and interest.

1.4 DIVISION OF LABOUR

The stellar photometric as well as the $H\alpha$ data used in studying the OB stars and H II regions of M33 (Chapter 2) were obtained prior to the start of this thesis. The U, B and V data had been obtained to study the OB associations within the

inner 1 kpc of the galaxy (Wilson 1991). The continuum-subtracted and calibrated $H\alpha$ image of the inner 1 kpc region of M33 was obtained from Wilson & Scoville (1991). Analysis of these data as well the application of the stellar ionization flux models (as discused in Chapter 2) was undertaken by myself. The article, "Are Galaxies Optically Thin to their own Lyman Continuum Radiation? I. M33" which has been submitted to The Astrophysical Journal, was entirely prepared by myself. The co-author, Dr. Christine Wilson, supervised the research and guided the writing of the paper by means of helpful comments on the content and style, as well as careful proof reading of the manuscript.

The photometric and $H\alpha$ data used in the investigation of the OB stars and H II regions of NGC 6822 (Chapter 3) were also obtained prior to the start of this thesis. The photometric B and V data had previously been used to investigate the OB associations of NGC 6822 (Wilson 1992a). Unpublished red-continuum and $H\alpha$ images of the galaxy were provided by P. Massey and G. Jacobi. A continuum-subtracted $H\alpha$ image of the galaxy was produced and calibrated by myself. As in Chapter 2, I was responsible for all the analysis of data as well as the application of the stellar ionization flux models. The spectroscopic data discused in Chapter 3 were obtained by Dr. Christine Wilson and myself in June, 1993. The data were reduced and preliminary spectral classes assigned by myself. The final spectral classifications of the observed stars were assigned in collaboration with Dr. Phil Massey. The manuscript "Are Galaxies Optically Thin to their own Lyman Continuum Radiation? II. NGC 6822" (submitted to The Astrophysical Journal) was prepared entirely by myself. Dr. Wilson supervised the research, proof read and provided helpful comments on the paper.

The spectroscopic data discussed in Chapter 4 were obtained by Dr. Christine

Wilson and I (for NGC 6822) and Dr. Phil Massey and I (in December of 1993 for M33). Reduction of the multi-object spectroscopic data for both the M33 and NGC 6822 stars was performed by myself. While preliminary spectral classes were independently determined by myself and Dr. Phil Massey, the final assignments for both data sets were based on a joint effort by the two of us.

Chapter 2

ARE GALAXIES OPTICALLY THIN TO THEIR OWN LYMAN CONTINUUM RADIATION? I. M33

2.1 ABSTRACT

Previously published $H\alpha$ data and UBV photometry of blue stars in the inner kpc of M33 are used to study the distribution of OB stars and H II regions in the galaxy and to determine whether individual regions of the galaxy are separately and/or collectively in a state of ionization balance. Based on the surface brightness of the $H\alpha$ emission, we identify three distinct ionized gas environments (bright, halo and field). We find that ~50% of the OB stars are located in the field, so that 1/2 of the lifetime of OB stars must be spent outside recognizable H II regions. If OB stars escape from bright H II regions by destroying their parent molecular clouds, this result would imply that molecular cloud lifetimes after forming OB stars could be as low as $\sim 5\times10^6$ yrs or 1/2 the typical lifetime of OB stars. We show that a possible origin for the large field OB population is that they were born in and subsequently percolated out of the $\sim 10^3$ giant molecular clouds with masses $\gtrsim 10^3 M_\odot$ predicted to exist within the inner kpc of the galaxy. Using ionization models, we predict $H\alpha$

fluxes in the bright, halo and field regions and compare them to those observed to find that the regions, separately as well as collectively, are not in ionization balance: predicted fluxes are a factor of ~3-7 greater than observed. The heaviest loss of ionizing photons appears to be taking place in the field. Observed and predicted $H\alpha$ luminosities in the field are in best agreement when Case A recombination is assumed. Therefore, our findings suggest that star formation rates obtained from $H\alpha$ luminosities must underestimate the true star formation rate in these regions of M33. We have performed a similar analysis of an individual, isolated region with bright and halo $H\alpha$ emission to find that comparable results apply and that the region, as a whole, is also not in ionization balance.

2.2 INTRODUCTION

Although massive OB stars have long been recognized as the source of the ionizing radiation that defines optically luminous H II regions, only recently has it become clear that OB associations and H II regions do not always coincide spatially. The Local Group galaxy M33 contains many examples of extragalactic OB associations that do not contain bright H II regions (Wilson 1990) while the edge-on spiral NGC 891 contains faint, filamentary $H\alpha$ structures high above the galactic disk with no obvious ionizing sources (Rand et al. 1990). In addition, the luminous young stars in M33 are not restricted to the spiral arms, traditionally believed to be the primary site of star formation (Madore 1978). Studies of the OB associations in the Magellanic Clouds show that there is an entire population of massive young stars that are located far enough away from neighbouring OB associations that they must have been born in the "field" and not in the associations (Massey *et al.* 1994). These observations suggest that massive stars must spend some portion of their lives far

from dense gas clouds and hence outside bright H II regions. The presence of significant numbers of field O stars has important implications for a number of key issues in star formation and the interstellar medium, including the evolution of molecular clouds, the ionization of diffuse interstellar gas and the calculation of extragalactic star formation rates (SFRs).

The length of time that an O star spends in the H II region phase, and thus at least partially embedded in its parent gas cloud, is important for estimating molecular cloud lifetimes after the formation of OB stars and, therefore, understanding the evolution of the molecular interstellar medium in galaxies. Estimates of molecular cloud lifetimes require an assessment of the destructive influence of massive stars and thus the time such stars spend in their natal environment is very important. The short lifetimes of $\sim 10^7$ yrs obtained by some authors (cf. Blitz & Shu 1980) assume this embedding time is a large fraction of the total lifetime of the star so that the first O stars that form will disrupt their parent cloud. Longer lifetime estimates ($\geq 10^8$ yrs, Solomon & Sanders 1980) are based on clouds being formed in a stable environment, the spiral interarm region of the Galaxy, where the overall SFR is low. Molecular clouds undergoing periods of intense star formation followed by quiescent star formation would result in long molecular cloud lifetimes so that each cloud could produce several OB associations of different ages (Elmegreen 1991). The fraction of self-gravitating clouds currently experiencing star formation ($\sim$0.5) can be combined with the duration of the process ($\sim 20 \times 10^6$yrs in OB associations) to obtain molecular cloud lifetimes of $\sim 4 \times 10^7$yrs (Elmegreen 1991). If OB stars destroy their natal environments, then the fraction of O stars seen in the field determines the time required to destroy the cloud. However, if these stars are seen in the field because they simply moved out of the clouds, then cloud lifetimes could be considerably longer.

The presence of OB stars in the field may be important to understanding the origin of the diffuse ionized gas (DIG) observed in our own Galaxy as well as extragalactic systems. This gas is characterized by its low density (electron density n_e ~0.2 cm^{-3}), cool temperatures (<10,000 K) and high [SII]/$H\alpha$ line intensities (Walterbos 1991). Observations of edge-on galaxies indicate scale heights of the DIG can be of the order of a few kpc (Walterbos 1991). Diffuse ionized gas in external galaxies is believed to account for a substantial fraction of the total $H\alpha$ emission from a galaxy (20-30% in the Large Magellanic Cloud. Kennicutt & Hodge 1986; 20-40% in M31, Walterbos & Braun 1994). Currently the most likely sources of ionizing photons for the DIG are OB stars. One problem with this scenario is that there is no clear understanding of how ionizing photons can traverse the large distances above the plane. If significant numbers of OB stars are found in field regions (where $H\alpha$ emission is low and optical depths are likely to be smaller than in bright H II regions), a potentially large reservoir of ionizing photons would be available to power the DIG.

Star formation rates that are calculated from observed $H\alpha$ fluxes rely on the assumption that the region in question is *ionization bounded* (Kennicutt 1983) *i.e.*, all Lyman continuum photons produced by massive stars are absorbed by the gas in the region (or galaxy). (The alternative scenario is for a region (or galaxy) to be *density bounded*, *i.e.*, the Lyman photons are more than sufficient to ionize all the (dense) gas.) The observed $H\alpha$ luminosity is then directly proportional to the Lyman continuum luminosity which can be converted into a SFR for massive stars via an assumed initial mass function (IMF) and theoretical models for the Lyman continuum luminosity as a function of stellar mass. The total SFR of a region can be obtained by extending the IMF over the full range of stellar masses. In these calculations, the assumption that the region is ionization bounded is crucial: since the SFR is directly

proportional to the Lyman continuum, and therefore $H\alpha$, luminosity, a region out of which continuum photons are escaping will have a smaller estimated SFR than one that is in ionization balance. The assumption of ionization boundedness may not be valid if large portions of the OB population lie outside bright H II regions. Considering the wide spread use of this technique for obtaining SFRs in extragalactic systems, it is vital to verify this underlying assumption of SFR measurements from $H\alpha$ luminosities.

Ionization balance calculations in extragalactic OB associations and H II regions have concentrated on single H II regions in the Large and Small Magellanic Clouds (LMC and SMC). Massey *et al.* (1989a) find the LMC OB associations NGC 2122 and LH 118 to be density rather than ionization bounded, since the predicted fluxes from stars in the association are a factor of two greater than what is observed. A similar study of NGC 346 in the SMC (Massey *et al.* 1989b) found the opposite to be true: the models predict less flux (up to a factor of $\sim$2) than what is observed and so the region is most likely ionization bounded. Finally, Parker *et al.* (1992) found that the LMC OB associations LH 9 and LH 10 were at the limit of being ionization bounded (observed fluxes were at most a factor of 1.5 greater than those predicted). To date there have been no such studies of systems more distant than the Magellanic Clouds and no attempt to measure the ionization boundedness of a large area of a galaxy.

At a distance of 0.79 Mpc (van den Bergh 1991), the Local Group galaxy M33 is an ideal system in which to conduct such an investigation. This Sc type galaxy is undergoing vigorous high mass star formation. The inner kpc region of the galaxy has recently received much attention: molecular gas maps in CO have identified a population of molecular clouds (Wilson & Scoville 1990), optical imaging

at $H\alpha$ has provided quantitative photometry of the H II regions (Wilson & Scoville 1991), and a UBV photometric survey of the region has identified luminous blue stars and OB associations (Wilson 1991). Diffuse ionized gas within the galaxy has been investigated by Hester & Kulkarni (1990).

In this chapter, we use $H\alpha$ and UBV photometry of the inner kpc region of M33 to study the distribution of the H II regions and luminous blue stars (hereafter OB stars) so as to calculate the fraction of an OB star's lifetime that is spent outside an H II region and to address the issues of post OB star formation lifetimes of molecular clouds, ionization balance, and the implications for the calculation of star formation rates and powering the diffuse ionized gas. The analysis of the $H\alpha$ data and UBV photometry and the theoretical ionization models used are outlined in section §2. A discussion of the OB star distribution is given in §3 and the results of the ionization balance calculations appear in §4. The results of our investigation are summarized in §5.

2.3 SELECTION AND ANALYSIS OF DATA

2.3.1 Photometric Data

We use the photometric UBV data from Wilson (1991), who used it to study the OB associations in the nucleus of M33. The observations were made at the Palomar 60-inch and Canada-France-Hawaii telescope (CFHT), using the blue sensitive Tektronix chip, CCD 6 (scale 0.235″ pixel^{-1}) at Palomar and the RCA2 double density CCD chip (scale 0.205″ pixel^{-1}) at the CFHT. The seeing was 1.2″-1.9″ at Palomar and ~0.8″ at the CFHT. Additional details of the observations can be found in Wilson (1991). Systematic uncertainties in the photometric zero points were estimated to be

±0.05 mag in B, ± 0.04 mag in V and ±0.15 mag in U. The data were estimated to be incomplete by 30% for 19.5<V<20, 55% for 20<V<20.5 and 65% for 20.5<V<21. Subsequent comparison of the data with independent photometry of M33 obtained by P. Massey (private communication) showed that there is a systematic offset (Massey-Wilson) of 0.14 mag in (U-B), while the B and V magnitudes agreed to better than 0.04 mag. Hence we have applied a +0.14 mag correction to the (U-B) colours. *i.e.*, the colours are shifted to the red relative to the values published in Wilson (1991).

This data set is particularly suitable for our use as it provides the most complete (to 21 mag in V) large-area census of the blue star population in the inner regions of the galaxy. The average reddening (foreground and internal) for the surveyed region is $\overline{E(B-V)}$=0.3±0.1 mag (Wilson 1991). We selected only those stars with $(B-V)\leq$0.4 mag. This criterion, which is based on the estimated average reddening for the galaxy, the intrinsic colour of O stars on the the zero age main sequence (ZAMS), $(B-V)$=-0.3 mag (Flower 1977), and the observed width of the main sequence, assures us that most potential OB stars will be selected.

2.3.2 $H\alpha$ Emission

We used a red-continuum subtracted Hα image of M33 from Wilson & Scoville (1991) to study the $H\alpha$ emission in the galaxy. The image was obtained on the Palomar 60-inch telescope (rebinned chip scale 1.3″pixel^{-1}). Visual inspection of the continuum subtracted $H\alpha$ image (henceforth the $H\alpha$ image) strongly suggested that three types of H II regions, bright, halo and field, are present in M33. The different regions were defined by their Hα surface brightness, I, such that $I \geq 1.37\times10^{-15}$ erg s^{-1}cm^{-2} arcsec^{-2} for the bright regions, $3.61\times10^{-16} \leq I < 1.37\times10^{-15}$ erg s^{-1} cm^{-2} arcsec^{-2} for the halo regions and $I < 3.61\times10^{-16}$ erg s^{-1} cm^{-2} arcsec^{-2} for the field

regions (see Figure 2.1a). The divisions into the three regions are motivated purely by visual inspection of the total image; the adopted dividing lines in surface brightness between each type of region are not based on any intrinsic physical quantity. The surface brightnesses, which have already been corrected for extinction in $H\alpha$ ($A_{H\alpha}=2.59\times E(B-V)=0.78$ mag (Schild 1977)) were measured above an observed average sky surface brightness over the galaxy of $I_{bg}=5.43\pm0.10\times10^{-16}$ erg s^{-1} $arcsec^{-2}$. The latter was obtained by averaging the observed surface brightness of four broad regions of the galaxy that appeared free of any $H\alpha$ emission. Because our $H\alpha$ image of M33 is restricted only to the inner kpc of the galaxy and does not cover any areas far from the galaxy, we cannot be certain that the background emission is in fact "sky", and not a very smooth emission component in M33. We will be in a better position to determine the true source of this background emission in our upcoming study of NGC 6822, for which we have $H\alpha$ images that extend past the optical limits of the galaxy. Finally, we note that these $H\alpha$ surface brightnesses as well as all measures of the $H\alpha$ luminosity have been corrected for contamination by the [NII] 6583$\AA$ line that was also observed through the filter used to obtain the $H\alpha$ image. To correct for this contamination, we used the data of Vilchez *et al.* (1988) to determine the average [NII]/$H\alpha$ line ratio of 21% $\pm$1% in three H II regions that lie within the surveyed region of M33. Scaling down all counts in the $H\alpha$ image by a factor of 0.79 then corrects for this contamination in the data.

The uncertainties associated with the observed $H\alpha$ luminosity include those in the calibration of the $H\alpha$ emission and the extinction at $H\alpha$. Wilson and Scoville (1991) estimate the calibration to be accurate to $\pm5\%$. The uncertainty in $A_{H\alpha}$ was determined to be $A_{H\alpha}=0.78\pm0.26$ mag from the assumed mean reddening for the galaxy $\overline{E(B-V)}=0.3\pm0.1$ mag and the uncertainty in the conversion factor between

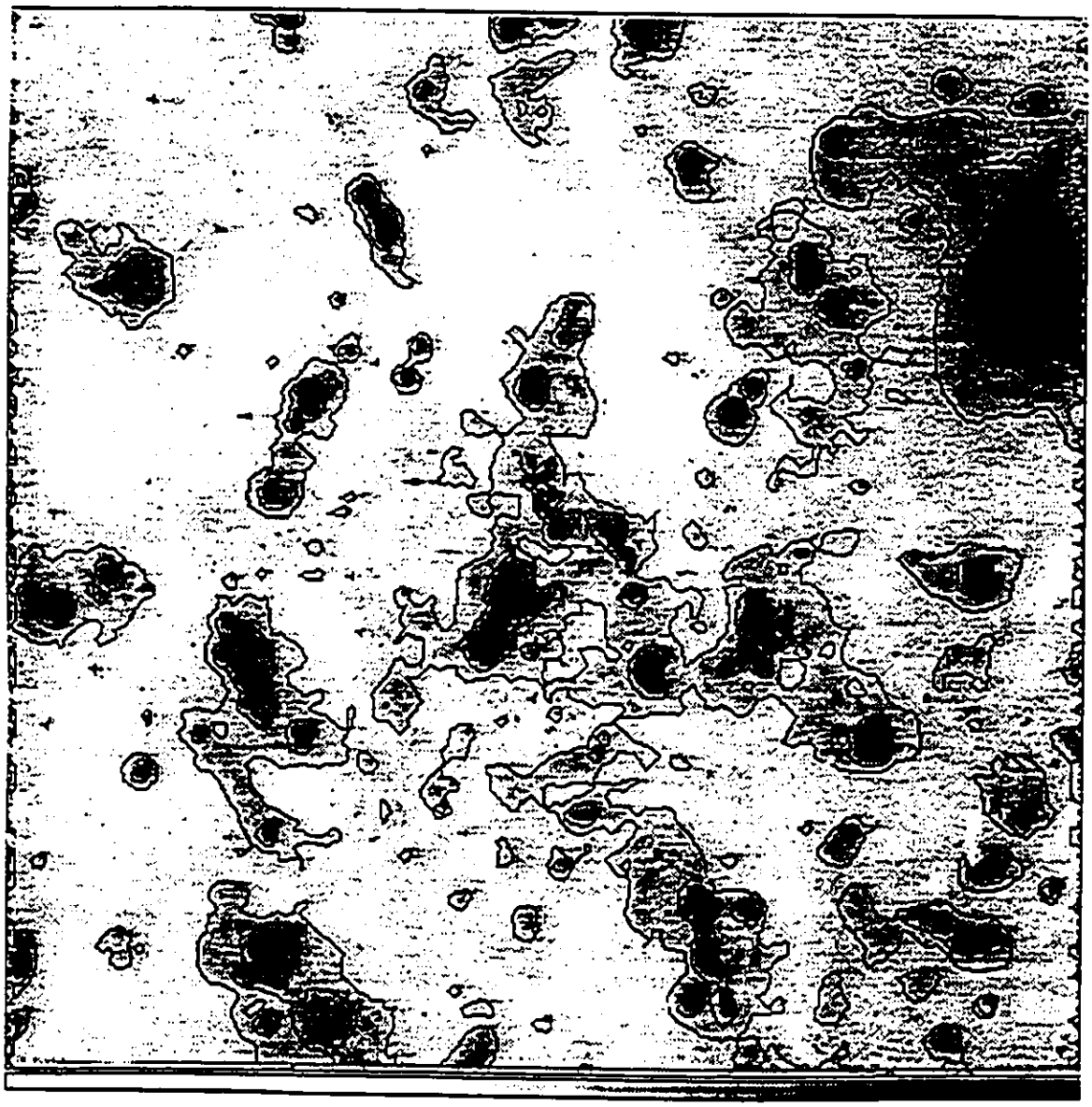

Figure 2.1a: The continuum subtracted $H\alpha$ image of the central 8.7′×8.7′ of M33 illustrating the distribution of the bright, halo and field $H\alpha$ emission regions. North is at the top and east is to the left. The contours, corresponding to surface brightnesses of I=1.74×10^{-15} and 4.57×10^{-16} erg s^{-1}cm^{-2}arcsec^{-2}, separate, respectively, the bright regions from the halo and the halo regions from the field. For orientation, the giant H II region NGC 595 is located on the top right-hand side of the image and the center of the galaxy coincides roughly with that of the image.

$A_{H\alpha}$ and $E(B-V)$, which we estimated at 0.07 mag or ~10% of $A_{H\alpha}$. We note that a radio continuum survey of the H II regions in M33 found an average $A_{H\alpha}$ of 0.91 mag (Viallefond & Goss 1986) which is comparable to our estimate. The total uncertainty in the observed $H\alpha$ luminosities is thus ~30%.

2.3.3 Predicted $H\alpha$ Luminosity from OB stars

In order to compare the observed $H\alpha$ fluxes with those expected from the associated stellar population, we estimate the Lyman continuum flux, and hence the $H\alpha$ luminosity, for stars with (B-V)≤0.4 by applying a number of stellar ionization models: blackbody, Auer & Mihalas (1972) (hereafter A&M), Kurucz (1979) and Panagia (1973). Both A&M and Kurucz calculate the expected number of Lyman continuum photons as a function of the effective temperature, T_{eff}, for various values of the effective gravity, g. The A&M results are based on nonblanketed NLTE model atmospheres composed of hydrogen and helium only. The Kurucz models, which include the effects of line blanketing, have LTE atmospheres of solar composition. The Panagia models are based on a combination of the NLTE A&M models and the LTE models due to Bradley and Morton (1969), Morton (1969) and Van Citters & Morton (1970), and appropriate values of g are used to calculate the flux of Lyman continuum photons as a function of T_{eff} for stars of luminosity class I, III, V as well as the ZAMS.

Effective temperatures (T_{eff}) and bolometric corrections (BC) for stars with $M_V \leq 21$ and $(B-V) \leq 0.4$ were obtained using the calibration equations given in Parker & Garmany (1993). The six equations (4a to 4f in Parker & Garmany 1993) give T_{eff} in terms of the reddening free index Q≡(U-B)-0.72(B-V) and the dereddened colour, $(B-V)_o$, for various luminosity classes. These equations which are, in

large part, taken from Massey *et al.* (1989a), are based on the data of Flower (1977), FitzGerald (1970) and Humphreys & McElroy (1984). The BC of the star was determined from T_{eff} using one of equations 5a to 5d in Parker & Garmany (1993). These calibrations are from Chelbowski & Garmany (1991) and Flower (1977). In applying these calibration equations, we followed the basic procedure outlined in Parker & Garmany, with a few modifications. We first selected all stars with $M_V \leq$-6 as potential supergiants. If the star had a (U-B) colour, we used equation (4f) to calculate T_{eff}. For -1.1<Q≤-0.9 or Q>0.0, we used equation (4a) (which is valid for main sequence stars) and subtracted 4000 K from the calculated T_{eff} (as per Parker & Garmany 1993; see their section 3.1 for a discussion of this point). For stars with Q<-1.1 or -0.3<Q≤0.0, we used (i) equation (4b) -4000 K if $(B-V)_o$<0.0. (ii) equation (4c) if 0.0≤ $(B-V)_o$<0.2 or (iii) equation (4d) if 0.2≤ $(B-V)_o$<0.5. Effective temperatures for all remaining, non-supergiant stars were calculated using one of equations (4a) to (4e) depending on the value of Q (if available) and $(B-V)_o$.

For the blackbody, A&M and Kurucz models, we applied Table XIV of Massey *et al.* (1989), which neatly summarizes the expected Lyman flux at the surface of the star for T_{eff} between 20,000 K and 50,000 K. For the Kurucz models, we have used log(g)=3.5 for stars with $T_{eff} \leq$ 35,500 K, and log(g)=5.0 for stars with T_{eff} >35,500 K while for the A&M models we take log(g)=4.0. The total flux in Lyman continuum photons is then found by integrating over the surface area of the star. For each star for which M_{bol} and T_{eff} were determined (as outlined above) and 18,000 K≤ T_{eff} ≤60,000 K, we calculate the stellar radius, R_*, using the luminosity-effective temperature relation, $L=4\pi R_*^2 \sigma_B T_{eff}^4$.

To apply the Panagia models, we need to know the luminosity class of the star as well as its T_{eff}. Panagia gives visual magnitudes (M_v^P) as a function of

effective temperature (16,100 K$\leq T^P_{eff} \leq$50,000 K) for ZAMS, supergiant, class III and main sequence stars. We estimate the luminosity class of the star by comparing the observed visual magnitude corrected for foreground and internal extinction, M_{V_o}, with M^P_v. Only stars with 15,100 K$\leq T_{eff} \leq T_{eff,U} \equiv$ 60,000 K are considered. We take all stars with $M_{V_o} \leq -6.0$ to be supergiants (class I). For the remainder of the stars, we compare the observed M_{V_o} to the values of the three M^P_v's (for class III, V and ZAMS) corresponding to the star's T_{eff}. The M^P_v that is closest to the observed M_{V_o} determines the luminosity class. In turn, the luminosity class and T_{eff} gives the total flux of Lyman continuum photons from the entire star.

To convert Lyman continuum photons to $H\alpha$, we refer to Osterbrock (1989) to find N(LyC)/N($H\alpha$)=2.22 assuming Case B recombination (appropriate for optically thick gas at 10,000 K and densities of 10^2-10^4 cm^{-3}). Although Case B recombination is the most commonly used approximation in the study of H II regions, we also consider Case A recombination for which N(LyC)/N($H\alpha$)=5.36 (Brockelhurst 1971), for stars in the "field" where the optical depth of the surrounding gas may be smaller. Clearly, Lyman continuum photons in optically thin gas produce fewer $H\alpha$ photons than those in optically thick gas.

2.4 IONIZED GAS AND OB STAR DISTRIBUTION

O and B stars in galaxies are commonly assumed to be located in bright H II regions. To study this assumption quantitatively, we identified the ionized gas environment of a star as either bright, halo, or field according to the average $H\alpha$ surface brightness inside a circle of radius of 2 pixels (~9.8 pc) centered on the star. Table 2.1 summarizes the total numbers of stars as a function of magnitude found in

the three different ionized gas environments.

Inspection of these tables reveals a number of surprising results. First and foremost, we find that *all O stars are not in bright H II regions*: there are a significant number of O stars in the field (see Figure 2.1b). From our analysis, roughly 50% of all blue ($(B-V)\leq 0.4$) stars brighter than V=21 are located in the field. In fact, the number of field stars outnumbers those in bright H II regions by almost a factor of three. This result is reflected also in the brightest stars ($V\leq 18$), where almost a third of the total are field stars. The halo component of the $H\alpha$ emission also contains a significant percentage (~30%) of the stellar population.

Additionally, the bright regions are predominantly populated by faint stars: 50% of all stars in the bright regions have $21<V\leq 20$ compared to 6% with $V\leq 18$. Although it appears that fainter stars form a larger fraction of the population in the field than in the bright H II regions (~64% in the field compared to ~50% in the bright regions), this may be due to a higher incompleteness level in the brighter regions where the crowding is larger (see Table 2.1).

From these results, we can estimate the fraction of the main sequence lifetime of an O star that is spent within a recognizable H II region (f_{HII}). We consider such an object to be composed of either a bright or halo emission region so as to obtain the most conservative estimate of this important quantity. With this assumption, we obtain $f_{HII} \equiv (N_B + N_H)/N_{TOT}=0.5$ where N_{TOT} is the total number of stars in the sample and N_B and N_H are the numbers of stars in, respectively, the bright and halo regions of the galaxy. Thus roughly 50% of the main sequence lifetime of an O star is spent *outside* of a recognizable H II region. If OB stars escape from bright H II regions by destroying their parent molecular clouds, this result

V MAG *	BRIGHT		HALO		FIELD		ENTIRE IMAGE	
	# of stars	% in region	# of stars	% in region	# of stars	% in region	# of stars	% in region
V ≤18	22 ±5	5.6 ±1.2%	15 ±4	2.2 ±0.6%	18 ±4	1.6 ±0.4%	55 ±7	2.5 ±0.3%
18 <V≤19	50 ±7	13 ±2%	66 ±8	10 ±1%	100 ±10	9 ±1%	216 ±15	10 ±1%
19<V≤20	123 ±11	32 ±3%	173 ±13	25 ±2%	276 ±17	25 ±1%	572 ±24	26 ± 1 %
20<V≤21	195 ±14	50 ±4%	434 ±21	63 ±4%	708 ±27	64 ±3%	1337±37	61 ±2%
V≤21(Total)	390 ±20		688 ±26		1102 ±33		2180	

Table 2.1: The Distribution of Blue Stars in Three Ionized Gas Environments of M33.

*Note : Only stars with (B-V)≤0.4

would imply that molecular cloud lifetimes after forming OB stars could be as low as $\sim$1-4$\times10^6$ yrs (or 1/2 the typical main sequence lifetimes of 2.6-8.1$\times10^6$yrs for 120-20 $M_\odot$ stars assuming Z=.020, Schaller *et al.* 1992). Since 50% of the molecular clouds in M33 contain optically visible H II regions (Wilson & Scoville 1991), under this scenario the lifetimes of the molecular clouds would be $\lesssim10^7$ yrs. This result, however, is inconsistent with the evidence that some OB associations in the galaxy have undergone at least two episodes of star formation separated by 10^7 yrs (Regan & Wilson 1993).

An alternative scenario is that the field O stars have percolated out of existing bright H II regions. In Table 2.2 we summarize a few key properties of the O star distribution and ionized gas environments. We see that although the field region occupies an area about 10 times that of the bright region, the surface density of stars in bright regions is only about 4 times that in the field. Assuming an average O star lives for 10 Myrs and has a velocity relative to the parental molecular cloud of 3 km s^{-1} (Churchwell 1991), it would travel only $\sim$30 pc over its lifetime. Typical dimensions of large field regions are 300$\times$600 pc (Figure 2.1b). Clearly, the field stars cannot all have simply percolated out of the H II regions we currently see.

Yet another scenario is one where the field stars originated in molecular clouds located in the field that have since been destroyed so as to leave the field O stars in a low density gas environment. The Owens Valley Millimeter-Wave Interferometer (OVRO) has been used to detect 38 giant molecular clouds (masses$\gtrsim5\times10^4M_\odot$) lying within an area of 1.5 to 2.0 kpc^2 in M33 (Wilson & Scoville 1990). The average surface density of molecular hydrogen in the OVRO fields is $\Sigma_{H_2}(OVRO)$=7.8$M_\odot$ kpc^{-2} (from Wilson & Scoville 1990, corrected by a factor of 1.44; see Thornley & Wilson 1994) while the average surface density in the inner kpc of the galaxy is Σ_{H_2}(1kpc)=6

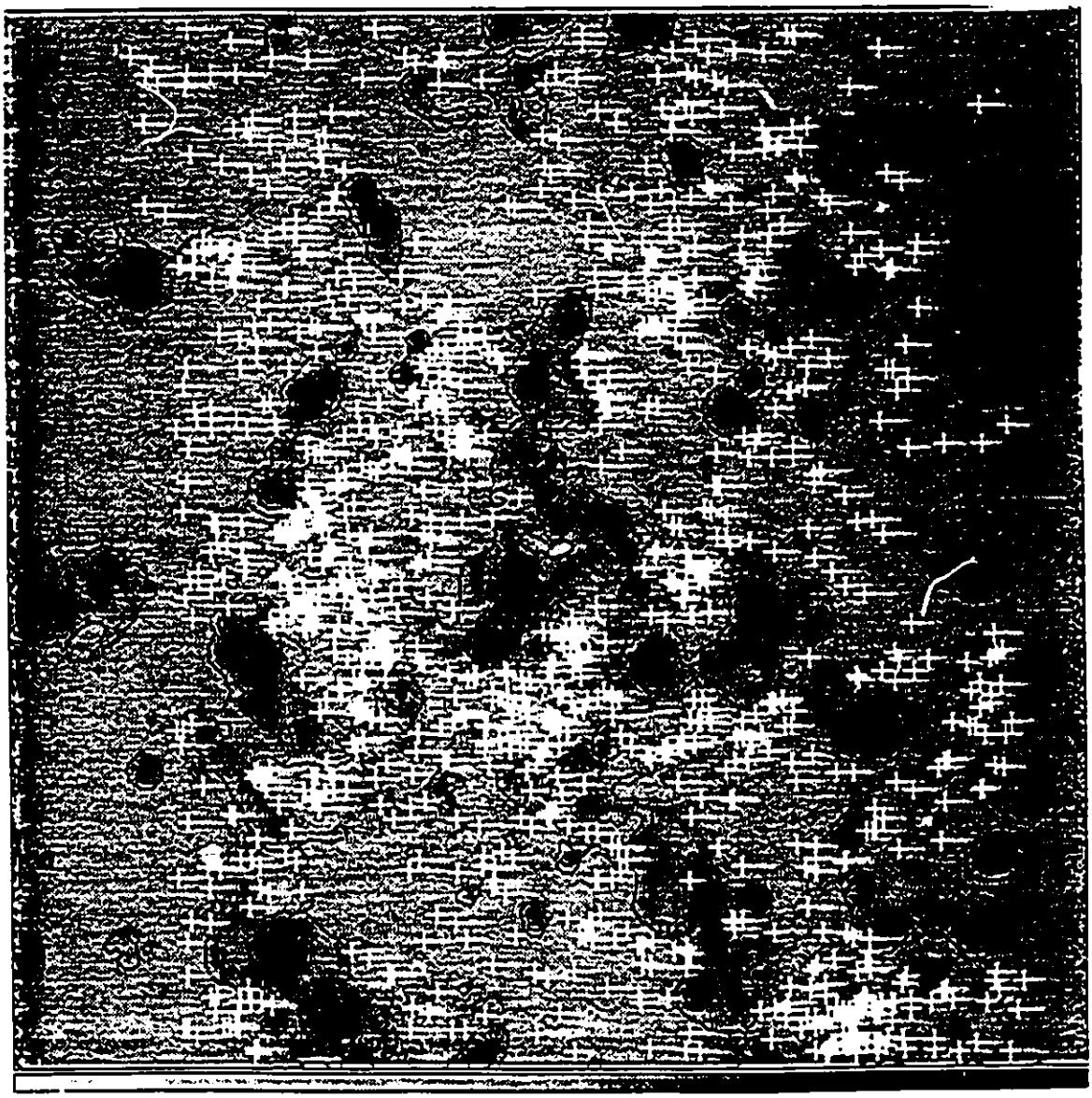

Figure 2.1b: The distribution of all field OB stars (V≤21 and (B-V)≤0.4) in the inner kpc of M33. As photometric coverage of the two vertical strips at the far left and right edges of the image was not available, these regions were excluded from the analysis.

	BRIGHT	HALO	FIELD	ENTIRE IMAGE
Total # of Stars $M_V \leq 21$	390	688	1102	2180
Area Covered (kpc^2)	0.22	0.83	2.28	3.33
Surface Density of Stars(kpc^{-2})	1770	829	483	655
Average Surface Brightness [I] [a]	3.44	0.62	0.09	4.15
Total Luminosity [L_{ob}] [b]	3.78	2.57	1.01	7.36
Relative Luminosity per Star [c]	1.0	0.38	0.10	0.35

Table 2.2: Average Properties of the Three Ionized Gas Environments in M33.

[a] In units of 10^{-15} erg $s^{-1}cm^{-2}$ $arcsec^{-2}$.This is measured above the average background.

[b] In units of $L_{39} \equiv 10^{39}$ erg s^{-1}. L_{ob} is measured above the average background luminosity $L_{bg} = 4.0 \pm 0.08 \times 10^{34}$ erg s^{-1}arcsec $^{-2}$. The total observed luminosity $L_{tot} = L_{ob} + L_{bg}$, for the bright, halo, field and entire image are, respectively, 3.9×10^{39}, 4.6×10^{39}, 7.0×10^{39} and 15.6×10^{39} erg s^{-1}.

[c] In units of 0.97×10^{37} erg s^{-1} $star^{-1}$. In the case where the average background was not subtracted off, the corresponding numbers are: 1., 0.67, 0.64 and 0.72 (in units of 1.0×10^{37} erg s^{-1}) for, respectively, the bright, halo, field and collective regions.

$M_\odot$ kpc^{-2} (Wilson & Scoville 1989, again corrected by a factor of 1.44). From the numbers of giant molecular clouds (GMCs) observed, the gas surface density, and the area covered in the OVRO survey (1.5-2 kpc), we estimate the expected number of GMCs (with masses$\gtrsim 5 \times 10^4 M_\odot$) within the inner kpc of M33 to be of the order of ~50. If the clouds are spread uniformly across a circular region of radius 1 kpc, the average distance between these clouds would be 130-150 pc. Clearly O stars that formed and percolated out from these large GMCs would not be able to fill the entire area of the field.

It is important to note, however, that the OVRO interferometer detected only ~40% of the flux measured in single dish observations of the same regions of the galaxy (Wilson & Scoville 1990). The missing flux was hypothesized to be distributed in a smooth component or dense molecular clouds less massive than $0.5 \times 10^5 M_\odot$ (Wilson

& Scoville 1990). If we assume that half of the missing flux (30% of the single dish flux) is due to small, dense molecular clouds, that the molecular cloud mass spectrum follows a power law of the form $N(m) \propto m^{-1.5}$ (as determined from the more massive molecular clouds in M33), and that the minimum mass of a molecular cloud of interest is 10^3 $M_\odot$ (a typical Taurus-type "dark cloud", Goldsmith 1987), then the estimated number of *low-mass* (10^3-$0.5\times10^5 M_\odot$) molecular clouds in the inner kpc of M33 is $\sim10^3$. Since the average separation between these clouds is 30 pc. O stars could easily disperse from these clouds to fill the entire field. Therefore, if even half the missing flux is in low-mass molecular clouds, most of the field O stars could have been born in and percolated out of (or destroyed) *low-mass* molecular clouds. Observational support for massive star formation in low-mass molecular clouds can be found within our own Galaxy. A survey of small Galactic H II regions ($\sim$1/5 the $H\alpha$ luminosity of Orion) and their associated molecular clouds (masses$\sim$1-$60\times10^3 M_\odot$) by Hunter & Massey (1990) showed that OB star formation has occurred in all of the molecular clouds. Finally, we point out that these energetic stars may be more effective at dispersing their lower-mass parental molecular clouds (compared to the more massive clouds associated with the bright H II regions) which could also account for the low $H\alpha$ emission in field regions.

Finally, it is possible that the field emission regions were created by supernovae that had swept out the gas and dust from large areas of the galaxy leaving behind low density gas as well as the field stars which must have already been formed prior to the explosions.

From Table 2.2 we see that the relative total $H\alpha$ luminosity per field star is $\sim1/10^{th}$ that of a star in a bright H II region. This result raises the question of whether the field is "leaking" Lyman continuum photons, which presumably escape

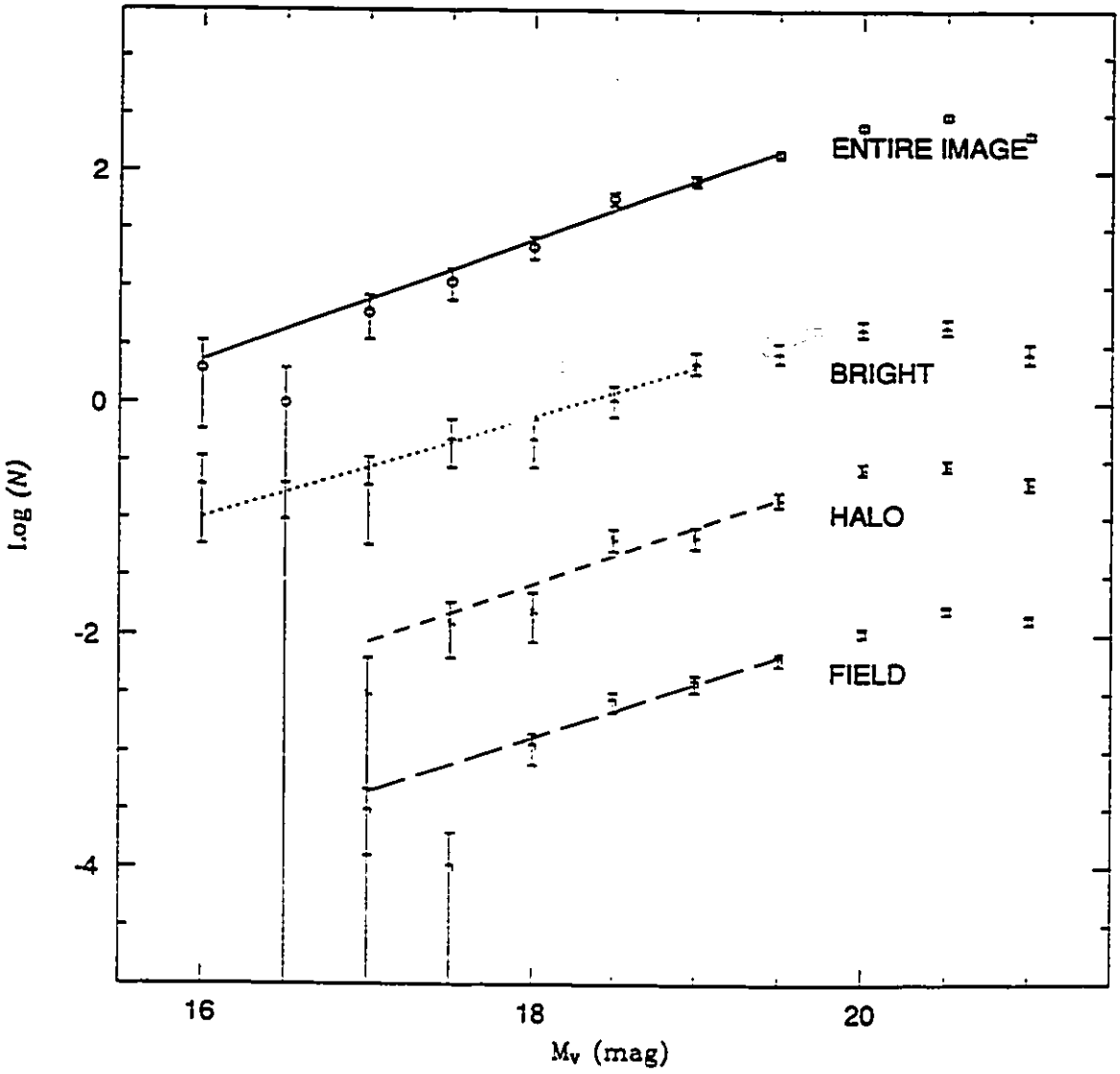

Figure 2.2: The luminosity functions for stars in the entire image as well as the bright, halo and field HII regions. An arbitrary offset in the ordinate has been applied for the purposes of clarity. Overlaid on the data are the weighted least squares fits (to a limiting magnitude of V=19 for the bright region and V=19.5 elsewhere).

from the galaxy. Alternatively, the field population may be older than that in bright H II regions so that fewer early type stars with large ionizing fluxes remain. To address these questions, we have determined the stellar luminosity functions for the three ionized gas environments as well as the entire sample to see if there is any indication of age segregation (Figure 2.2). Weighted least-squares fits to the data to a limiting magnitude of 19 for the bright H II region (to reduce incompleteness effects) and 19.5 for all others yield slopes of 0.44 ±0.09 (bright), 0.49 ±0.08 (halo), 0.47 ±0.07 (faint) and 0.52 ±0.04 (entire image). The uniformity of the luminosity function slopes does not suggest that the stellar populations of the three H II environments have different average ages. Although including stars up to V=19.5 in the bright H II regions decreases the slope to 0.40 ±0.07, the difference is still not significant enough to suggest a younger population. As age differences could affect the distribution of the bright stars most severely, we also examined the distribution of stars that are brighter than V=18, normalized to the total number brighter than V=19. The percentage of stars with V≤18 in the bright, halo and field regions are respectively, 30 ±10% , 18 ±7% and 15 ±5% . Clearly again, no region appears to have an over-abundance of luminous stars and therefore there is no evidence for age segregation between the different $H\alpha$ emission regions. It appears therefore that the difference in the $H\alpha$ luminosity per O star in the field compared to that in the bright regions is not due to a difference in age but is perhaps indicative that ionizing radiation from field stars may be escaping out of the surveyed region.

2.5 IONIZATION BALANCE IN THE INNER 1 KPC

Star formation rates calculated from $H\alpha$ luminosities assume that all the Lyman continuum flux emitted by the stars remains in the galaxy (or region) so

that the galaxy (or region) is ionization bounded (*e.g.*, Kennicutt 1983). To test this hypothesis, we have estimated the Lyman continuum and hence $H\alpha$ flux emitted by the stars and compared it to that observed in the $H\alpha$ image. In carrying out these ionization balance calculations, we have relied heavily on the models of Panagia (1973) which are applicable to zero age main sequence stars (ZAMS) as well as main sequence (class V), luminosity class III and supergiant stars. As an estimate of the uncertainties in the theoretical models, we have also used the blackbody, Kurucz, and A&M models.

In all applications of the ionizing radiation models, we have imposed an upper and lower limit to T_{eff}, respectively $T_{eff,U}$ and $T_{eff,L}$. For comparative purposes, we have set $T_{eff,U}$ =60,000 K and $T_{eff,L}$=30,000 K. The lower limit $T_{eff,L}$ is chosen as the minimum effective temperature for which all ionization models are defined. Although all four models are defined up to T_{eff}=50,000 K (for an O4, class V star), we have chosen $T_{eff,U}$ =60,000 K so as to provide a small margin of error at the high T_{eff} end as well as to roughly account for the Lyman continuum flux for stars earlier than O4. Stars that had calculated effective temperatures between 50,000 K and 60,000 K were all assigned Lyman fluxes corresponding to 50,000 K from the models. By doing this, we are most likely under estimating the true Lyman continuum flux from those stars earlier than O4. Stars with effective temperatures outside the limits set by $T_{eff,U}$ and $T_{eff,L}$ have no ionizing flux assigned to them. We have not attempted to account for stars with $T_{eff}>T_{eff,U}$ as these effective temperatures may most likely be the result of photometric errors (for example, Massey *et al.* (1989a, 1989b) have found many stars with unrealistic (B-V) or (U-B) colours the cause of which they attributed to photometric errors). Similarly, stars with $T_{eff}<T_{eff,L}$ are also not accounted for as these stars are most likely to be late type stars (with correspondingly small ionizing

fluxes) or more evolved stars. We note that the presence of Wolf-Rayet stars is also not taken into account. While the ionizing Lyman continuum flux from these stars is estimated to be significant, the exact values are highly uncertain (Massey *et al.* 1989b). Therefore not accounting for the presence of Wolf-Rayet stars in the surveyed regions of M33 serves to underestimate the predicted theoretical flux. Finally, studies in the LMC and SMC have shown that effective temperatures calculated from photometry are in general lower than those determined from spectroscopy (Massey *et al.* 1989b; Parker *et al.* 1992) so that here again, predicted ionizing fluxes from photometry are most likely to be underestimated.

In terms of the $H\alpha$ fluxes (assuming Case B recombination), the total flux in $H\alpha$ from all stars with $T_{eff,L} < T_{eff} < T_{eff,U}$ calculated from the four ionization models are (in units of 10^{39}erg s^{-1}), $F_{H\alpha}$= 14.46 (Panagia), 15.15 (blackbody), 11.05 (Kurucz) and 13.49 (A&M). The agreement amongst the different models is quite good: the lowest (Kurucz) and highest (blackbody) estimates of $F_{H\alpha}$ differ by a factor of 1.4. At low T_{eff}, the blackbody model predicts more Lyman continuum photons than the A&M and Kurucz models so that it is not surprising that the total flux from all stars (many of which have low T_{eff}) for the blackbody model is the highest estimate. In the remainder of the section we will discuss only the $H\alpha$ flux estimated using the Panagia models. As the minimum effective temperature for which these models are defined depends on the luminosity class of the star, *i.e.*, T_{eff}=15,100 K (for class I), T_{eff}=16,900 K (for class V and ZAMS) and T_{eff}=16,000 K (for class III), we have defined for each luminosity class the corresponding $T_{eff,L}$ inferred from the models. As such, the percentage of stars with (B-V)$\leq$0.4 that have T_{eff} between $T_{eff,L}$ and $T_{eff,U}$ is then 54% (V<18), 60% (18<V<19), 74% (19<V<20) and 75% (20<V<21).

To obtain the most complete and accurate estimate of the Lyman continuum, and hence the $H\alpha$, luminosity, we have applied two corrections to the data. The first concerns incompleteness of the photometric survey at the faint end of the luminosity function (V≤21). Wilson (1991) determined that the data were incomplete by 30% for 19.5<V≤20, 55% for 20<V≤20.5 and 65% for 21<V≤21 by comparing the observed luminosity function with a power law with slope of 0.65. Thus the corrected fluxes are obtained by scaling the uncorrected fluxes by 1.4 for stars with 19.5<V≤20, 2.2 for stars with 20<V≤20.5 and 2.9 for stars with 20.5<V≤21. Secondly, we must account for flux from stars that are below our faint magnitude limit. We have calibrated a relation between main sequence mass and M_V using theoretical evolutionary tracks between the ZAMS and the terminal age main sequence (TAMS) for metallicity Z=0.020 from Schaller *et al.* (1992). The tracks were interpolated in steps of 1 $M_\odot$ and then transformed to the observational plane using the equations outlined in section three of Massey *et al.* (1989a). As was done in Wilson (1992), we determined the total range of stellar masses possible for each range in M_V and assigned to each magnitude bin the average of the maximum and the minimum possible stellar mass. At the distance and reddening of M33, V=21 corresponds to 24 $M_\odot$. Linearly interpolating the spectral type-mass calibrations given by Popper (1980) and Schmidt-Kaler (1982), we find that 24 $M_\odot$ corresponds to roughly an O7.5-O8 star. We determined the total number of stars for each spectral (sub)class from O7.5 to B3 (the latest class for which the Panagia models give theoretical fluxes) using our spectral type-main sequence mass calibration and the Salpeter initial mass function (IMF) $N(m)d(M)=Am^{\alpha}dm$ (Salpeter 1955), where α=2.35. The normalization constant A is determined by integrating the initial mass function between 24 $M_\odot$ and 65.5 $M_\odot$ and equating this to the total number of stars for which we could determine T_{eff}, either uncorrected (N_* ~240 (bright), ~400 (halo) and ~640 (field)) for

the conservative flux estimate, or corrected for incompleteness brighter than V=21 (N. ~540 (bright), ~1020 (halo) and ~1280 (field)) for the best flux estimate. We determined the total flux in each spectral class (or subclass) bin between O7.5 and B3 due to main sequence stars fainter than V=21 by multiply the average theoretical flux for that bin (class V assumed) by the total predicted number of stars in the bin.

In Table 2.3 we summarize the observed and predicted $H\alpha$ fluxes, with theoretical values given in several steps correcting in turn for the effects discussed above. Included are the theoretical fluxes predicted from all stars with $T_{eff,L} \lesssim T_{eff} \lesssim T_{eff,U}$ (1) for the stars actually observed ("minimum flux"); (2) corrected for stars fainter than V=21 ("conservative flux"); (3) corrected for incompleteness for both stars brighter and fainter than V=21. Based on the limited reliability of the Panagia model in assigning ionizing fluxes from photometric data alone (see Chapter 3), we will consider any agreement between the observed and predicted $H\alpha$ fluxes that are within a factor of two to be acceptable.

If we make no corrections to the data, we find that the predicted fluxes are in very good agreement with what is observed: over the total image, the two differ by less than a factor of 2. The best agreement between theory and observation is in the bright region (~1.3:1 correspondence) followed by the halo region, where the predicted flux is ~1.6 times the observed flux. The field may be losing some ionizing photons as the predicted flux is a factor of ~2.4 (Case A) and ~5.7 (Case B) greater than that observed.

Including the flux from stars below the faintness limit of the survey increases the predicted fluxes by a factor of ~2 over both the individual ionized gas regions as well as the entire survey area. The total theoretical flux exceeds that observed by

	BRIGHT	HALO	FIELD (Case A/ B)	TOTAL (Case A/ B)
Minimum Flux[a]	4.90	4.07	2.40 / 5.75	11.48 / 14.79
Incompleteness (V≤21)[b]	8.13	8.32	4.75 / 11.48	21.20 / 27.93
Best Estimate [c]	15.03	21.47	13.23/31.88	49.73 / 68.38
Conservative Estimate [d]	7.92	9.32	5.42 / 13.00	22.66 / 30.24
Observed Flux[e]	3.78	2.57	1.01	7.36

Table 2.3: Observed and Predicted Hα Flux in the Three Ionized Gas Environments of M33.

[a]Minimum: no corrections applied. All fluxes in units of $L_{39} \equiv 10^{39}$ erg s^{-1} $arcsec^{-2}$.

[b]Incompleteness: corrected for incompleteness for stars brighter than V=21.

[c]Best estimate: corrected for incompleteness at bright (V≤21) and faint (V>21) magnitudes.

[d]Conservative estimate: corrected only for stars with V>21.

[e]Observed fluxes do not include the average sky background. If the average background is included, the relevant numbers are: 3.9 (bright), 4.6 (halo), 7.0 (field) and 15.6 (entire image).

factors of 2.1 (bright), 3.6 (halo), 5.4 (field: Case A), 12.9 (field: Case B), 3.1 (total image: Case A) and 4.1 (total image: Case B). Clearly adopting Case B recombination for the field results in predicted ionizing fluxes that are substantially larger than observed. Including stars below the faintness limit of our survey is the minimum correction we must make to our data and thus these fluxes represent a lower limit to the theoretically predicted $H\alpha$ fluxes.

Correcting the data for incompleteness ($V \leq 21$) increases the predicted fluxes by a factor of less than 2 over the different ionized gas environments. The most complete estimate of the predicted flux includes both incompleteness corrections for $V \leq 21$ and main sequence stars with $V > 21$. From Table 2.3 we see that over the entire surveyed region, these final fluxes are a factor of $\sim$6.7 (Case A) to $\sim$9.3 (Case B) greater than observed. The best agreement is again found in the bright regions where the predicted flux is $\sim$4 times that observed and the worst agreement is in the field where the predicted flux exceeds the observed by factors of $\sim$13 (Case A) to $\sim$31 (Case B). This most generous estimate of the theoretical fluxes after corrections and the most conservative estimate differ by less than a factor of 3 from each other.

The best agreement between observations and theory in the field, as well as for the entire surveyed region, is obtained when we assume Case A (optically thin) recombination. Bright H II regions are likely to have larger opacities than faint regions where gas densities are likely to be smaller. Although we have no direct measure of the density of gas in the various regions, we can place limits on this quantity by comparing the observed $H\alpha$ surface brightness with that expected for H II regions of various different gas densities. If we consider a B0 star ($L_{H\alpha}$=5.82$\times 10^{35}$ erg sec^{-1} and $N_{Ly C}$=4.27$\times 10^{47}$ photons sec^{-1}; Panagia 1973) located in the field, then the maximum surface brightness observed in the field (I_F=3.61$\times 10^{-16}$ erg s^{-1}cm^{-2}

arcsec^{-2}) limits the gas density to be $\lesssim$5 cm^{-3}. We have used the Stromgren radius (*e.g.*, Spitzer 1978) to estimate the radius of the H II region and assumed the gas within the Stromgren sphere of the star is completely ionized. For the H II region of a field O5 star to have a surface brightness equal to I_F, the density of gas would have to be $\lesssim$0.5 cm^{-3}. In contrast, if the surface brightnesses of H II regions formed by B0 and O5 stars are to equal the average surface brightness observed in bright H II regions (I_B=3.44$\times$10^{-15} erg s^{-1}cm^{-2} arcsec^{-2}), the gas density must be $\sim$15 cm^{-3} (B0) and $\sim$1 cm^{-3} (O5). Thus the density of gas in the field is likely to be lower than that in the bright H II regions which lends some support to our assumption of Case A recombination in the field and Case B elsewhere in the galaxy.

Comparing the corrected final theoretical fluxes with the observed fluxes *when the uniform background has not been removed* reveals that the two still differ by up to a factor $\sim$2-5. Clearly the field region is most sensitive to the inclusion or exclusion of the uniform background: the field could be in ionization balance if Case A recombination is assumed and the uniform background is not removed. However, including the background and assuming Case A recombination where appropriate, comparison of the theoretical best estimate fluxes with the observed fluxes suggests that *over the total, as well as the bright and halo regions surveyed, the galaxy is not in a state of ionization balance.*

With so much ionizing flux missing we are left with the question: where does it go? One possible fate for leaked photons is in powering the halo ionized gas. The low density and expected small opacities in the field combined with the enormous reservoir of leaked flux provided by the OB stars would clearly increase the chances for the photons to reach the large distances above the plane before recombining and producing the halo ionized gas. Additionally, the large pool of ionizing photons avail-

able would be advantageous in producing a halo ionized gas with a total luminosity that is a sizable fraction of the total $H\alpha$ emission measured in the galaxy.

Star formation rates from $H\alpha$ luminosities are based on the assumption that all the ionizing radiation from stars remains in the galaxy. If a significant portion of the ionizing flux is leaking out of the galaxy, SFRs calculated from observed $H\alpha$ fluxes would underestimate the true SFR. Our results suggest that this is the case in M33. We find, in fact, that SFRs calculated from observed $H\alpha$ luminosities alone underestimate those calculated from the most realistic predicted fluxes (best estimate scenario and assuming Case A recombination in the field) by a factor of ~4 (bright), ~8 (halo), ~13 (field) and ~7 (total image). The implications of this result for SFR calculations in other systems could be serious. Clearly much will depend on how ionizing photon leakage correlates with other characteristics of a galaxy such as its morphology, age and the state of the interstellar medium. If M33 is typical of its class, then applying this technique in late-type spiral galaxies could severely underestimate the actual SFR. The outcome for irregular galaxies (due to their patchy gas distribution) and elliptical galaxies (due to their low gas densities) may be comparable to that found here for M33 but would certainly need to be verified by a similar type of investigation before any conclusions can be drawn.

2.5.1 IONIZATION BALANCE IN AN ISOLATED REGION

Having looked at the question of ionization balance on the large scale, we consider now the small scale and focus on one isolated region of the galaxy containing both bright and halo H II emission. The chosen region, denoted Region A, lies in the south-east portion of the galaxy, and covers an area of ~300×500 pc (90″×130″; Figure 2.3). We have photometry for 19 stars located in the region with bright $H\alpha$

	BRIGHT	HALO	COMBINED (BRIGHT + HALO)
Minimum Flux[a]	0.24	0.01	0.25
Incompleteness (V≤21)[a]	0.69	0.03	0.72
Best Estimate [a]	1.00	0.37	1.37
Conservative Estimate [a]	0.40	0.14	0.54
Observed Luminosity [L_{ob}][b]	0.13	0.07	0.20
# Stars Observed [S_{ob}]	19	17	36
# Stars with $T_{eff,L} < t_{eff} < T_{eff,U}$	11	14	25
L_{ob}/S_{ob}[c]	1	0.64	0.82

Table 2.4: The Observed and Predicted Hα Fluxes and OB Star Content in Region A.

[a]Predicted $H\alpha$ luminosity accounting for incompleteness (as in Table 2.3). All fluxes in units of $L_{39} \equiv 10^{39}$ erg s^{-1} arcsec^{-2}.

[b]Observed luminosities have been background subtracted. If the background is included, the numbers are: 0.18 (bright) and 0.14 (halo) and 0.32 (combined bright and halo).

[c]In units of 6.8×10^{36}erg s^{-1} arcsec^{-2} star^{-1}.

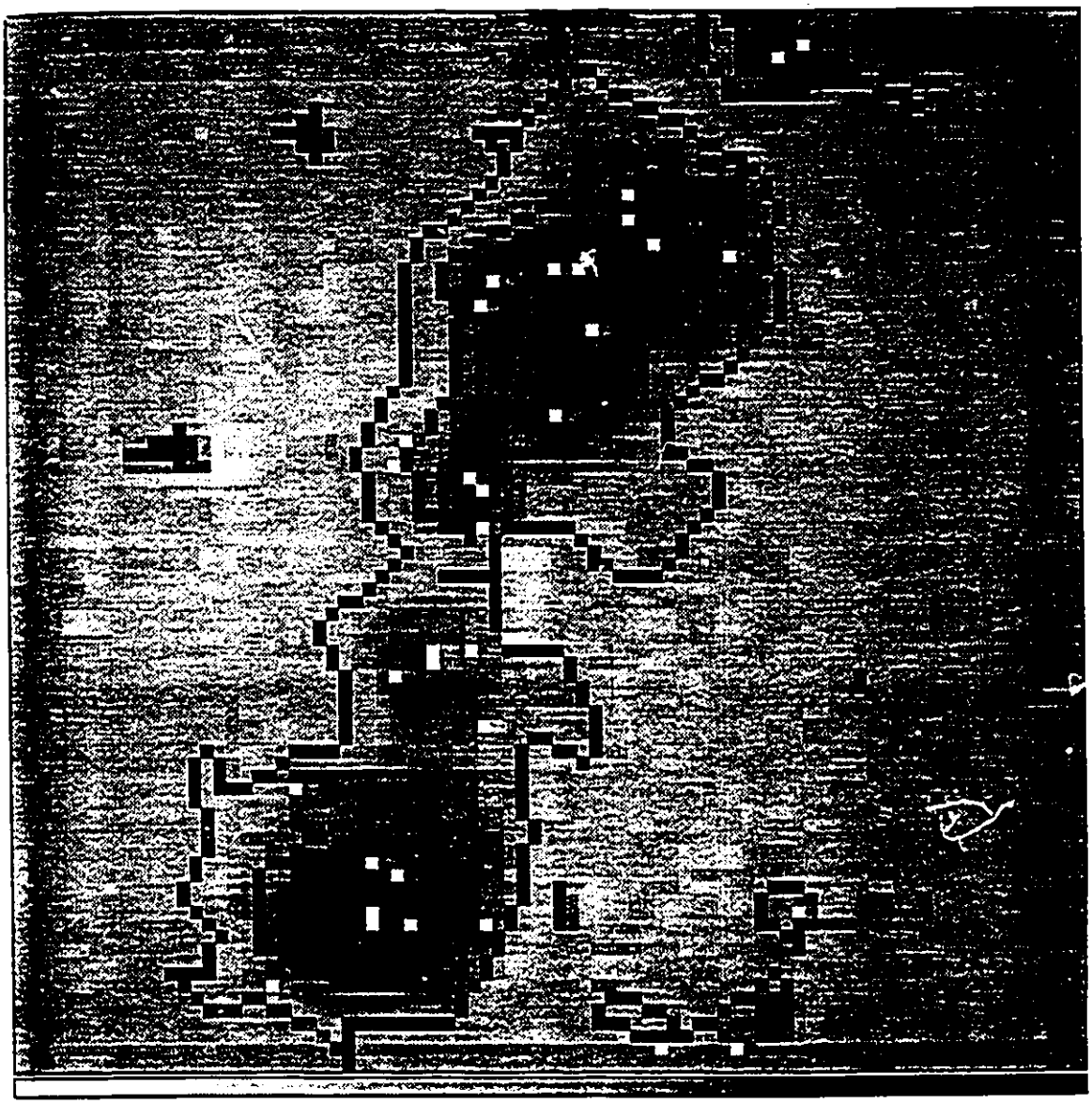

Figure 2.3: Expanded View of Region A which was selected for individual investigation. Overlaid are the stars in the bright and halo $H\alpha$ emission areas within the region.

emission and 17 stars in the halo emission region. Table 2.4 summarizes the observed and theoretical $H\alpha$ fluxes in the bright, halo and combined (bright and halo) regions. We find that observations and model predictions are best matched for the simplest situation where no corrections are made: the predicted fluxes in the bright and halo regions are, respectively, a factor 1.8 and 0.1 times that observed so that the region as a whole is in balance. Correcting for stars fainter than V=21 increases the predicted fluxes by factors of $\sim$2 in the bright, $\sim$14 in the halo region and $\sim$1.4 over the combined region. This result can be considered to be the most conservative corrected estimate of the theoretical flux in Region A. Correcting for incompleteness ($V \leq 21$) increases the minimum theoretical flux by a factor of $\sim$3 over both the bright and halo regions. The best estimate of the predicted fluxes are a factor of 8 (bright), 5 (halo) and 7 (combined bright+halo) greater than that observed. Therefore, only in the simplest situation of the uncorrected data is Region A close to being ionization bounded. In the more realistic case where the data has been corrected for incompleteness in stars brighter than V=21 and flux from stars fainter than V=21, this region is *clearly not ionization bounded.* Even the conservative estimate of the corrected flux indicates this region is leaking photons to its surroundings. Furthermore, including the uniform background cannot bring the combined bright and halo emission regions into ionization balance. Thus our results for a small, individual region confirm those obtained for the larger surveyed area: ionizing flux from OB stars is found to be missing on both large and small scales in M33.

2.6 CONCLUSIONS

Using $H\alpha$ data and UBV photometry of blue stars, we have investigated the distribution of H II regions and OB stars and tested the hypothesis of ionization

balance within the inner kpc of M33. The main results are summarized below.

(1) The $H\alpha$ emission appears to be distributed in three distinct components, denoted bright, halo and field, that are spread out over the galaxy. Roughly one third of the brightest blue stars (V$\leq$18) are found in the field region. Including all stars within the photometric limit V=21, we find that $\sim$50% of the OB stars (luminous blue stars with $(B-V)\leq 0.4$) are located in the field. From this result we estimate 50% of the main sequence lifetime of an OB star is spent outside a recognizable H II region. The implication of this for molecular cloud lifetimes is that if the field stars escape from bright H II regions by destroying their parent molecular clouds, then molecular cloud lifetimes after the formation of OB stars must be shorter than $\sim 10^7$ yrs. On the other hand, if OB stars simply move out of the clouds, molecular cloud lifetimes could be considerably longer.

(2) Assuming typical OB star velocities are $\sim$3 km s^{-1} we find field stars could not all have originated in and percolated out of existing H II regions or for that matter, a strictly massive ($\gtrsim 0.5\times 10^5 M_\odot$) GMC population. If the galaxy contains GMCs with masses down to $\sim 10^3 M_\odot$ (typical Taurus-type dark clouds), there would exist sufficient numbers of GMCs to make the average separation between them comparable to the maximum distance an OB star can travel over its lifetime. Therefore, the field star population could have originated from and percolated out of a GMC population with masses $\gtrsim 10^3 M_\odot$.

(3) The slopes of the luminosity functions for stars in the bright, halo and field regions are comparable to one another, which suggests that the stellar populations in the different ionized gas environments must have similar ages. This result is supported by the brightest (V$\leq$18) blue stars which show no evidence of being concentrated in

any one type of ionized gas environment.

(4) We have estimated the theoretical ionizing flux from the observed OB stars using the Panagia (1973) models and converted these to theoretical $H\alpha$ fluxes assuming Case B recombination for the bright and halo regions and Case A and B recombination for the field region. Ionization balance calculations show that the inner region of M33 *is not in ionization balance*: the observed fluxes are a factor of ~7-9 (Case A-Case B) less than the predicted best estimate fluxes and a factor of ~3-4 (Case A-Case B) less than the predicted conservative estimate fluxes. The greatest loss of ionizing flux occurs in the field region: even in the conservative case, the predicted $H\alpha$ flux is a factor of 5 (Case A recombination) greater than that observed. The discrepancy between the two increases to a factor of 13 (Case A recombination) for the best estimate case of the predicted flux. We find Case A recombination provides the best agreement between observed and predicted $H\alpha$ fluxes in the field. Of the three ionized gas environments, the bright regions are closest to being ionization bounded. Investigation of an individual, isolated region containing both bright and halo emission produces comparable results: the region is unbalanced by a factor of ~3 and ~7 for respectively, the conservative and best estimate cases.

(5) Based on our result that the separate ionized gas environments and individual regions of the galaxy are leaking ionizing flux, SFRs calculated from $H\alpha$ luminosity must underestimate the true SFR. Over the entire surveyed region, the difference between the true SFR and that calculated from $H\alpha$ could differ by a factor of ~3-7.

2.7 REFERENCES

Auer, L.H. & Mihalas, D. 1972, ApJS, 24, 193

Blitz, L. & Shu, F. 1980 ApJ, 235, 148

Brandley, P.T. & Morton. D.C. 1969. ApJ. 156. 687

Brockelhurst. M. 1971. MNRAS. 153. 471

Chelbowski, T. & Garmany. C.D. 1991. ApJ. 368. 241

Churchwell, E. 1991, in the Physics of Star Formation & Early Stellar Evolution, ed. C. Lada & N.D. Kylafis (Dordrecht:Kluwer), p. 221

Elmegreen. B.G. 1991. in The Physics of Star Formation & Early Stellar Evolution, Ed. C.J. Lada & N.D. Kylafis (Dordrecht:Kluwer), p. 35

Flower. P.J. 1977. A&A. 54. 31

FitzGerald, M.P. 1970. A&A. 4. 234

Goldsmith, P.F. 1987 in Interstellar Processes. eds. D. Hollenbach & H. Thronson (Dordrecht:Reidel), p. 51

Humphreys. R.M. & McElroy. D.B. 1984. ApJ. 284. 565

Hester, J.J & Kulkarni. S.R. 1990. in The Interstellar Medium in External Galaxies, NASA-3084. eds. D. Hollenbach & H. Thronson (Washington:NASA), p. 288

Hunter, D.A. & Massey. P. 1990. AJ. 100. 1915

Kennicutt, R.C. 1983, ApJ, 272, 54

Kennicutt, R.C. & Hodge, P. 1986, ApJ, 306, 130

Kurucz, R.L. 1979, ApJS, 40, 1

Massey. P., Lang, C.C., Degioia-Eastwood, K. & Garmany, C.D. 1994, ApJ, in press

Madore, B.F. 1978, Observatories, 98, 169

Massey. P., Garmany, C.D., Silkey, M. & Degioia-Eastwood, K. 1989a, AJ, 97, 107

Massey. P., Parker, J.W. & Garmany, C.D. 1989b, AJ, 98, 1305

Morton, D.C. 1969, ApJ, 158, 629

Osterbrock, D.E. 1989, Astrophysics of Gaseous Nebulae and Active Galactic Nuclei (Mill Valley: University Science Books)

Panagia, N. 1973, AJ, 78, 929

Parker, J.W. & Garmany, C.D. 1993, AJ, 106, 1471

Parker, J.W., Garmany, C.D., Massey, P. & Walborn, N.R. 1992, AJ, 103, 1205

Popper, D. 1980, ARA&A, 18, 115

Rand, R.J., Kulkarni, S.R. & Hester, J.J. 1990, ApJ, 352, L1.

Regan, M.W. & Wilson, C.D. 1993, AJ, 105, 499

Salpeter, E.E. 1955, ApJ, 129, 608

Schaller, G., Schaerer, D., Meynet, G., Maeder, A. 1992 A&AS, 96, 296S

Schild, R. 1977 AJ, 82, 337

Schmidt-Kaler, Th. 1982, in Landolt-Bornstein: Numerical Data and Functional Relationships in Science and Technology, New Series, Vol 2, Astronomy and Astrophysics, eds K. Schaiffer and H.H. Voigt (Berlin: Springer-Verlag), p. 1

Spitzer, L. 1978, Physical Processes in the Interstellar Medium (New York:Wiley)

Solomon, P.M. & Sanders, D.B. 1980, in Giant Molecular Clouds in the Galaxy, eds P.M. Solomon and M.G. Edmunds (Oxford:Pergammon Press), p. 41

Thornley, M.D. & Wilson, C.D. 1994, ApJ, 421, 458

Van Citters, G.W. & Morton, D.C. 1979, AJ, 161, 695

Van den Bergh, S. 1991, PASP, 103, 609

Viallefond, F. & Goss, W.M. 1986, A&A, 154, 357

Vilchez, J.M., Pagel, B.E.J., Diaz, A.I., Terlevich, E. & Edmunds, M.G. 1988, MNRAS, 235, 633

Walterbos, R.A.M. & Braun, R. 1994, ApJ, 431, 156

Walterbos, R.A.M. 1991, in The Interstellar Disk-Halo Connection in Galaxies, ed. H. Bloemen (Dordrecht:Kluwer), p. 223

Wilson, C.D. 1992, AJ, 104, 1374

Wilson, C.D. 1991, AJ, 101, 1663

Wilson, C.D. & Scoville, N.Z. 1991, ApJ, 370, 184

Wilson, C.D. & Scoville, N.Z. 1990, ApJ, 363, 435

Wilson, C.D. & Scoville, N.Z. 1989, ApJ, 347, 743

Wilson, C.D. 1990, Ph.D. thesis, Caltech

Chapter 3

ARE GALAXIES OPTICALLY THIN TO THEIR OWN LYMAN CONTINUUM RADIATION? II. NGC 6822

3.1 ABSTRACT

In this paper we study OB stars, H II regions, and the state of ionization balance in the Local Group galaxy, NGC 6822. Using $H\alpha$ data and BV photometry of the blue stars in this dIrr galaxy, we investigate the distribution of OB stars and H II regions and determine whether individual areas of the galaxy are separately and/or collectively in a state of ionization balance. Four distinct components of the $H\alpha$ emission (bright, halo, diffuse and field) differentiated by their surface brightnesses are identified. We find that approximately 1/2 of all OB stars in NGC 6822 are located in the field while only 1/4 are found in the combined bright and halo regions, suggesting that OB stars spend roughly 3/4 of their lifetimes outside "classical" H II regions. If OB stars escape from bright H II regions by destroying their parent molecular clouds, then cloud lifetimes after forming OB stars could be as low as ~1-3×10^6 yrs or 1/4 the typical main sequence lifetimes of OB stars. However, if the stars are simply escaping from the clouds without destroying them, then these data place

no limits on molecular cloud lifetimes. We find that the entire field population of OB stars cannot have originated in and percolated out of existing H II regions. Comparing the observed $H\alpha$ emission with that predicted from stellar ionizing flux models and hydrogen recombination theory, we find that although the bright, halo and diffuse regions are probably in ionization balance, the field region is producing at least 6 times as much ionizing flux as is observed. The ionization balance results in NGC 6822 suggest that star formation rates obtained from $H\alpha$ luminosities must underestimate the true star formation rate in this galaxy by about 50%. Comparing our results for NGC 6822 with previous results for the Local Group spiral galaxy M33, we find that the inner kiloparsec of M33 is in a more serious state of ionization imbalance, perhaps due to its higher surface density of blue stars. Thus the morphological class of a galaxy may be an important factor in how accurately we can determine star formation rates from $H\alpha$ luminosities.

3.2 INTRODUCTION

Evidence that massive OB stars are not always associated with optically luminous H II regions has been steadily increasing. Previous indications of this phenomenon included a study of the OB associations of M33 that showed many of the associations do not contain bright H II regions (Wilson 1990). As well, a study of the edge-on spiral galaxy, NGC 891, revealed the existence of filamentary $H\alpha$ structures high above the galactic disk which are not associated with any obvious ionizing sources (Rand *et al.* 1990). In addition, the neighbouring Large and Small Magellanic Clouds were found to house an entire population of OB stars that were located in the "field" far from any OB associations (Massey *et al.* 1994). These findings raise a number of interesting question, such as how are the OB star and H II region distributions

related? What fraction of the OB star lifetime is spent within an optically bright H II region? How prevalent are the "field" stars? What is the state of ionization balance in individual and collective regions of the galaxies? The answers to these questions have important implications to issues in star formation and the interstellar medium, including the determination of extragalactic star formation rates (SFRs) and molecular cloud lifetimes. To answer these questions, we have investigated the OB and H II region population and the state of ionization balance within Local Group galaxies. We began with a study of the spiral galaxy, M33 (Patel & Wilson 1995, hereafter Chapter 2). The present work is focused on the dIrr member of the Local Group, NGC 6822.

We begin by outlining some of the key issues (further details can be found in Chapter 2). The length of time an O star spends in the H II region phase, and thus partially embedded in its parent cloud, will have some bearing on the lifetime of the parent molecular cloud. Short lifetimes ($\sim 10^7$ yrs Blitz & Shu 1980) assume the embedding time is a large fraction of the total lifetime of the star so that the first O stars that form will disrupt their parent cloud. Molecular clouds undergoing periods of intense star formation followed by more quiescent star formation would result in long molecular cloud lifetimes ($\gtrsim 10^7$ yrs) so that each cloud could produce several OB associations of different ages (Elmegreen 1991). If O stars destroy their natal environments, then the fraction of O stars seen in the field or outside of bright H II regions (which is proportional to the length of time a typical O star spends outside a bright H II region) determines the time required to destroy the cloud. However, if these field O stars have simply moved out of their parent clouds, then cloud lifetimes could be considerably longer.

The second issue in this study concerns one of the most common methods of

determining SFRs in extragalactic systems, namely using the $H\alpha$ luminosity. This method relies heavily on the assumption that the region in question is *ionization bounded* (Kennicutt 1983) *i.e.,* all Lyman continuum photons produced by massive young stars are absorbed by the gas in the region. (The alternative scenario is for a region (or galaxy) to be *density bounded, i.e.,* the Lyman photons are more than sufficient to ionize all the (dense) gas.) Since the observed $H\alpha$ luminosity is directly proportional to the Lyman continuum luminosity, by assuming an initial mass function (IMF) and theoretical models for the Lyman continuum luminosity as a function of stellar mass the "observed" Lyman continuum luminosity can be converted into a SFR for massive stars. The total SFR of a region is obtained by extending the IMF over the full range of stellar masses. In all of this, the assumption that the region is ionization bounded is crucial: since the SFR is directly proportional to the Lyman continuum luminosity and therefore the observed $H\alpha$ luminosity, a region out of which continuum photons are escaping will have a smaller estimated SFR than one that is ionization bounded. The assumption of ionization balance is not certain to be valid if a large fraction of the OB population lies outside bright H II regions. In view of the wide spread use of this technique in extragalactic systems, it is vital to verify this important assumption of the theory.

Until very recently, ionization balance calculations in extragalactic systems had concentrated on individual OB associations in the Large and Small Magellanic Clouds (respectively, LMC and SMC). NGC 2122 and LH 118 in the LMC were found to be density rather than ionization bounded (Massey *et al.* 1989a) while NGC 346 in the SMC is, most likely, ionization bounded (Massey *et al.* 1989b). The results of the M33 study (Chapter 2) showed that the entire (inner 1 kpc) surveyed area, as well as individual ionized gas regions of the galaxy are not in ionization balance and in fact,

in total, the surveyed region was producing between 3 and 7 times the observed flux.

At a distance of 0.5 Mpc (McAlary *et al.* 1983), NGC 6822 is very well suited for our investigation. While its low galactic latitude makes this a somewhat difficult system to study, there is a substantial body of research in the Local Group literature that is associated with the galaxy. Photometric surveys of the stellar populations and OB associations include the photographic surveys of Hodge (1977), and most recently, CCD imaging in the B and V filters by Wilson (1992a). Luminous blue stars in NGC 6822 have been studied by Humphreys (1980), while the Wolf-Rayet star population has been surveyed by Armandroff & Massey (1991, 1985). Over 140 H II regions of the galaxy have been catalogued and studied by Hodge *et al.* (1989,1988). The recent evolutionary history, including determinations of the SFR within NGC 6822 have been discussed by Hodge *et al.* (1991) and Hodge (1980). Finally, the molecular gas content of the galaxy has recently received some attention with the CO surveys by Wilson (1992b), Ohta *et al.* (1993) and Wilson (1994).

In this paper, we use $H\alpha$ and BV photometric data of NGC 6822 to study the distribution of the H II regions and luminous blue stars (hereafter OB stars) in order to determine the fraction of an OB star's lifetime that is spent outside a bright H II region and hence, to address the issues of molecular cloud lifetimes after the formation of OB stars. With the aid of stellar ionization models, we use the data to determine whether the individual regions are separately and/or collectively in a state of ionization balance. Additionally, optical spectra of a number of stars in NGC 6822 have been used to test the performance of the principal ionization model used in the investigation. The implications of the state of ionization balance for the SFRs estimated from $H\alpha$ luminosities are also discussed. Finally we compare our results for NGC 6822 with the results obtained previously for M33. The analysis of

the data ($H\alpha$ and BV photometry), discussion of the theoretical ionization models used and the limitation of these models appear in section §2. The OB star and H II region distributions are discussed in §3 and the findings of the ionization balance calculations appear in §4. M33 and NGC 6822 are compared in §5 and the results of our investigation are summarized in §6.

3.3 SELECTION AND ANALYSIS OF DATA

3.3.1 PHOTOMETRIC DATA

We use BV photometric data from Wilson (1992a) which had previously been used to study the OB associations in the galaxy. The observations were made at the Palomar 60-inch telescope using the blue sensitive Tektronix chip, CCD 6 (chip scale 0.235″pixel^{-1}). The "T" shaped area surveyed included the main body of the galaxy as well as the northern bar region which contains many OB associations previously identified by Hodge (1977). The average seeing in B and V was, respectively, 1.4 arcsec and 1.3 arcsec. Additional details of the observations can be found in Wilson (1992a). The average photometric uncertainties are 0.03 mag for B,V<20 and 0.06 mag for 20<B,V<21. Incompleteness in the data was estimated to be 30% for 20<V<20.5 and 55% for 20.5<V<21.

This data set is ideally suited for our use as it provides the most complete (to 21 mag in V over all the surveyed regions) census of the blue star population of NGC 6822. Wilson (1992a) has estimated the colour excess of the main sequence stars in the galaxy to be $E(B-V)$=0.45±0.05 with 0.3 mag of reddening coming from foreground sources and 0.15 mag from sources internal to the galaxy. For the purposes of our investigation, we have selected only those stars with V≤21 and $(B-V)$≤0.5

mag. The colour criterion, which is based on the estimated average reddening for the galaxy, the intrinsic colour of O stars on the zero age main sequence ($(B-V)$=-0.3 mag, Flower 1977) and the observed width of the main sequence, assures us that the maximum number of potential OB stars will be selected for further investigation.

3.3.2 $H\alpha$ EMISSION

We used red-continuum and $H\alpha$ CCD images of the entire galaxy as well as its immediate surroundings kindly provided by P. Massey and G. Jacoby. The images were obtained using the KPNO 4-m telescope and 2048×2048 T2KB chip (scale 0.48″ pixel^{-1}) on the night of January 7, 1992. Exposure times were 60 sec for the red-continuum and 500 sec for the $H\alpha$ frame. These frames have been trimmed and overscan subtracted, flat fielded and bias subtracted in the usual manner using the image processing package CCDPROC within IRAF. The $H\alpha$ image was scaled to the same flux level as the red-continuum image using a number of bright, unsaturated stars. As the seeing in the $H\alpha$ image was slightly worse than that in the continuum image, the latter was gaussian convolved so that stars on both images had the same full width at half maximum. The final continuum-subtracted image for NGC 6822, hereafter referred to as the $H\alpha$ image, was then obtained by subtracting the convolved red-continuum image from the $H\alpha$ image.

The $H\alpha$ image was calibrated by comparing published $H\alpha$ fluxes from Hodge *et al.* (1989) with the observed number of counts above the mean background for 15 bright (surface brightness I$\geq 10^{-13}$ erg cm^{-2} sec^{-1}) isolated regions in the galaxy. The slope of this relation, which is illustrated in Figure 3.1, determines the uncorrected calibration constant, γ. As the Hodge *et al.* (1989) $H\alpha$ fluxes were measured above the atmosphere, for our purposes γ had to be corrected for foreground and internal

extinction. Taking $A_{H\alpha}$=2.59×E(B-V)=1.17 ±0.13 (Schild 1977), we determined the extinction corrected calibration constant, Γ, to be 6.5±0.8×10^{-18} erg cm^{-2} sec^{-1} $count^{-1}$. The uncertainty in Γ was estimated at ∼12%. This figure included the error in γ (estimated at ∼2% based on the rms error in the slope of the $H\alpha$ luminosity versus count graph) as well as that in $A_{H\alpha}$. In addition to the reddening, the data had to be corrected for contamination from the [NII] line at 6583Å which was also observed through the $H\alpha$ filter used. This was done by using the data of Pagel *et al.* (1980) that give an average [NII]/$H\alpha$ ratio of 5.5% ±1% over seven H II regions in NGC 6822. Thus scaling down all counts on the $H\alpha$ image by a factor of 0.945 corrects for the [NII] contamination in the data.

Motived by the investigation in M33 as well as visual inspection of the $H\alpha$ image, we separated the galaxy into four types of emission regions: bright, halo, diffuse and field. The four regions were defined by their Hα surface brightness, I, such that $I \geq 1.6\times10^{-15}$ erg $s^{-1}cm^{-2}$ $arcsec^{-2}$ for the bright regions, $4.4\times10^{-16} \leq I < 1.6\times10^{-15}$ erg s^{-1} cm^{-2} $arcsec^{-2}$ for the halo regions, $1.3\times10^{-16} < I \leq 4.3\times10^{-16}$ erg s^{-1} cm^{-2} $arcsec^{-2}$ for the diffuse regions and $I < 1.3\times10^{-16}$ erg s^{-1} cm^{-2} $arcsec^{-2}$ for the field regions (see Figure 3.2). For comparative purposes, the dividing lines in surface brightness between the bright, halo and diffuse regions are consistent with those adopted in M33 (without the [NII] correction applied to the data) but that between the diffuse and field emission regions was motived by visual inspection of the $H\alpha$ image of NGC 6822. We note that the diffuse and field regions were not separated in M33 as it was not clear whether they were two distinct components of the emission in the M33 study or, rather, a single component that was smoothly declining in surface brightness. The surface brightnesses quoted above have been corrected for extinction in $H\alpha$ and are measured above an observed average sky surface brightness over the

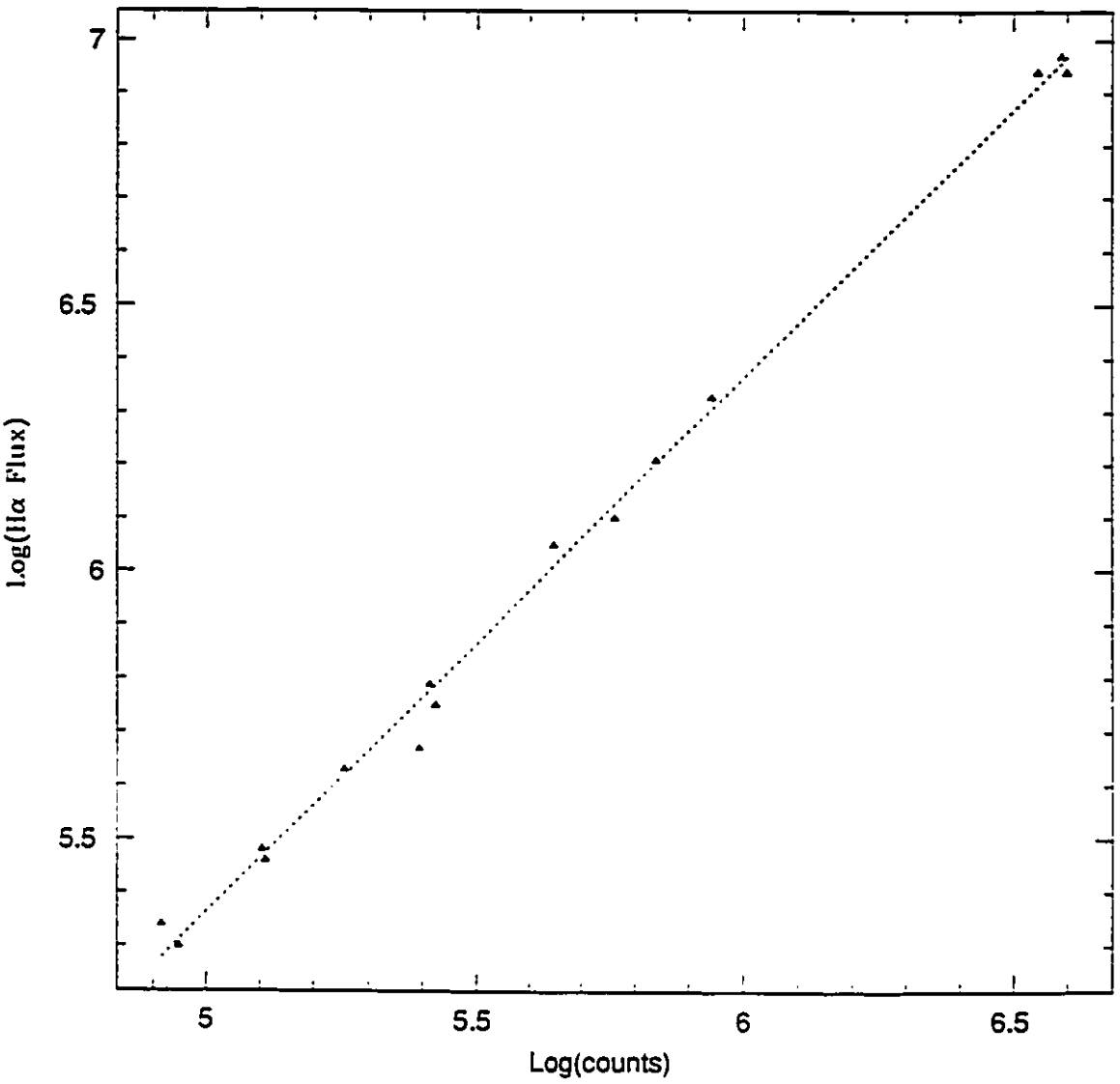

Figure 3.1: A graph of the observed number of counts above the mean background level versus published $H\alpha$ fluxes (in units of 10^{-18} erg cm^{-2} s^{-1}) from Hodge *et al.* (1989) for 15 bright (surface brightness I$\geq 10^{-13}$ erg cm^{-2} sec^{-1}) isolated regions in the galaxy. The best fit slope through the data determines the calibration constant γ=2.22$\times 10^{-18}$ erg cm^{-2} s^{-1} count^{-1}.

galaxy of I_{bg}=5.32±0.53×10^{-16} erg s^{-1} cm^{-2} $arcsec^{-2}$. The sky emission level was obtained by averaging the modal photon counts of a number of isolated regions past the optical limits of the galaxy. As this emission was observed to be fairly uniform over the entire image, it is assumed to be "sky" and not a smooth emission component within NGC 6822. As such, it was not included in calculating the $H\alpha$ luminosity of a region. One final point to note is that although the $H\alpha$ emission in the entire galaxy is available for study, we have restricted our attention to only those regions for which BV photometric data are available *i.e.*, the main body and northern bar regions of NGC 6822.

3.3.3 PREDICTED $H\alpha$ LUMINOSITY FROM OB STARS

To enable a comparison of the observed $H\alpha$ fluxes with those expected from the associated stellar population, we have used the stellar ionization models of Auer & Mihalas (1972) (hereafter A&M), Kurucz (1979) and Panagia (1973) as well as the blackbody approximation. Given the effective temperature (T_{eff}) and effective gravity (g) of a star, the models predict the expected Lyman continuum flux from the star. The predicted ionizing flux is, in turn, used to obtain an $H\alpha$ luminosity by an assumed recombination scenario. The models differ in their treatment of the stellar atmospheres. In particular, the A&M results are based on nonblanketed NLTE model atmospheres composed of hydrogen and helium only, while the Kurucz models, which include the effects of line blanketing, have LTE atmospheres of solar composition. Finally the Panagia models are based on a combination of the NLTE A&M models and the LTE models due to Bradley and Morton (1969), Morton (1969) and Van Citters & Morton (1970), and appropriate values of g are used to calculate the flux of Lyman continuum photons as a function of T_{eff} for stars of luminosity class I, III,

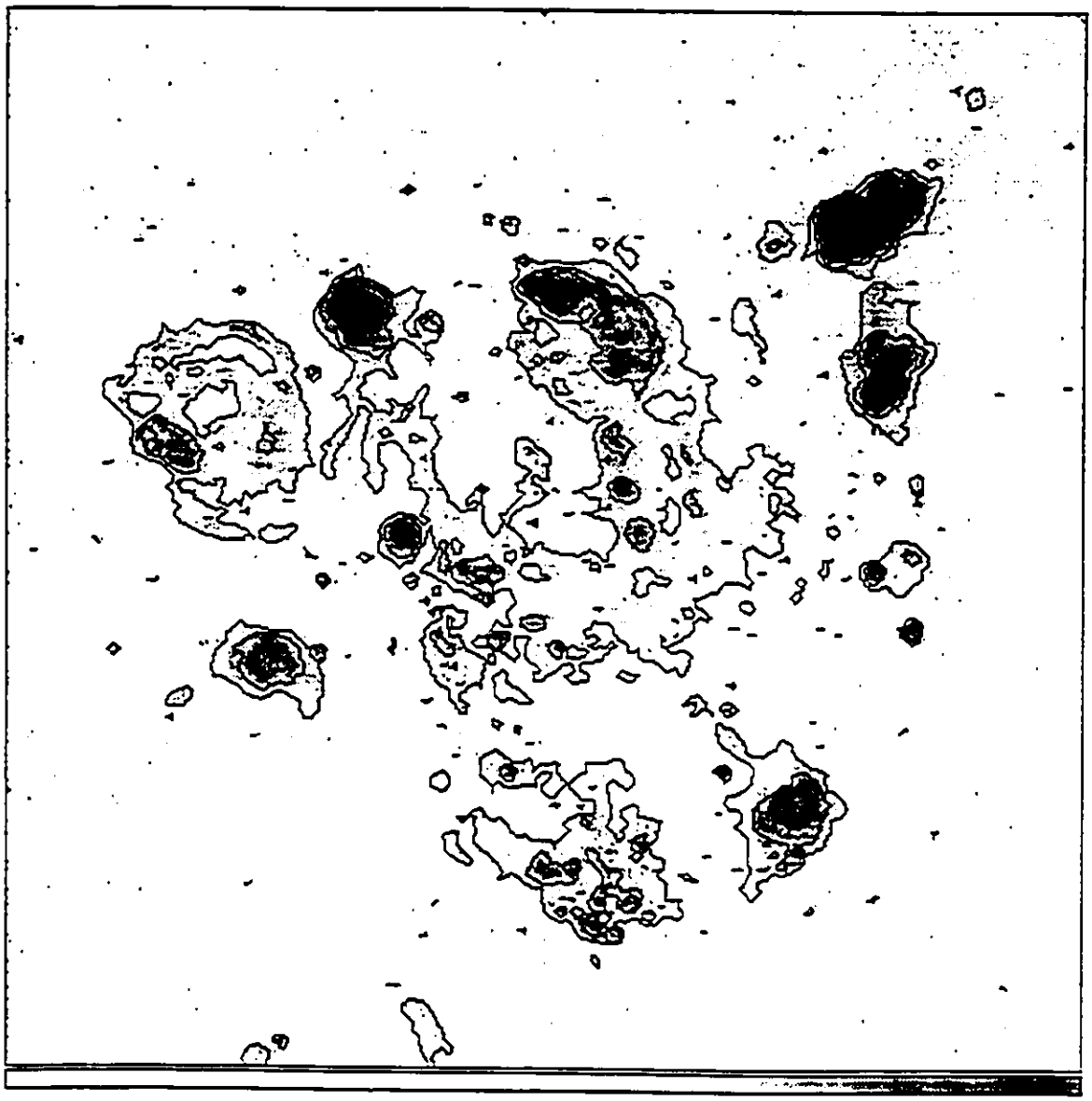

Figure 3.2: The $\sim$7.5′×7.5′continuum subtracted $H\alpha$ image of NGC 6822 illustrating the distribution of the bright, halo, diffuse and field $H\alpha$ emission regions. North is at the top and east is to the left. For reference, the giant HII regions Hubble I and III are to the top right. The contours, corresponding to surface brightnesses of I=1.7×10^{-15}, 4.6×10^{-16} and 1.4×10^{-16} erg s^{-1}cm^{-2}arcsec^{-2}, separate the bright, halo, diffuse and field regions.

V as well as the zero age main sequence (ZAMS).

We have used the calibration equations given in Parker & Garmany (1993) to calculate the effective temperatures and bolometric corrections (BC) for all stars with $M_V \leq 21$ and $(B-V) \leq 0.5$. As only B and V photometry is available, we have used only those equations which are independent of the reddening free index $Q \equiv (U-B) - 0.72(B-V)$. The effective temperature was calculated using one of equations 4b to 4e in Parker & Garmany (1993) while the BC of the star was determined from T_{eff} using one of equations 5a to 5d (ibid). Effective temperatures thus calculated were used as inputs to the ionization models while the BCs were used to estimate, where necessary, the radius of the star emitting the ionizing flux.

Details of the application of the various ionization models used here are given in Chapter 2. Briefly, for the blackbody as well as the A&M and Kurucz models for various effective gravities, we have used Table XIV from Massey *et al.* (1989b) which neatly summarizes the expected Lyman flux at the surface of the star for T_{eff} between 20,000° K and 50,000 K. We have adopted $\log(g)=3.5$ for stars with $T_{eff} \leq 35{,}500$ K, and $\log(g)=5.0$ for stars with $T_{eff} > 35{,}500$ K for the Kurucz models and $\log(g)=4.0$ for the A&M models. In order to apply the Panagia models, we were required to determine the luminosity class of the star as the models give the total ionizing flux (as a function of T_{eff}) separately for ZAMS, supergiant, class III and main sequence stars. We estimated the luminosity class of the object by comparing the model V mag, M_V^p (for a given T_{eff}), with that observed. The M_V^p that was closest to the observed M_{V_o} determined the luminosity class. All stars with $M_{V_o} \leq -6.0$ were taken to be supergiants (class I).

To convert Lyman continuum photons to $H\alpha$ photons, we used the relations

N(LyC)/N($H\alpha$) =2.22 (Osterbrock 1989) for Case B recombination, which is appropriate for optically thick gas at 10,000 K and densities of 10^2-10^4 cm^{-3}, as well as N(LyC)/N($H\alpha$)=5.36 (Brockelhurst 1971) for Case A recombination which is appropriate for gas at 10,000 K that is optically thin in all Lyman transitions. Clearly, Lyman continuum photons in optically thin gas produce fewer $H\alpha$ photons than those in optically thick gas. While Case B recombination is the most commonly used approximation in the study of H II regions, Case A recombination was included for stars found in the diffuse and field emission regions where the optical depth of the surrounding gas may be smaller.

3.3.4 GAUGING THE RELIABILITY OF THE IONIZATION FLUX

In order to gauge the reliability of the ionization fluxes determined from photometry plus the Panagia models, we compared the photometric spectral classes (which determine the predicted ionizing flux due to each star) for a number of stars in NGC 6822 with spectral classes obtained from optical spectroscopy. The optical spectra for 37 stars were obtained during the nights of July 19-21, 1993 using the multi-object spectrometer ARGUS on the CTIO 4-m telescope. Details of the observation, reductions and spectral classifications are described in detail in Chapter 4 and will be published in Massey *et al.* (1995, in preparation). The stars selected for spectroscopic study were some of the brightest, blue stars from the photometric list of Wilson (1992a). Seven of the stars are found to be Galactic foreground stars (based on their spectral classification as A or G type) and 2 were identified as Wolf-Rayet star thus leaving only 28 OB type stars in NGC 6822 for which we have obtained spectral classes. Due to the small number statistics, we have not used these stars to perform a direct test of the ionization balance in the galaxy.

Although a number of the ARGUS spectra were strong enough to identify the subclass as well as the luminosity class of the object, in some cases only an approximate identification of spectral type or subclass was possible. Spectral classes determined from photometry plus Panagia models were based on the calculated T_{eff} and observed M_V of the star (as in §2.3). As the theoretical ionizing flux models are not defined for stars of spectral classes later than B3 (or photometrically determined $T_{eff}<T_{eff,L}$), all such stars were left unclassified. The 7 Galactic foreground stars and Wolf-Rayet stars were included in the sample in order to test the model predictions for respectively, late type (or low T_{eff}) and evolved stars.

Before proceeding further we note that the results of this type of comparison must be treated with caution due to the limited resolution and signal-to-noise (S/N) of the observed spectra as well as the uncertainties in the colour-magnitude-ionizing flux and absolute magnitude-spectral class relations from Panagia (1973) which were used to determine the photometric classifications. The uncertainties in the spectroscopic classifications can be up to 6 classes and/or up to 2 or more luminosity classes for spectra where classification was even possible. The reason for this large an error is mainly due to the extreme distance of NGC 6822. Even with the long integration times, typically 3.5 to 4 hours per star, the S/N ratio per resolution element was 50-80. Characteristically, an S/N ratio greater than 100 is required for good identifications. To gauge the uncertainty in the photometric spectral classification, we included the photometric errors associated with each star to the model inputs (V and (B-V)) to find the average change in spectral class was $\sim$4 classes.

In light of the above, inspection of Table 3.1 reveals that the match between spectral classes determined from the ARGUS spectra with those from photometry+models is reasonably good: ignoring the luminosity class, of the 37 stars, 19 or just over 50%

of the identifications agreed or were within a few subclasses of each other. Of the 18 stars with poor matches, 16 had photometric classifications that were significantly earlier than those observed spectroscopically while the remaining 2 were classified later than those observed. The results for stars spectroscopically identified to be later than B3 or Wolf-Rayet were similar: 9 out of 17 spectral classifications were in agreement.

In conclusion, it would appear that photometric classifications are slightly biased towards earlier spectral types. This trend can be explained by the presence of unresolved binary stars in the galaxy. In light of the fact that T_{eff}, and hence the photometric classification of high mass stars, is much more sensitive to their V mag than their (B-V) colours (as the colours of massive stars on the main sequence are degenerate), an unresolved binary would be detected as a more luminous, and therefore earlier type star then the individual stars making up the binary. Furthermore, studies indicate that roughly $\sim$50% of all stars are found in binary systems (Abt 1978; Duquennoy & Mayor 1991) which matches surprisingly well with the fraction of photometric identifications that did not agree with the spectroscopic ones. While we cannot gauge the exact quantitative effect of the photometric bias on the theoretical ionizing fluxes, we can safely say that its overall effect is to predict more flux then if spectroscopic data were used. In light of the results of this section and for the purposes of our investigation, we shall consider any agreement between observed and predicted fluxes that is within a factor of 2 to be acceptable.

STAR	V	(B-V)	SPECTRAL CLASS		MATCH?
			Spectra	Photometry	
OB13-9	18.08	-0.76	Early-Mid O	———	YES
CW030	17.49	-0.03	Early O	———	YES
CW029	18.58	0.11	Early O	O7.5 I	NO
OB6-16	18.11	-0.82	O9II	———	NO
OB3-7	18.53	-1.42	O9III / O9.5II	———	NO
CW102	18.27	0.18	O9 / Early B	B0.5 I	YES
OB9-12A	18.17	-0.46	Late O / Early B	———	NO
OB15-15	18.53	-0.94	Composite : O + other	———	NO
CW138	18.40	0.18	B0.2 V	B0.5 I	YES
OB8F-2	6.92	-0.68	B2.5 V / B1.5 III	———	NO
OB11-8	18.41	-0.64	Early B	———	NO
OB15-9	18.08	-0.78	Early B	———	NO
CW114	18.20	0.12	Early B	O8.5 I	YES
CW107	18.22	0.12	Early B	O8.5 I	YES
CW117	18.95	0.14	Early B	O9 III	YES
OB7F-40	18.89	-0.51	Early B I	———	NO
OB7-15	17.50	-0.73	B1 V	———	NO
CW057	18.48	0.12	Early B / B5	O8.5 I	YES
CW120	17.97	0.16	B1 V	B0.5 I	YES
CW008	17.73	0.09	B0 III	O6 I	NO

Table 3.1: Comparison of Spectral Classes Obtained from ARGUS Data with those Determined from Photometry.

STAR	V	(B-V)	SPECTRAL CLASS		MATCH?
			Spectra	Photometry	
CW126	18.40	0.12	B2 IV / B3 I-II	O8.5 I	YES
CW100	18.06	0.21	B5 I	B2 I	YES
CW077	16.61	0.26	B5 I	———	YES
CW061	18.28	0.22	B8 I	B2 I	NO
CW052	18.39	0.04	B8	O4 I	NO
CW089	18.48	0.10	Late B	O6.5 I	NO
CW069	18.83	0.08	Late B / Early A	O4 I	NO
CW122	17.73	0.29	Late B / Early A I	———	YES
CW017	17.92	0.41	Early A I	———	YES
CW067	16.57	0.17	A V	B0.5 I	NO
CW068	18.54	0.26	A I (classic)	———	YES
CW116	18.85	0.20	A	B0.5 I	NO
CW111	17.33	0.34	A I	———	YES
CW112	18.81	0.22	A	B1 I	NO
CW047	19.09	0.43	G	———	YES
CW080	18.92	-0.01	WR (N6822-W12)	———	YES
OB2-3	19.37	-0.80	WR (N6822-W3)	———	YES

Table 3.1: Comparison of Spectral Classes Obtained from ARGUS Data with those Determined from Photometry. Table continued from previous page.

3.4 IONIZED GAS AND OB STAR DISTRIBUTION

To study the common assumption that O and B stars are predominantly found in bright H II regions, we looked at the distribution of these stars as a function of their surrounding ionized gas environment. We identified the ionized gas environment of a star as either bright, halo, diffuse, or field according to the average $H\alpha$ surface brightness inside a circle of radius of 3 pixels (~3.5 pc) centered on the star. The distribution of the OB stars (as a function of their visual magnitude) within the four ionized gas environments is summarized in Table 3.2.

It is immediately clear that OB stars are not all located in the bright H II regions: in fact, ~50% of all the stars with V<21 and (B-V)<0.5 are found in the field (see Figure 3.3). Moreover, field stars outnumber those in the bright regions by a factor of three. This trend is also suggested by the brightest stars in the survey where slightly less than half of all stars with V$\leq$18 are seen to be in the field while only a quarter are in the bright regions. At ~11%, the halo houses the smallest percentage of OB stars in the galaxy while the diffuse emission region carries a substantial 24% of the total. We see faint stars dominate all four regions and that percentage of these stars within the different regions is comparable.

We can now determine the important quantity, the fraction of the main sequence lifetime of an O star that is spent within a recognizable H II region, defined as $f_{HII} \equiv (N_B + N_H)/N_{TOT}$ where N_{TOT} is the total number of stars in the sample and N_B and N_H are the numbers of stars in, respectively, the bright and halo regions of the galaxy. By defining a recognizable H II region to be composed of either a bright or halo emission region, we are assured of obtaining the most conservative estimate of this key quantity. From Table 3.2, we find f_{HII}=0.29, implying that roughly 70% of

Figure 3.3: The distribution of all OB stars (V≤21 and (B-V)≤0.5) in the inner kpc of NGC 6822. Photometric coverage of the galaxy was restricted to inside the "T" shaped region outlined. The location of field OB stars are marked by plus signs while the OB stars in the bright, halo and diffuse regions are marked by a small square.

V MAG *	BRIGHT		HALO		DIFFUSE		FIELD		ENTIRE IMAGE	
	# stars	% region	# stars	% region	# stars	% region	# stars	% region	# stars	% region
V ≤18	5 ±2	4 ±2 %	1 ±1	2 ±2 %	4 ±2	2±1 %	9 ±3	3±1 %	19 ±4	3±1 %
18<V≤19	16 ±4	13±4%	8 ±3	10±5%	6 ±2	3±1 %	25 ±5	7±2 %	55 ±7	8±1 %
19<V≤20	35 ±6	30±8 %	27 ±5	35±11%	44 ±7	25±6 %	88 ±9	25±4 %	194 ±14	27±3 %
20<V≤21	62 ±8	52±11%	41 ±6	53±14%	121 ±11	69±11 %	232 ±15	67±8 %	456 ±21	63±5 %
V≤21(Total)	118 ±11		77 ±8		175 ±13		354 ±19		724 ±27	

Table 3.2: The Distribution of Blue Stars in Four Ionized Gas Environments in N6822.

*Note : Only stars with (B-V)≤0.5 selected.

the main sequence lifetime of an OB star is spent *outside* of a recognizable H II region. The consequence of this result to the lifetimes of molecular clouds is that if OB stars escape from bright and halo H II regions by destroying their parent molecular clouds, the molecular cloud lifetimes after forming OB stars could be as short as $\sim$1-3$\times10^6$ yrs (or 1/3 the typical main sequence lifetimes of 3-8$\times10^6$yrs for 120-20 $M_\odot$ stars assuming Z=.020, Schaller *et al.* 1992).

We summarize in Table 3.3 a few important properties of the ionized gas environments and the associated OB star distribution. A striking point to note is that while the surface density of stars in the bright region is a factor of $\sim$6 times greater than that in the field, the field occupies an area that is $\sim$17 times that of the bright region. These two results provoke the puzzling question of whether the field stars could have originated in and percolated out of existing bright ionized gas environments. Citing a study of the Trapezium cluster in Orion by Zuckerman (1973), Churchwell (1991) suggests a typical O star velocity relative to its parent molecular cloud is 3 km s^{-1}. At this speed, an O star could travel $\sim$30 pc over its lifetime of $\sim$10 Myr. This scales falls far short of the characteristic distances ($\sim$200-500 pc) of the large field regions and, therefore, field stars cannot all have simply percolated out of the H II regions currently visible.

Also from Table 3.3 we find that the relative total $H\alpha$ luminosity per field star is $\sim$4% that of a star in a bright H II region, which raises the question of whether the field is "leaking" Lyman continuum photons that presumably escape from the galaxy. An alternative possibility is that the field population is older than that in bright H II regions so that fewer early type stars with large ionizing fluxes still remain. One way to investigate this possibility is to look at the bright star distribution, which is most sensitive to age differences, in the different ionized gas environments. The distribution

	BRIGHT	HALO	DIFFUSE	FIELD	ENTIRE IMAGE
Total # of Stars [a]	118	77	175	354	724
Area Covered (kpc^2)	0.06	0.13	0.56	1.04	1.79
Surface Density of Stars (kpc^{-2})	1967	592	312	340	404
Average Surface Brightness [I] [b]	71.56	8.03	0.99	0.20	1.44
Total Luminosity [L_{ob}] [c]	2.19	0.53	0.83	0.29	3.85
Relative Luminosity per Star [d]	1	0.37	0.26	0.04	0.28

Table 3.3: Average Properties of the Four Ionized Gas Environments.

[a] All stars with (B-V)$\leq$0.5 and V$\leq$21.

[b] In units of 10^{-16} erg $s^{-1}cm^{-2}$ $arcsec^{-2}$. This is measured above the average background.

[c] In units of $L_{39} \equiv 10^{39}$ erg s^{-1}.

[d] In units of 1.86×10^{37} erg s^{-1} $star^{-1}$.

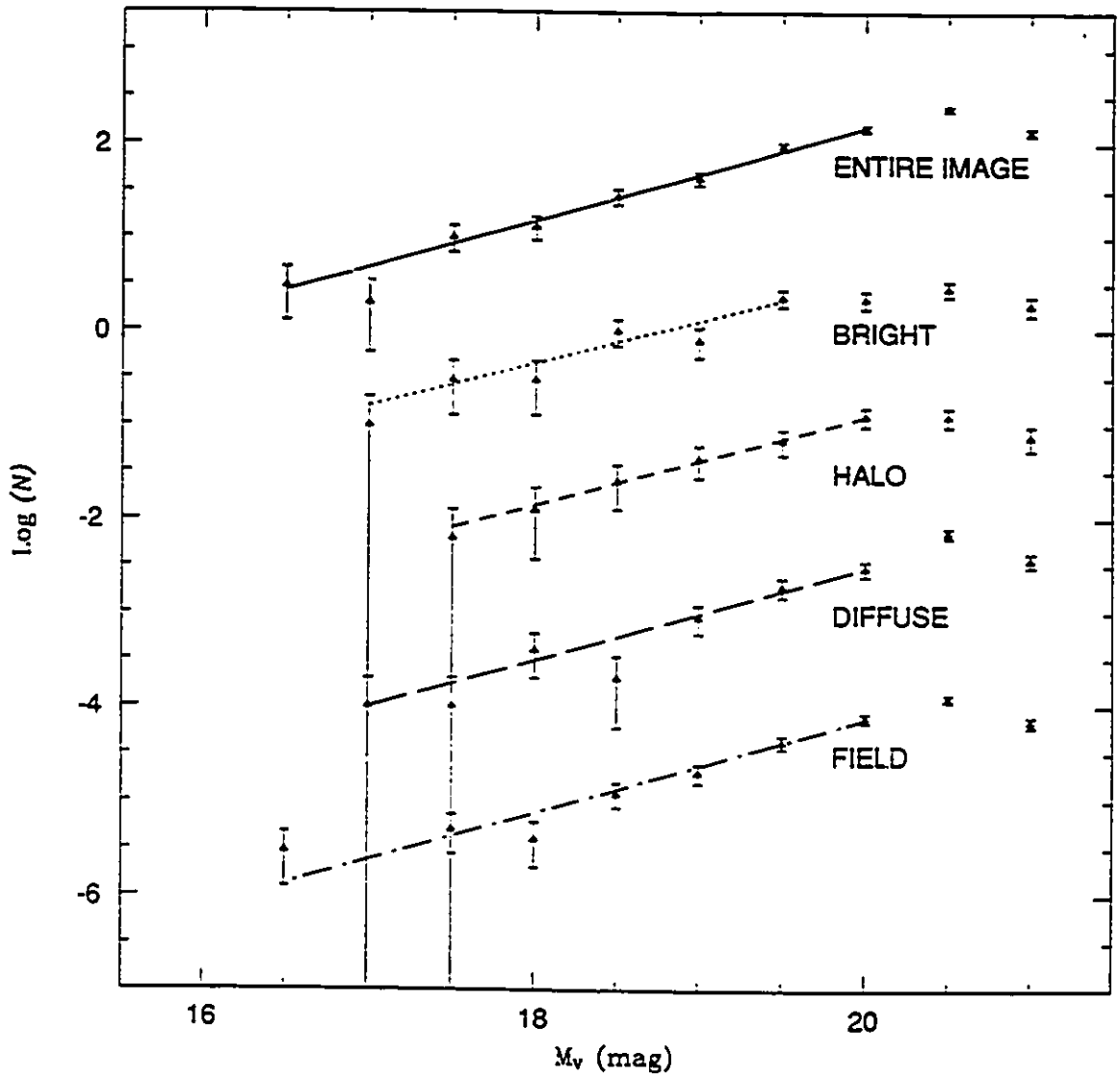

Figure 3.4: The luminosity functions for all blue ((B-V)≤0.5) stars in the survey as well those in the bright, halo, diffuse and field ionized gas environments. An arbitrary offset in the ordinate has been applied for the purposes of clarity. Overlaid on the data are the weighted least squares fits (to a limiting magnitude of V=19 for the bright region and V=19.5 elsewhere).

of stars brighter than V=18, normalized to the total number brighter than V=19, in the bright, halo, diffuse and field regions are, respectively, 7% ±4%, 1% ±1%, 5% ±3% and 12% ±5%. Clearly, there is no firm indication that any one of the ionized gas environments has an over-abundance of bright stars and therefore there is no evidence for age segregation between the different regions. The slope of the stellar luminosity function can be another indicator of an age difference: shallow slopes imply younger stars dominate the region while steep slopes indicate older populations dominate. Plots of the luminosity functions, in terms of M_V versus Log(N_*) where N_* is the total number of stars in the magnitude bin (width 0.5 mag), are given in Figure 3.4. Weighted least-squares fits to the data to a limiting V magnitude of 19 for the bright region (to reduce the effects of incompleteness) and V=19.5 for all others yield slopes of 0.36 ±0.05 (bright), 0.37 ±0.19 (halo), 0.53 ±0.16 (diffuse), 0.47 ±0.07 (faint) and 0.53 ±0.05 (entire image). Clearly there is no evidence for significant differences in the luminosity function slopes and therefore, no indication that the stellar populations of the four H II environments have different average ages. As such, it appears that the differences in the $H\alpha$ luminosity per O star in the field compared to that in the bright regions indicates a difference in the gas environment of the O stars and may indicate that ionizing radiation from field stars is escaping out of the galaxy.

3.5 IONIZATION BALANCE

In this section, we test one of the fundamental assumptions of star formation rate calculations from $H\alpha$ luminosities, namely that the region under consideration is ionization bounded *i.e.*, the Lyman continuum flux emitted by the stars remains in the region. This is accomplished by comparing the observed $H\alpha$ emission from stars with that predicted from stellar ionization models. Although the detailed analysis is

based on the models of Panagia (1973), we have also used the blackbody, Kurucz, and A&M models for comparative purposes as well as to serve as a check on the Panagia results.

In all applications of the ionizing flux models, we have followed a method similar to that described in Chapter 2. In brief, for comparative purposes, we have imposed an upper and lower limit to T_{eff}, $T_{eff,U}$=60,000 K and $T_{eff,L}$=30,000 K. The lower limit $T_{eff,L}$ is chosen as the minimum effective temperature for which all ionization models are defined. Although all four models are defined up to T_{eff}=50,000 K (for an O4 class V star), we have chosen $T_{eff,U} = 60,000$ K so as to provide a small margin of error at the high T_{eff} end as well as to roughly account for the Lyman continuum flux for stars earlier than O4. Stars that had calculated effective temperatures between 50,000 K and 60,000 K were all assigned Lyman fluxes corresponding to 50,000 K from the models. Stars with $T_{eff} < T_{eff,L}$ and $T_{eff} > T_{eff,U}$ are assigned zero flux. Note that we have not attempted to account for the ionizing flux from stars with effective temperatures outside these limits: stars with $T_{eff} < T_{eff,L}$ are most likely to be evolved late type stars with very small contributions to the total Lyman continuum luminosity while those with $T_{eff} > T_{eff,U}$ would not only entail extrapolating the T_{eff}-Lyman continuum flux relations to highly uncertain limits, but more importantly, such high effective temperatures may be a result of photometric errors rather than reflecting the true T_{eff} of the star (for example, Massey *et al.* (1989a, 1989b) have found many stars with unrealistic (B-V) or (U-B) colours which they attributed to photometric errors). Finally, we did not consider the presence of Wolf-Rayet stars in the galaxy as the ionizing flux from these stars, while likely to be very high, is rather uncertain (Massey *et al.* 1989b). The effect of accounting for Wolf-Rayet stars in NGC 6822 would be to increase the predicted ionizing flux.

Assuming Case B recombination, the $H\alpha$ flux from all stars with $T_{eff,L}<T_{eff}<T_{eff,U}$ predicted by the four different ionization models (in units of 10^{39}erg s^{-1}) is: 10.7 (Panagia), 7.2 (blackbody), 5.7 (Kurucz) and 6.8 (A&M). The highest (Panagia) and lowest (Kurucz) estimates differ by a factor of roughly 2. Considering the differences in the models and the arguments of §2.4, the agreement between them is acceptable. In the remainder of the section we will restrict our discussion to the results obtained using the Panagia models only, keeping in mind that the corresponding results from the other models scale as above.

As the minimum effective temperature for which the Panagia models are defined depends on the luminosity class of the star, *i.e.*, T_{eff}=15100 K (for class I), T_{eff}=16,900 K (for class V and ZAMS) and T_{eff}=16,000 K (for class III), we have defined for each luminosity class the corresponding $T_{eff,L}$ inferred from the models. Of the 724 stars for which we had photometry, 428 had effective temperatures between $T_{eff,L}$ and $T_{eff,U}$. The percentage of stars with $T_{eff}<T_{eff,L}$ or $T_{eff}>T_{eff,U}$ (and therefore for which no ionizing flux could be assigned) was 58% (V<18), 28% (18<V<19), 27% (19<V<20) and 48% (20<V<21). As such, it would appear that a significant fraction of the stars are not contributing to the total $H\alpha$ luminosity observed.

Photometric incompleteness for all stars with 20<V≤21 as well as incompleteness due to stars fainter than the survey limit of 21 mag have also been accounted for. To correct for the photometric incompleteness of the data, we have multiplied the predicted fluxes by a factor of 1.43 for 20<V≤20.5 and 2.22 for 20.5<V≤21 where the correction factors follow from the estimated incompleteness of ~30% (for 20<V≤20.5) and ~55% (for 20.5<V≤21) (Wilson 1992a). In order to correct for stars with V>21, we have used a method similar to the one used in the study of M33

(Chapter 2). Briefly, we calibrated a main sequence mass-M_V relation (using theoretical stellar evolution tracks for Z=0.020 from Schaller *et al.* (1992)) to find that, at the distance and reddening of NGC 6822, V=21 corresponds to 18 $M_\odot$ or roughly an O9.5 to B0 star (Popper (1980) and Schmidt-Kaler (1982)). We then used the Salpeter initial mass function $N(m)d(M)=Am^{\alpha}dm$ (α=2.35, Salpeter 1955) to calculate the total number of stars for each spectral (sub)class from O9.5 to B3 (the latest class for which the Panagia models give theoretical fluxes). For each of the four ionized gas environments, a different normalization constant A was determined by equating the integral of the initial mass function between 18 $M_\odot$ and 65.5 $M_\odot$ to the total number of stars in the region for which we could determine T_{eff} (either uncorrected for the conservative flux estimate, or corrected for incompleteness for the best flux estimate). With A in hand, we then calculated the total ionizing flux in each spectral class (or subclass) bin between O9.5 and B3 by multiply the average theoretical flux for that bin (class V assumed) by the total predicted number of stars in the bin. The correction to the flux from stars fainter than V=21 was then simply the sum of the ionizing flux from the individual bins.

Observed and theoretical fluxes from stars in the four ionized gas environments corrected, in turn, for the various effects described above, are summarized in Table 3.4. The theoretical fluxes are organized in the following manner: (1) no corrections for incompleteness (minimum flux case); (2) corrected for incompleteness for stars brighter than V=21; (3) corrected for incompleteness for V$\leq$21 and V>21 (best estimate) and (4) corrected for stars below the survey limit (*i.e.*, V>21).

The best overall agreement between theory and observation is obtained for the case where the data are uncorrected for any incompleteness. Over the total image, the two differ by a factor of $\sim$1.8 (Case A used in the diffuse and field) and $\sim$2.8

	BRIGHT	HALO	DIFFUSE (CASE A/B)	FIELD (CASE A/B)	TOTAL (CASE A/B)
Minimum Flux[a]	3.16	1.10	0.95 / 2.29	1.72 / 4.16	6.93 / 10.71
Incompleteness (V<21)[b]	4.28	1.52	1.36 / 3.28	2.33 / 5.64	9.75 / 14.72
Best Estimate [c]	4.32	1.55	1.39 / 3.33	2.39 / 5.73	9.65 / 14.93
Conservative Estimate [d]	3.19	1.22	0.96 / 2.32	1.74 / 4.22	7.11 / 10.95
Observed Flux[e]	2.19	0.53	0.83	0.29	3.85

Table 3.4: Observed and Predicted H_α Flux in the Four Ionized Gas Environments.

Note: All stars with V≤21 and all fluxes in units of $L_{39} \equiv 10^{39}$erg s^{-1}.

[a]Minimum: no corrections applied.

[b]Incompleteness: corrected for incompleteness in stars brighter than V=21.

[c]Best estimate: corrected for stars brighter and fainter than V=21.

[d]Conservative estimate: corrected only for stars with V>21.

[e]Observed fluxes are measured above the average sky background.

(Case B used everywhere). The predicted flux exceeds that observed by a factor of 1.4 in the bright, 2.1 in the halo, 1.1 in the diffuse (2.8 for Case B recombination) and 5.9 in the field (14 for Case B recombination). While the bright, halo and diffuse regions appear to be relatively close to ionization balance, the field is clearly not in ionization balance. Since 50% of the blue stars in NGC 6822 are found in the field, up to 50% of the ionizing photons produced may be escaping from the galaxy.

The effect of correcting the data for V>21 incompleteness is minor: the minimum flux estimates for the four regions, separately and combined, are increased by roughly 1% when the flux expected from stars fainter than the survey limits are included. In contrast, correcting the data for photometric incompleteness for $20<V\leq21$ increases the predicted flux from the uncorrected, uniform reddening case by a factor of ~1.4. The total theoretical flux, after this correction has been made, exceeds that observed by a factor of 2.0 in the bright, 2.9 in the halo, 1.6 in the diffuse (4.0 for Case B), 8.0 in the field (19 for Case B), and 2.5 for the entire galaxy (3.8 for Case B used everywhere). Clearly, of all the different corrections, only that of photometric incompleteness for stars with $20<V\leq21$ is significant. It is reassuring that the more uncertain, model dependent correction for stars with V>21 is unimportant compared to the simpler and more easily measured photometric correction.

The best estimate of the predicted flux corrects for photometric incompleteness over $20<V\leq21$ and includes flux from main sequence stars fainter than V=21. Over the entire surveyed region, these fluxes are a factor ~2.5 (Case A) to ~3.9 (Case B) greater than observed. The best case for ionization balance is in the diffuse and bright emission regions where the predicted fluxes are, respectively, ~1.7 and ~2.0 (assuming Case A recombination) times those observed. The worst case

for ionization balance is in the field, where predicted and observed fluxes for Case A and B differ from that observed by factors of, respectively, ~8 and ~20. On average, the best estimate fluxes are approximately 1.4 times the corresponding conservative estimates.

It is clear from Table 3.4 that the predicted and observed fluxes in the diffuse and field emission regions are best matched when Case A (optically thin) recombination is assumed. That the gas density in these regions should be lower than that in the bright and halo regions is not unreasonable. While we have no direct measure of the gas density in the different ionization regions, we can place limits on this quantity by comparing the observed $H\alpha$ surface brightness with that expected for an H II region in gas of known density. For a B0 star ($L_{H\alpha}$=5.82×10^{35} erg sec^{-1} and $N_{Ly C}$=4.27×10^{47} photons sec^{-1}; Panagia 1973) located in the diffuse emission region, the maximum surface brightness observed (I_F=4.32×10^{-16} erg s^{-1}cm^{-2} arcsec^{-2}) limits the gas density to be $\lesssim$5 cm^{-3}. In obtaining the above result, we have used the Stromgren radius (*e.g.*, Spitzer 1978) to estimate the radius of the H II region and assumed the gas within the Stromgren sphere of the star is completely ionized. Similarly, if the ionizing source is an O5 star, the gas density in the diffuse region would have to be $\lesssim$0.5 cm^{-3} for the surface brightness of the H II region to match the maximum level observed. As the maximum surface density in the field is lower than that in the diffuse region, the field gas density would be correspondingly smaller. If the surface brightnesses of H II regions formed by B0 and O5 stars are to equal the average surface brightness observed in bright H II regions (I_B=4.11×10^{-15} erg s^{-1}cm^{-2} arcsec^{-2}), the gas density must be ~15 cm^{-3} (B0) and ~1 cm^{-3} (O5). Thus the gas density in the diffuse and field regions is likely to be lower than that in the bright H II regions which lends some support to our assumption of Case A recombination in

the diffuse and field regions and Case B elsewhere in the galaxy.

What are the implications of the above findings to the determination of high mass SFRs from $H\alpha$ luminosities? Recalling from our earlier discussion that the SFR scales with the Lyman continuum luminosity, we would expect the SFR in NGC 6822 to underestimate the "true" SFR i.e., that which would be measured if all the stellar ionizing radiation is converted into, and observed as, $H\alpha$ emission. Over the entire galaxy, the difference between the observed and true SFR is a factor of ~2-4. Moreover, while the difference is less than a factor of 4 in the bright, halo and diffuse regions, in the field the discrepancy between the observed and true SFR is a factor of ~6-20. Clearly, this technique to obtain the rate of formation of massive stars is sensitive to the stellar environment and cannot be used indiscriminately in any environment. For the field region, which houses a significant ~50% of the total number of OB stars in the galaxy but is losing the greatest amount of ionizing flux, this technique is most unreliable. Our results also illustrate the importance of choosing a recombination scenario that is appropriate to the region under investigation.

Assuming Case B recombination when Case A is more likely to be appropriate systematically underestimates the SFR. This may be a problem for many SFRs that are determined using Kennicutt's (1983) relation which assumes Case B recombination over the entire galaxy. In NGC 6822, the SFR obtained by applying the Kennicutt formula to the observed $H\alpha$ luminosities in all four ionized gas regions (SFR_K) underestimates by ~30% the SFR obtained when Case A is used in the field and diffuse regions. Moreover, by taking the flux lost from the field region into account (by assuming the actual $H\alpha$ luminosity in the field is the minimum flux estimated from the Panagia ionization models and Case A recombination in the diffuse and field regions) we find SFR_K underestimates the true SFR by ~50%.

	BRIGHT	HALO	COMBINED (BRIGHT + HALO)
Minimum Flux[a]	1.24	0.0035	1.24
Incompleteness (V≤21)[a]	1.72	0.0080	1.73
Best Estimate [a]	1.74	0.0082	1.73
Conservative Estimate [a]	1.25	0.0049	1.26
Observed Luminosity [L_{ob}][b]	0.75	0.05	0.80
# Stars Observed [N_{ob}]	40	3	43
# Stars with $T_{eff,L} < t_{eff} < T_{eff,U}$ [c]	35	3	38
Relative Luminosity per star [L_{ob}/N_{ob}][c]	1.01	0.89	1.00

Table 3.5: The Observed and Predicted Hα Fluxes and OB Star Content in Hubble I and III.

[a]Predicted $H\alpha$ luminosity accounting for incompleteness and/or differential reddening (as in Table 3.4).
All stars with V≤21 and all fluxes in units of L_{39}.
[b]Observed luminosities have been background subtracted.
[c]In units of 1.86×10^{37}erg s^{-1} arcsec^{-2} star^{-1}.

3.5.1 IONIZATION BALANCE IN HUBBLE I AND III

What is the state of ionization balance on a small scale? To answer this question we focus on the bright H II knot consisting of Hubble I and III located in the northern bar of the galaxy (see Figure 3.5). First identified by Hubble in 1925, Hubble I and III collectively encompass an area roughly 0.3 kpc^2 (for I$\gtrsim1.3\times10^{-16}$ erg s^{-1}cm^{-2} arcsec^{-2}). This region was among the many H II regions of NGC 6822 studied by Hodge & Lee (1989) who measured the $H\alpha$ luminosity of the region to be 6.21×10^{-16} erg s^{-1}cm^{-2}. We have summarized in Table 3.5 the observed and predicted $H\alpha$ emission in the bright, halo and combined (bright and halo) components of Hubble I and III. The theoretical fluxes are calculated by applying the models of Panagia (1973) to the 43 stars in the region for which we have photometry. In all

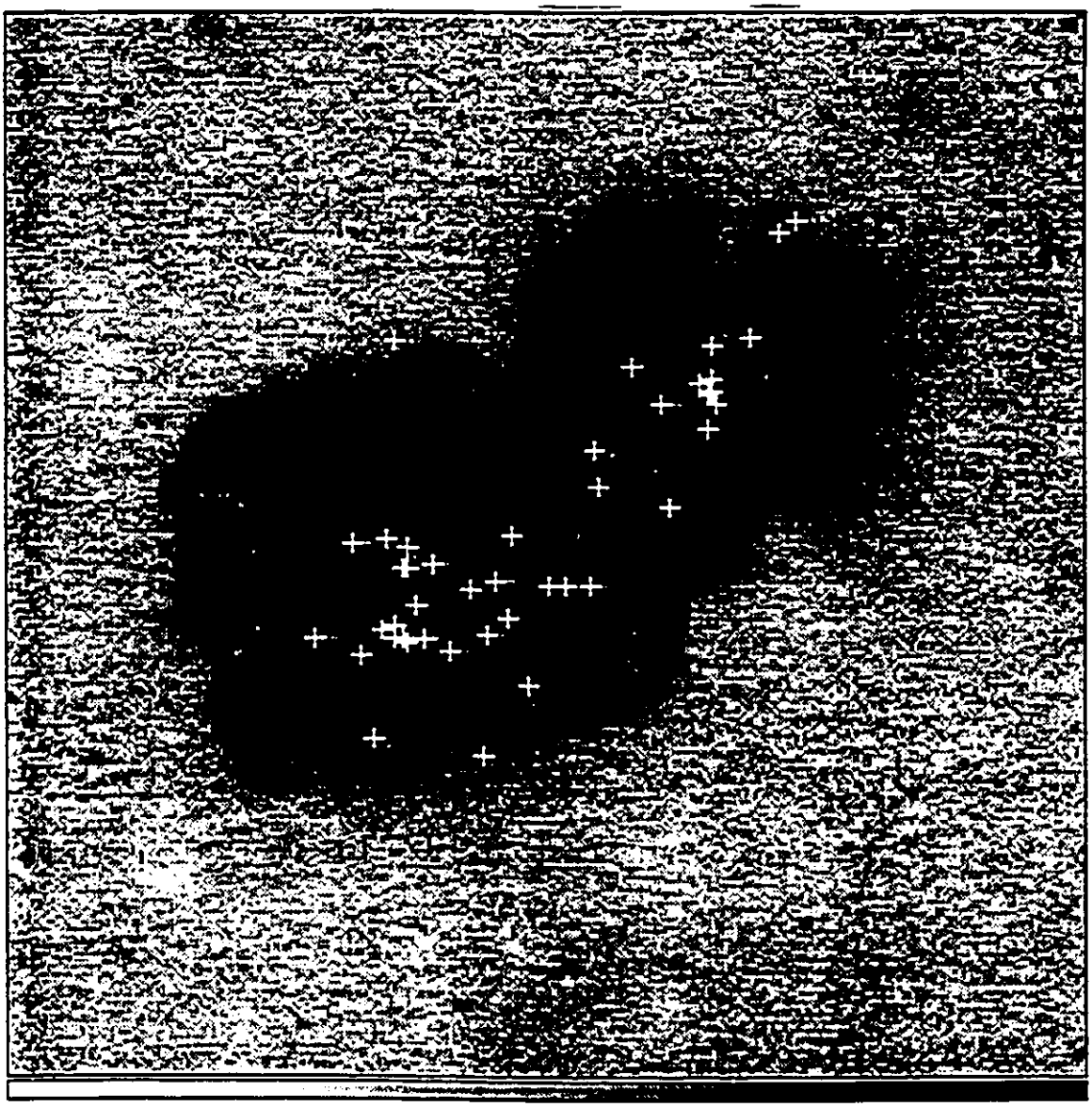

Figure 3.5: The $H\alpha$ image of the giant H II regions, Hubble I and III. Overlaid are the OB stars within the bright and halo emission regions.

cases, the models predict more flux than observed in the bright emission region and less flux than observed in the halo region. Moreover, the agreement between theory and observations is very good (within a factor of 1.7 to 2.3) in the bright regions but rather poor in the halo (between a factor of 0.07 to 0.16). This large discrepancy in the halo region is most likely due to the very few (only 3) stars located there. As it turns out, the flux measured and predicted in the halo is almost negligible when compared to that in the bright region and so does not affect the overall conclusions of ionization balance in this individual region. Concentrating on the combined (bright and halo) regions, we find that the predicted and observed fluxes are best matched when the data are left uncorrected where the two differ by a factor of $\sim$1.6. Correcting for incompleteness ($V \leq 21$) has the greatest overall effect on the predicted fluxes which are seen to increase by a factor of $\sim$0.4 from the minimum flux case and are a factor of $\sim$2.2 greater than that observed. Finally, the best estimate case which corrects for incompleteness above and below V=21, yields predicted fluxes that are slightly more than twice those observed and therefore within the allowed range of uncertainty. Based on these results, we conclude that Hubble I and III are collectively likely to be in ionization balance.

3.6 COMPARISON WITH M33

Having investigated the ionized gas-OB distribution as well as considered the question of ionization balance in NGC 6822, we can now address the question of how the results for this dwarf irregular system compare with those found for the spiral galaxy M33. In order to do so, it is important that the colour and brightness cutoffs in the two galaxies are matched so that the same types of OB stars are sampled. In the case of M33, only those stars with $V \leq 21$ and $(B-V) \leq 0.4$ were selected for

study. Assuming a total reddening of E(B-V)=0.3 mag (Wilson 1991), and a distance of 0.79 Mpc to the galaxy (van den Bergh, 1991), the absolute magnitude cutoff corresponding to the limit of V=21 is M_V=-4.4 mag. At the NGC 6822 distance and adopted reddening of E(B-V)=0.45, the selection criterion for matching the two galaxies is V$\leq$20.5 and (B-V)$\leq$0.55.

Although the diffuse emission component was not differentiated from the field component in the M33 investigation (Chapter 2), we have, for sake of comparison, done so here (see Figure 3.6). The limiting surface brightness separating the field and diffuse regions in M33, $I_{FD,M33}$, is chosen to match that in NGC 6822 *before correcting for [NII] emission* so that $I_{FD,M33}$=1.3$\times10^{-16}$ erg s^{-1} cm^{-2} arcsec^{-2} uncorrected and $I_{FD,M33}$=1.03$\times10^{-16}$ erg s^{-1} cm^{-2} arcsec^{-2} corrected fro [NII] emission. A number of interesting features of the ionized gas distributions are revealed on comparing Figures 3.3 and 3.6. Unlike NGC 6822, where the diffuse emission is extended over the galaxy, in M33 the diffuse gas appears to be confined to a narrow region around the halo emission, thus giving the impression that the diffuse gas is, in fact, a thin "halo" of the latter. Additionally, the distinction between the bright and halo regions in M33 is much clearer than that in NGC 6822: while the halos in M33 are broad, extended regions, those in NGC 6822 are narrow rings or bands confined around the bright emission regions. The field regions in both galaxies are similar in that the emission is highly uniform and low level. It appears therefore that although M33 and NGC 6822 both contain bright, halo, diffuse and field emission regions, the spatial distribution of these components are not the same in the two galaxies. The main difference is seen in the halo and diffuse emission regions that appear to have exchanged roles between M33 and NGC 6822.

In Table 3.6 we summarize the distribution of the brightest OB stars ($M_V\leq$-

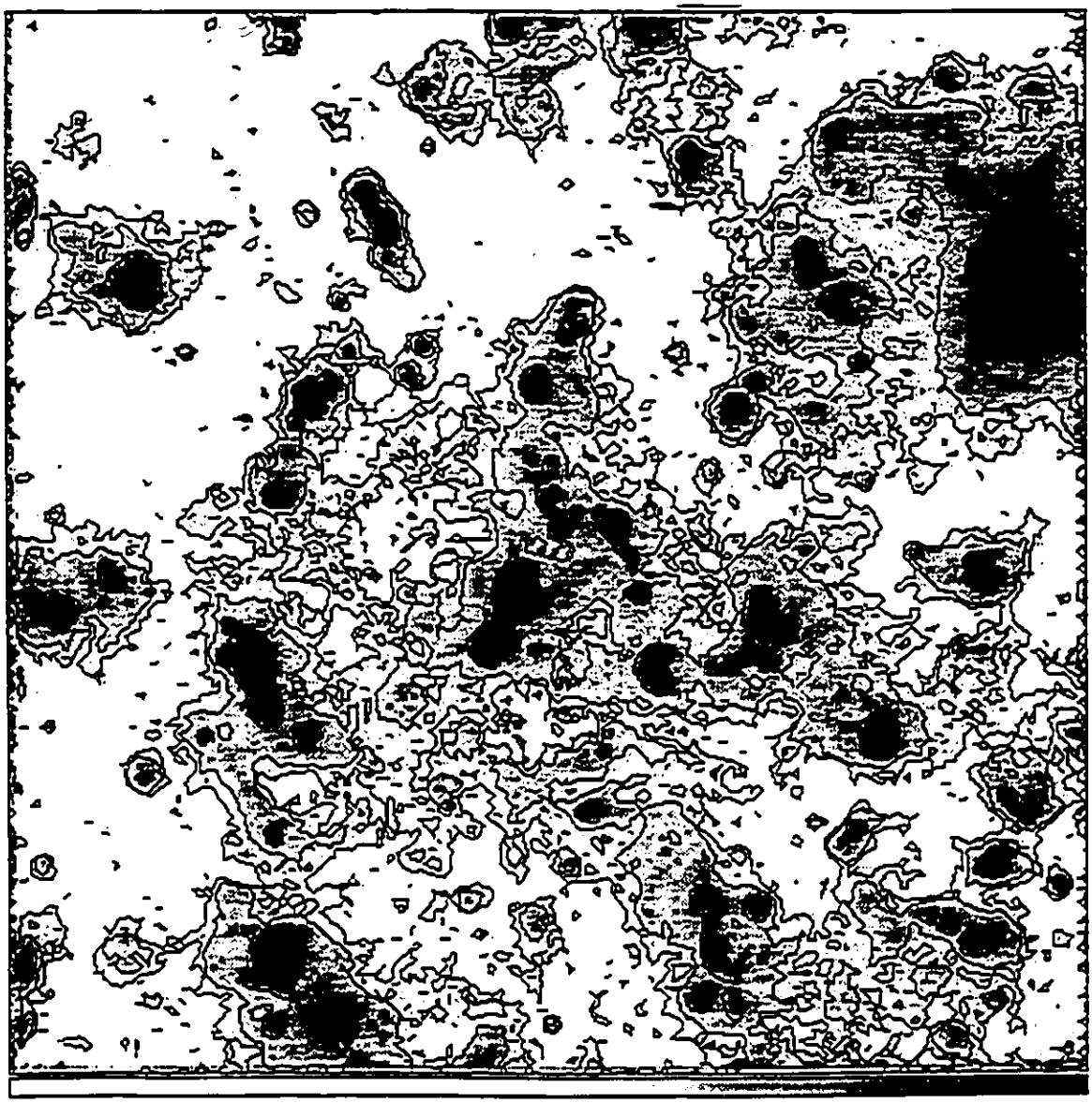

Figure 3.6: The continuum subtracted $H\alpha$ image of the central 8.7′×8.7′ of M33 illustrating the distribution of the bright, halo, diffuse and field $H\alpha$ emission regions. North is at the top and east is to the left. For orientation the giant HII region NGC 595 is located in the top right-hand corner of the image and the center of the galaxy coincides roughly with the center of the image.

	GALAXY	BRIGHT # of stars	HALO # of stars	DIFFUSE # of stars	FIELD # of stars	TOTAL # of stars
Brightest Stars [a]	M33	22 ±5	15 ±4	7 ±3	11 ±3.3	55 ±7
	NGC 6822	2 ±1	0	2 ±1	6 ±2	10 ±3
Total in Survey [b]	M33	390 ±20	688 ±26	519 ±23	583 ±24	2180 ±47
	NGC 6822	84 ±9	51 ±7	119±11	224 ±15	481 ±22

Table 3.6: The Distribution of OB Stars in M33 and NGC 6822.

[a]The brightest stars are selected such that M_V <-7.45 in both galaxies and (B-V)<0.4 for M33 and (B-V)≤0.5 for NGC 6822. Note that M_V ≤-7.45 corresponds to V≤18 in M33 and V≤17.5 in NGC 6822.

[b]Total number of stars to a limiting absolute magnitude M_V ≤-4.45 (corresponding to V≤21 in M33 and V≤20 in NGC 6822) for both galaxies. The colour cutoff as is above.

7.45 corresponding to V≤18 in M33 and V≤17.5 in NGC 6822) and total number of OB stars down to the M33 survey completeness limit V≤21 or M_V≤-4.45 (corresponding to V≤20.5 in NGC 6822). Considering the sample of stars brighter than M_V <-4.45, the results in the two galaxies are well matched in the bright and diffuse emission components (~18% (M33) and ~17% (NGC 6822) are located in the bright and ~24% (M33) and ~25% (NGC 6822) in the diffuse) but somewhat different in the halo and field regions (~32% (M33) compared to ~11% (NGC 6822) in the halo and ~27% (M33) compared to ~46% (NGC 6822) in the field). NGC 6822 has a proportionately larger field population then M33. Due to the significant percentage of halo stars in M33, the fractional lifetimes of an O star spent in a recognizable H II region, and thus in its parent molecular cloud, is greater in M33 (f_{HII} ~50%) than in NGC 6822 (f_{HII} ~28%).

What might the value of f_{HII} be telling us about molecular clouds in M33

	GALAXY	BRIGHT (CASE B)	HALO (CASE B)	DIFFUSE (CASE A)	FIELD (CASE A)	TOTAL
MINIMUM	M33[a]	1.29	1.58	1.30	17.09	2.29
	NGC 6822[b]	1.14	1.54	0.91	4.07	1.46
CONSERVATIVE	M33[c]	2.10	3.62	2.98	40.11	5.28
	NGC 6822[d]	1.20	1.74	1.00	4.66	1.49
BEST ESTIMATE	M33[e]	3.97	8.35	6.20	88	6.51
	NGC 6822[f]	1.29	1.73	1.13	4.93	1.59
OBSERVED Hα [g]	M33	3.78	2.57	0.95	0.06	7.36
	NGC 6822	2.19	0.53	0.83	0.29	3.85

Table 3.7: Predicted and Observed Hα Fluxes in the Four Ionized Gas Environments of M33 and NGC 6822.

All predicted fluxes are expressed as a fraction of the observed *Hα* flux in the particular ionized gas environment of the galaxy. Magnitude and colour cutoffs in respectively, M33 and NGC 6822 are, respectively, $V \lesssim 21$ and $(B-V) \lesssim 0.4$ and $V \lesssim 20.5$ and $(B-V) \lesssim 0.55$.

[a] Minimum flux M33: no corrections applied.

[b] Minimum flux NGC 6822: no corrections applied.

[c] Conservative estimate M33: corrected only for stars with V>21.

[d] Conservative estimate NGC 6822: corrected only for stars with V>20.5.

[e] Best estimate M33: corrected for stars with $V \leq 21$ and V>21.

[f] Best estimate NGC 6822: corrected for stars with $V \leq 20.5$ and V>20.5.

[g] Observed fluxes are in units of $L_{39} \equiv 10^{39}$ erg s^{-1} $arcsec^{-2}$.

and NGC 6822? If in both galaxies OB stars escape from bright and halo H II regions by destroying their parent molecular clouds, then molecular cloud lifetimes after the formation of OB stars are shorter in NGC 6822. This could be explained if the molecular clouds in NGC 6822 are smaller on average than those in M33, since smaller clouds would be easier to destroy. It could also be that the star formation efficiency (defined as SFE=$M_*/(M_*+M_{gas})$ where M_* and M_{gas} are respectively the mass in stars and gas in the cloud) is higher in NGC 6822 so that more stars are formed and, therefore, the probability of destroying or dissipating the natal molecular clouds is much increased. Alternatively, if OB stars simply move out of their parent molecular clouds and H II regions, then the quantity f_{HII} does not imply a molecular cloud lifetime but suggests that perhaps molecular clouds are smaller in NGC 6822 than M33. Evidence that molecular clouds may be smaller in dwarf irregular galaxies than in spirals comes from a recent CO study of the SMC (Rubio *et al.* 1993).

Inspection of Table 3.7 reveals a number of interesting results from the ionization balance calculations in the two galaxies. Based on the simple minimum flux case, the bright, halo and diffuse emission regions, as well as the entire surveyed regions of both galaxies are likely to be ionization bounded. This is also suggested by the conservative and best estimate of the ionizing flux in NGC 6822. The problem area in the minimum case, as in all the others, is the field which appears to be leaking the most Lyman photons: from ~4 (in NGC 6822) and ~17 (in M33) times the observed flux in the uncorrected, minimum estimate case to ~ 5 (in NGC 6822) and a staggering ~88 (in M33) times the observed flux in the best estimate case. The field, therefore, does not appear to be in a state of ionization balance in either galaxy and furthermore, the problem is much more severe in M33 than NGC 6822. The fact that even in the minimum flux case (where no corrections for incompleteness have been

made) the field stars in M33 are producing so much more ionizing flux than observed suggests that the field is truly leaky to Lyman continuum photons. Although NGC 6822 has a higher percentage of field stars contributing to the ionizing flux (*i.e.*, stars with $T_{eff,U} < T_{eff} < T_{eff,L}$ ~60% in NGC 6822 and ~45% in M33), it is still more effective at holding on to the ionizing photons produced by these stars than M33. This is also seen to be the case in the other individual ionized gas environments as well as the entire surveyed regions of the galaxies as a whole: for both the conservative and best estimate cases, the difference between the predicted and observed $H\alpha$ fluxes in the bright, halo, diffuse and collective regions are consistently higher in M33 than NGC 6822, which thus implies that the inner kiloparsec of M33 is in a more serious state of ionization imbalance than NGC 6822. All three models support the finding that the likelihood of ionization balance decreases in going from the bright to faint emission regions. Finally, while NGC 6822 as a whole appears to be in a state of ionization balance, the surveyed inner 1 kpc region of M33 is clearly not.

In conclusion, it would appear that the morphological class of the galaxy may be an important factor in these types of studies. The fact that M33 appears to be so much less effective at holding on to the ionizing radiation than NGC 6822 suggests that the shapes of the galaxy are important: the flat discs of spiral galaxies may not provide a thick enough layer of gas to capture all or most of the Lyman continuum photons emitted by the OB stars, especially from those stars in the field. The surface density of stars may also be an important factor in the extent of ionization imbalance in that for two areas of similar column densities of neutral gas, the one with a larger surface density of OB stars may have much less gas left to ionize and would therefore be more likely to be leaking ionizing photons then one that has fewer stars per unit area. As an example consider the field regions in M33 and NGC 6822: the M33 field

star surface density is twice that of NGC 6822 (~416 stars kpc^{-2} compared to ~215 stars kpc^{-2}). Given that the average H I column density in these two galaxies is of the order of ~10^{20} cm^{-2} (Deul & van der Hulst 1987; Skillman 1987), this would mean that M33 should be twice as efficient at losing ionizing flux as NGC 6822. *i.e.*, we would expect the ratio of the predicted to observed $H\alpha$ luminosities in the field regions of M33 to be a factor of two larger then that in NGC 6822. While what we observe is more than this (in the minimum flux case, M33 is 17.09/4.07~4.2 times more effective at losing ionizing flux than NGC 6822), the general outcome is clear: based on the surface density of OB stars, M33 can be expected to be more susceptible to leaking ionizing photons then NGC 6822.

3.7 CONCLUSIONS

We have investigated the distribution of H II regions and OB stars and tested the hypothesis of ionization balance within NGC 6822 using $H\alpha$ data and BV photometry of blue stars. We divide the $H\alpha$ emission in NGC 6822 into four distinct components, denoted bright, halo, diffuse and field, based on the surface brightness of the gas. The major findings of our study are summarized below.

(1) The distribution of OB stars brighter than V=21 within the bright, halo, diffuse and field regions is such that ~16% are located in the bright, ~10% in the halo, ~24% in the diffuse and ~49% in the field regions. Combining the bright and halo regions reveals that only 1/4 of the blue stars are found in the optically prominent H II regions. These results suggest that roughly 3/4 of the main sequence lifetime of an O star is spent outside of such H II regions.

(2) The OB star and H II region distributions imply that if OB stars destroy

their parent molecular clouds while escaping their H II regions, then molecular cloud lifetimes after the formation of OB stars must be shorter than $\sim$1-3$\times10^6$ yrs. Alternatively, if the stars escape the H II regions without destroying their parent molecular clouds, then molecular cloud lifetimes could be much longer.

(3) Comparing the spectral classes determined from photometry with those deduced from optical spectroscopy shows that the former are biased towards earlier spectral types, perhaps due to unresolved binaries. Due to this effect, the theoretically predicted $H\alpha$ fluxes are likely to be over-estimated. We therefore consider any ionization balance calculations that agree to within a factor of two to be in acceptable agreement.

(4) Comparing the observed $H\alpha$ luminosities in the four ionized gas environments both separately and collectively with those predicted theoretically we find that the models consistently predict more flux than observed. The bright regions are likely to be ionization bounded as the predicted fluxes are, at most, a factor of 2 larger than observed. The halo and diffuse regions appear to be at the limit of ionization balance as the predicted fluxes can differs from that observed by up to a factor of, respectively, $\sim$3 and $\sim$4. In the field however, the observations and model predictions differ by a factor of $\sim$6-15 (assuming Case A and B recombination) for the conservative case and $\sim$8-20 for the best estimate case. This region is clearly not in ionization balance and thus fully 50% of the blue stars in NGC 6822 may be losing most of their ionizing radiation to interstellar space.

(5) In determining a SFR from the $H\alpha$ luminosity in a galaxy, the assumption is made that the galaxy is ionization bounded and that Case B recombination is appropriate everywhere. For NGC 6822, our results show that the true SFR would

be underestimated by ~50% due to the leakiness of the field and the use of Case A recombination in the diffuse and field regions.

(6) Significant differences between the distributions of the OB stars within the ionized gas environments as well as the state of ionization balance in M33 and NGC 6822 suggest that the morphological class of the parent galaxy may be an important factor in the state of ionization balance of the gas and therefore in determining the SFR from the $H\alpha$ luminosity. The field in the inner kiloparsec of M33 appears to be in a more serious state of ionization imbalance than NGC 6822: M33 is losing at least ~17 times the observed $H\alpha$ flux while the figure for the field in NGC 6822 is ~4. The difference in the number of ionizing photon leaking from the two galaxies may be due to the surface density of OB stars, which is higher in M33: since the two galaxies have comparable H I column densities, the likelihood of losing ionizing photons is increased when the stellar surface density is increased. Based on the ionization balance results, SFRs from $H\alpha$ luminosities are less likely to reflect the true SFR in the central region of M33 than in NGC 6822.

3.8 REFERENCES

Abt, H.A. 1978 in Protostars and Planets, ed. T. Gehrels (Univ. of Arizona Press:Tucson), p. 323

Armandroff, T.E. & Massey, P. 1985 ApJ, 291, 685

Armandroff, T.E. & Massey, P. 1991 AJ, 102, 972

Auer, L.H. & Mihalas, D. 1972, ApJS, 24, 193

Blitz, L. & Shu, F. 1980 ApJ, 235, 148

Brandley, P.T. & Morton, D.C. 1969, ApJ, 156, 687

Brockelhurst, M. 1971, MNRAS, 153, 471

Churchwell, E. 1991, in the Physics of Star Formation & Early Stellar Evolution, ed. C. Lada & N.D. Kylafis (Dordrecht:Kluwer), p. 221

Deul, E.R. & van der Hulst, J.M. 1987, AAS., 67, 509

Duquennoy, A. & Mayor, M. 1991, A&A, 248, 485

Elmegreen, B.G. 1991, in The Physics of Star Formation & Early Stellar Evolution, Ed. C.J. Lada & N.D. Kylafis (Dordrecht:Kluwer), p. 35

Flower, P.J. 1977, A&A, 54, 31

Hodge, P.W. 1977, APJS, 33, 69

Hodge, P.W. 1980 ApJ, 241, 125

Hodge, P.W., Lee, M.G. & Kennicutt, R.C. 1988 PASP, 100, 917

Hodge, P.W., Lee, M.G. & Kennicutt, R.C. 1989 PASP, 101, 32

Hodge, P.W., Smith, T., Eskridge, P., Macgillivray, H.T. & Beard, S. 1991, ApJ, 379, 621

Humphreys, R. M. 1980, ApJ, 238, 65

Kennicutt, R.C. 1983, ApJ, 272, 54

Kurucz, R.L. 1979, ApJS, 40, 1

McAlary, C.W., Madore, B.F., McGonegal, R., McLaren, R.A. & Welch, D.L. 1983, AJ, 273, 539

Massey, P., Garmany, C.D., Silkey, M. & Degioia-Eastwood, K. 1989a, AJ, 97, 107

Massey, P., Parker, J.W. & Garmany, C.D. 1989b, AJ, 98, 1305

Massey, P., Lang, C.C., Degioia-Eastwood, K. & Garmany, C.D. 1994, ApJ, in press

Massey, P., Pyke, R., Armandroff, T.E., Patel, K. & Wilson, C.D. 1995, in preparation

Morton, D.C. 1969, ApJ, 158, 629

Osterbrock, D.E. 1989, Astrophysics of Gaseous Nebulae and Active Galactic Nuclei (Mill Valley: University Science Books)

Ohta, K., Tomita, A., Saito, M., Sasaki, M. & Nakai, N. 1993, PASJ, 45, L21

Pagel, B.E.J., Edmunds, M.G. & Smith, G. 1980, MNRAS, 193, 219

Panagia, N. 1973, AJ, 78, 929

Parker, J.W. & Garmany, C.D. 1993, AJ, 106, 1471

Patel, K. & Wilson, C.D. 1995 (Paper I), ApJ, submitted

Popper, D. 1980, ARA&A, 18, 115

Rand, R.J., Kulkarni, S.R. & Hester, J.J. 1990, ApJ, 352, L1

Rubio, M., Garay, G., Montani, D. & Thaddeus, D. 1993, A&A, 271, 7

Salpeter, E.E. 1955, ApJ, 129, 608

Schaller, G., Schaerer, D., Meynet, G., Maeder, A. 1992 A&AS, 96, 296

Schild, R. 1977 AJ, 82, 337

Schmidt-Kaler, Th. 1982, in Landolt-Bornstein: Numerical Data and Functional Relationships in Science and Technology, New Series, Vol 2, Astronomy and Astrophysics, eds K. Schaiffer and H.H. Voigt (Berlin: Springer-Verlag), p. 1

Skillman, E. 1987, in Star Formation in Galaxies, NASAP-2466, ed. C. L. Person (Washington:NASA), p. 263

Spitzer, L. 1978, Physical Processes in the Interstellar Medium (New York:Wiley)

Van Citters, G.W. & Morton, D.C. 1970, AJ, 161, 695

Van den Bergh, S. 1991, PASP, 103, 609

Wilson, C.D. 1990, Ph.D. thesis, Caltech

Wilson, C.D. 1991, AJ, 101, 1663

Wilson, C.D. 1992a, AJ, 104, 1374

Wilson, C.D. 1992b, ApJ, 391, 144

Wilson, C.D. 1994, AJ, 434, L11

Zuckerman, B. 1973, ApJ, 183, 863

Chapter 4

SPECTROSCOPY OF LUMINOUS BLUE STARS IN NGC 6822 AND M33

4.1 INTRODUCTION

In order to obtain accurate effective temperatures and therefore accurate masses and ionization fluxes of OB stars, it is vital to supplement photometric observations with spectroscopic data. The reason that photometry alone is not sufficient is due to the fact that the broadband colours of massive stars on the main sequence are degenerate so that T_{eff} cannot be uniquely determined and one cannot use the H-R diagram and stellar evolutionary tracks to accurately determine the mass of a star. In fact, photometry systematically underestimates the mass of a star (Massey *et al.* 1989a, 1989b) and moreover, these masses are uncertain by at least 50% (Wilson 1990). In addition to the problems related to the colour degeneracy are the uncertainties introduced by the reddening and the fact that mapping from the colour ((B-V) or (U-B)) or reddening free index (Q≡(U-B)-0.72(B-V)) to T_{eff} is dependent on the effective gravity (g) so that stars of the same colour but different luminosity class (*i.e.*, supergiant, main sequence etc.) do not have the same T_{eff}. Optical spectroscopy

resolves this problem by allowing a direct, reddening independent determination of T_{eff} from the spectral class of the star. Accurate masses and ionization fluxes as well as many other important quantities that depend on the masses of stars, such as the IMF (initial mass function) and SFR (star formation rate) can then be more precisely estimated.

We undertook a program of spectroscopic investigation of candidate OB stars in M33 and NGC 6822 to determine accurate masses and T_{eff}. Our original intention was to use the spectroscopic masses to estimate directly the high mass IMF and, combined with the main sequence lifetimes of stars from stellar evolution models, the high mass SFR. Effective temperatures deduced from knowledge of spectral classes would have been used to assign accurate Lyman continuum fluxes from the stellar ionization models and thus improve the ionization balance calculations for the two galaxies. Finally, we hoped to contribute towards an existing and on-going spectroscopic data base of individual massive stars in Local Group galaxies that already included OB and evolved OB or Wolf-Rayet stars in the LMC (Massey *et al.* 1987; Parker *et al.* 1992; Breysacher 1981, Conti & Garmany 1983 Azzopardi & Breysacher 1979), SMC (Massey *et al.* 1989; Azzopardi & Breysacher 1979), M33 and NGC 6822 (Armandroff & Massey 1985, 1991). While that was the intention, the results turned out to be somewhat different. Due to time limitations and extremely poor weather conditions during the M33 observations, the signal-to-noise (S/N) ratio of the data was not sufficiently high to allow spectral classifications (accurate or rough) for many of the stars in the original sample: only 15 stars or 40% of the data were classifiable. While the conditions were somewhat better for the NGC 6822 observing run, we were able to classify only 35 or ~50% of the spectra. With such small number statistics, we could not use the spectra to investigate the massive star IMF and SFR. Moreover,

even in some of the high S/N spectra only approximate spectral classes could be assigned and it was often not possible to determine the luminosity class of the star. For these reasons, we abandoned most of our original plans for these data. While the individually studied stars are, in their own right, significant and will be a welcome addition to the existing bank of information on the massive star content of nearby galaxies, for the purposes of this study we used only the NGC 6822 spectra as a tool to test the performance of the stellar ionizing flux models of Panagia (1973) used in the ionization balance calculations.

In §2 of this chapter, we outline the method of obtaining the optical spectra of the OB stars in M33 and NGC 6822. A discussion on spectral classification is given in §3 followed by the classification scheme used in our investigation in §4. The M33 and NGC 6822 spectra are presented and discussed in §5.

4.2 DATA ACQUISITION

We describe, in this section, the instruments and the procedures used to obtain the spectroscopic data for the blue stars of NGC 6822 and M33. As many of the steps for reducing the raw images into individual spectra ready for analysis are similar for the two galaxies, we will discuss one of these, NGC 6822, in greater detail.

4.2.1 ARGUS Spectroscopic Data for NGC 6822

The spectra were obtained during three clear nights in July 1993 at the CTIO 4m telescope using the multifiber spectrograph ARGUS. ARGUS, which rests at the prime focus of the telescope, consists of 24 independent computer controlled arms that are used to position 48 optical fibers (24 object + 24 adjacent sky) within a

flat field of view 46 arcmin in diameter. Each arm holds both an object and sky fiber: the object fiber is found at the tip of the arm and is separated by 2mm (or 36 arcsec) from its respective sky fiber. The 24 4μm (1.86 arcsec at the prime focus) fibers can be positioned within 10 arcsec (center to center distance) of each other. Transmission characteristics at all wavelengths longer than 450 nm are excellent but decline towards the blue and UV. The fibers carry light from the prime focus cage to a bench-mounted spectrograph housed in a thermally and mechanically isolated chamber near the base of the telescope. Additional technical details of the instrument and the spectrometer can be found in Ingersol (1988), Ingersol (1994) and Sunzeff (1993). We used the blue Schmidt camera with the 400×1240 Reticon CCD (pixel scale 27μm) and the KPGILF grating, combined with a first order blocking filter, to select wavelengths centered on λ=4350$\AA$. Spectra obtained using the Reticon chip have a resolution element of ~2.5 pixels at the center and ~4 pixels near the edges of the chip.

Comparison spectra for wavelength calibration covering the wavelength range 3800 to 4850$\AA$ were obtained using the He-Ar lamp at the beginning, middle and end of each night. Conventional flat field spectra were obtained by pointing the telescope to a flat, uniformly illuminate white spot inside the dome. Additional flat field spectra, called milk flats, were also taken each night. Milk flats are highly defocused spectra of the twilight sky or dome white spot obtained by placing a piece of diffusive opal glass in front of the optical fibers in the spectrograph. Combined with conventional flat fields, they can be used to obtain the very precise flat fielding required to obtain high S/N spectra. Numerous zero second bias exposures as well as high S/N spectra of both the twilight and dawn sky were obtained during each of the three nights.

The stars selected for spectroscopic study were some of the brightest, blue stars from the photometric list of Wilson (1992). In total, four program fields were observed. Typical integration times on each field were 3.5 to 4 hours. All images, except biases, were trimmed and corrected for overscan and bias in the normal manner using the IRAF package CCDPROC in CCDRED. The milk flats were scaled by the mean value and combined (using IMCOMBINE) to form a single average milk flat (Figure 4.1). (For clarity, all images names given are followed by an ".IMH" extension. The data presented are from the first night of observing.) After removing cosmic rays and dead pixels, the package IMSURFIT (in IMAGES) was used to fit and subtract a two-dimensional surface from the average milk flat to produce a final normalized response flat field image (Figure 4.2). This normalized flat, which will still contain the pixel-to-pixel variations but will be free of all low order (wavelengths of a few pixels or more) effects, is then used to flatten (by being divided into) all the data (twilight, combined dome flats, comparison lamps and object) using CCDPROC. This step removes the variations in the spectra due to pixel-to-pixel response variations in the CCD chip.

Using the APALL task in ARGUS, the dome flat (processed, combined and corrected for pixel-to-pixel variations; Figure 4.3) was used to find, recenter, trace and extract the reference apertures. A vertical slice of DOMECOMB.IMH used to find, trace and extract the 23rd aperture is shown in respectively, Figures 4.4, 4.5a and 4.5b. These reference apertures were then used to extract the 48 spectra found on each object, twilight sky and comparison lamp image. The next step in the reduction was to remove the cosmic rays and normalize (by fitting a curve and taking the ratio) the combined and extracted dome spectra (using the task CONTINUUM). Then we need to correct the resulting image for the absolute and colour transmis-

sion variations (or "throughput") of the fibers which we measure from each of the *twilight* sky spectra using the task MSRESP1D in SPECRED. This task calculates an individual scale factor (less than 1. in magnitude) per aperture as well as the average shape of the spectra using all the apertures. The throughput image used in MSRESP1D was a master twilight sky image which was obtained by combining the separate twilight sky images taken each night. An example of the effect of the task MSRESP1D, used to remove the transmission and colour variations in each fiber, is given in Figure 4.6 for aperture #23 of the normalized, combined dome flat image (NORMDOMECOMB.IMH). Also given in Figure 4.6 is the throughput uncorrected spectrum from aperture #23 of NORMDOMECOMB.IMH which has an intensity, on the y-axis, that is centered on unity. In this example, we can clearly see the greatest effect of MSRESP1D was to shift the entire spectrum down in intensity by ~5% of the total uncorrected intensity.

The output of MSRESP1D is the dome flat image that has been throughput corrected, normalized, extracted, combined and corrected for pixel-to-pixel variations. This image was divided into all the remaining data (object and comparison arc spectra that were already extracted and corrected for pixel-to-pixel variations) so as to remove from each spectrum, the absolute and colour transmission variations introduced by the optical fibers. This concluded the processing and extracting of the raw data.

The next step in the reduction was to obtain the wavelength calibrations. Using the ARGUS task IDENTIFY, a few features on one reference He-Ar spectrum were identified by hand after which the remaining lines were then automatically assigned from a master list of the features in the arc spectrum (Figure 4.7). The disperson solution was obtained by deleting poor assignments and changing the fit parameters until a solution with an acceptable fit and residual was obtained. The

typical rms error in the dispersion-solution, based on 15-23 spectral features in each of the 24 apertures, was less than 0.02Å (Figure 4.8). This solution was used by the task REIDENTIFY to obtain the dispersion solutions of the remaining arc spectra on the reference image as well as all the spectra on the remaining comparison images. Using the package REFSPEC, each object spectrum was assigned a comparison arc spectrum that was taken closest in time to the object spectrum. The purpose of this type of arc assignment is to minimize the effects of any systematic horizontal drifts or shifts of the spectra on the CCD chip that may have occurred during the course of the night. Following this step, the spectra were dispersion-corrected over the range 3800 to 4850 Å using the task DISPCOR in ARGUS. The spectra were then cleaned of cosmic rays using the task CONTINUUM. Figure 4.9a shows the extracted, pixel-to-pixel, throughput and dispersion corrected, cosmic ray cleaned spectrum of OB8F-2.

The individual spectra for each multiply-observed star were combined to produce one final spectrum of increased S/N using the package SCOMBINE in SPECRED. Finally, the adjacent sky spectrum was subtracted from each object spectrum using the task SKYSUB in ARGUS and the continuum was removed from the resultant spectra using the task CONTINUUM. This concluded the reduction of the ARGUS images.

Where necessary, the spectra were smoothed (using BOXCAR in IMAGES) in order to enable clearer identification of the spectral features present. The effect of removing the average sky lines from the spectrum of OB8F-2 is illustrated in Figure 4.9b: the continuum subtracted spectrum (including sky lines) is on the bottom and the continuum and sky subtracted spectrum is at the top. The two spectra have been shifted in intensity by an arbitrary amount to facilitate comparison. The effect

of removing the sky lines is rather small in this object. This final sky subtracted spectrum was used to obtain the spectral classification of OB8F-2.

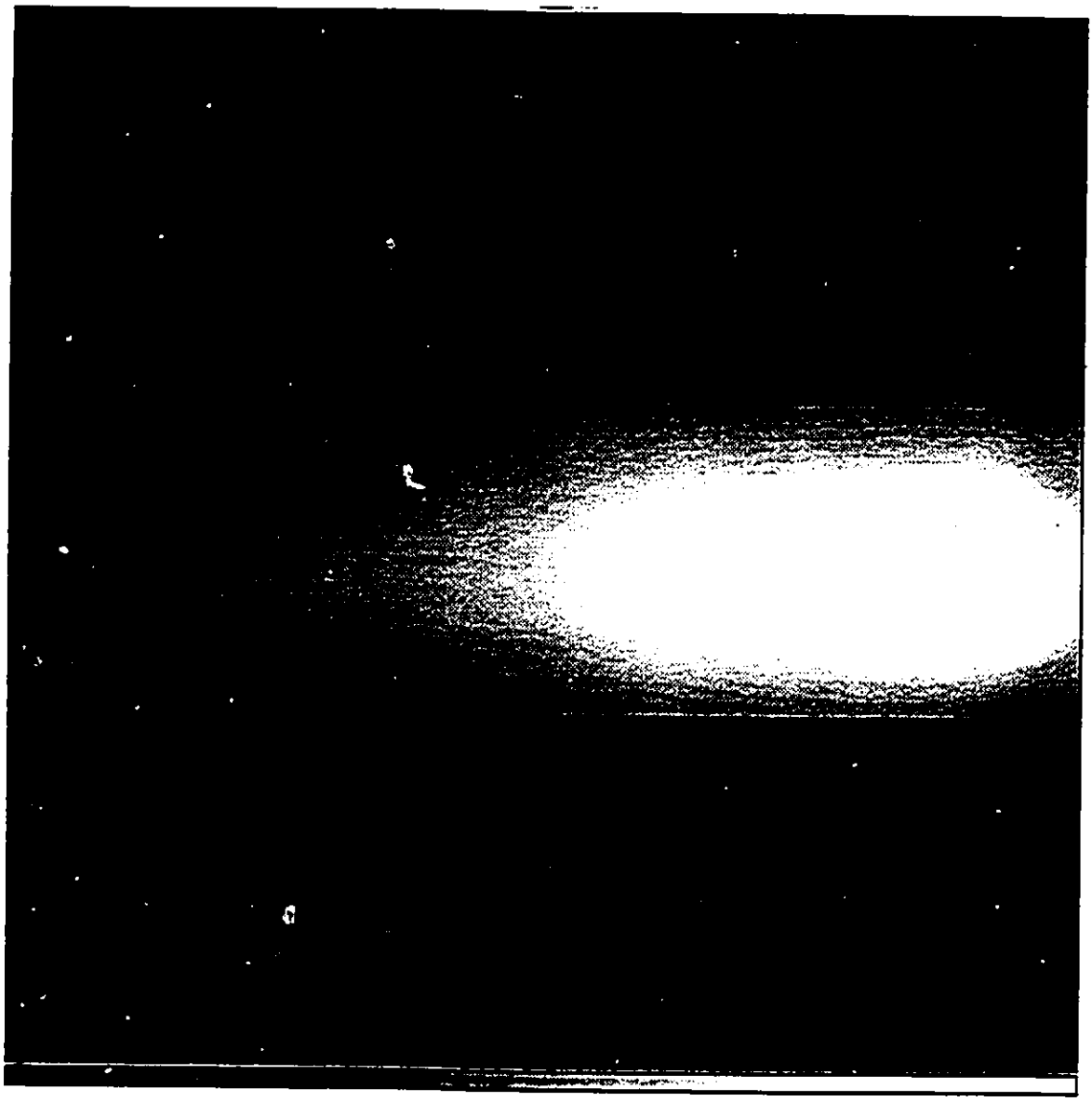

Figure 4.1: An image of the average milk flat, MILK.IMH, obtained by scaling and combining the individual milk flats obtained on the first night of observing. Milk flats are highly defocused spectra of the dome white spot obtained by placing a piece of diffusive opal glass in front of the optical fibers in the spectrograph.

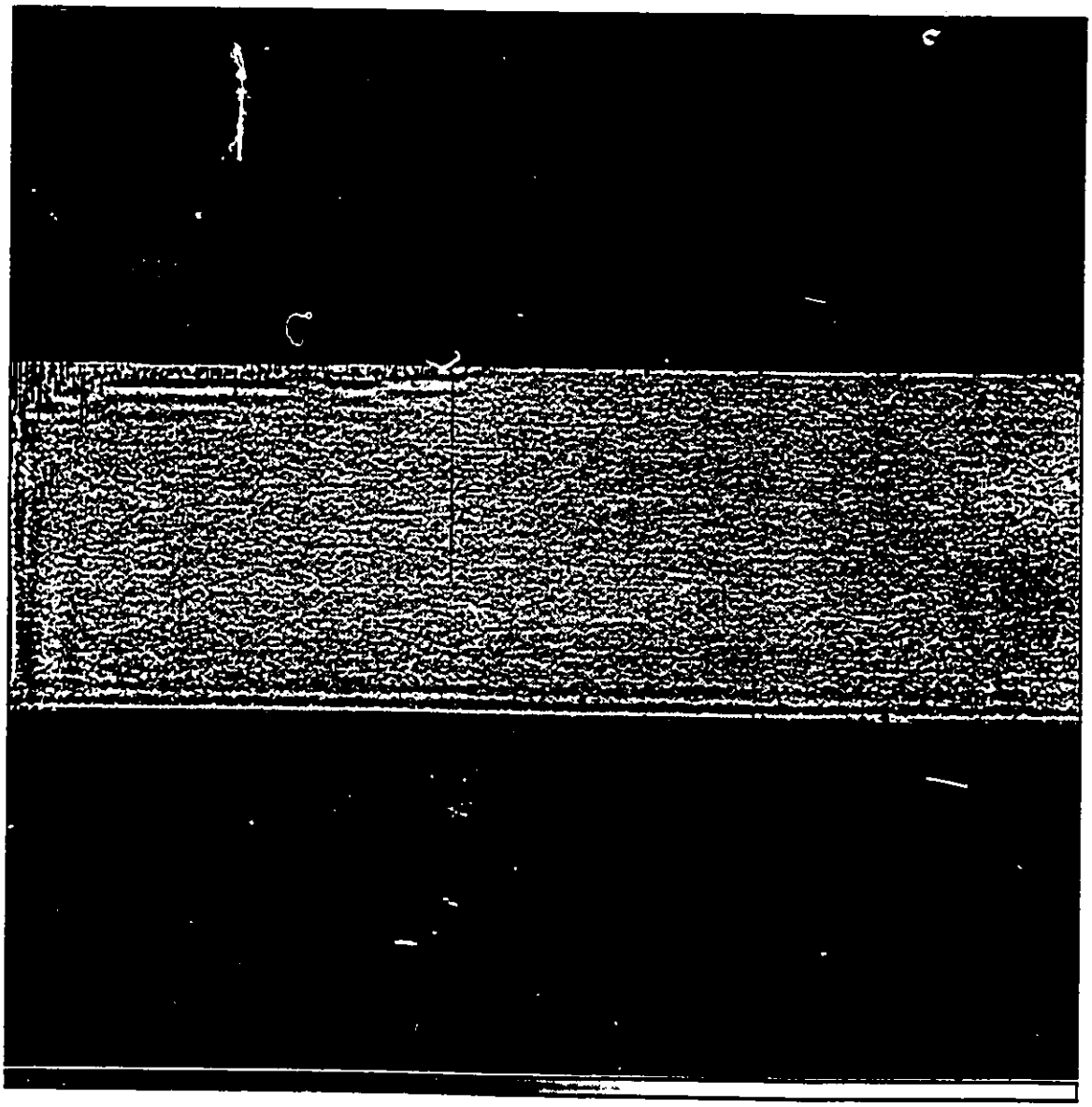

Figure 4.2: The ratio of the MILK.IMH image to the two-dimension fit to the image (obtained using the task IMSURFIT in ARGUS) that was used to remove the pixel-to-pixel variation from all data.

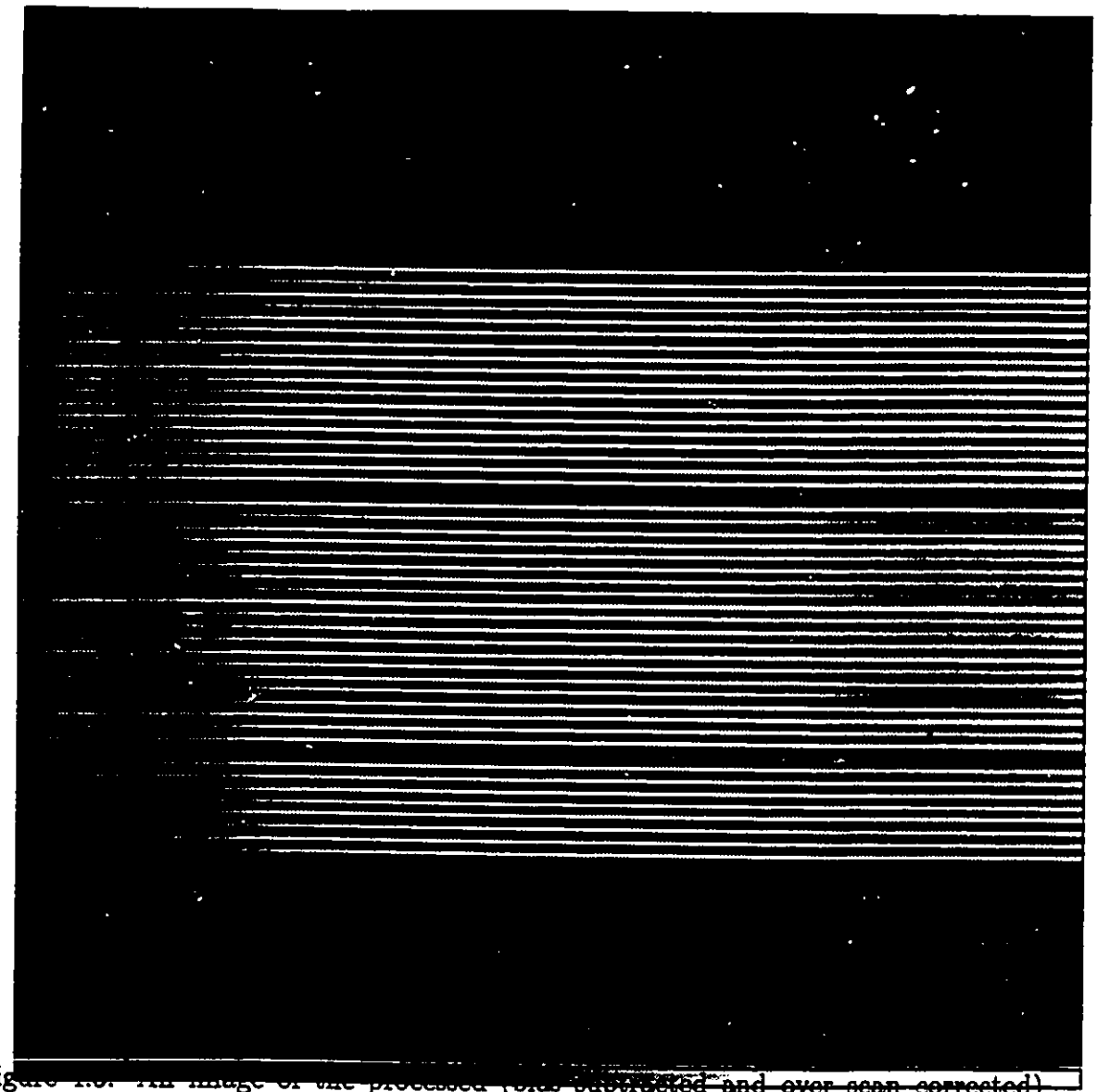

Figure 4.5: An image of the processed (bias subtracted and over scan corrected) and combined dome image DOMECOMB.IMH which clearly shows the 48 horizontal bands that correspond to the 48 spectra recorded on each ARGUS image. The high S/N of the dome images are ideal for finding, tracing and extracting the individual apertures (and therefore spectra).

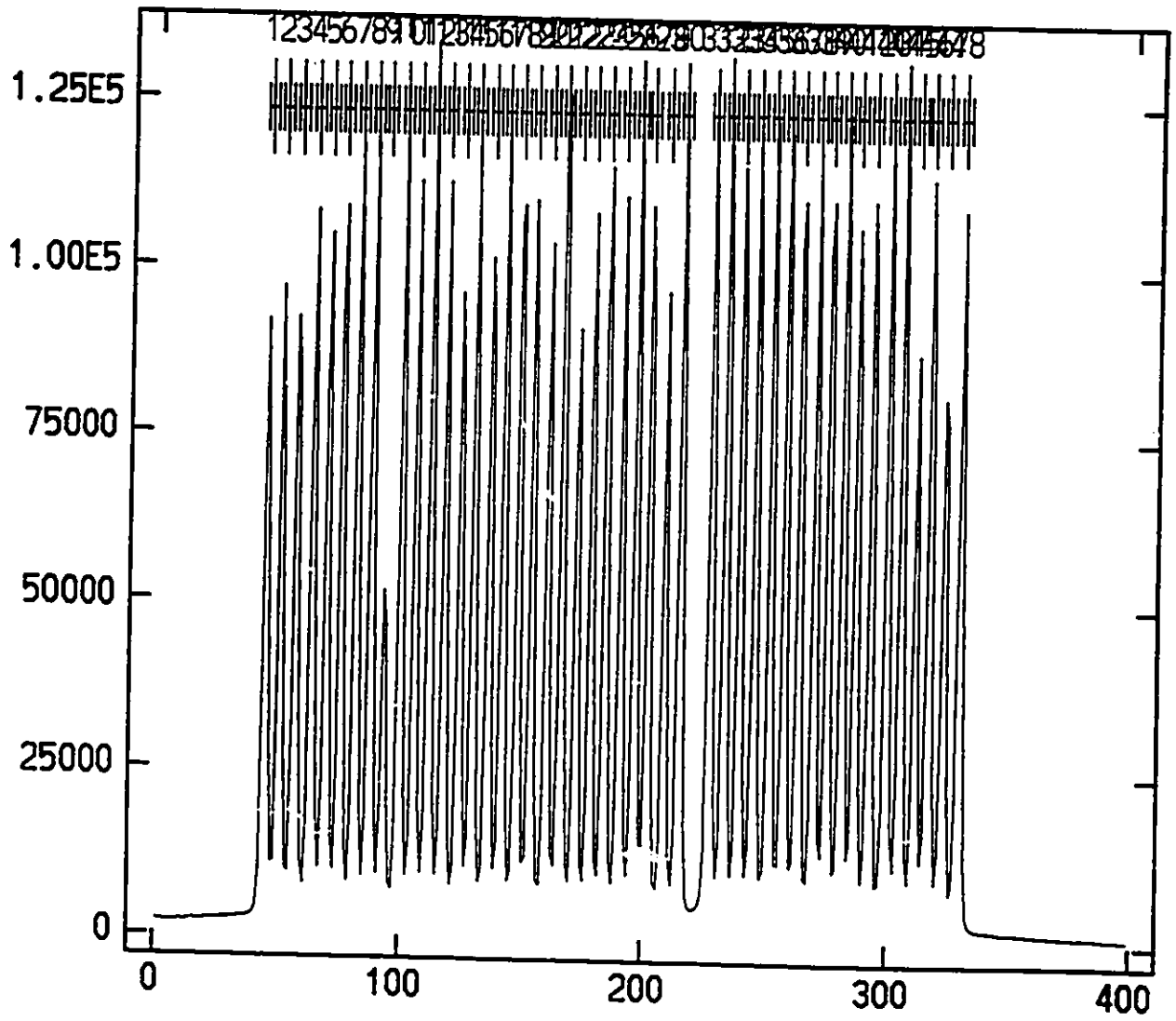

Figure 4.4: A vertical slice of DOMECOMB.IMH used to find and recenter the 48 reference apertures from which all other apertures and spectra can be extracted.

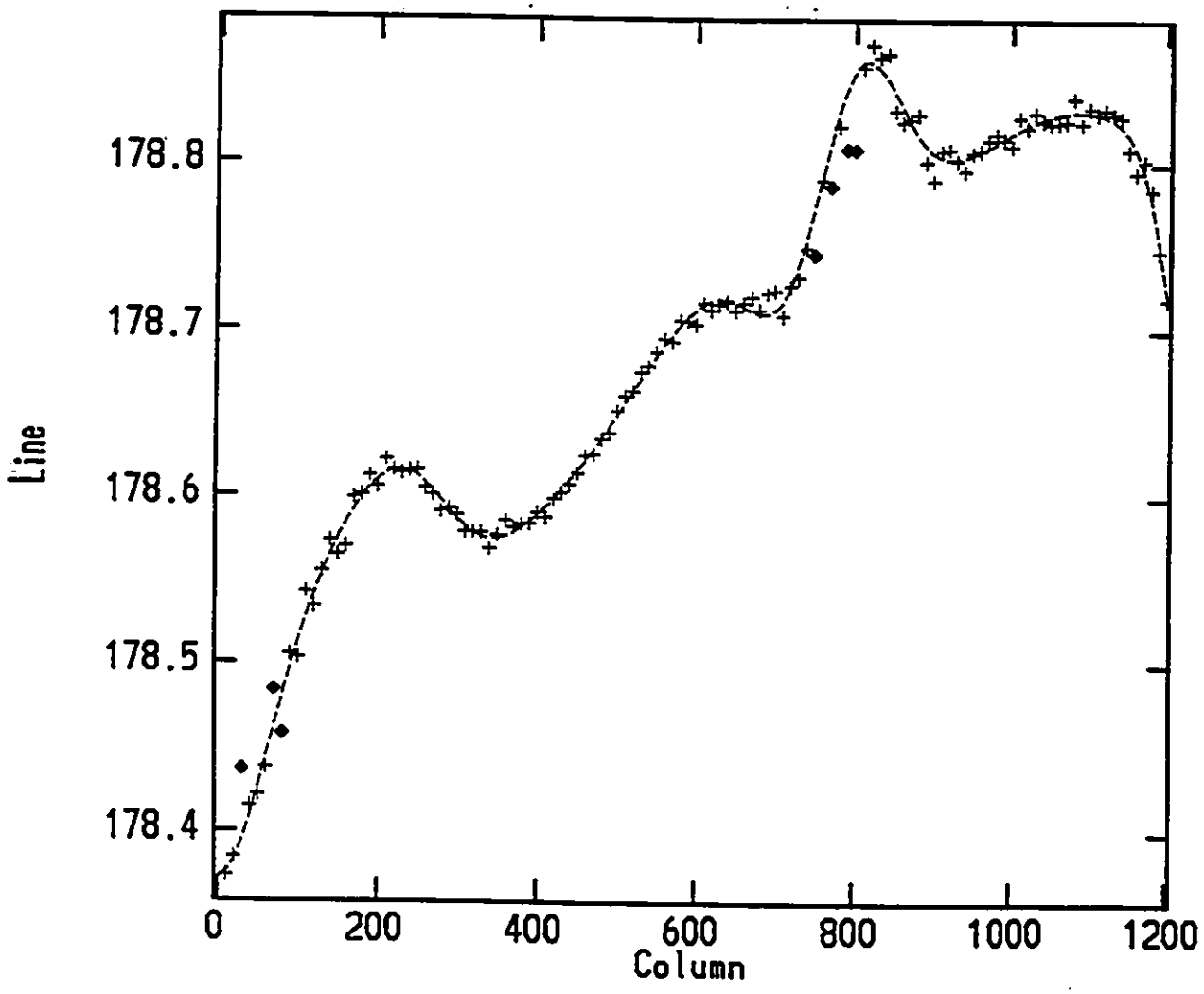

Figure 4.5a: A trace of the 23rd aperture of DOMECOMB.IMH. Notice that the variation of the fiber position along the dispersion axis is less than 1 pixel.

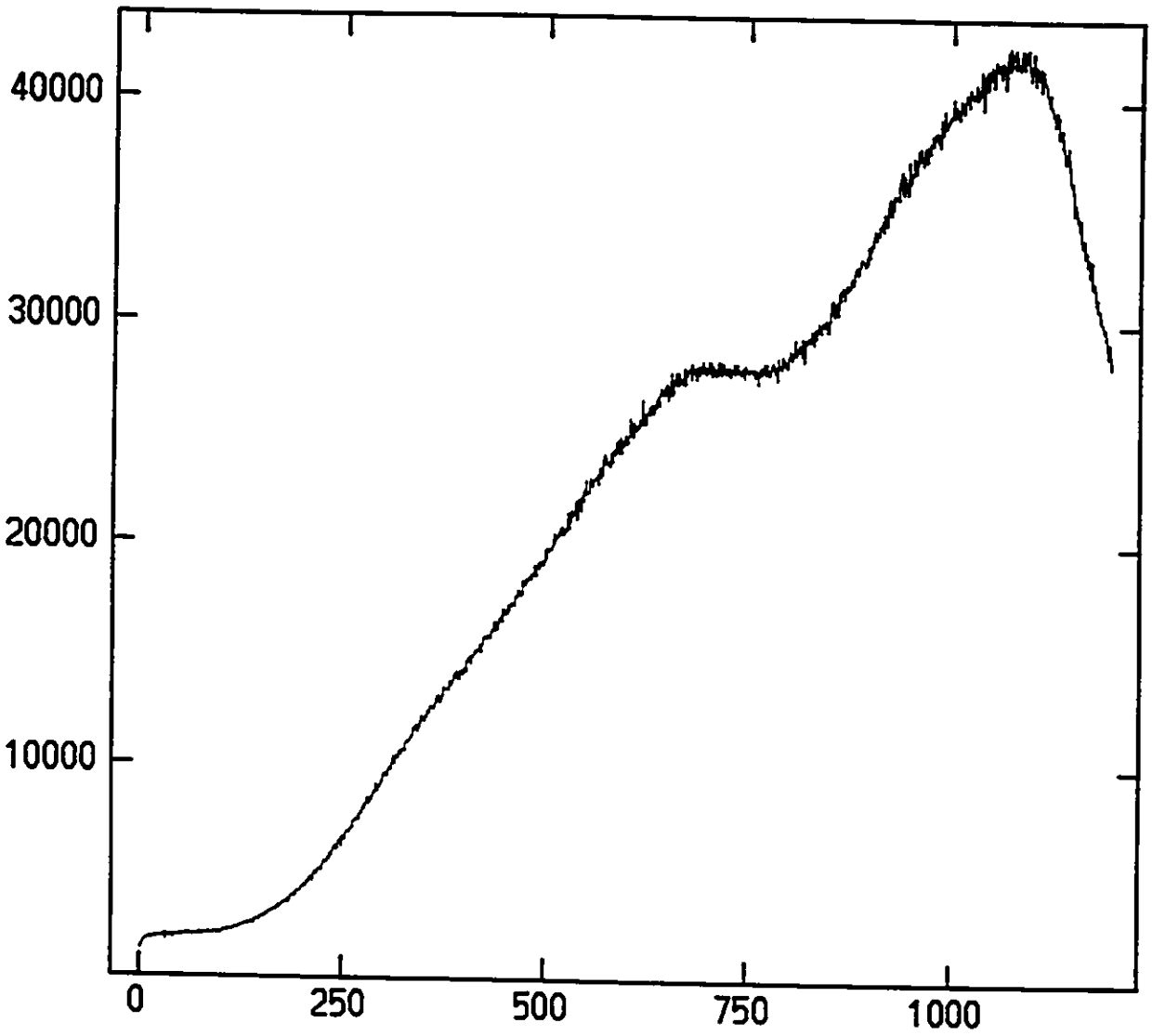

Figure 4.5b: The extracted spectrum from the 23rd aperture of DOMECOMB.IMH. The drop off at the blue (left) end is due mainly to atmospheric extinction and the rapidly declining quantum efficiency of the T2KB CCD chip.

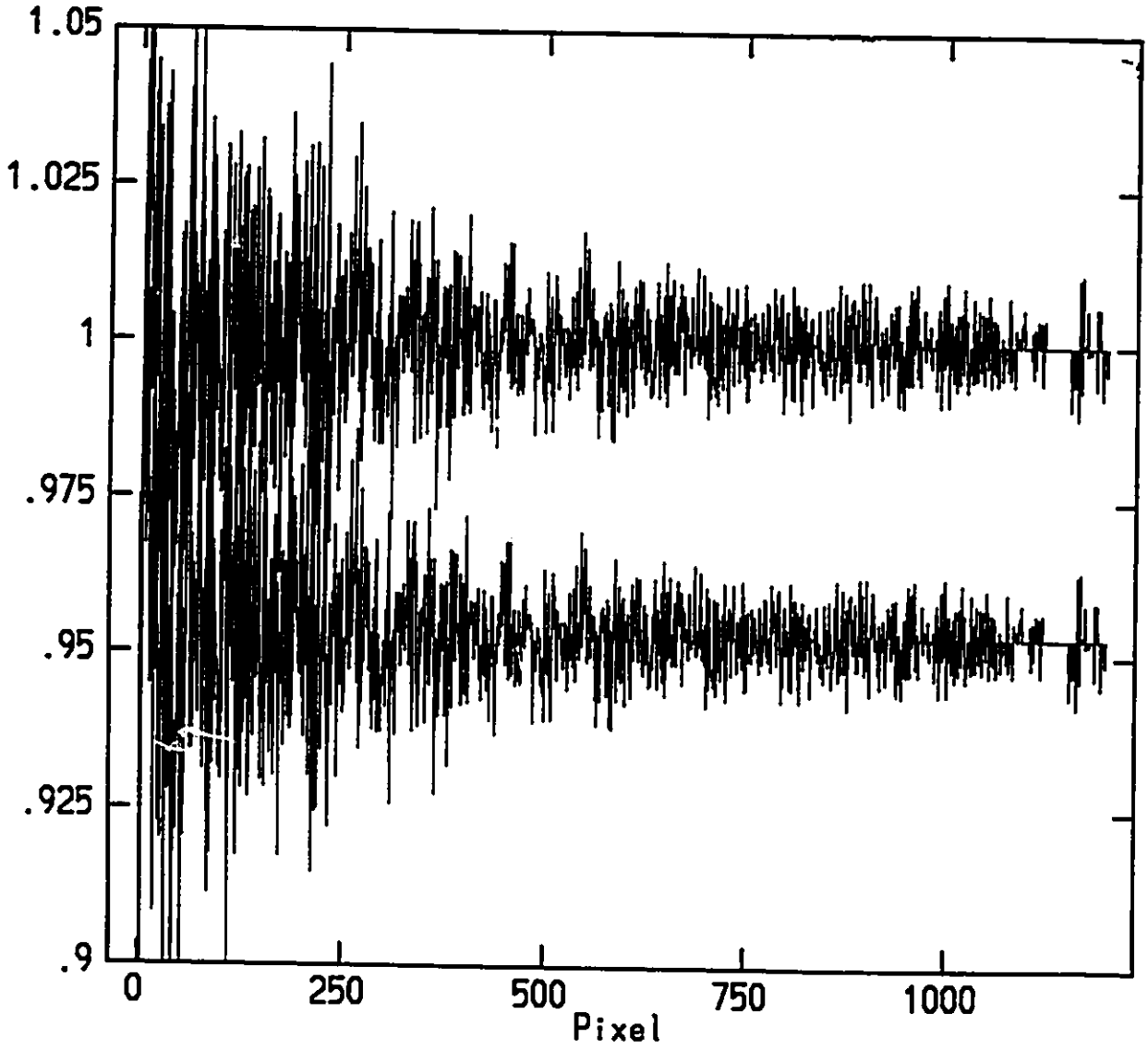

Figure 4.6: The input and output spectra from MSRESP1D (which corrects for the transmission and colour variations in each fiber) for aperture #23 of NORMDOME-COMB.IMH. The throughput corrected (output) spectrum is shifted down by ~0.05 units on the y (intensity) scale from the uncorrected (input) spectrum which is centered on Y=1.0.

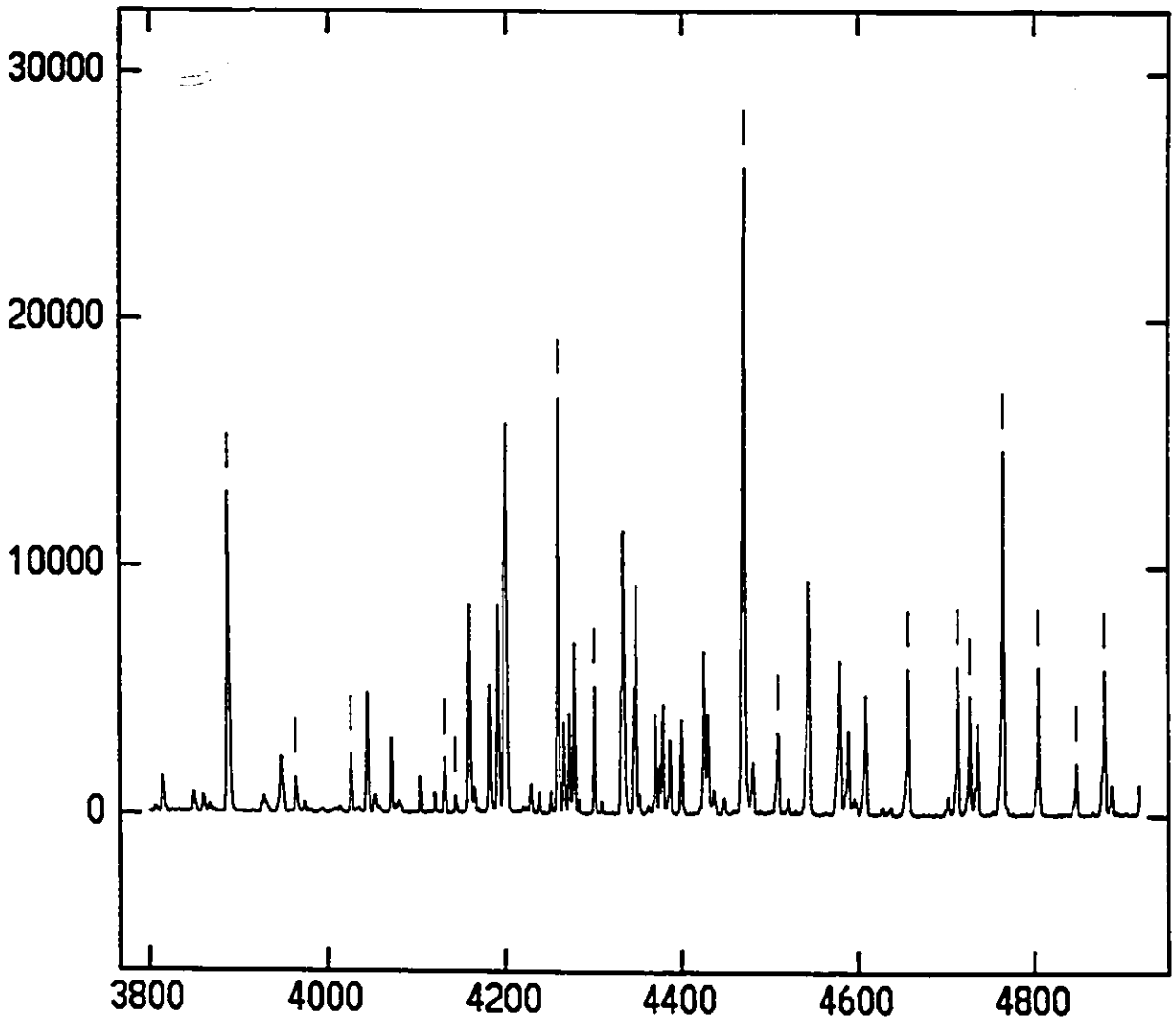

Figure 4.7: An example of a reference He-Ar spectrum from COMP.IMH used by the task IDENTIFY to determine the dispersion solution to the program data. The spectral features which are marked by vertical lines were selected and assigned wavelength coordinates (in $\AA$) upon which the dispersion solutions determined by the task IDENTIFY were based.

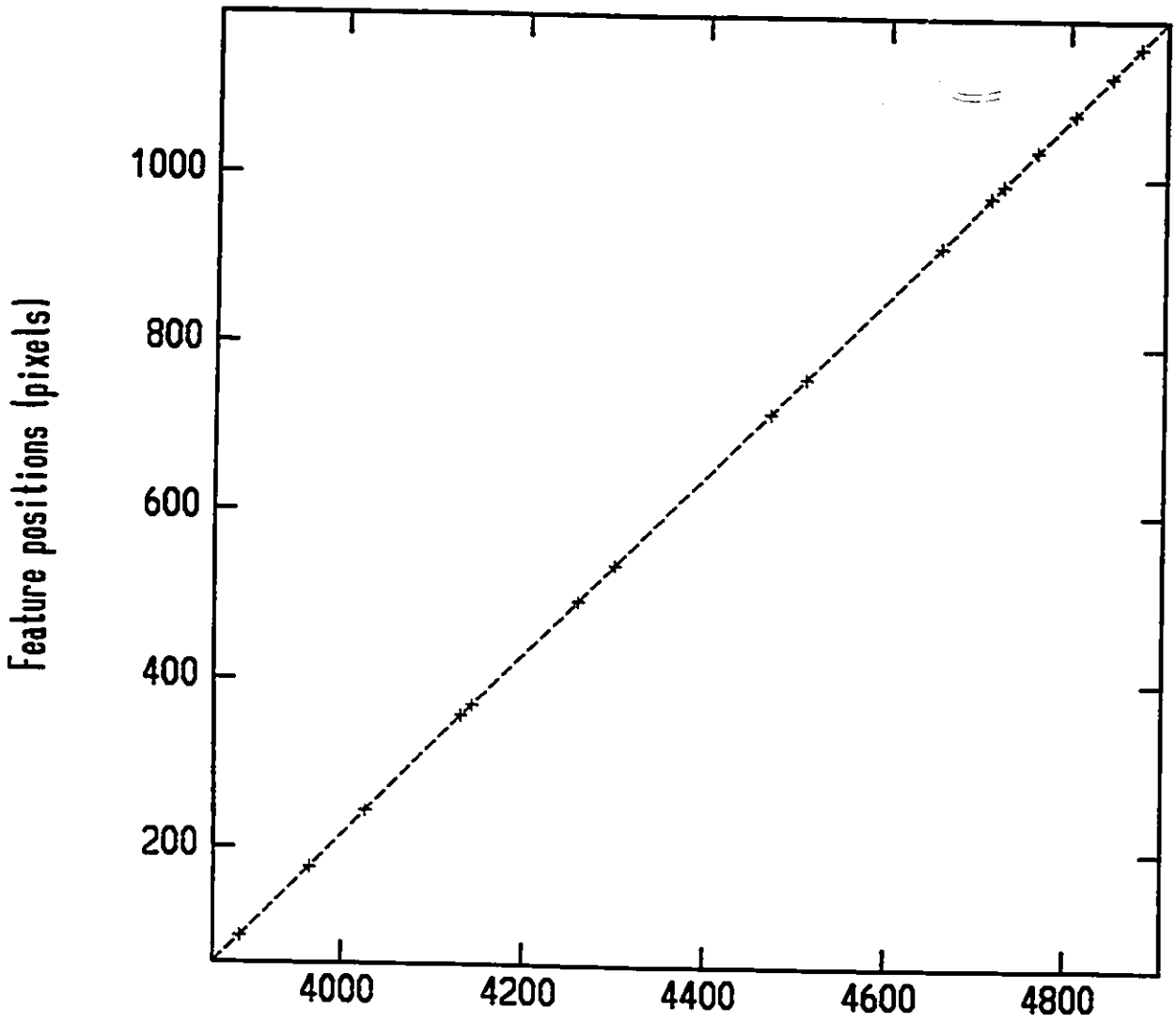

Figure 4.8a: The results of spline interpolation of order 6 between the input wavelengths and pixel coordinates used to obtain the dispersion solutions of the ARGUS spectra. Given is a plot of the pixel coordinate (X) versus the user inputed wavelength coordinate (Y) for a reference arc spectrum from COMP.IMH. The fit is made to 16 points and the rms is 0.0195$\AA$

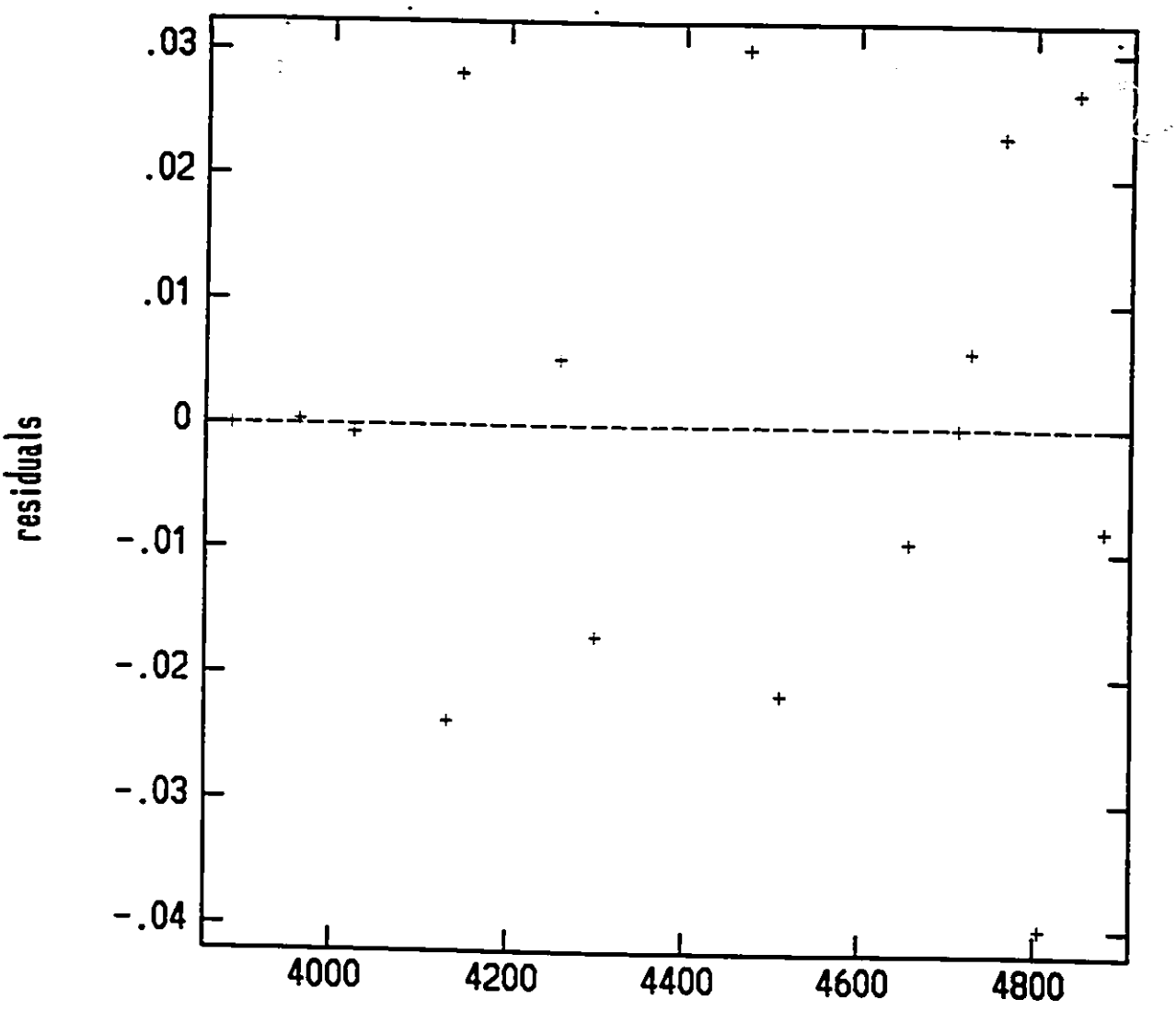

Figure 4.8b: From the spline interpolation of order 6 for the same reference spectrum as in Figure 4.8. Given is a plot of r=(Y-f), the residual of the user inputed wavelength coordinate (Y) minus the fitted (f) wavelength solution, versus Y.

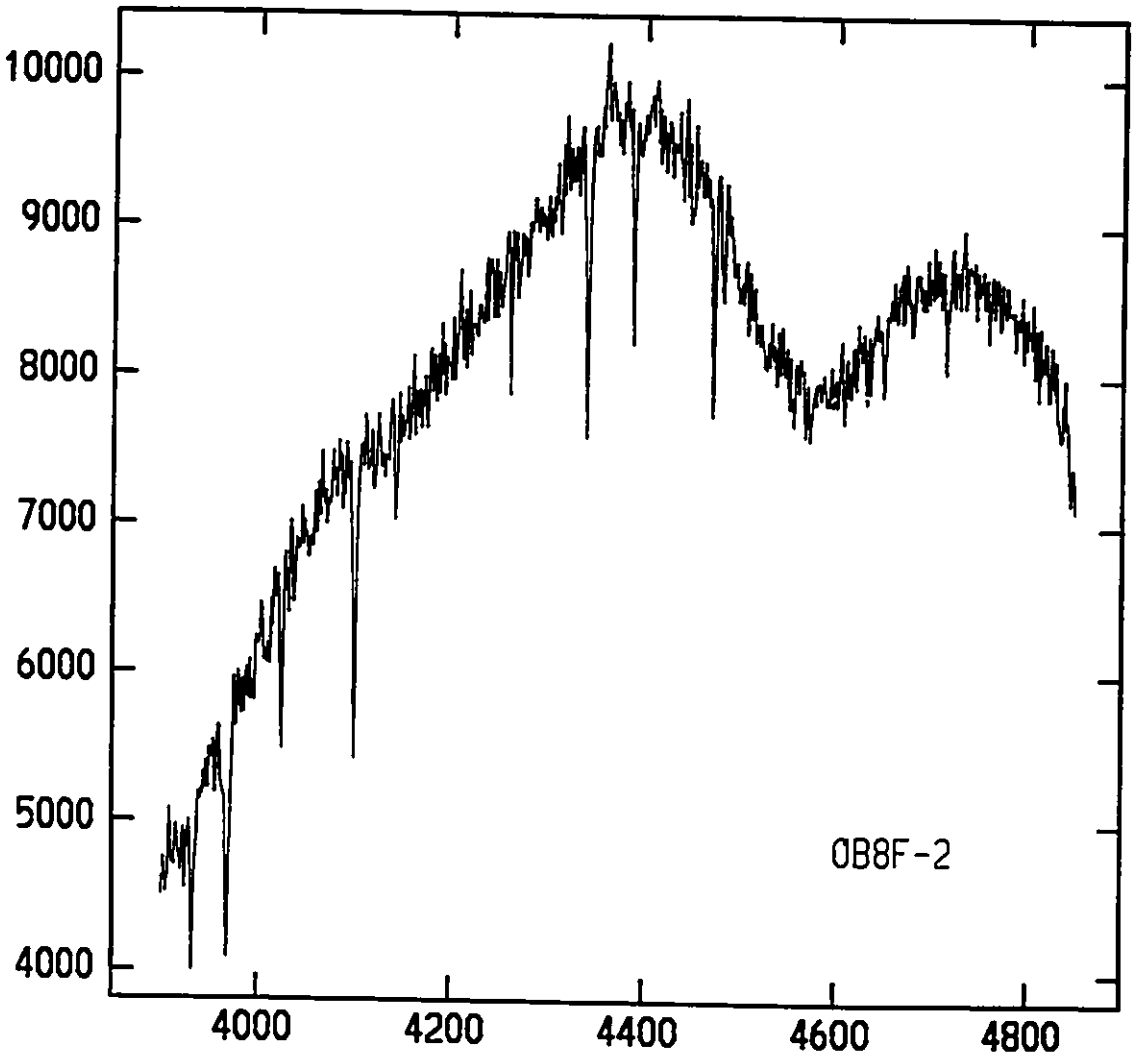

Figure 4.9a: The extracted, pixel-to-pixel, throughput and dispersion corrected, cosmic ray cleaned spectrum of the star observed through aperture #23 on the first night of observing, OB8F-2. The continuum level and sky spectra have not been removed.

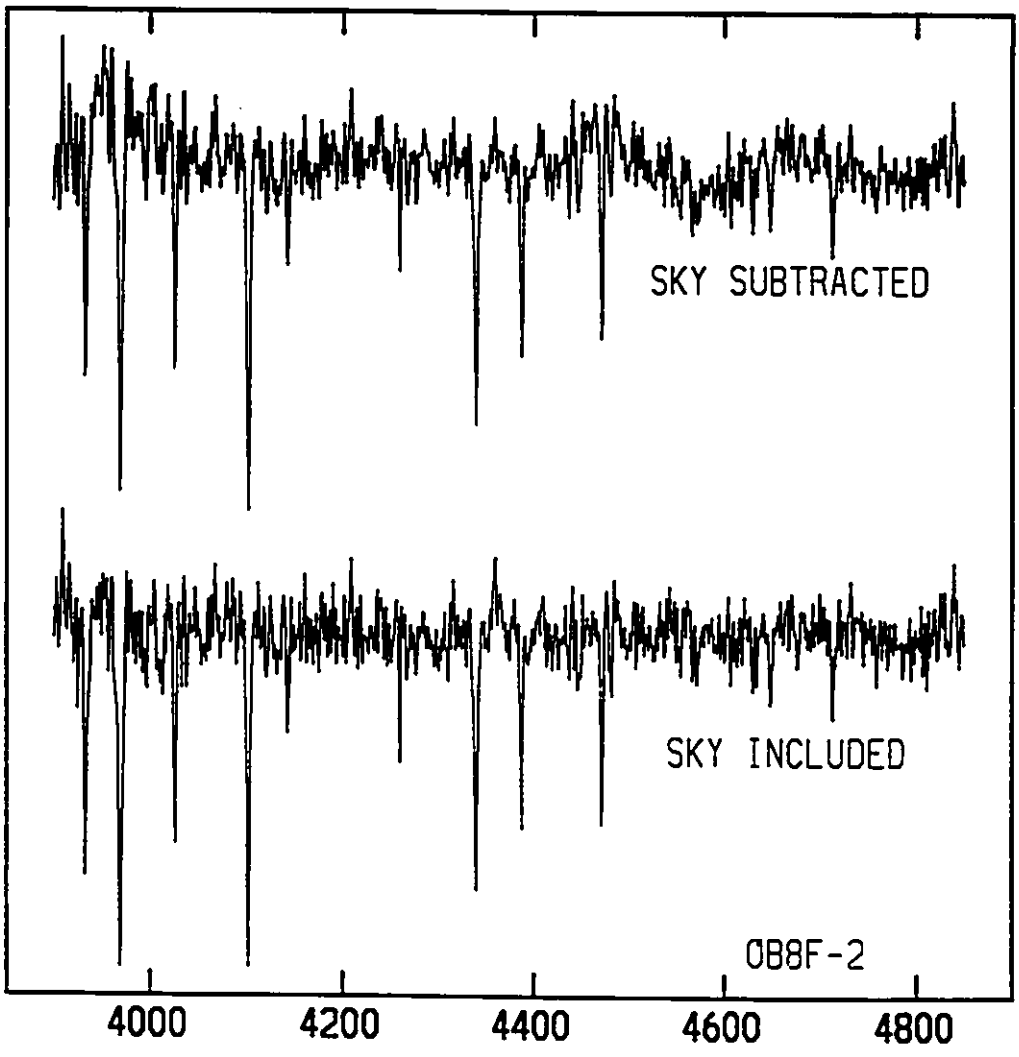

Figure 4.9b: The spectrum of OB8F-2 now with the spectral features from the sky and continuum level removed.

4.2.2 HYDRA Spectroscopic Data for M33

The observations were made during the nights of December 13-14, 1993 using the fiber positioner, HYDRA, and Bench Spectrograph at the Mayall 4-m telescope at Kitt Peak National Observatories (KPNO). Since details of HYDRA have been described elsewhere (Barden *et al.* (1992a), Barden *et al.* 1992b), we will give here only a brief summary. Hydra, which resides at the R-C focal plane of the telescope, consists of 97 red and 97 blue sensitive fibers (core diameter corresponding to 2 arcsec on the sky) and positioning mechanism. Twenty-four feet of optical fiber carry light from the R-C focal plane to the Bench Spectrograph located in an isolated, stable coude room near the base of the telescope. At the R-C focal plane end, each fiber is polished and has optically cemented to it a small right angle prism. The fiber/prism pair is aligned and centered within a magnetic button which is used by a gripper arm to position the fibers along the focal plate. The gripper, based on an "iris-type" shutter mechanism, can position fibers to cover a field up to ~49 arcmin in diameter (vignetted) and ~40 arcmin (unvignetted). The minimum separation between two fibers is 26.5 arcsec. There are also 6 Field Orientation Probes, consisting of seven 200 μm diameter fibers hexagonally packed together, which are used to lock on to the target field. In the coude room, light leaving the fiber is passed through a rear slit viewing TV (for viewing the fibers end), reflected off an aluminum-coated paraboloid collimator and passed through a grating and an axis mount camera (used to optimize the efficiency for a given central wavelength and grating blaze angle) before it falls incident on the CCD detector. To better envision the setup of the fibers at the R-C focal plane as well as in the coude room, we have reproduced, in Figures 4.10 and 4.11, the schematic diagrams of respectively, the fiber button assembly and the Bench Spectrograph from the Hydra Users Manual.

For the M33 observations, we used the blue sensitive fibers and the 2048×2048 thinned Tektronics CCD chip, T2KB. The blue fibers were selected for their good transmission in the wavelength range 3600 to 7000$\AA$ (see Figure 4.12). Note that some fiber to fiber throughput variations exist and are believed most likely to be caused by the quality of the prism at the incoming end of the fiber but this effect is corrected for in the data reduction. The 24 μm per pixel T2KB chip was chosen for its high quantum efficiency at blue wavelengths (see Figure 4.13). The grating used was the KP22 (central wavelength 4500 $\AA$, blaze angle 32.1°) and the axis mount camera used was the Simmons. Spectra obtained using the T2KB chip were found to have a resolution element (*i.e.*, smallest scale for which structure in the spectrum could be resolved) of ~5 pixels across the chip.

Stars selected for spectroscopic investigation were some of the brightest blue stars observed by Wilson (1991). Due to the time of year during which we were granted telescope time, we could observe M33 for only ~5 hours each night. Moreover, although we were granted three nights of observing time, extremely high winds during the second night forced us to close the dome and abandon the project after a little more than 2 hours of integrating on the M33 sources. Similar weather conditions on the third and final night resulted in unacceptably high seeing (on average larger than 3 arcsec) forcing us again to abandon the project. Therefore, the bulk of the object spectra were taken on the first night (when fortunately the weather was favorable) with a few spectra (obtained under poor but not completely unacceptable seeing conditions) on the second night. Object images contained spectra from both program stars as well as random sky spectra. Typical exposure times were 3600 sec. Flat field spectra were obtained before every Hydra field configuration by pointing the telescope towards the Great White Spot on the side of the dome. Comparison spectra, using

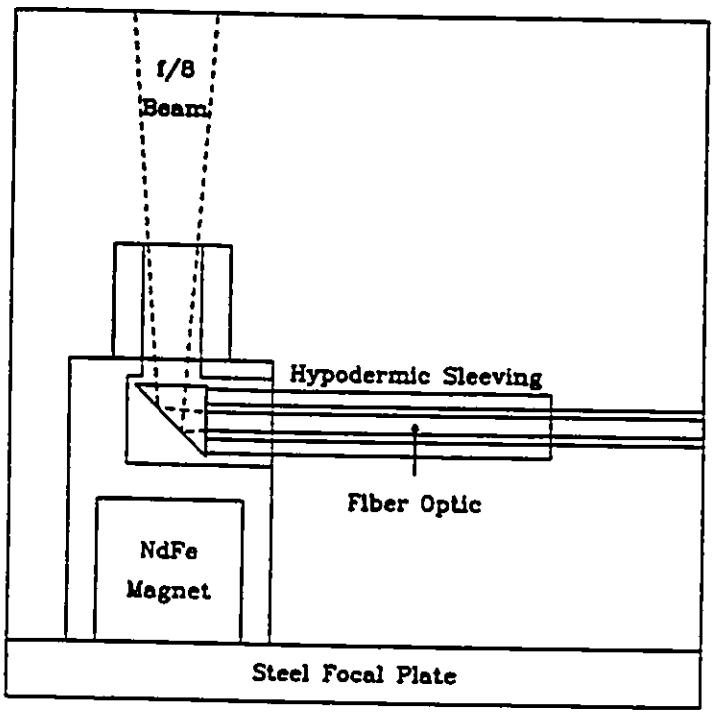

Figure 4.10: A schematic view of a HYDRA fiber button at the R-C focal plane of the telescope. The figure is from the HYDRA Users Manual (Barden *et al.* 1992b) page 12

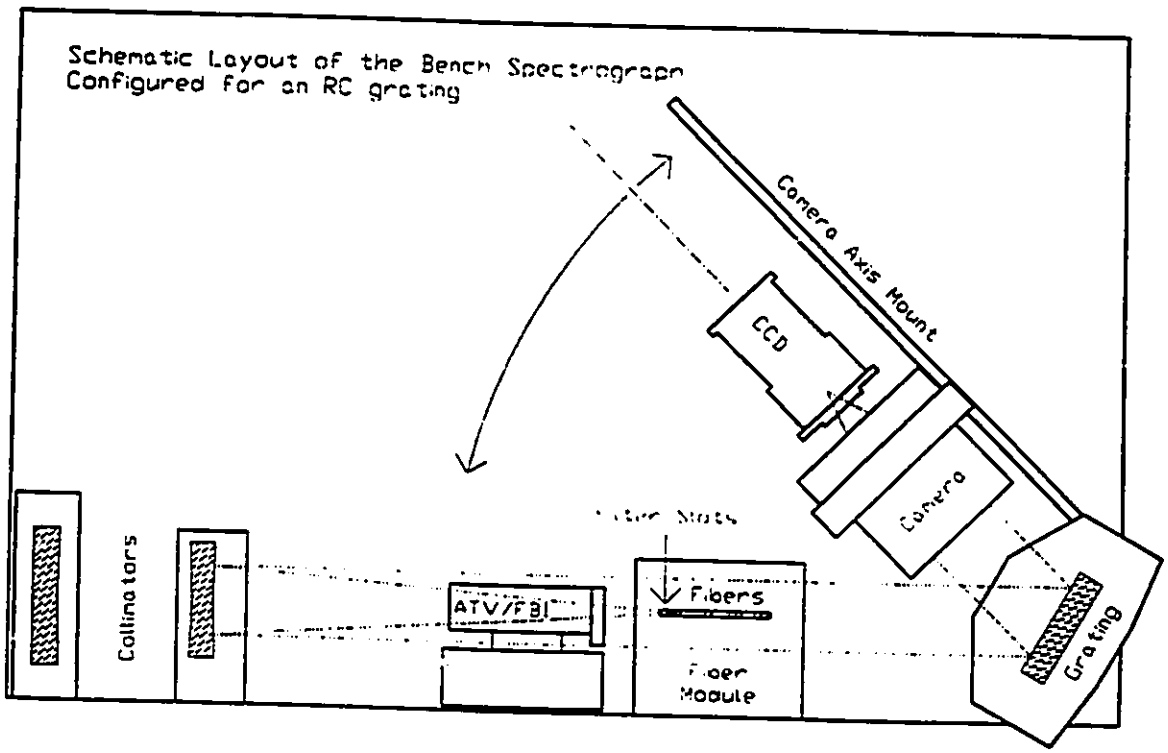

Figure 4.11: A reproduction (from the HYDRA Users Manual, page 16 (Barden *et al.* 1992b)) of the Bench Spectrograph used with the HYDRA fiber positioner on the KPNO Mayall 4-m telescope.

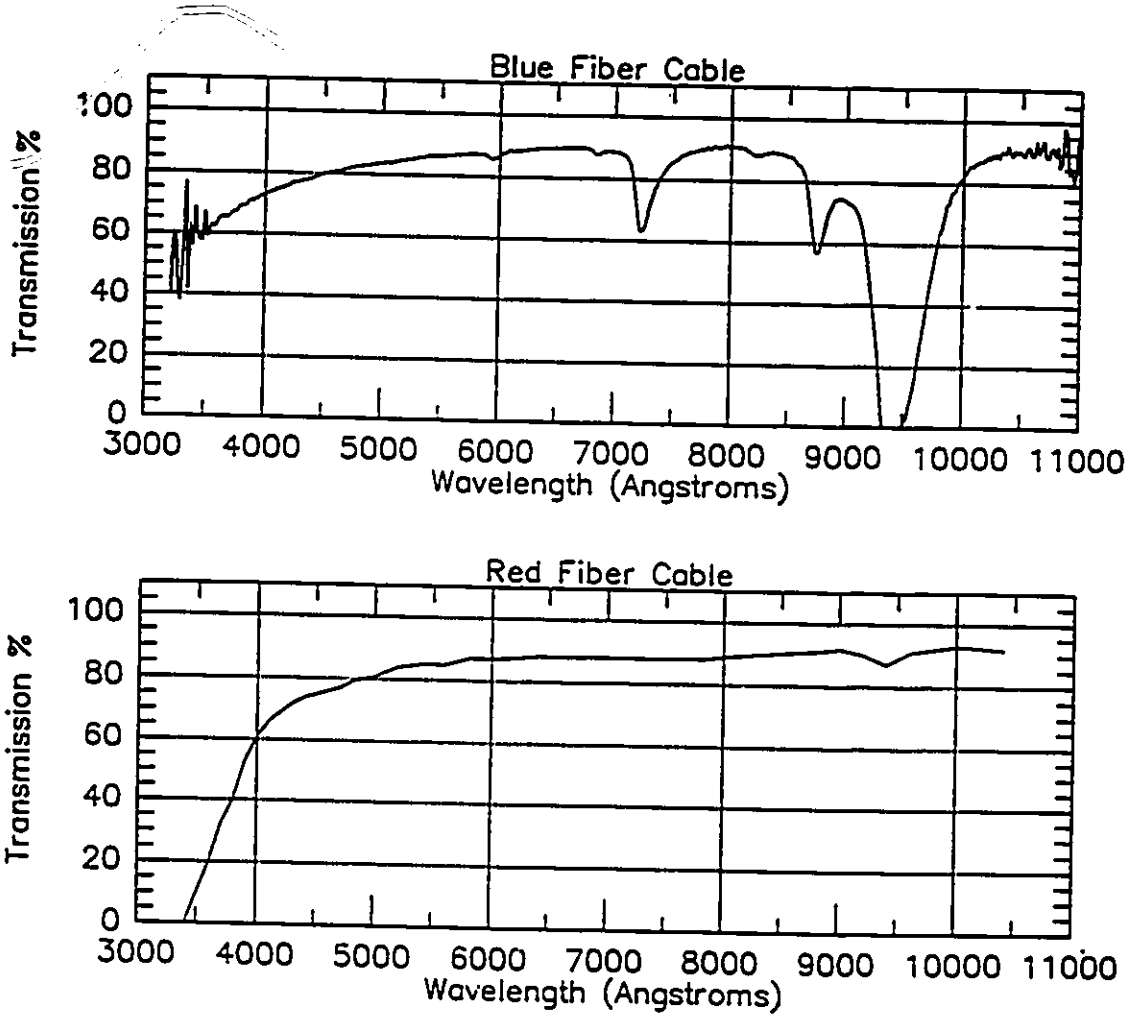

Figure 4.12: The transmission characteristics, as a function of wavelength, of the blue and red fiber cables used to carry light from the R-C focal plane of the telescope to the bench spectrograph in the Coude room. Notice the increased sensitivity of the blue cables at wavelengths λ<4500Å. This figure is taken from the HYDRA Users Manual, page 18 (Barden *et al.* 1992b).

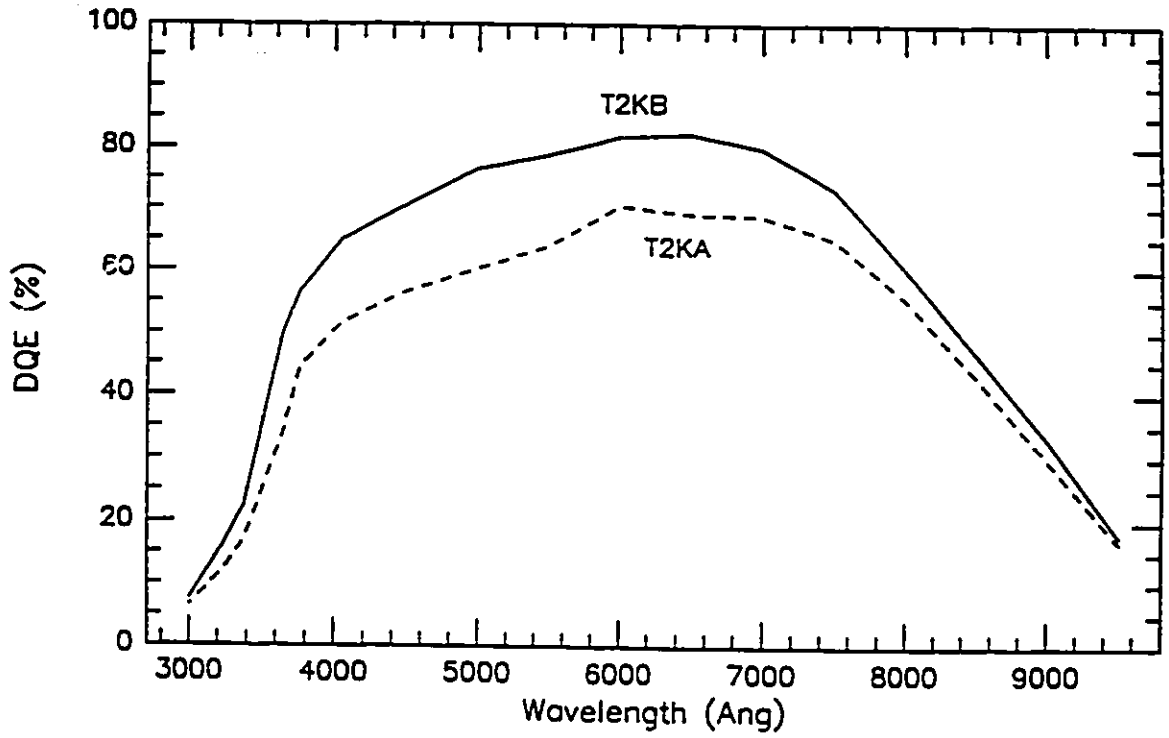

Figure 4.13: The Quantum Efficiency (QE) of the T2KB (used in the M33 HYDRA observations) and T2KA CCD chips as a function of the wavelength. Notice the rapid drop off of the chip response at λ<4000$\mathring{A}$.

a Cu-Ar arc lamp, were taken at both the beginning and end of each configuration while high S/N twilight sky spectra were taken only at the start of each night. Finally, a few zero second bias exposures were taken to verify the uniform bias level of the T2KB chip.

The data were reduced using IRAF image processing packages (CCDPROC *etc.* in CCDRED) and the DOHYDRA task in HYDRA. The first step in processing the raw data was to fit the overscan region of the chip and subtract this level from all program images. Next, the images were trimmed so that only sections containing relevant data remained. Following this, the bias exposures were examined for their structure and zero level. We found that the bias frames were all very uniform: typical count levels were 29 $\pm$1, standard deviations of 1.9 to 3.6 over an area covering 25 pixels. Examination of the averaged frame (obtained using ZEROCOMBINE) showed that a 0.2 adu (=0.64 photons) gradient was running across the chip. The rms of the average bias was 0.98 adu. At this level, correcting for the bias level would not improve the data and therefore the bias was not subtracted from the program data. Dome flats from each configuration were combined (using FLATCOMBINE) to obtain a single flat field image, FLAT.IMH.

The spectra were all extracted and calibrated using the DOHYDRA task in the standard manner. In summary, the location and size of the reference apertures to be extracted (up to 97) were defined using the image FLAT.IMH and traced so as to determine how the spectra shift along the dispersion axis of the chip. The next step was to fit a function to the "average" flat field spectra and divide this fit into each of the individual flat field spectra in order to obtain a normalized flat spectra. The comparison arc spectra were then extracted (using the reference apertures and traces) and normalized (using the appropriate normalized flat field spectrum). Dis-

persion solutions for the comparison spectra was found by using the IDENTIFY and REIDENTIFY task which was called by DOHYDRA. This was in a similar manner to that described in the previous section for the ARGUS spectra. The dispersion solution obtained was used for all other apertures in the reference comparison arc image as well as in the remaining comparison images. This done, the object spectra were extracted and wavelength calibrated. An average sky spectrum was determined and subtracted from the stellar spectra. This concluded the processing, extraction and calibration of the object spectra. Fields that were observed more than once were combined using the SCOMBINE task. Finally, using CONTINUUM, the combined spectra were cleaned of cosmic rays as well as the continuum level removed.

4.3 SPECTRAL CLASSIFICATIONS: THEORY AND SYSTEM

The aim of spectral classification is to group together stars of very similar physical characteristics based on the morphology of their spectra. While the whole spectrum may, in principle, be used, in practice classifications are based on the part of the spectrum transmitted through the earth's atmosphere. The forerunners of the standard system in use today, the empirical MK system developed by W.W. Morgan and P.C. Keenan (Morgan *et al.* 1943) and subsequently revised and extended by Johnson & Morgan (1953), Morgan & Keenan (1973), Abt *et al.* (1978) and Morgan *et al.* (1978), date back to the mid-1800s (see Underhill 1966 and Kaler 1989 for the evolutionary history of spectral classifications). The MK system uses two labels (*i.e.*, is a two-dimensional system) to classify stars: the *spectral* (or temperature) class and a luminosity class. The spectral sequence (A, B, C, D,...), initially motivated by the progression of line patterns in the spectra, was later recognized as a temperature sequence (O, B, A, F, G, K, M, C and S), primarily from observed variations of ratios

of line strengths of successive ionization stages of certain chemical elements in the spectra. The luminosity sequence (classes I to V) was motivated by the finding that stars of the same spectral class could have vastly different luminosities and, therefore, different radii and atmospheric densities. Physically, while the spectral sequence correlates with the temperature of the star, the luminosity sequence correlates with the surface gravity of the star.

The MK system is defined only by standards and therefore is independent of stellar models and is unaffected by changes in the theories and/or interpretations of the theories of stellar structure and evolution. For this reason, characteristics defining spectral classes can only be illustrative (Mihalas & Binney 1981). This said, we have reproduced (in Tables 4.1 and 4.2) Tables 2-1 and 2-2 of Mihalas & Binney (1981) which summarize the primary spectral features characterizing each spectral class. The "early"-type or hot stars are at the beginning of the sequence (*e.g.*, O, B) while the cool or "late"-type stars are at the end (*e.g.*, G, K, M). (The designation "early" and "late" are remnants of a defunct theory of stellar evolution and have no physical meaning but remain widely used in literature.) Spectral subclasses, ranging from 0 at the hot (early) to 9 at the cool (late) end also exist and therefore an O4 star can be referred to as an early type O star, while an O9 is a late type O star; a B0 star is an early type B but of course is later than O9. Note that not all (integer) subdivisions are defined for every spectral class and furthermore, fractional subclasses are also defined in some cases: for example in the MK system *as it stands today*, the O star sequence begins at O3, continues, in steps of whole integers, to O9 and ends at O9.5 while the B star sequence begins at B0 and includes subclasses B0.3 and B0.5 but lacks subclass B4 and B6. Additionally, spectral classes can also be suffixed by an alphabetic letter to convey further information: for example, *n* to denote nebulous

lines, *p* (peculiar) to indicate some lines are unusually strong or weak and *f* to indicate emission at He II λ4686 and at the N III multiplet λ4634-41. We note that the MK classification system is evolving and therefore, subject to change.

Even with the enormous range of different types stars that can be classified using the MK system, there still remain many that lie outside the standard sequences. One such class that is of interest to us are the evolutionary products of massive ($M \gtrsim 20$-$40\ M_\odot$) O stars, the Wolf-Rayet (WR) stars. Named after the astronomers who first discovered them in 1867 (Wolf & Rayet, 1867), these stars are distinguished by the presence of broad, strong emission features due to highly ionized elements (especially helium and carbon and/or nitrogen). The hydrogen emission lines are usually missing. In the rare instances where they are present, they are usually in emission. WR stars are arranged in two sequences based on the dominance of carbon ions (defining the carbon WR or WC stars) or nitrogen ions (defining the nitrogen WR or WN stars). Subclasses to WN and WC stars also exist based, respectively, on ionization stages of nitrogen and the relative widths of the carbon ions (Beals 1938, Smith 1968). For further detail of WR stars and their classifications, we refer the interested reader to reviews by Conti & Underhill (1988), van der Hucht (1992) and Maeder & Conti (1994).

4.4 CLASSIFICATION OF OB SPECTRA: METHODS

In this section we will describe the technique and outline the criteria we used to obtain spectral classifications for the blue stars in M33 and NGC 6822. The classification scheme we are following for the OB stars is based on one used extensively in the field (and described to us originally by P. Massey). The main idea is to

Spectral Class	Characteristic Spectral Features [a]
O	He II lines visible; H lines relatively weak; highly ionized atoms *e.g.*, N III, O III, C III, Si IV visible; strong UV continuum
B	He I lines strong reaching maximum at B2; He II lines missing; H lines stronger; lower ions lines *e.g.*, C II, O II, Si III visible;
A	H lines maximum at A0 and decrease for later types; Mg II and Si II strong; Ca II weak but increasing towards later types
F	H weaker; Ca II stronger; prominent lines of neutral atoms and first states of ionization
G	Ca II lines very strong; prominent neutral metal lines; weak ion lines: strong CH or G band; H lines weakening; Solar-type spectra
K	dominant neutral metal lines; H lines very weak; molecular bands more common; weak continuum at blue wavelengths
M	Strong molecular bands, particularly TiO; some neutral atom lines; Ca I strong

Table 4.1: Principle Characteristics of Spectral Classes

[a] After Table 2-1 of Mihalas & Binney (1981).

MK	Luminosity Class Designations [a]
Ia-0	Extreme supergiant stars
Ia	Luminous supergiant stars
Iab	Moderate supergiant stars
Ib	Less-luminous supergiant stars
II	Luminous giant stars
III	Normal giant stars
IV	Subgiant stars
V	Dwarf or Main Sequence stars

Table 4.2: Principle Characteristics of Luminosity Classes

[a] After Table 2-1 of Mihalas & Binney (1981)

obtain first an approximate spectral and luminosity class for the object by looking for characteristic primary and secondary lines in the spectra and to refine the rough estimates into a final classification by using the extensive OB spectra atlas of Walborn & Fitzpatrick (1990). As we are primarily interested in the O and B stars, we have not attempted to obtain detailed spectral or luminosity classifications for other classes such as A, G or WR stars. Identifications and rough spectral classifications of the A and G type stars were based on comparisons with standard spectra from Janchek & Janchek (1987) while those for the WR stars were based on the comparisons with the spectra of known Wolf-Rayet stars in M33 and NGC 6822 (Massey *et al.* 1987 and Armandroff & Massey 1991)

The first step when looking at any of the spectra is to determine whether the star in question is of type O or B (hereafter OB). The answer to this depends on whether (a) the hydrogen Balmer absorption lines such as Hϵ(λ3970), Hδ(λ4101), Hγ(λ4340) and Hβ(λ4861) and (b) the helium He I λ4471 and/or He II λ4542 are

present. If so, the answer is yes, it is an OB star. Occasionally, the hydrogen absorption lines may be seen in emission, indicating the star is inside an HII region. In this case, it may still be a OB star. Having established the above, we distinguish which class, O or B, the star belongs to. Generally, if the helium lines, He II λ4200 and/or He II λ4542 are observed, the star is an O or perhaps B0 star. If these lines are not seen, the star is B type.

The next step in the classification scheme is to estimate the approximate spectral and if possible, the luminosity class of the star. We begin by considering the O stars. The first step in estimating the spectral class is to establish whether the star is of early (hotter *i.e.*, O3) or late type (cooler *i.e.*, O9). In the case of O stars, the separation is based completely on the relative strength of He II λ4200 and He I λ4471: the two are equal for spectral classes O7/O7.5 and He II gets progressively stronger (weaker) towards earlier (later) type. Having done this, the next step is to estimate the luminosity class of the object. The luminosity class of stars later than O7.5 is set by the relative strength of Si IV λ4116 and He I λ4121. Characteristically, Si IV is much stronger than He I in supergiants but is of about equal strength to He I in main sequence and giant (class III) stars. Additionally, a secondary line, He II at λ4686 is seen in weak emission in supergiants and strong absorption in main sequence stars. The luminosity class of early O stars is based on the He II λ4686 and the two N III λ4634 and λ4642 lines. He II goes from being seen in absorption in main sequence stars, to either "filled in" (or very weak absorption or emission) in giants to finally in strong emission in supergiants. The N III lines are seen in weak emission in main sequence stars and stronger emission in the giants and supergiants.

We now outline the steps to approximately determine the spectral and luminosity classes of B stars. Whether a B star is of early or late type will depend on the

relative strengths of the Si IV λ4089, Si III λ4553 and Si II λ4128 lines, with Mg II λ4481 and He I λ4471 playing some part. The Si IV and Si III lines are seen in all early to mid type B stars: while Si IV is stronger than Si III for stars earlier than B0.5, it becomes increasingly weaker than Si III for stars later than B1 and eventually disappears from the spectrum of stars of class B2 or later. Additionally, stars earlier than B0.2 show He II λ4542 in their spectra while those later do not. Other indicators of the rough spectral class of a B star include the CIII λ4650 and He I λ4713 lines: at around B1, the two are of equal strength with CIII becoming progressively weaker in later types. Mid to late type stars are characterized by the presence of the Mg II λ4481 line in their spectra: while this line is seen in stars as "early" as B1.5, in the late type stars, Mg II is found to be of comparable strength to the neighbouring He I λ4471 line. The luminosity class of late type stars can be estimated by looking at the width of the hydrogen Balmer lines (Hβ, Hδ, Hγ etc.): these lines are seen to be very thin and weak in supergiant stars but become noticeably gradually thicker and stronger in giants and main sequence stars. The luminosity class of the mid type (B0.7 to B2) stars can be estimated by looking at the relative strengths of the Si III λ4553 line to He I λ4471or λ4387: in the supergiant stars, these lines are of roughly equal strength with Si II becoming increasingly weaker than He I in the giants and main sequence stars. Finally in the early type stars, the relative strength of the Si IV λ4116 and He I λ4121 lines determine the luminosity class: in the main sequence stars He I is seen to be much stronger than the Si IV line while in the supergiants, the Si IV is seen to be stronger than the He I line.

Having determined the approximate spectral and luminosity classes of the OB stars, the next step is to fine tune these estimates using the spectral atlas of Walborn and Fitzpatrick (1990). This was done by visually comparing the observed spectrum

with that for a standard star of approximately the same spectral and luminosity class as estimated. In all cases, independent classifications were obtained by the author and P. Massey. These were compared and any differences were examined until an agreement was reached. We note that in the spectral atlas, all early type O stars are of luminosity class "If" or a "III(f)" or "V((f))". As luminosity classes with the "f" designation are redundant with the common classifications V, III and I (without the "f" designation) for the early type O stars, we have used the latter notation in our identifications.

4.5 THE OBSERVED SPECTRA

Using the techniques outlined above, we have obtained spectral classifications for blue stars in M33 and NGC 6822. Due to the relative proximatity of NGC 6822 as well as the excellent weather at CTIO during the observing run, we were able to obtain some very fine data with a moderately high S/N ratio averaging around 60-80 per resolution element. In contrast, the data for M33 were rather poor with an average S/N per resolution element of ~40. This was due to the distance of the galaxy as well as the extremely poor weather conditions at the Kitt Peak summit during the HYDRA run. In both cases, the spectra were often extremely difficult to classify: only 50% of the ARGUS data and less than 40% of the HYDRA data had a high enough S/N to allow even a rough estimate of the spectral type or class. In light of this, we have taken the greatest care not to imply in our classification more confidence than justified by the data. For this reason, some of the classifications consist of only an approximate spectral type or a range of possible spectral classes or subclasses.

The Blue Stars of NGC 6822

Tables 4.3 and 4.4 summarize the results of the spectral classification of the blue stars in NGC 6822 which were observed using ARGUS. Of the 37 stars for which classifiable spectra were obtained, we find 7 to be most likely Galactic foreground stars (based on their spectral classification as A or G type) and 2 to be WR stars in NGC 6822 and thus leaving 28 stars in the galaxy with approximate or definite spectral classes. In the remainder of this section, we will briefly highlight the features of the individual spectra that were used to classify the stars. The discussion follows the order given in Table 4.3 and 4.4 beginning with the earliest types and ending with the evolved WR stars.

The first three objects in Table 4.3, CW030, OB13-9 and CW029 were found to have nearly identical early O star type spectra (see Figures 4.14 and 4.15). The fact that the three stars lie within 2 arcsec of each other inside a bright HII knot in the northern bar of the galaxy suggests that the three spectra may in fact be of one or contaminated by one very strong early type star. From both Figures 4.14 and 4.15, the Balmer lines as well as the He I line at λ4471 can be seen to be self-absorbed indicating that the stars are in an HII region. Lines that give away the spectral class are the strong He II λ4200, λ4542 and λ4686. In OB13-9 (Figure 4.14), the He I 4713 line can also be seen in emission. Based on the clear He I λ4686 absorption and barely visible N III λ4634 lines, the object(s) would be of luminosity class V.

The identification of objects OB6-16 and OB3-7 (Figure 4.16) as late O type stars is based on the presence of the He II λ4200 and λ4542 lines as well as the strong He I λ4471 absorption line. The late nature of these two stars is implied by He I > He II. Luminosity class I for either object is ruled out by the fact that the He II

STAR	α(1950)	δ(1950)	V	(B-V)	SPECTRAL CLASS
OB13-9	19 42 15.77	-14 50 30.4	18.08	-0.76	Mid-Early O
CW030	19 42 15.76	-14 50 33.2	17.49	-0.03	Early O
CW029	19 42 15.84	-14 50 33.0	18.58	0.11	Early O
OB6-16	19 41 59.80	-14 51 20.	18.11	-0.82	O9II
OB3-7	19 41 44.67	-14 49 35.3	18.53	-1.42	O9III / O9.5II
CW102	19 42 12.74	-14 54 12.1	18.27	0.18	O9 / Early B
OB9-12A	19 42 6.60	-14 51 35.3	18.17	-0.46	late O / Early B
OB15-15	19 42 26.01	-14 52 42.5	18.53	-0.94	Composite : O + other
CW138	19 41 56.87	-14 59 23.3	18.40	0.18	B0.2 V
OB8F-2	19 42 0.73	-14 50 10.4	6.92	-0.68	B2.5 V / B1.5 III
OB11-8	19 42 10.80	-14 51 52.4	18.41	-0.64	Early B
OB15-9	19 42 23.74	-14 52 26.5	18.08	-0.78	Early B
CW114	19 42 13.97	-14 56 4.2	18.20	0.12	Early B
CW107	19 42 8.30	-14 53 45.8	18.22	0.12	Early B
CW117	19 42 6.60	-14 56 10.3	18.95	0.14	Early B
OB7F-40	19 42 5.74	-14 53 48.5	18.89	-0.51	Early B I
OB7-15	19 41 59.50	-14 52 43.6	17.50	-0.73	B1 V
CW057	19 42 7.96	-14 51 22.9	18.48	0.12	Early B / B5
CW120	19 42 10.18	-14 56 15.0	17.97	0.16	B1 V
CW008	19 41 44.72	-14 49 35.5	17.73	0.09	B0 III
CW126	19 41 58.84	-14 57 18.7	18.40	0.12	B2 IV / B3 I-II
CW100	19 42 3.09	-14 53 57.9	18.06	0.21	B5 I
CW077	19 42 6.68	-14 52 20.3	16.61	0.26	B5 I
CW061	19 42 0.50	-14 51 45.2	18.28	0.22	B8 I
CW052	19 42 8.18	-14 51 17.3	18.39	0.04	B8
CW089	19 42 30.63	-14 53 0.4	18.48	0.10	Late B
CW069	19 42 6.20	-14 51 57.1	18.83	0.08	Late B / Early A
CW122	19 42 5.86	-14 56 47.1	17.73	0.29	Late B / Early A I

Table 4.3: NGC 6822: OB Spectral Classes from ARGUS spectroscopic data.

STAR	α(1950)	δ(1950)	V	(B-V)	SPECTRAL CLASS
CW017	19 41 41.95	-14 50 11.7	17.92	0.41	Early A I
CW067	19 42 34.27	-14 52 1.0	16.57	0.17	A V
CW068	19 42 6.13	-14 51 53.2	18.54	0.26	A I (classic)
CW116	19 42 8.55	-14 56 10.1	18.85	0.20	A
CW111	19 42 10.84	-14 55 40.5	17.33	0.34	A I
CW112	19 42 13.52	-14 55 47.6	18.81	0.22	A
CW047	19 42 26.17	-14 51 11.6	19.09	0.43	G
CW080	19 42 23.98	-14 52 31.3	18.92	-0.01	WR (N6822-W12)
OB2-3	19 41 42.47	-14 51 24.5	19.37	-0.80	WR (N6822-W3)

Table 4.4: NGC 6822: Other Spectral Classes from ARGUS data.

λ4686 line is seen very weakly in absorption in both spectra. In OB6-16, the N III λ4634 line is seen somewhat in absorption, while in OB3-7 it is in weak emission. The appearance and relative strengths of the Si IV λ4116 and He I λ4144 lines are primarily responsible for the O9-O9.5 subtype classifications.

We identify CW102 as either a very late O or early B star based on the presence of strong He I λ4471, the (weak) He II λ4200 and (very weak) He II λ4542 lines (Figure 4.17). This is a somewhat difficult star to classify due to the filled-in Balmer lines as well as the significant noise level in the spectra. OB9-12A is another star that can only be identified as either a late type O or early type B. Although the He II λ4200 and λ4542 lines are not visible above the noise in Figure 4.17, the presence of the strong He I λ4471 and Si IV λ4089 lines suggests that the star could perhaps be a O8 supergiant which characteristically have very weak He II λ4471 and λ4542 lines.

OB15-15 appears to have a composite O and B spectrum: the presence of the He II λ4200 line suggests the former while that of Mg II λ4481, He I λ4471 and N II at λ3995 and λ4045 suggest the later (Figure 4.18). The Balmer lines are all seen in partial self-absorption implying that there is some nebulosity in the region.

CW138 is classified as a B0.2 star based on the presence of He I λ4143, λ4387, λ4471 and λ4710, the C III/O II blend λ4070, the O II λ4415 and Si IV λ4089 (Figure 4.19). Luminosity class V is assigned based on the strong Si IV λ4121 line compared to λ4116. The very deep absorption line around 4220$\AA$ is not intrinsic to the stellar spectrum, but rather due to a flawed pixel in the CCD chip.

The extremely clean and simple spectrum of OB8F-2 (Figure 4.19) which is composed primarily of sharp He I lines (λ40226, λ4144, λ4387, λ4471 and λ4713) and a weak Mg II λ4481 line suggests a classical B2.5 V star. The spectral type B1.5 III is an alternate possibility and is based on the (very) faint features around λ4552-78 and λ4415 that could be due to the Si III (λ4552-68-75) and O II λ4415 lines.

The spectra of OB11-8 and OB15-9 (Figure 4.20), CW114 and CW107 (Figure 4.21), CW117 and OB7F-40 (Figure 4.22) allow only a rough classification of early B type. There is no indication of the He II λ4200 and λ4542 lines in any of the spectra, suggesting that the stars are later than B0.2. The strong He II λ4471 line unaccompanied by the Mg II λ4481 suggests that the stars are earlier than B1.5. The C III λ4650 line is seen in the spectra of OB15-9, CW107 and CW117, which lends further support to the early B classification. We note that although He λ4471 is fairly weak in OB7F-40, there is some indication that Si III λ4552-68-75 lines are present.

OB7-15 is also identified as an early B type star based on the strong He I

lines (λ3995, λ4009, λ4026, λ4471, λ4713) and missing He II lines (λ4542, 4200 etc.) and Mg λ4481 lines in its spectra (Figure 4.23). The subclass classification follows from relatively weak (compared to other early type B stars) to missing O II λ4640 and C III λ4650 lines. We note that there is some hint of Si III lines at λ4552-68-72 seen in absorption. The luminosity class is based on the strength of the He I λ4471 which is much greater than that of the barely visible Si III λ4553.

CW057 is classified as either an early type or mid-type B star. The uncertainty is a result of a weak absorption feature around 4480$\AA$ which may be either Mg II λ4481 or noise. The lack of Mg II in the spectrum (Figure 4.23) would make CW057 an early type star. Support for the B5 classification is given by the presence of He I (λ4144, λ4387, λ4713) and the strong Si II lines at 4128-30$\AA$. Note that the deep absorption line at ~4500$\AA$ is a result of a flaw on the CCD chip and not due to the object observed.

CW120 is classified as B1 V based on the presence of the He I λ4121, λ4144, λ4471 and λ4713 as well as the O II λ4070 and λ4415-17 and O II-C III λ4650 blend in its spectrum (Figure 4.24). One inconsistency between the observed spectrum and the classification is that the observed C III λ4650 line is somewhat weaker than He I λ4710 suggesting that spectral class B1.5 may also be appropriate.

CW008 is identified as a B0 III star due to the presence of He II λ4542, the very strong Si IV λ4086 and λ4116 and C III-O II blend at λ4650 as well as C III λ4070 in the spectrum (Figure 4.24). Also prominent are the He I λ4387 and λ4713 lines. One puzzling feature in the complete lack of He I λ4144 which is, characteristically, of the same strength as Si IV λ4116 in B0 III stars.

The spectrum of CW126 (Figure 4.25) is relatively easy to classify as an early

to mid type B star due to the clear presence of Mg II λ4481, which is about one half the strength of He I λ4471, as well as C III λ4650 and He I λ4026, λ4144. Most likely, this is a B2 IV star but B3 I-III is also a possibility.

The two stars CW100 and CW077 are both classified as B5 I. While the spectrum of CW100 is noisier than that of CW077 (both in Figure 4.26), the characteristic B5 I lines can be seen in both. The primary indicator of spectral class is the relative strengths of Mg II λ4481 and He I λ4471: it is clear from the CW077 spectrum that Mg II is about half as deep as He I. This is also the case in the CW100 spectrum but harder to see as Mg II is sandwiched between He I and a deep absorption feature due to noise. Other support for the B5 I classification comes from the deep Si II λ4128 and He I λ4144, λ4387 lines as well as the thin Balmer lines in the spectra.

Stars CW061 and CW052 are both classified as B8 I type stars on the basis that He I λ4471 and Mg II λ4481 are of equal strength (Figure 4.27). Although the He I λ4121 and λ4144 line are seen in both spectra, the Si II λ4128-30 line is missing from that of CW061. While similar features, especially the equally strong He I λ4471 and Mg II λ4481 lines, seen in the spectrum of CW089 motivate a late B identification for the star, the rather noisy spectrum makes it difficult to say anything more (Figure 4.28).

The spectra of CW069 and CW122 (Figure 4.29) allow only an approximate late B to early A type classification. The primary indicator for the late B classifications is the relative strengths of the Mg λ4481 and He II λ4471 lines: Mg II is noticeable stronger than He II in the spectrum of CW069 while the two are of roughly equal strength in CW122. There is some evidence for the Fe II λ4233 and λ4583 lines in the spectrum of CW122 lending further support to the late type classification. The

high level of noise in the CW069 spectrum makes it impossible to refine the rough estimate. The possible A star classification is based on the stronger Balmer lines and in some cases, evidence of the Fe II lines.

The six stars CW017, CW067, CW068, CW116, CW111 and CW112 are all identified as A (or potential A for CW112) stars based on their relatively simple looking spectra that are dominated by hydrogen lines. The spectra of CW017 and CW068 (Figure 4.30) are those of classical A I stars: the Balmer lines are very thin and no He I lines to be seen. In contrast, CW067 is a typical A V star: while the spectrum is still very simple and composed primarily of the hydrogen Balmer lines, these are seen to be very broad. The difference between the class V and I A stars is easily seen in (Figure 4.31) which compares the spectrum of CW017 with CW067. The stars CW116 and CW111 both show some indication of the Fe I, IIλ4383 (Figure 4.32). Finally, although the spectrum of CW112 (Figure 4.33) resembles that of an A type star, the large noise level makes the classification only approximate.

It is immediately clear from the spectrum of CW047 (Figure 4.34) that it is a G type star: the primary indicator of this is the glaringly obvious deep, broad G-band near λ4300 as well as the very strong Fraunhofer H and K lines of Ca II at λ3634 and λ3968 in its spectrum. The "late type" classification is based on the presence of the Fe I lines at λ4046, λ4385 and the Ca I lines at λ4227 and λ4435-55. Mn I at λ4031-34 is also clearly visible in the spectrum.

Finally, CW080 and OB2-3 are identified as WR stars based on the large number of broad emission and relatively few absorption lines their spectra (Figure 4.35). Subsequent to our classification, we realized that both these stars had previously been identified and confirmed as WN stars by Westerlund *et al.* (1983) for CW080

and Armandroff & Massey (1985) and Armandroff & Massey (1991) for OB2-3. The WR nature of both stars is determined by the Hydrogen Balmer lines Hϵ(λ3970), Hδ(λ4101) and Hγ(λ4340) as well as He II λ4542 , λ4686 seen in strong emission. We can also see that OB2-3 is a WN star based on the strong and broad N III emission features at λ4515 and λ4634-41. Evidence that CW080 is a WN star is somewhat shakier: although the N III λ4515 line appear slightly in emission, the N III λ4634-41 lines cannot be distinguished from the noise.

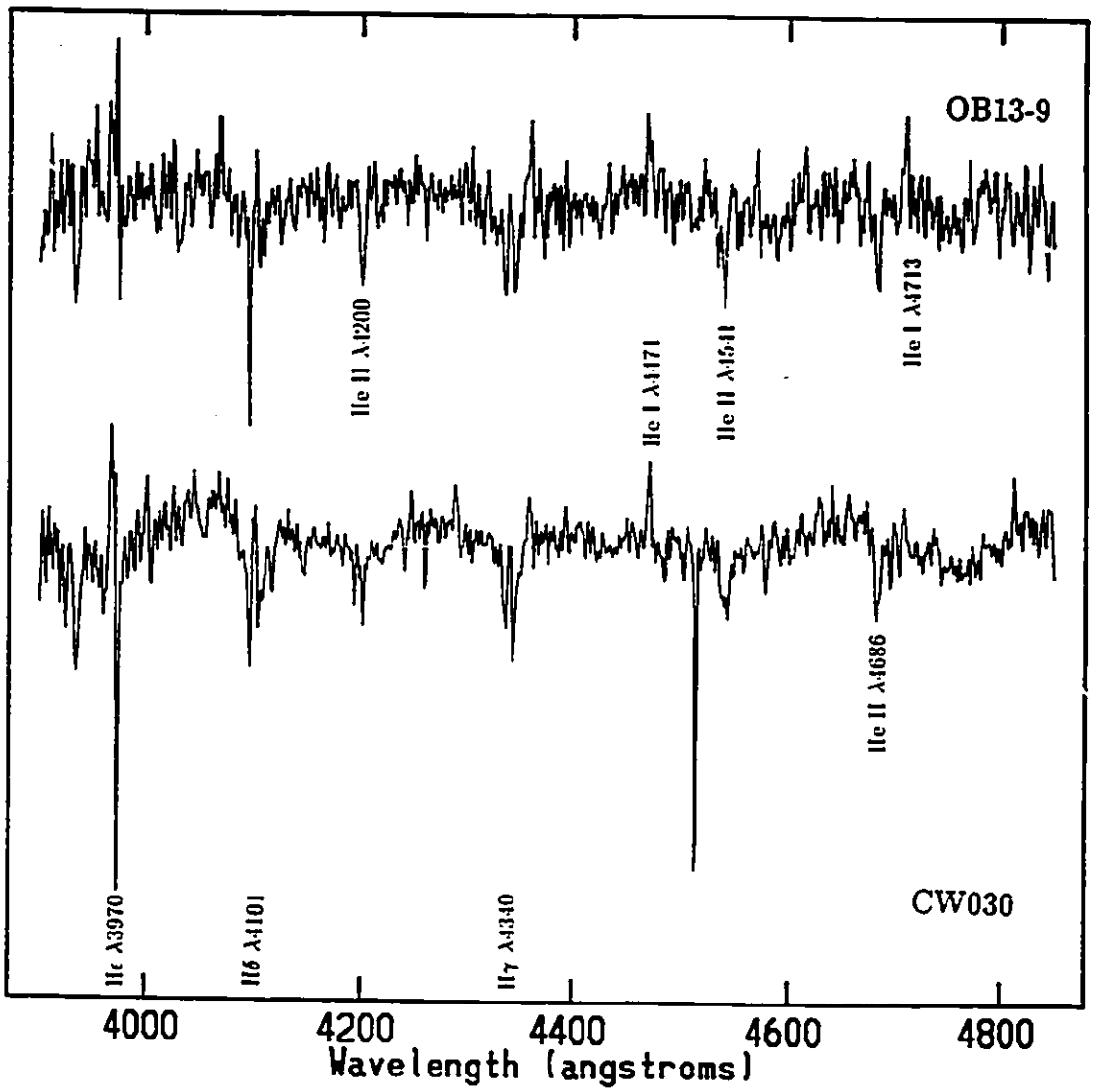

Figure 4.14: The spectra of early O type stars CW030 and OB13-9 located within a tight HII region in NGC 6822. Notice the strong He II λ4200, λ4542 and λ4686 lines which are characteristic of an O star. The self-absorbed Balmer lines and He I λ4471 indicate the stars are in an HII region.

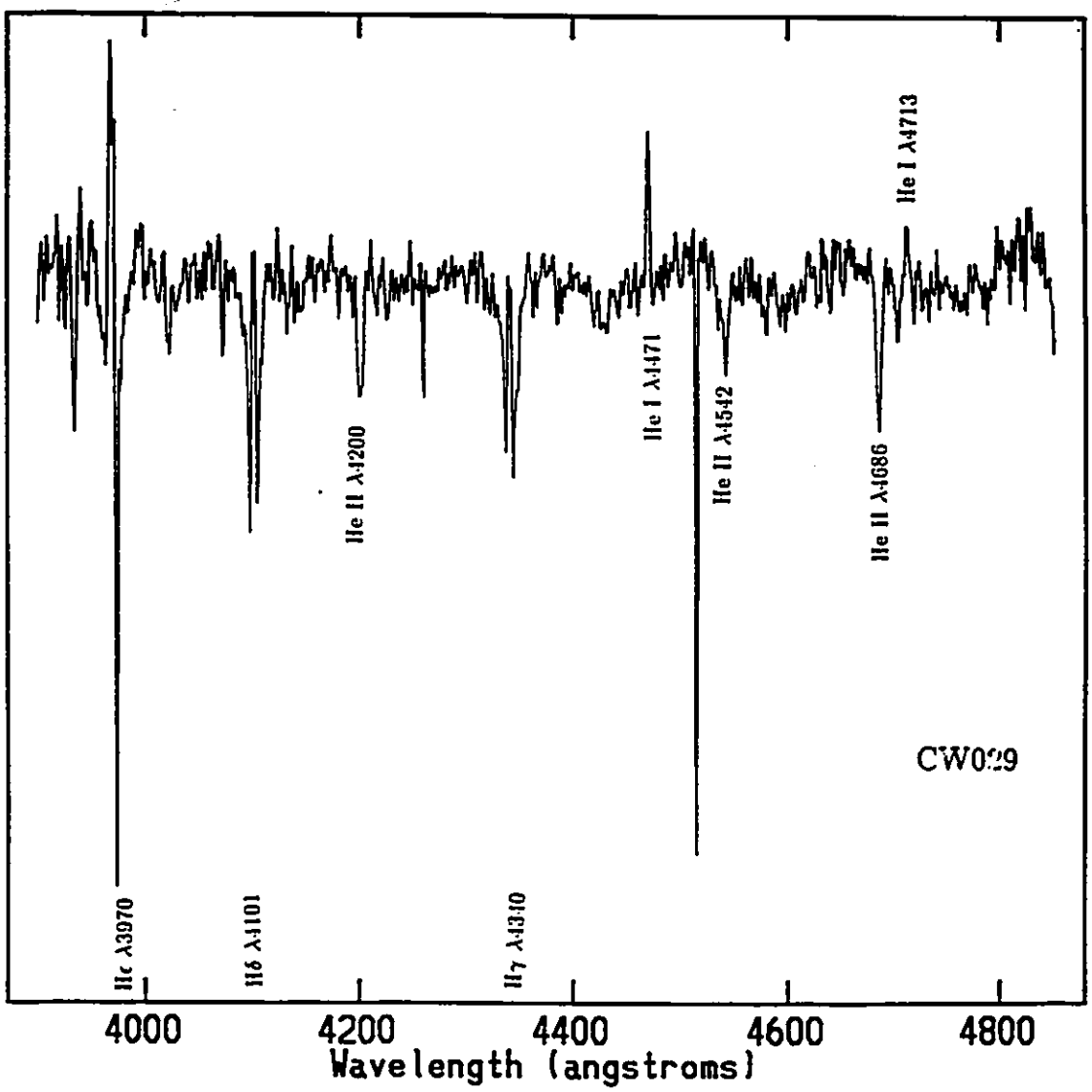

Figure 4.15: The spectra of the early O type star CW029 in the same HII knot as CW030 and OB13-9 in NGC 6822.

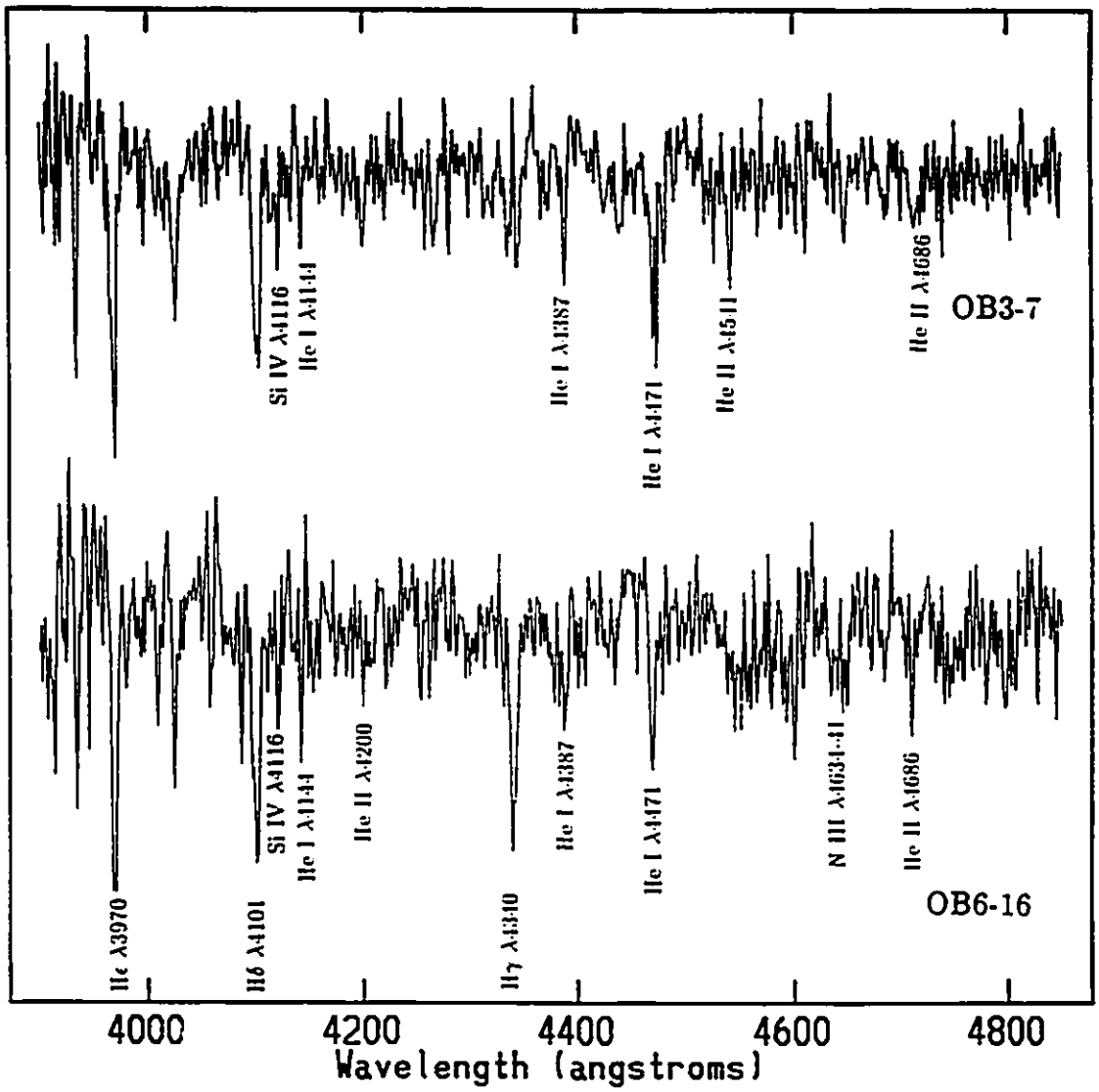

Figure 4.16: The spectra of the late O type stars OB6-16 and OB3-7. Notice the presence of the He II λ4200 and the strong He I λ4471> He II λ4542.

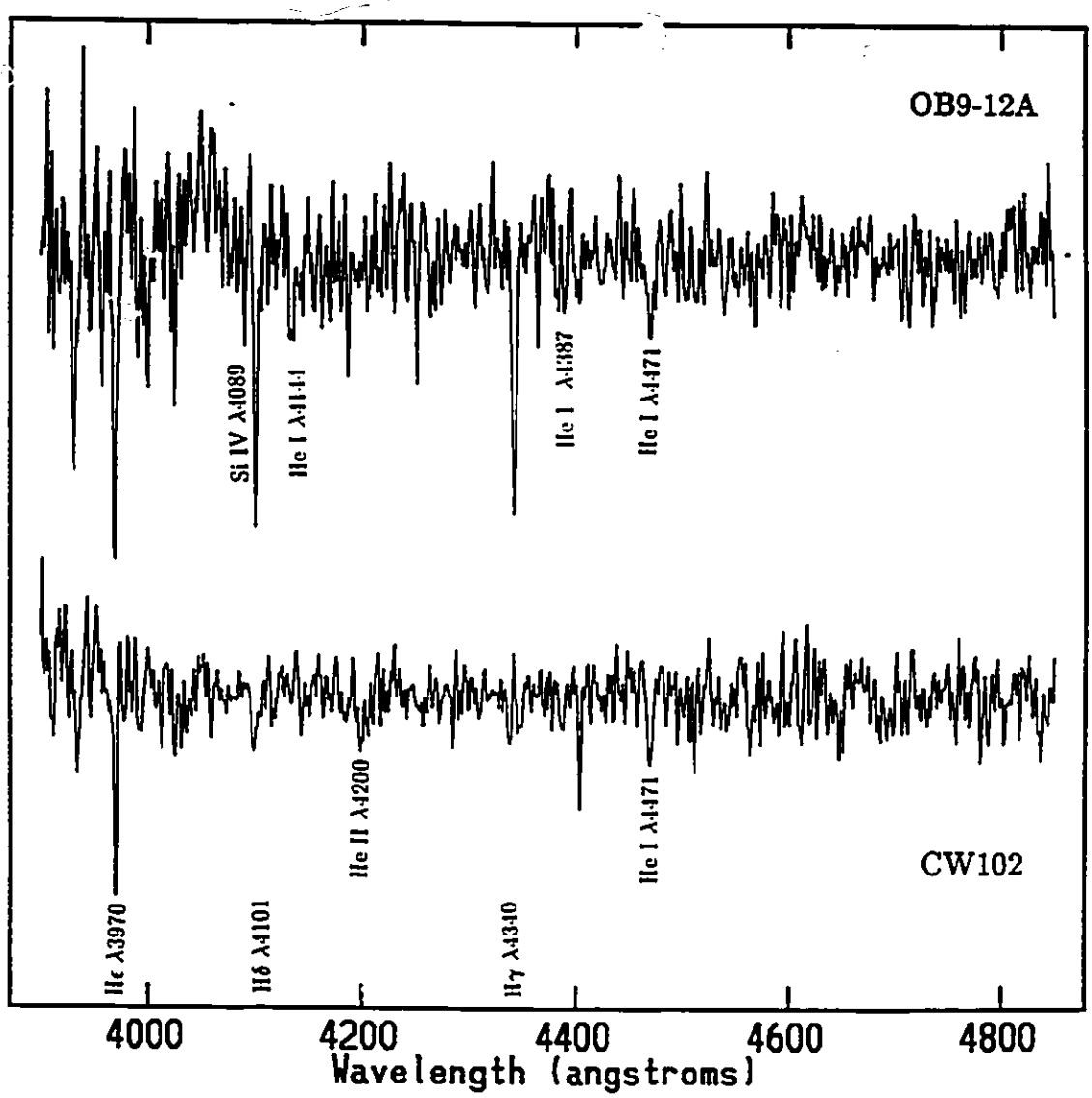

Figure 4.17: The spectra of the late O or early B type stars CW102 and OB9-12A. Notice the presence of strong He I λ4471 and weak to non-existent He II λ4200, λ4542 lines. The Si IV λ4089 line in OB9-12A suggests that the star could perhaps be a O8 supergiant.

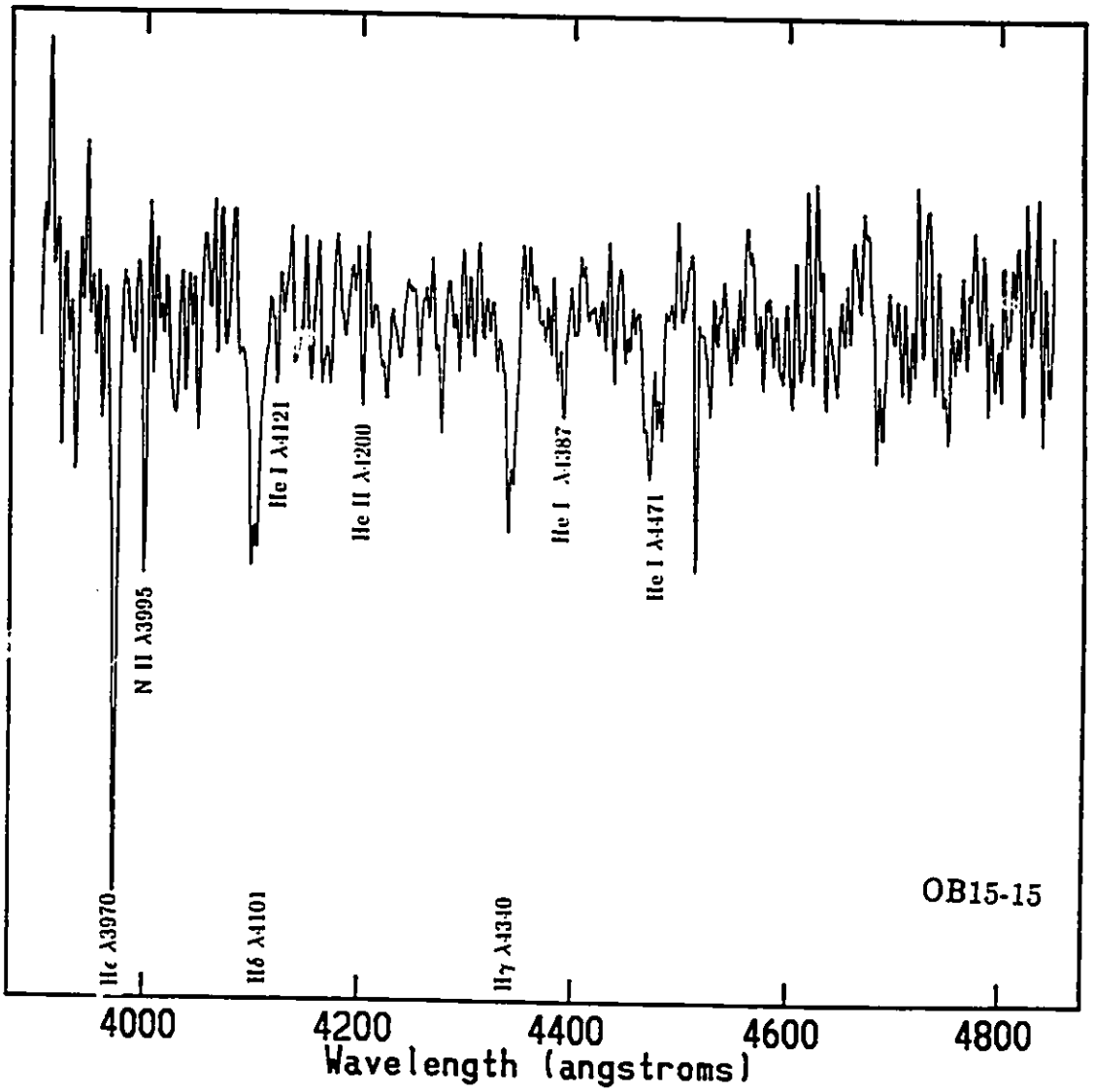

Figure 4.18: The spectra of the composite O and B type star OB15-15. The early classification follows from the presence of He II λ4200 while the late classification from the presence of Mg II λ4481, He I λ4471 and N II at λ3995 and λ4045.

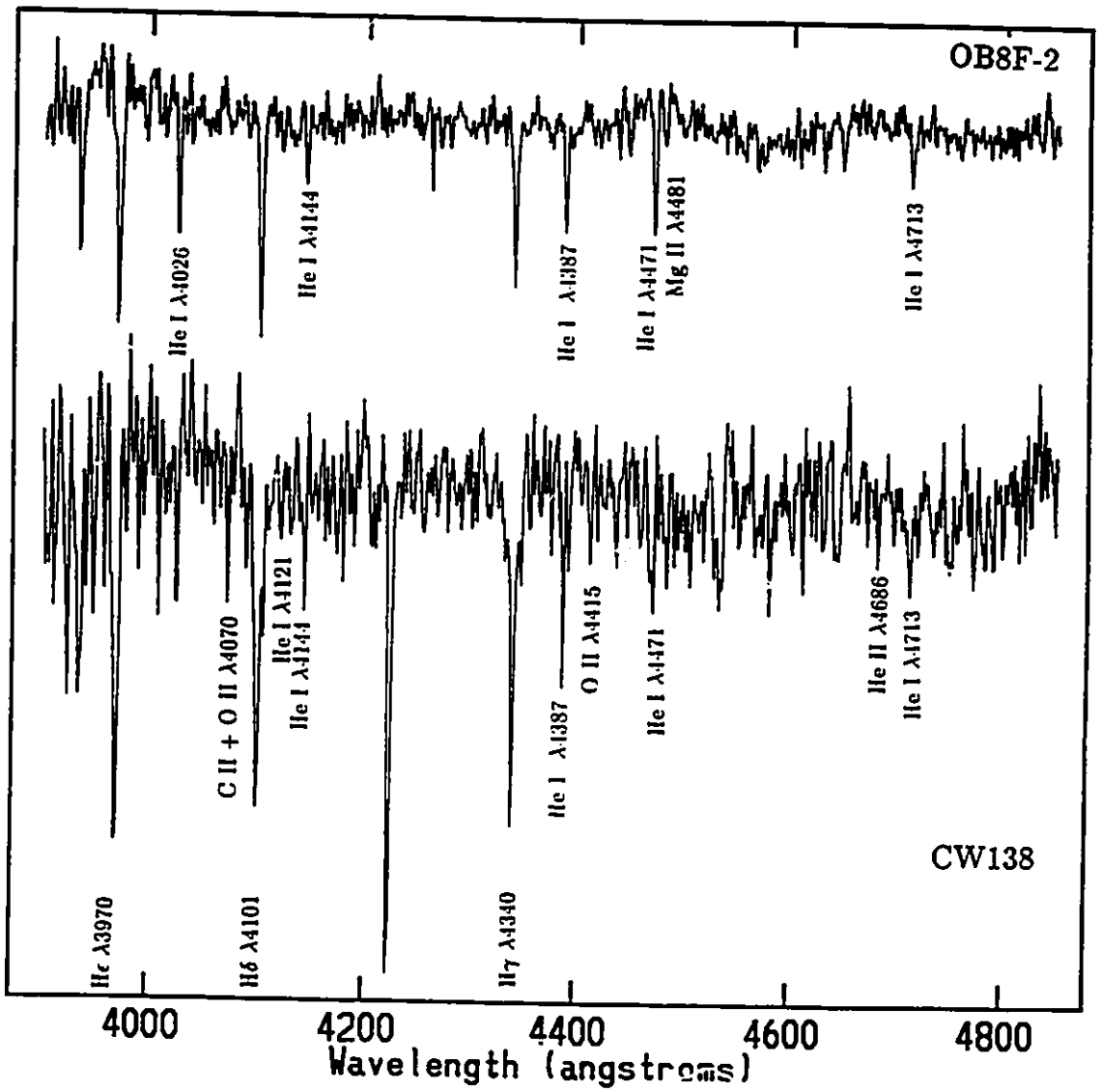

Figure 4.19: The spectra of the early to mid B type stars CW138 and OB8F-2. CW138 is classified as a B0.5V star and OB8F-2 is either a B2.5 or B1.5 III star.

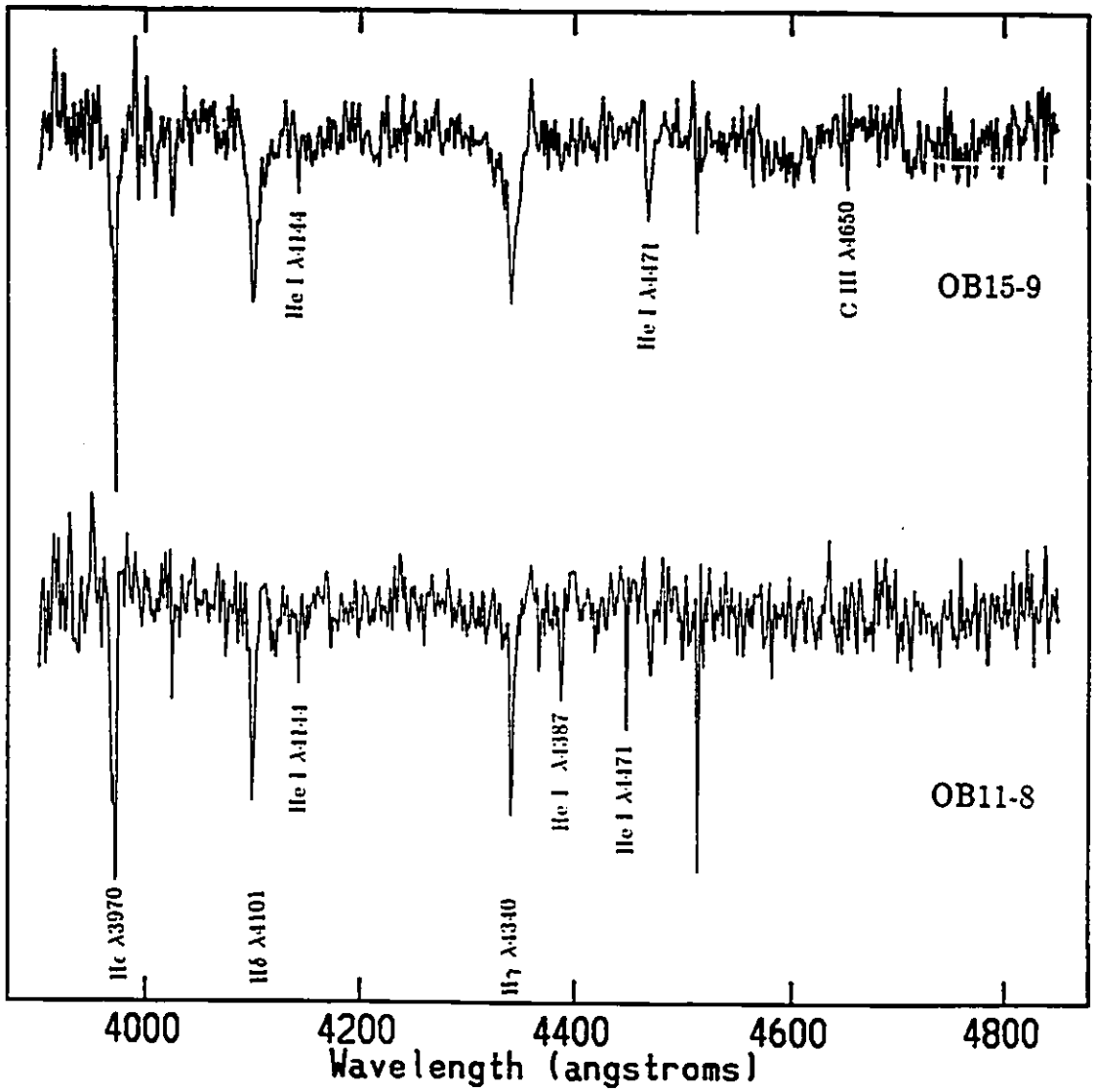

Figure 4.20: The spectra of B type stars OB11-8 and OB15-9. Note the presence of the strong He II λ4471 line unaccompanied by Mg II λ4481 in both stars and C III λ4650 in OB15-9.

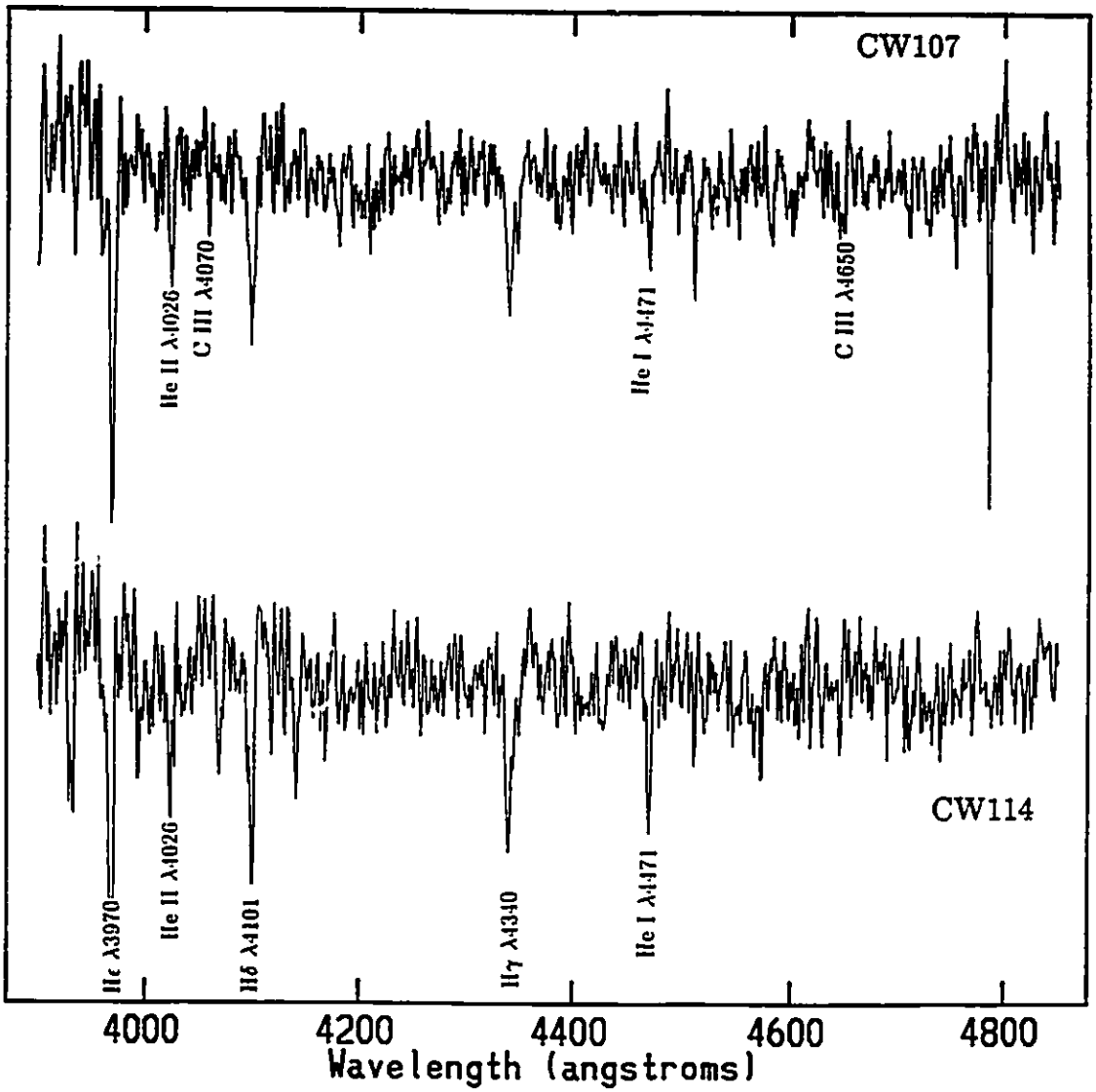

Figure 4.21: The spectra of B type stars CW114 and CW107. Here as in the case of OB11-8 and OB15-9, He II λ4471 is unaccompanied by Mg II λ4481. Note also the presence of C III λ4650 in CW107.

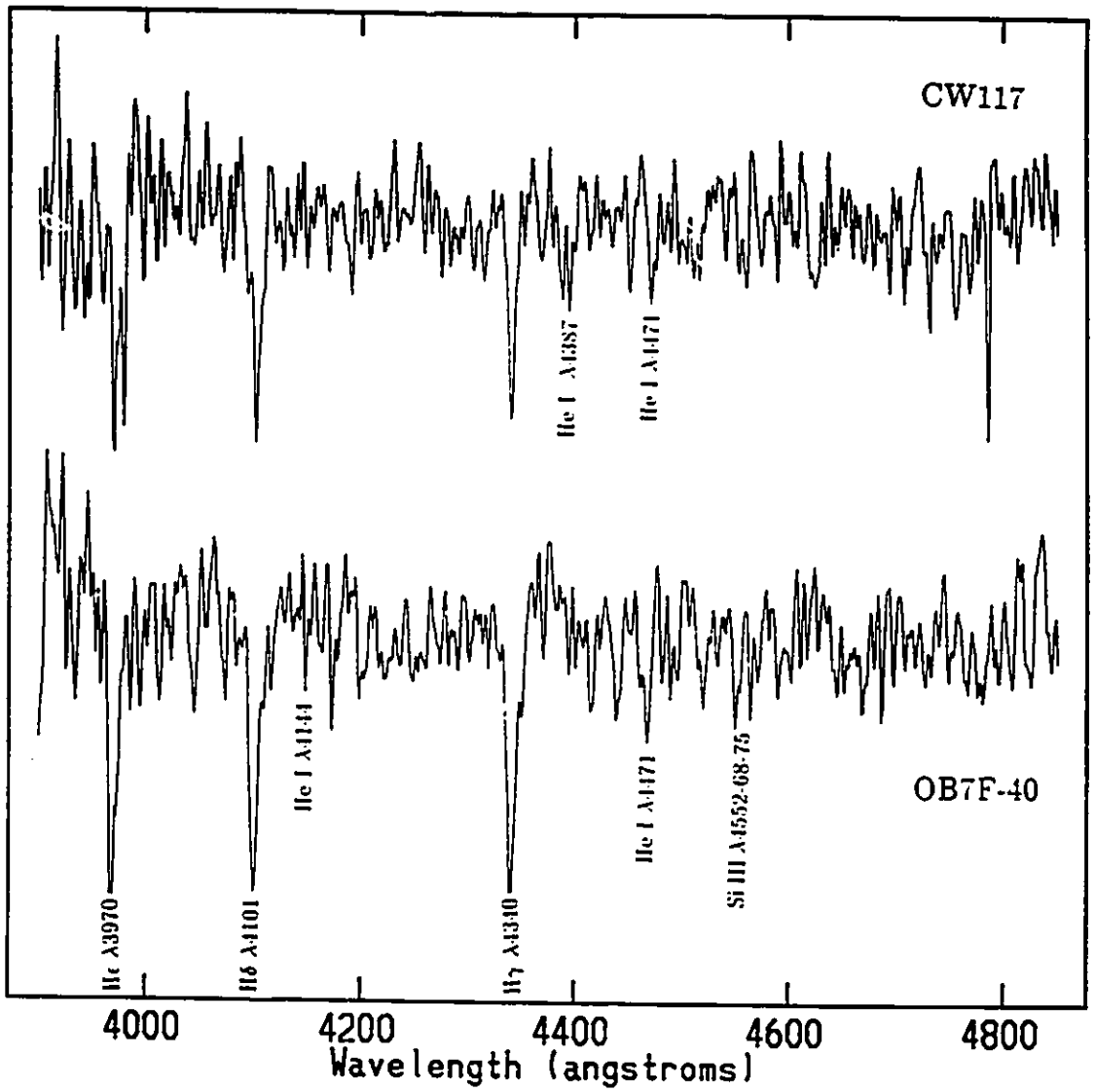

Figure 4.22: The spectra of B type stars CW117 and OB7F-40. Note the presence of He II λ4471 and absence of Mg II λ4481. C III λ4650 is seen in CW117.

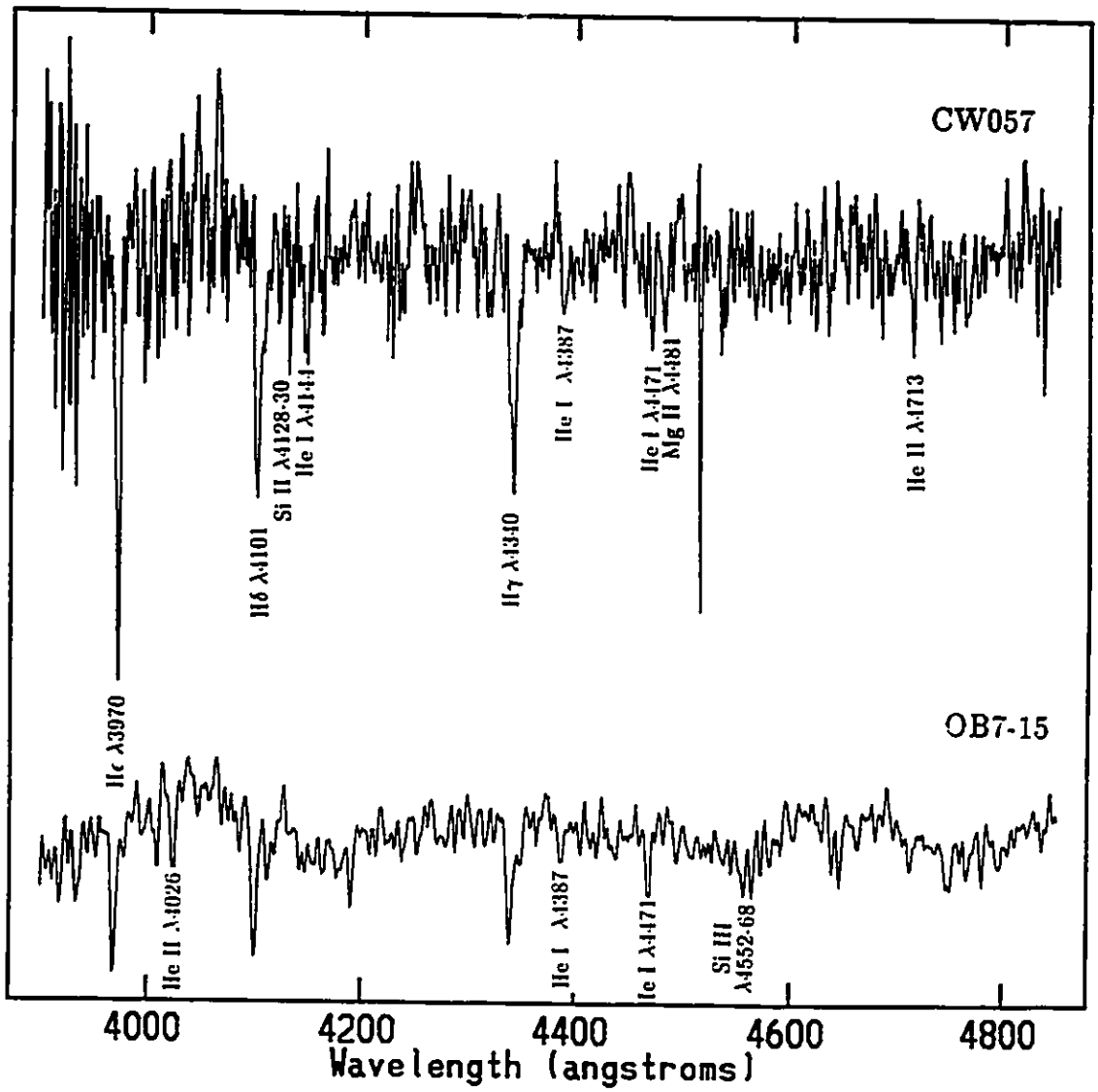

Figure 4.23: The spectra of the early B type star OB7-15 and the early to mid B type star CW057. Note the strong He I lines (λ3995, λ4009, λ4026, λ4471, λ4713) and missing He II lines (λ4542, 4200 etc.). While Mg λ4481 is missing in the spectrum of OB7-15, there is some (but not definitive) evidence that it is present in that of CW057.

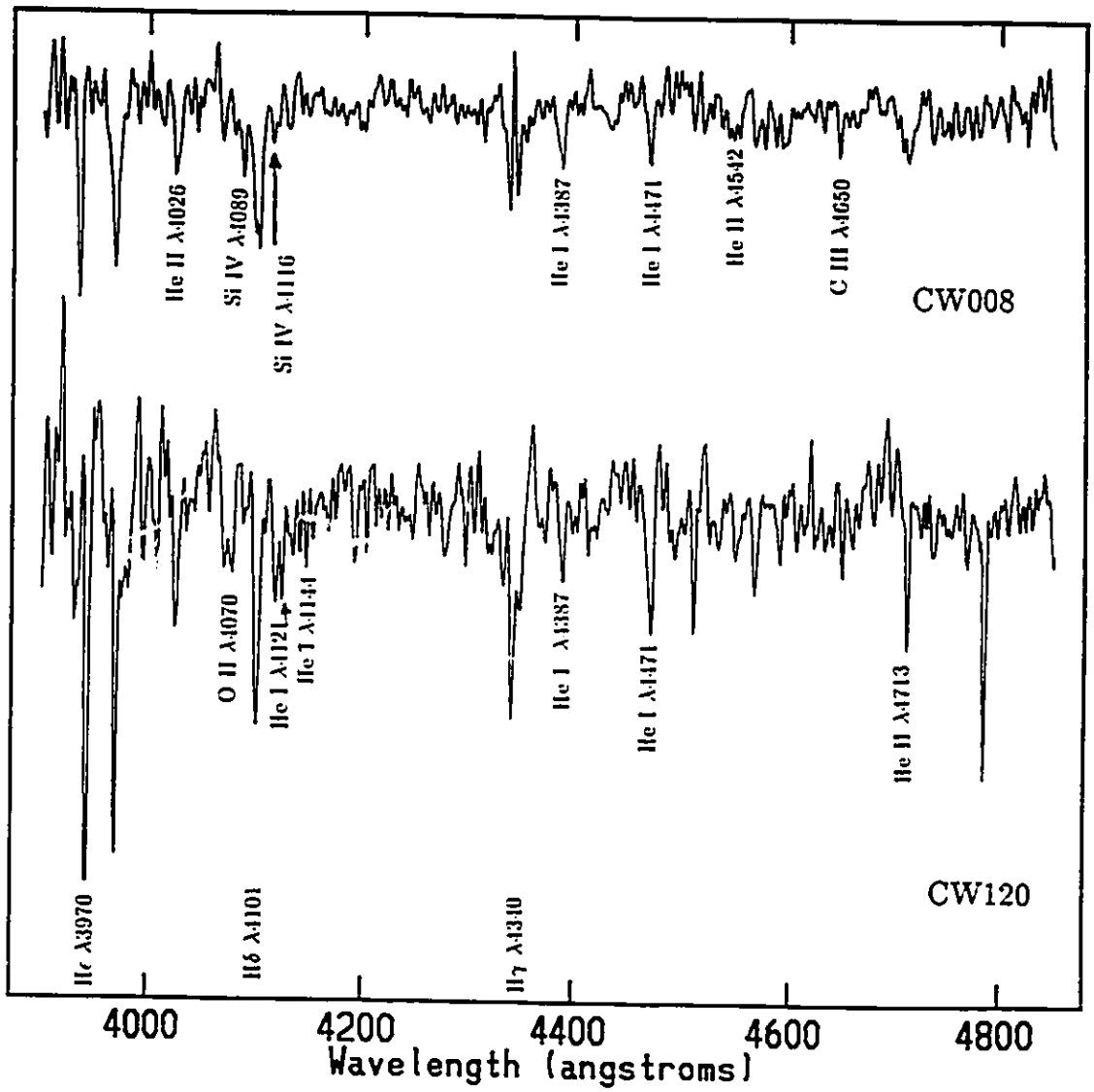

Figure 4.24: The spectra of the star CW120 and CW008. CW120 is classified as a B1 V or potential B1.5 V star while CW008 is identified as a B0 III star. Notice the presence of O II λ4070 and λ4415-17 and O II-C III λ4650 blend in the spectrum of CW120. Characteristic B0 lines in CW008 include He II λ4542, the strong Si IV λ4086 and λ4116, C III-O II blend at λ4650 as well as C III λ4070.

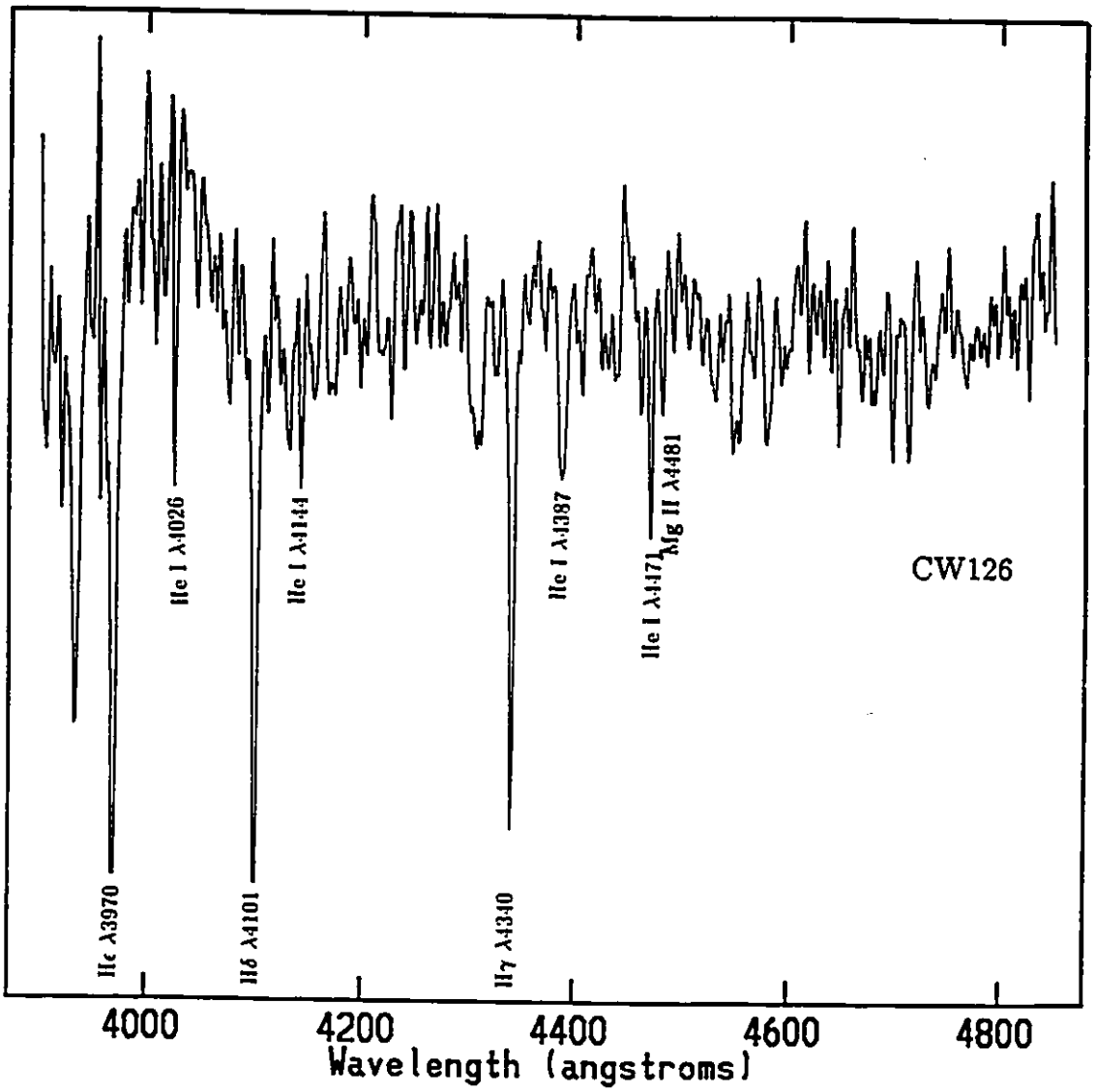

Figure 4.25: The spectrum of the star CW126 classified as either B2 IV or B3 I-III. Note the clear presence of Mg II λ4481, which is about one half the strength of He I λ4471, as well as C III λ4650 and He I λ4026, λ4144.

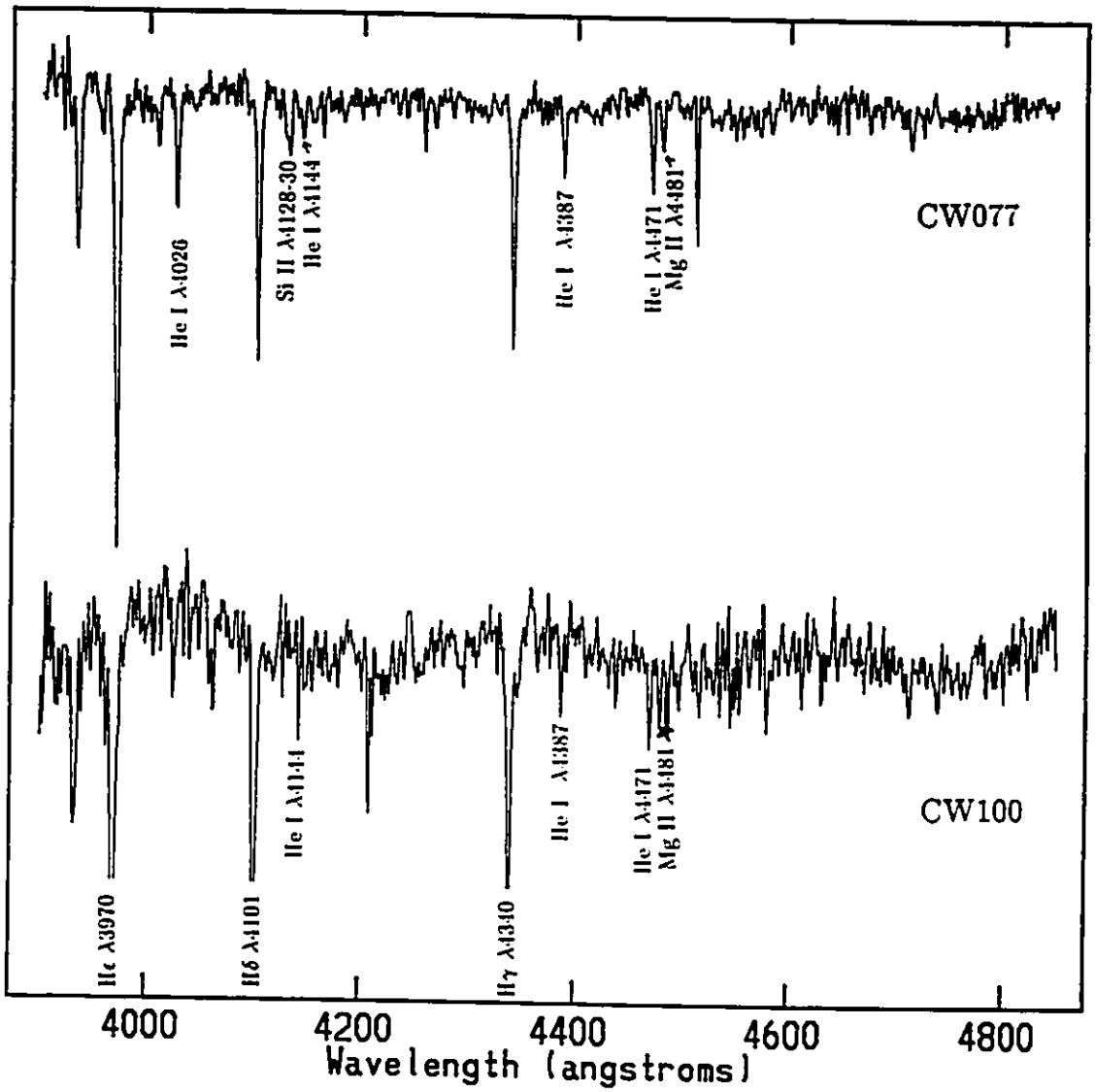

Figure 4.26: The spectrum of the B5 I stars CW100 and CW077. Note the strength of Mg II λ4481 relative to He I λ4471.

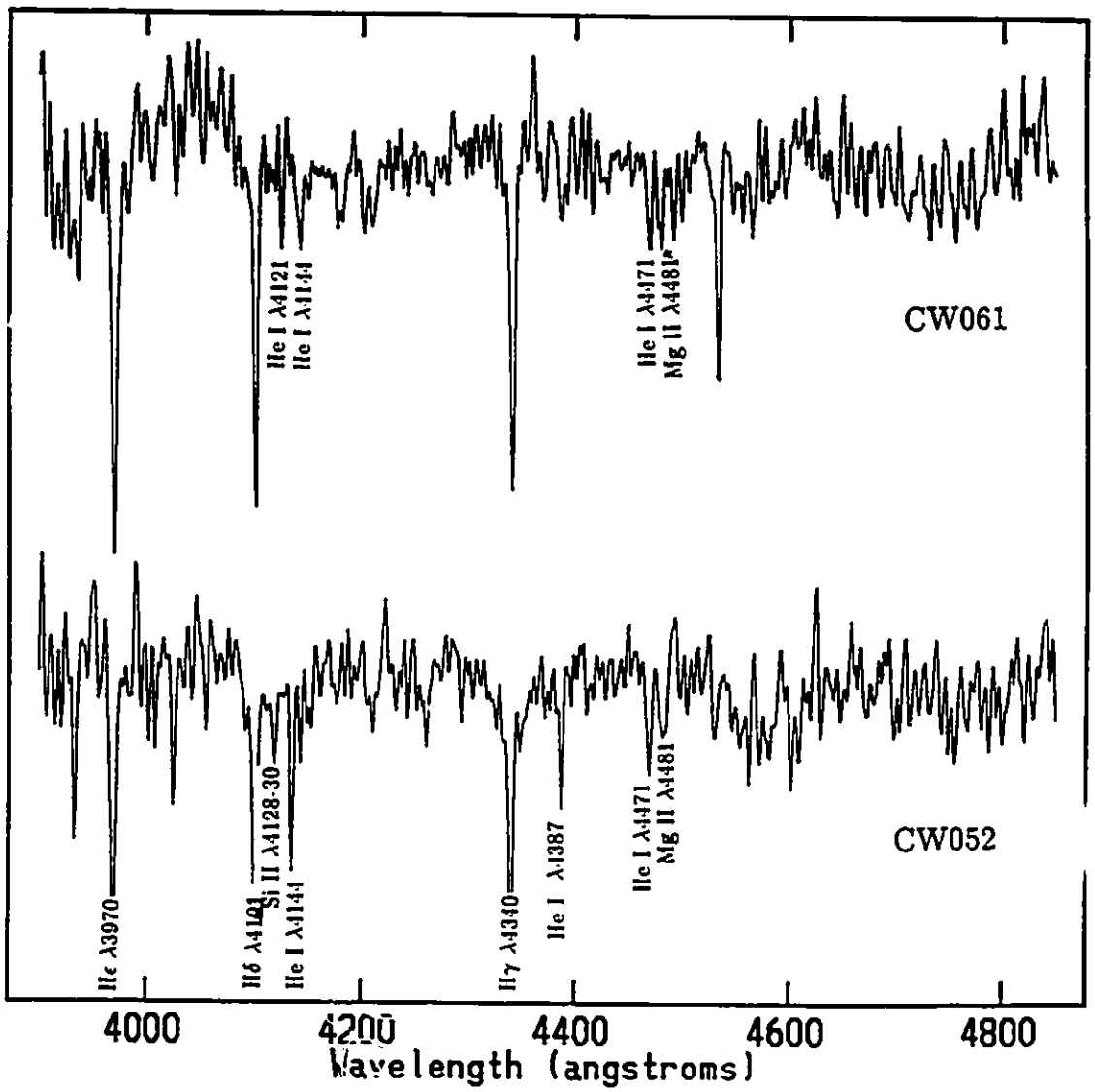

Figure 4.27: The spectrum of the late B8 I stars CW061 and CW052. The classification is based on the roughly equal strengths of He I λ4471 and Mg II λ4481.

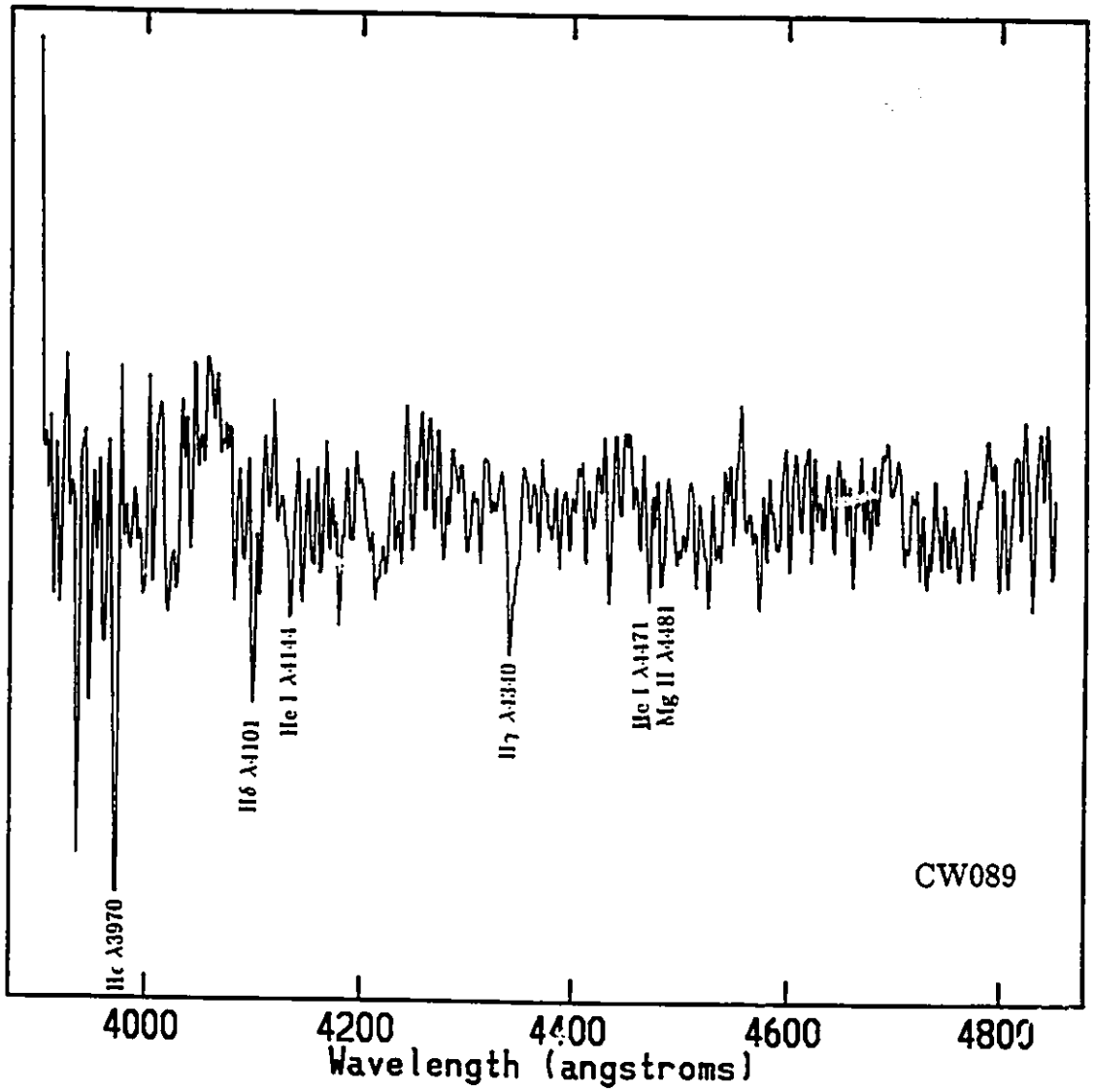

Figure 4.28: The spectrum of the late type B star CW089. The estimated spectral type is based on the presence of the strong He I λ4471 and Mg II λ4481 lines. The poor S/N ratio makes it difficult to be more precise.

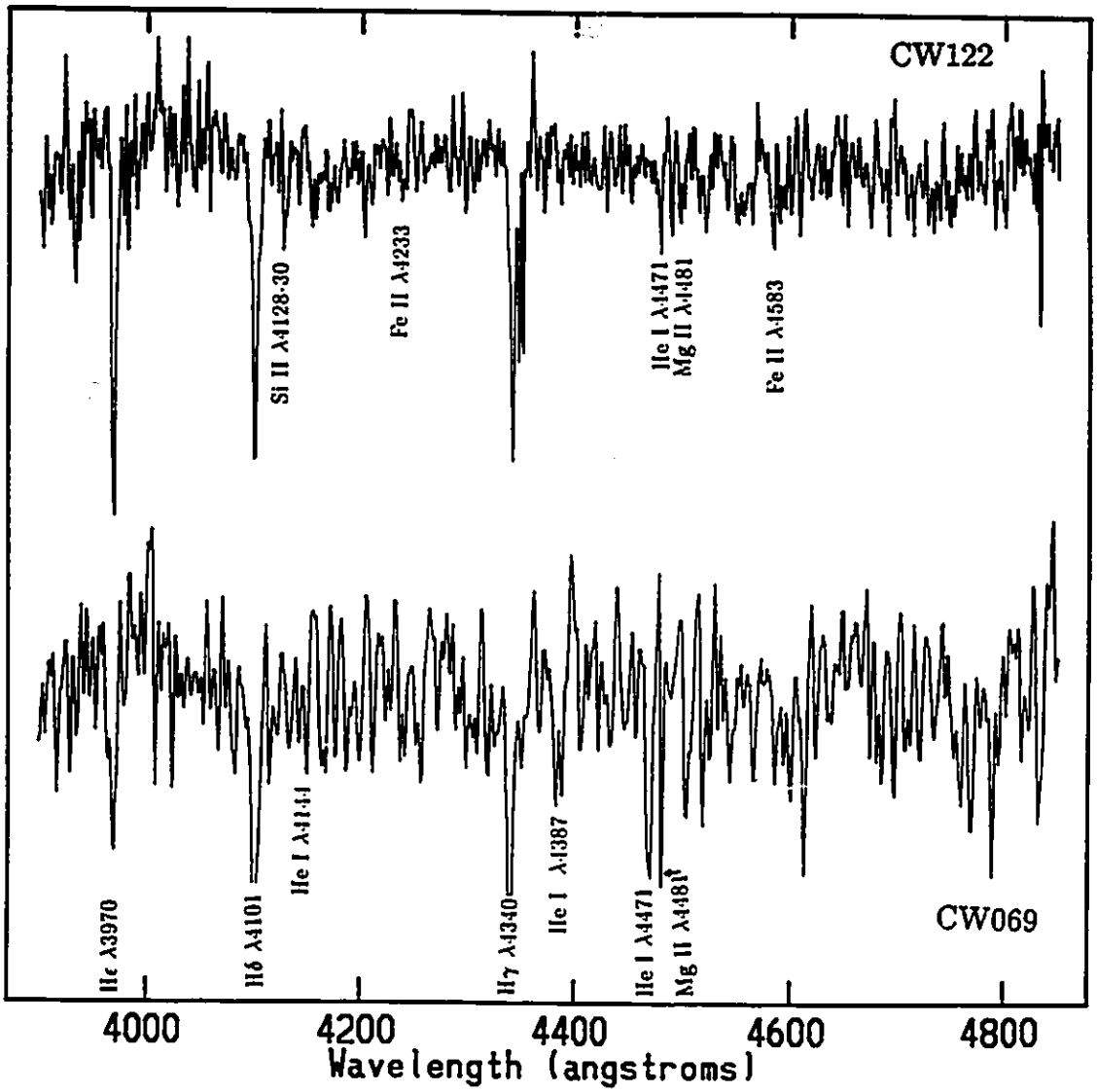

Figure 4.29: The spectra of the stars CW069 and CW122. Only an approximate spectral classification of late B to early A is possible based on the strong Balmer lines and Mg λ4481 which is stronger than He II λ4471. Notice the potential Fe II λ4233 and λ4583 lines in the spectrum of CW122.

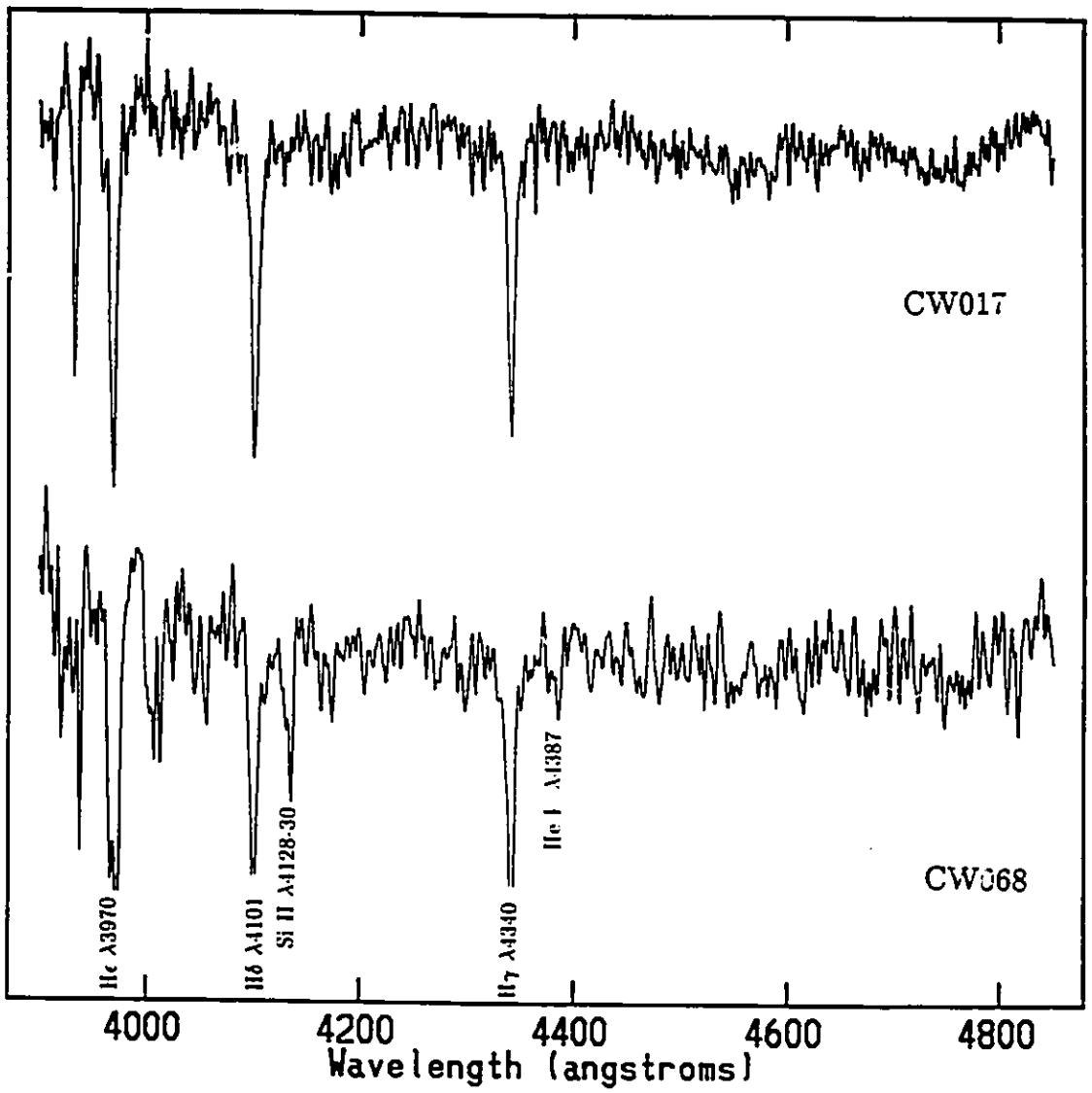

Figure 4.30: The spectra of the classical A I type stars, CW017 and CW068. Note the extremely thin hydrogen Balmer lines and absence of He I lines.

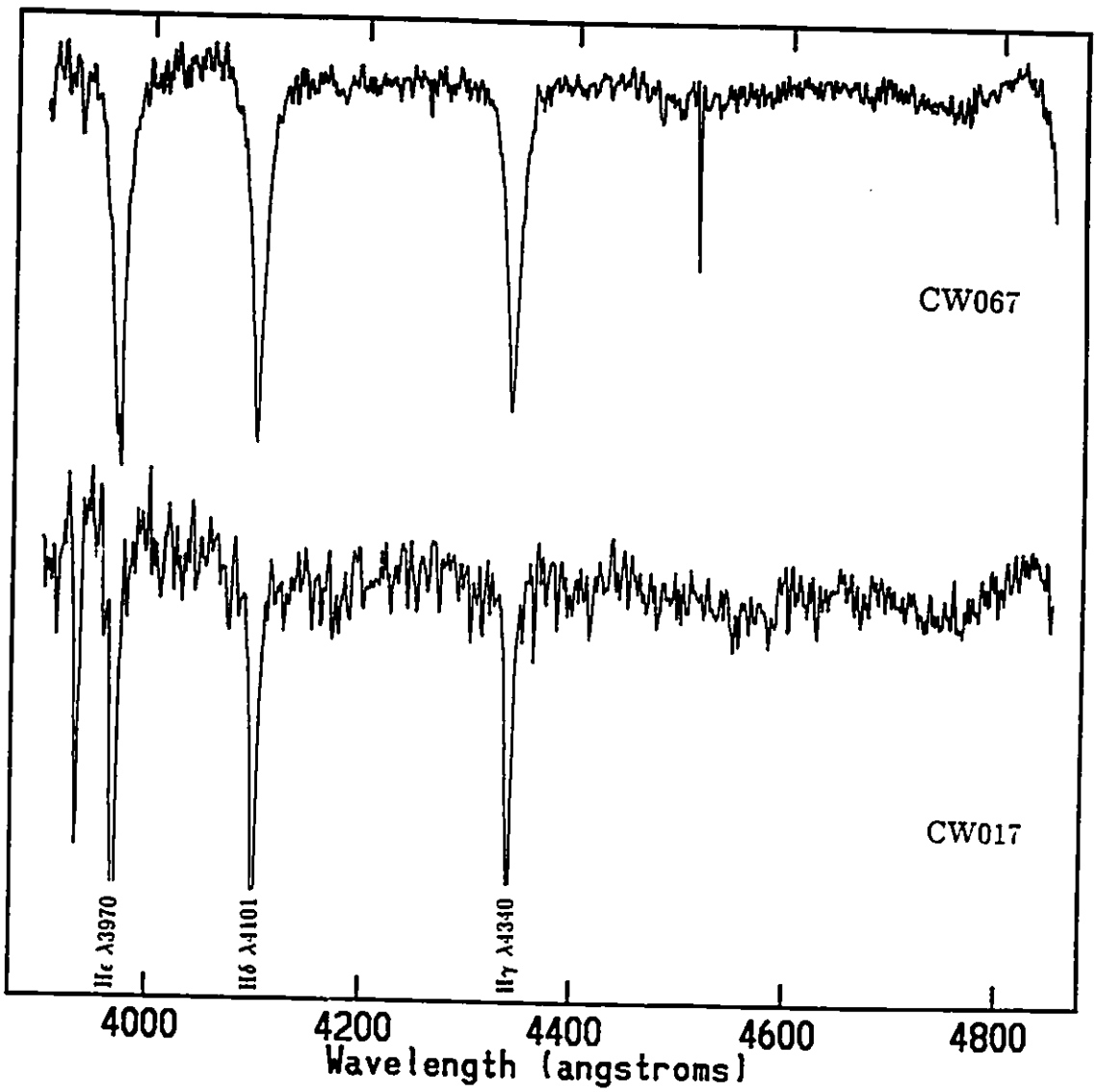

Figure 4.31: The spectra of the stars CW017 and CW067 illustrating the luminosity effect in A type stars. CW017 is classified as A I while CW067 is classified as A V based on the broad hydrogen Balmer lines.

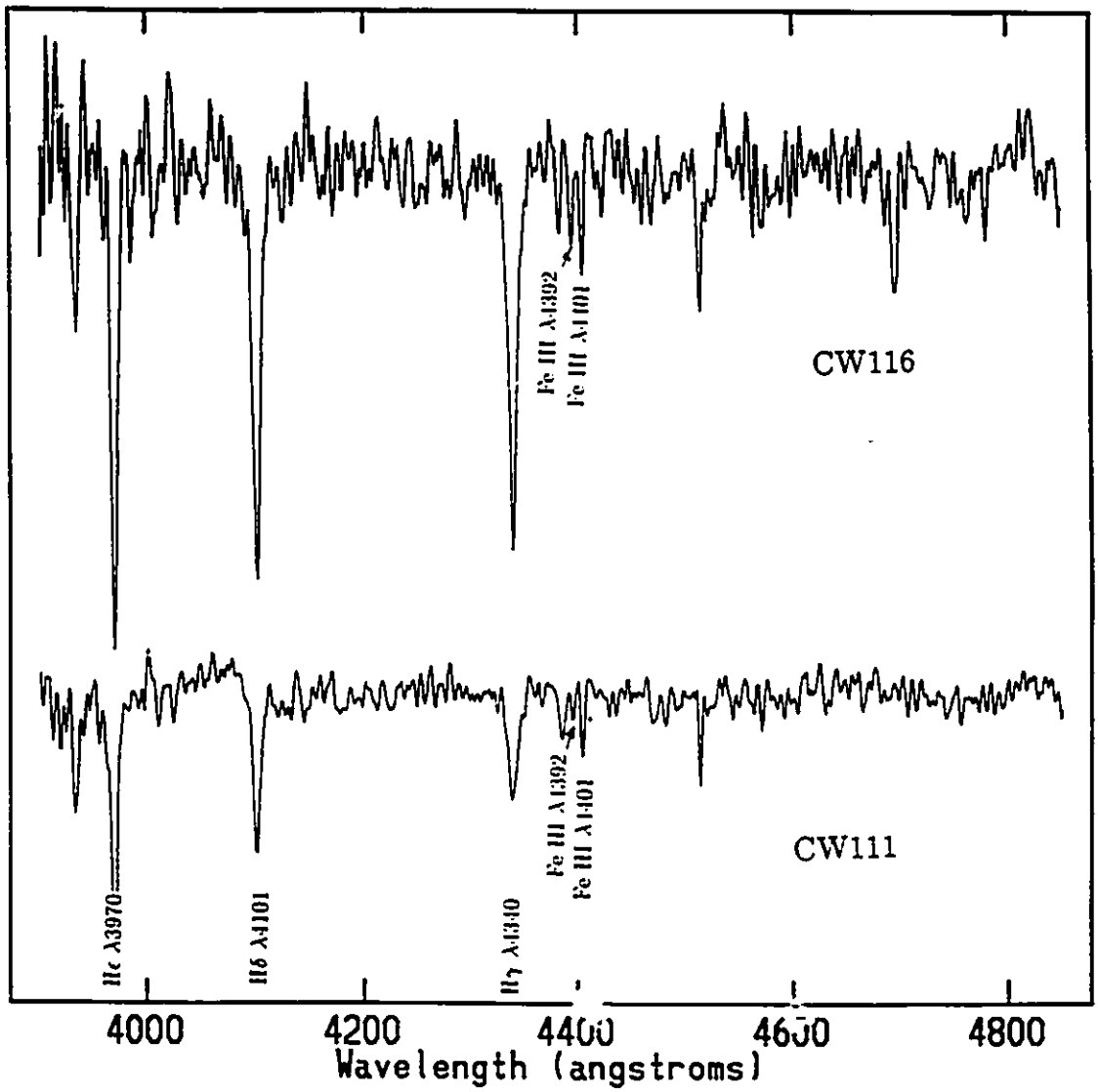

Figure 4.32: The spectra of the stars CW111 and CW116. CW111 is identified as an A type star while CW116 is identified as a potential A type star due to poor S/N. Notice the Fe I, IIλ4383 line in the spectrum of CW111.

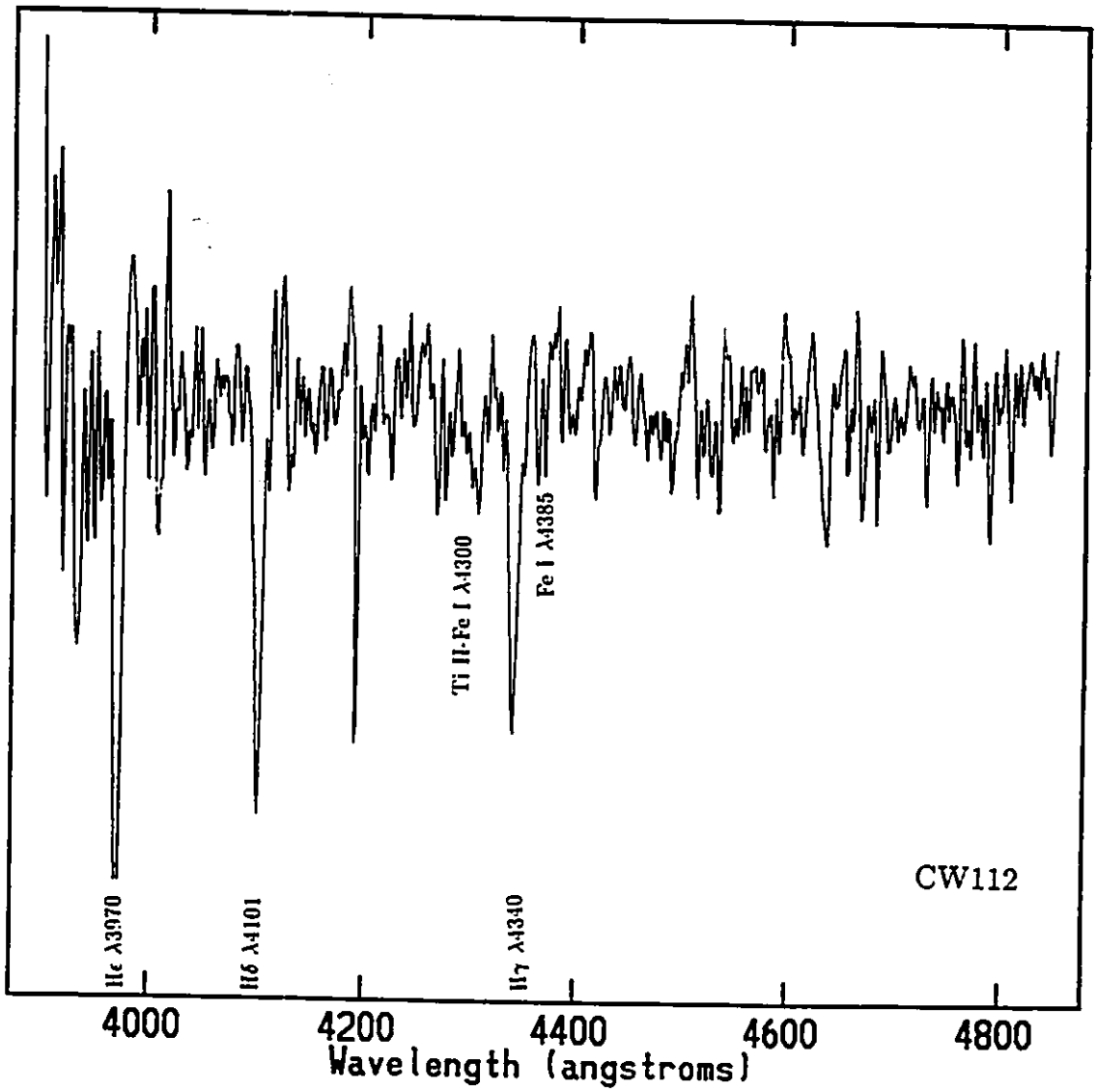

Figure 4.33: The spectrum of CW112 resembles that of an A type star, although the high noise level makes the classification only approximate.

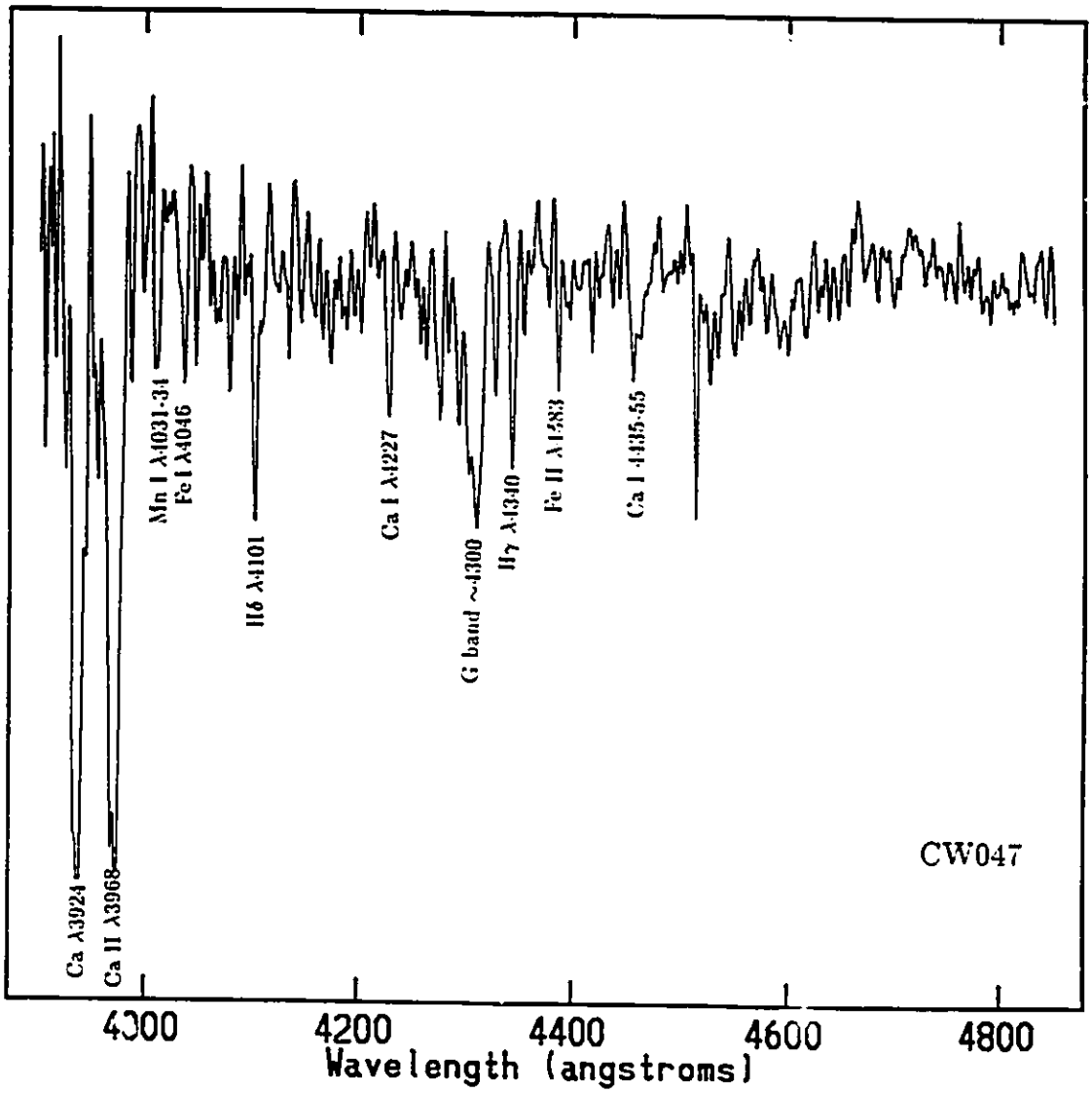

Figure 4.34: The spectra of the G type star CW047. Notice the deep, broad G-band near λ4300 as well as the very strong Fraunhofer H and K lines of Ca II at λ3634 a d λ3968.

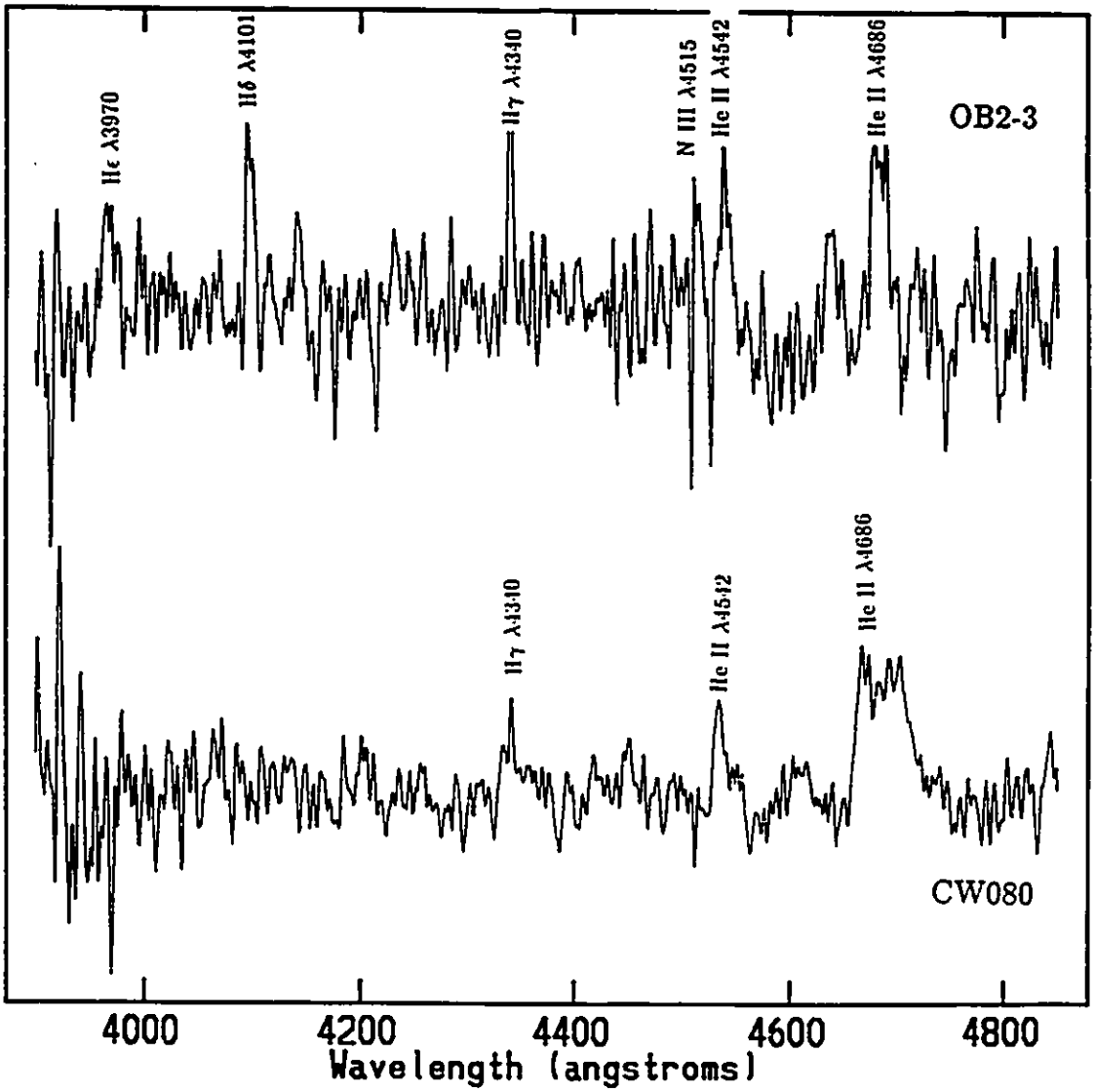

Figure 4.35: The spectra of the Wolf-Rayet type stars CW080 and OB2-3. The primary indicators of the spectral class are large number of broad emission (hydrogen Balmer and He II λ4542 , λ4686) and relatively few absorption lines in the spectra. Notice the N III emission features at λ4515 and λ4634-41 in the spectrum of OB2-3 which indicates it is a WN star.

STAR	α(1950)	δ(1950)	V	(B-V)	SPECTRAL CLASS
CW042	1 30 52.08	30 16 50.1	18.28	-0.0	O (potential)
CW011	1 31 3.95	30 20 3.4	17.15	-0.04	B1 III
CW018	1 30 54.02	30 20 11.5	17.55	-0.03	B0.5 I
CW012	1 30 55.34	30 20 36.6	17.23	-0.03	B1.5-B5
CW008	1 30 48.84	30 15 47.8	16.91	-0.01	B5 I
CW016	1 30 44.02	30 18 45.3	17.43	-0.05	Mid B
CW025	1 31 7.13	30 24 30.5	17.90	0.02	B5-B8 I
CW024	1 30 55.93	30 21 4.0	17.71	-0.02	B
CW047	1 31 2.37	30 25 41.5	18.34	0.14	B
CW049	1 30 50.11	30 20 8.2	18.38	-0.11	B
CW043	1 31 1.20	30 23 27.4	18.29	-0.01	B
CW006	1 30 53.82	30 23 44.0	16.80	0.06	WN7
CW010	1 30 44.84	30 26 14.6	17.05	0.06	WN7 or Of+nebula
CW001	1 30 59.90	30 22 46.8	15.78	0.12	G I ?
CW002	1 30 45.79	30 20 37.8	16.39	0.12	LBV ?

Table 4.5: M33: Spectral Classifications from HYDRA data.

The Blue Stars of M33

We summarize, in Table 4.5, the results of the spectral classification of the M33 stars observed using the Mayall 4-m telescope and the HYDRA spectrometer at KPNO. Out of the 15 stars that had classifiable spectra we found 2 potential WR stars, 1 G star, 1 potential luminous blue variable (LBV), 1 potential O star and 10 B stars. The following is a brief summary of the noteworthy features in the individual spectra that prompted the classifications that appear in Table 4.5.

The star CW042 is identified as a potential O star as the He II λ4541 line is

clearly seen and there is some, but not definitive, evidence for He II λ4200 (Figure 4.36). The spectrum also shows little or no He I λ4471. It is difficult to say more about this star as it appears, from the self absorbed Balmer lines, that it is located in an area of some nebulosity.

From Figure 4.37, it is clear that CW011 and CW018 are early B type stars. The presence of Mg II λ4481, He I λ4121 and λ4144, N II λ4631, C II-O II blend at λ4070 and C III-O II blend λ4650 as well as the noticeable lack of Si IV λ4116 or Si II λ4128-30 suggests that CW011 is perhaps a B1 III star. Clear evidence of Si IV λ4089 and λ4116 combined with the strong C III lines at λ4070 and λ4650 and virtually non-existent weak Mg II λ4481 lines in the spectrum of CW018 is indicative of a B0.5 I type star.

CW012 is classified as an early to mid-B type (B1.5-B5). supergiant star based on the preponderance of the O II (λλ4415, λ4591-95) and N II (λ4631 and λ4640) lines as well as the strong Mg II λ4481, C II λ4267 and Si III λ4553-68 features in its spectrum (Figure 4.38). Evidence for the later classification lies in the strength of Mg λ4481 which is approximately half that of He I λ4471. This is particularly well illustrated in the spectrum of CW008 (also Figure 4.38) where Mg II λ4481 appears very prominent in relation to He I. Support for the B5 I classification for this star comes from the relatively few but strong absorption lines such as Si II λ4128 and He I λ4144, λ4386 and the narrow Balmer lines.

The spectrum of CW016 (Figure 4.39) allows only an approximate mid-B classification for this star. This is based on the relative strength of Mg II λ4481 and He II λ4471 as well as the presence of the C III-O II blend λ4650. There is some indication that O II λ4640 is also present, lending further support to the classification.

A more specific subclass cannot be determined for this star due to the low signal-to-noise level in the spectrum.

CW025 is identified as a supergiant B5 to B8 type star based on the strength of Mg II λ4481, which is greater than He I λ4471, and the relatively thin Balmer lines seen in its spectra (Figure 4.39). The same criterion (Mg II > He II) is used to assign class B8 I to the star CW020 (Figure 4.40).

The spectra of CW024, CW047, CW049 and CW043 allow only an approximate classification of the objects as B type stars. In all cases, it is the presence of Mg II λ4481 that is primarily responsible for the classification. In both CW024 and CW047 (Figure 4.41) the hydrogen Balmer lines are self-absorbed suggesting that the stars are located inside HII regions. Also visible are the C III λ4650, O II λ4415, He I λ4686 and λ4144 lines. The He I and Mg II lines are of roughly equal strength in CW049 (Figure 4.42) suggesting perhaps a late type star, but the additional presence of the O II λ4415 line is not consistent with such an identification.

CW006 is classified a WN7 star based on the very broad He II λ4686 and N III λ4634 as well as the strong, partially absorbed Balmer and He I λ4141 lines which all appear in emission in Figure 4.43. The subclass "7" is based on the relative strength of N V λ4608 and N III λ4640. Subsequent to our investigation, we discovered that this star had been previously identified as a WR7 star by Armandroff & Massey (1985). CW010 is classified as either a WN7 or an Of star in a nebular region. The W7 classification is suggested by the strong emission, self-absorbed Balmer lines while the Of+nebulosity classification is based on the strong N III λ4640 and He II λ4686 emission features as well as the He I lines (λ4026, λ4387, λ4471) and He II λ4541 lines that are all seen in absorption. The nebulosity would explain why the hydrogen

Balmer lines are self-absorbed or in slight emission. There is no indication in the literature that this star has been previously identified as a WR star.

The star CW001 is tentatively identified as a late type star, perhaps a G supergiant, based on the broad, if somewhat cut-up, G band in the vicinity of 4300Å (Figure 4.44). The Ca II K line at λ3968 is also visible. Finally, CW002 is tentatively classified as a luminous blue variable star based on extreme brightness of the star (V=16.4) and the enormous number of emission lines in the spectrum (Figure 4.44). Luminous blue variables, also known Hubble-Sandage variables, show signs of variability, irregular and violent outbursts and high mass loss (rates up to $\sim 10^{-3} M_{\odot} yr^{-1}$ (Davidson *et al.* 1986). They are most often interpreted as a short stage in the evolution of massive O stars into WR stars (Meader & Conti, 1994).

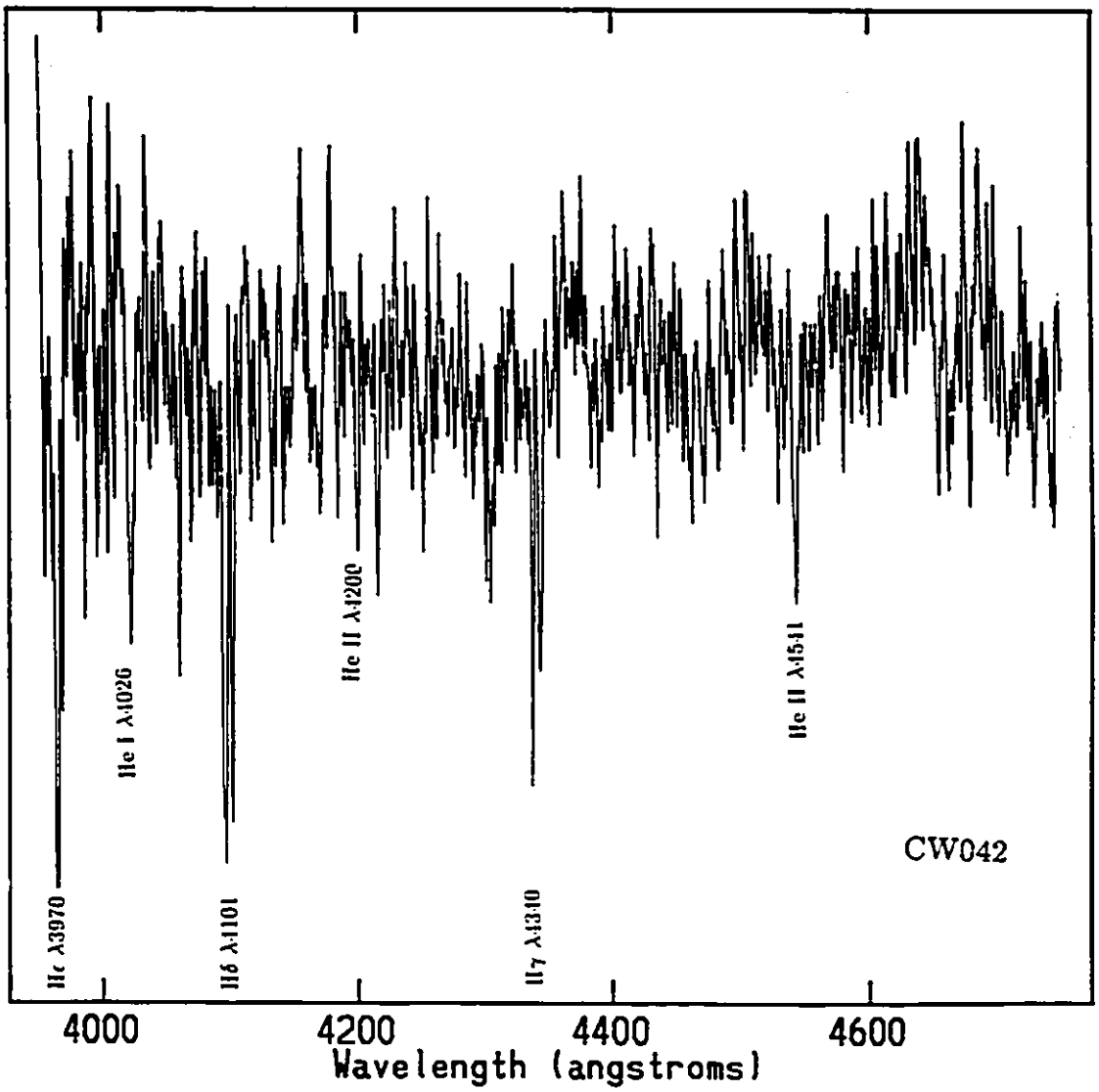

Figure 4.36: The spectra of the potential O star, CW042. Note the clear presence of He II λ4541 but the missing He II λ4200.

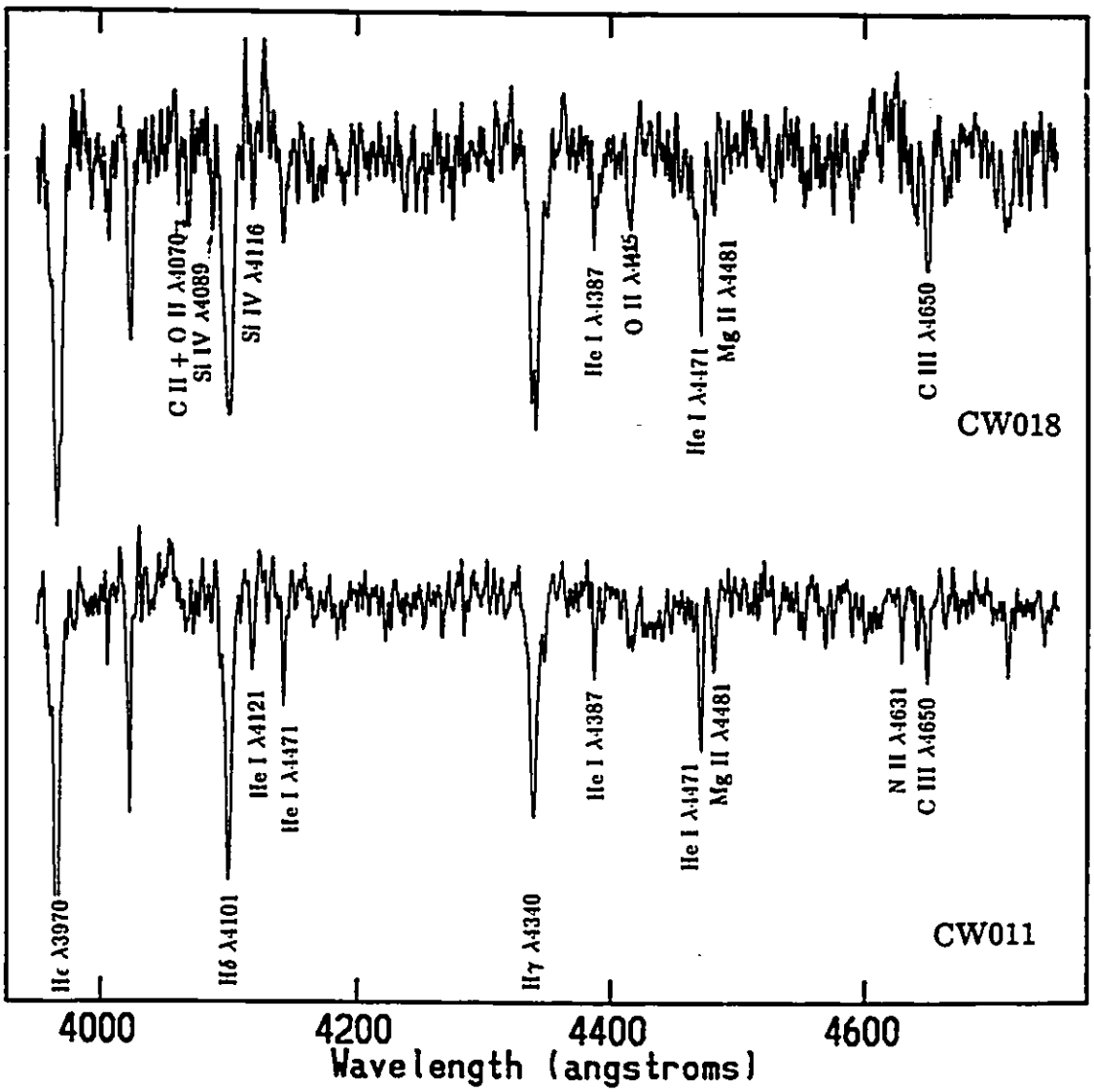

Figure 4.37: The spectra of the B1 III star CW011 and the B0.5 I type star CW018. Characteristic features to look for in the spectrum of CW011 include the presence of Mg II λ4481 and the absence of Si IV λ4116 or Si II λ4128-30 while those in the spectrum of CW018 include Si IV λ4089, λ4116, strong C III λ4070, λ4650 and the absence of Mg II λ4481.

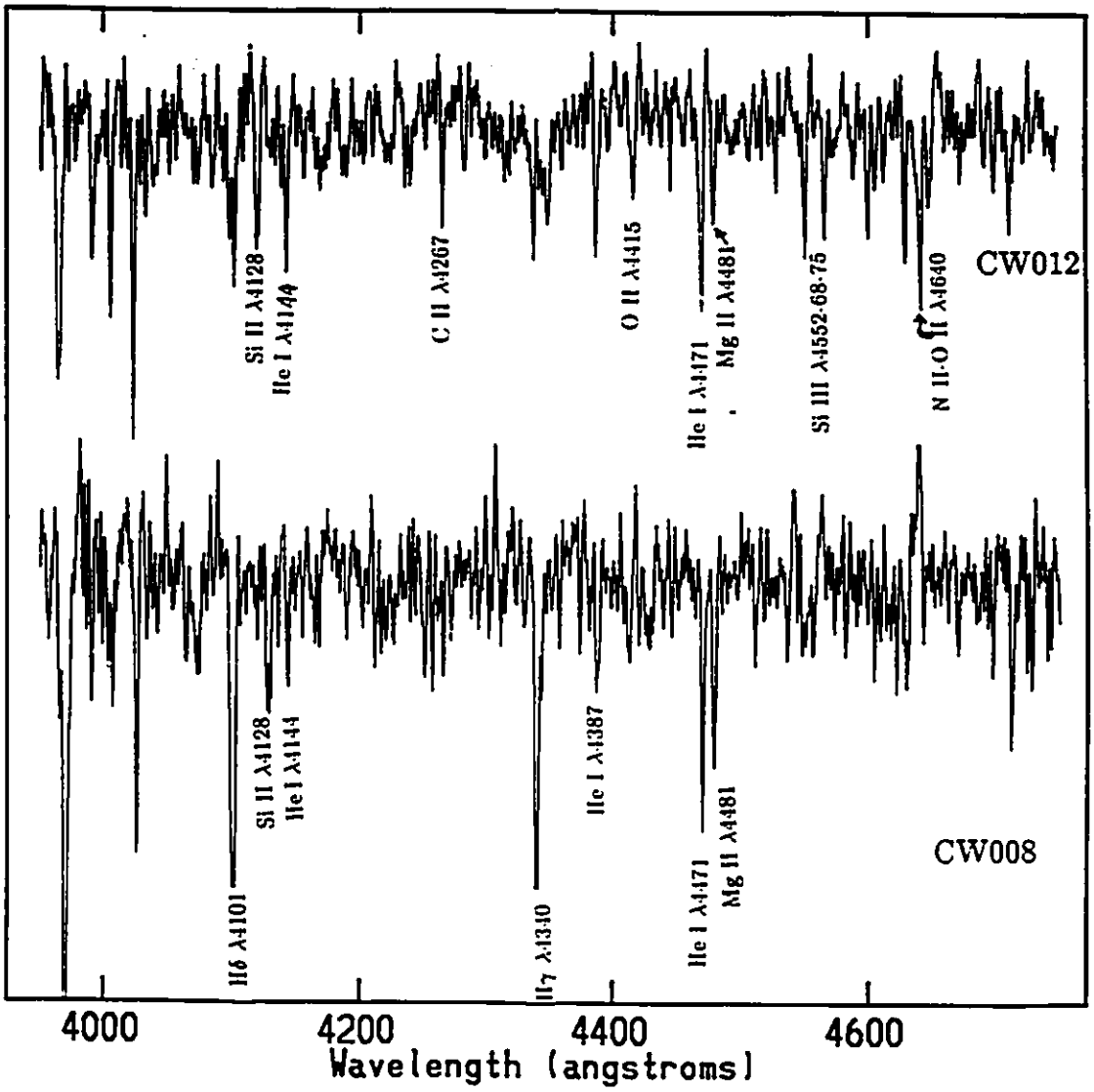

Figure 4.38: The spectra of the early to mid-B type star CW008 and the B5 I star CW012. Note the strong Mg II λ4481 line as well as the abundance of O II (λλ4415, λ4591-95) and N II (λ4631 and λ4640) lines in the spectrum of CW012. Characteristic B5 V features seen in the spectrum of CW008 include the strong Si II λ4128, He I λ4144, λ4386 and thin hydrogen Balmer lines.

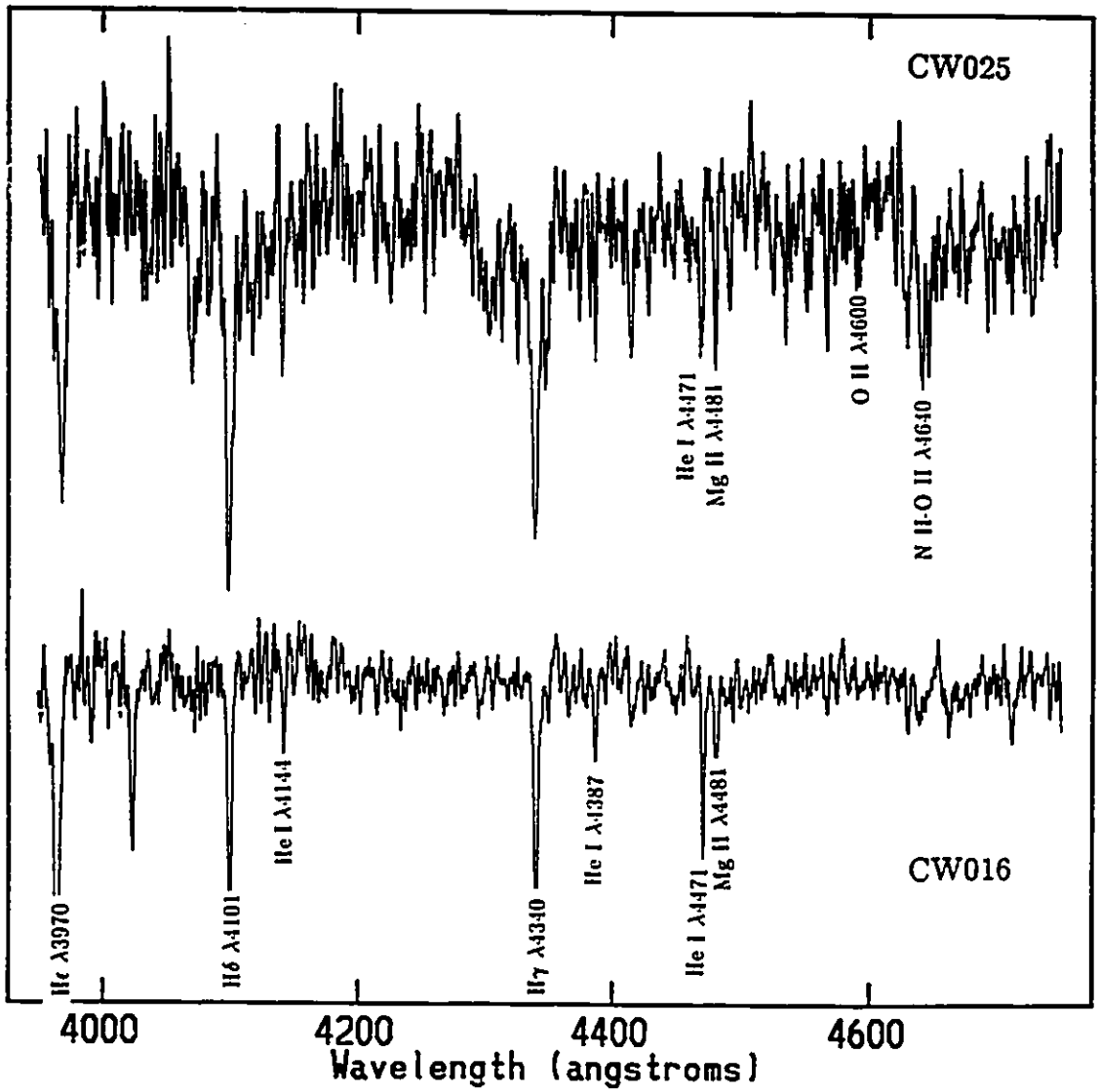

Figure 4.39: The spectra of the mid-B type star CW016 and the B5 to B8 supergiant star CW025. The characteristic mid to late B type feature in these spectra is the Mg II λ4481 line that is stronger than He I λ4471. Note the thin hydrogen Balmer lines that are prominent in the spectrum of CW025.

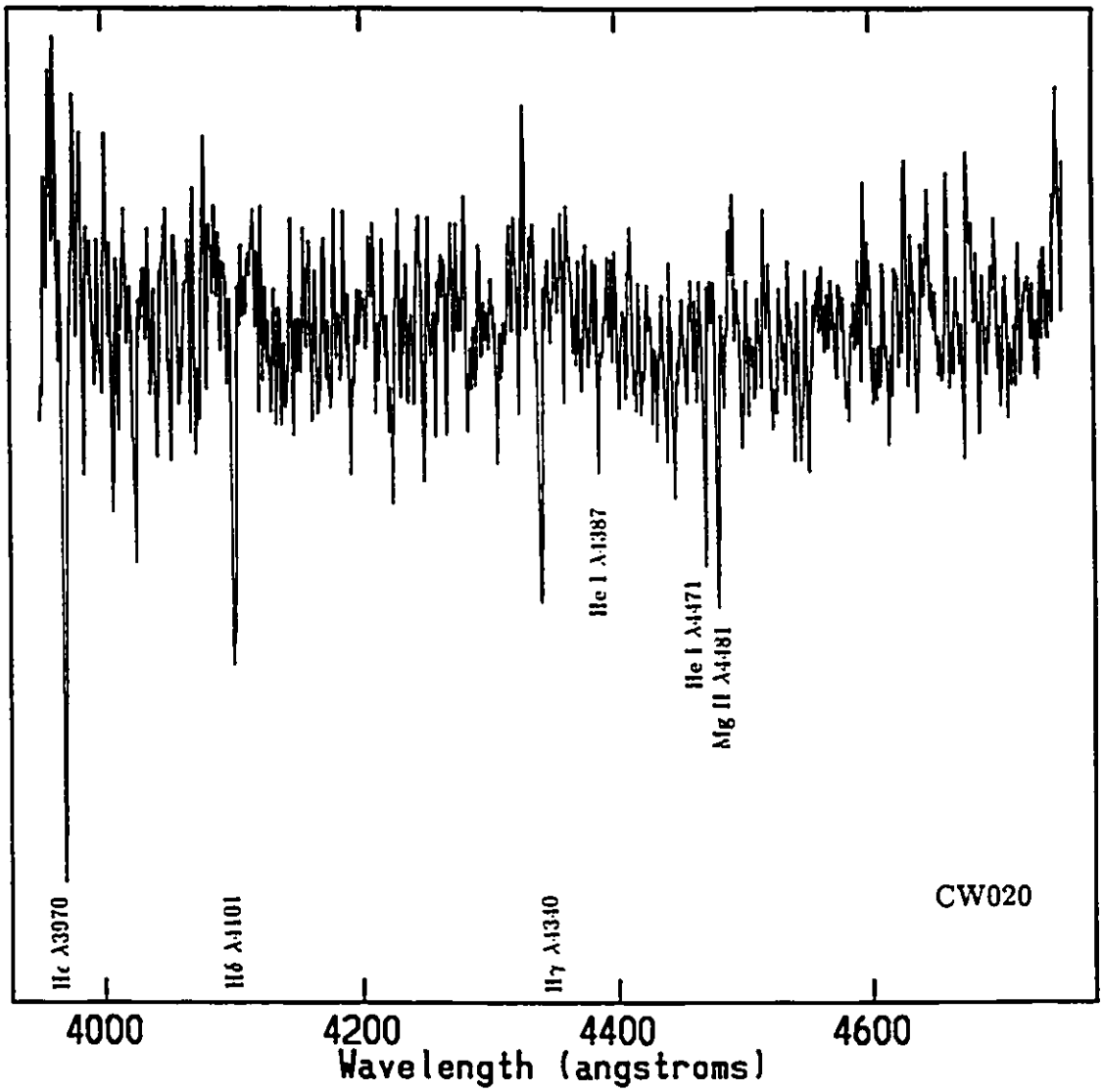

Figure 4.40: The spectra of the B8 I star CW020. The primary features are thin hydrogen Balmer lines and Mg II λ4481>He I λ4471.

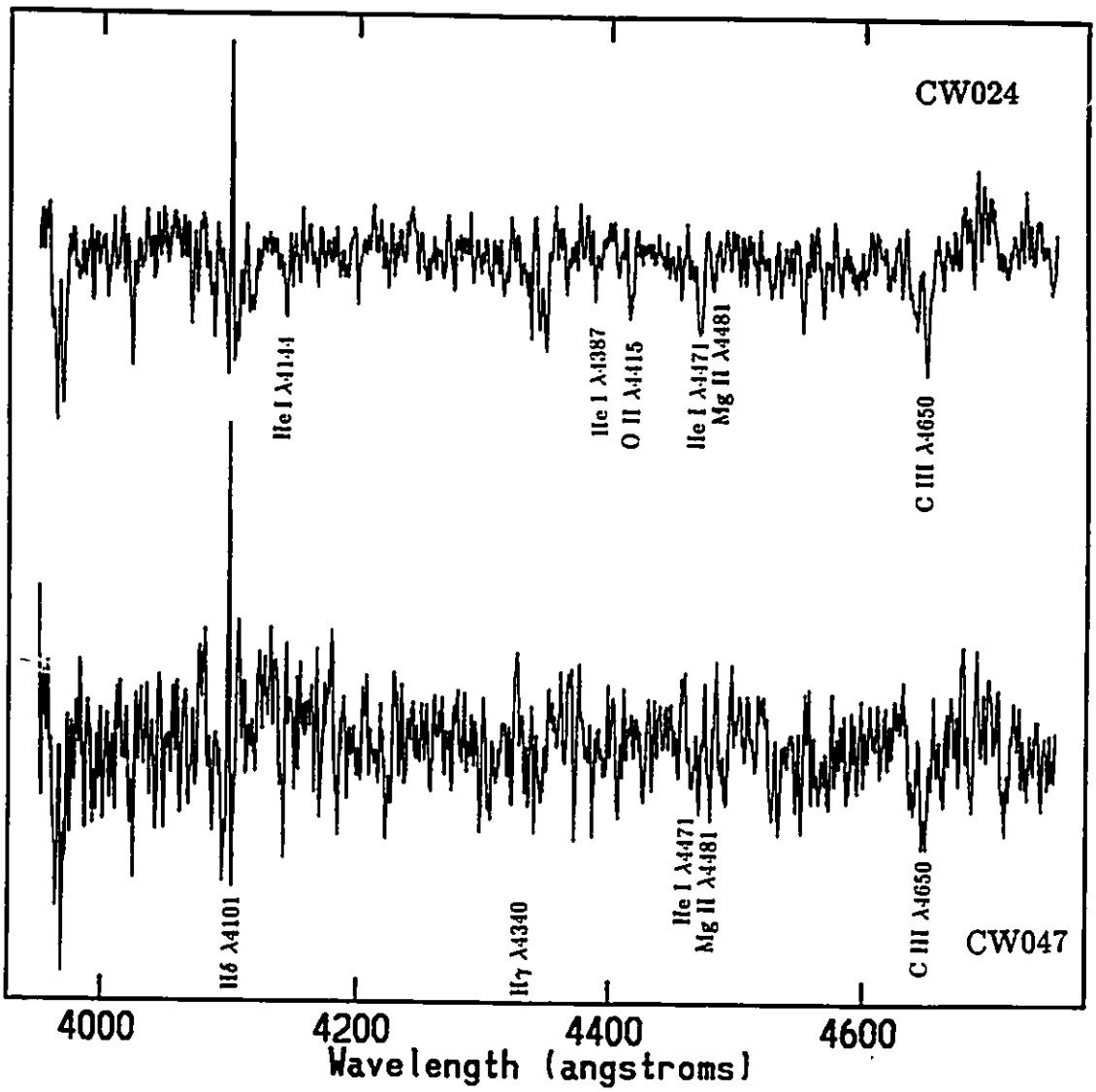

Figure 4.41: The spectra of the B type stars CW047 and CW024. Only an approximate class B classification based on the presence of Mg II λ4481 is possible from these spectra. Notice self-absorbed hydrogen Balmer lines indicative of the stars being in an HII region.

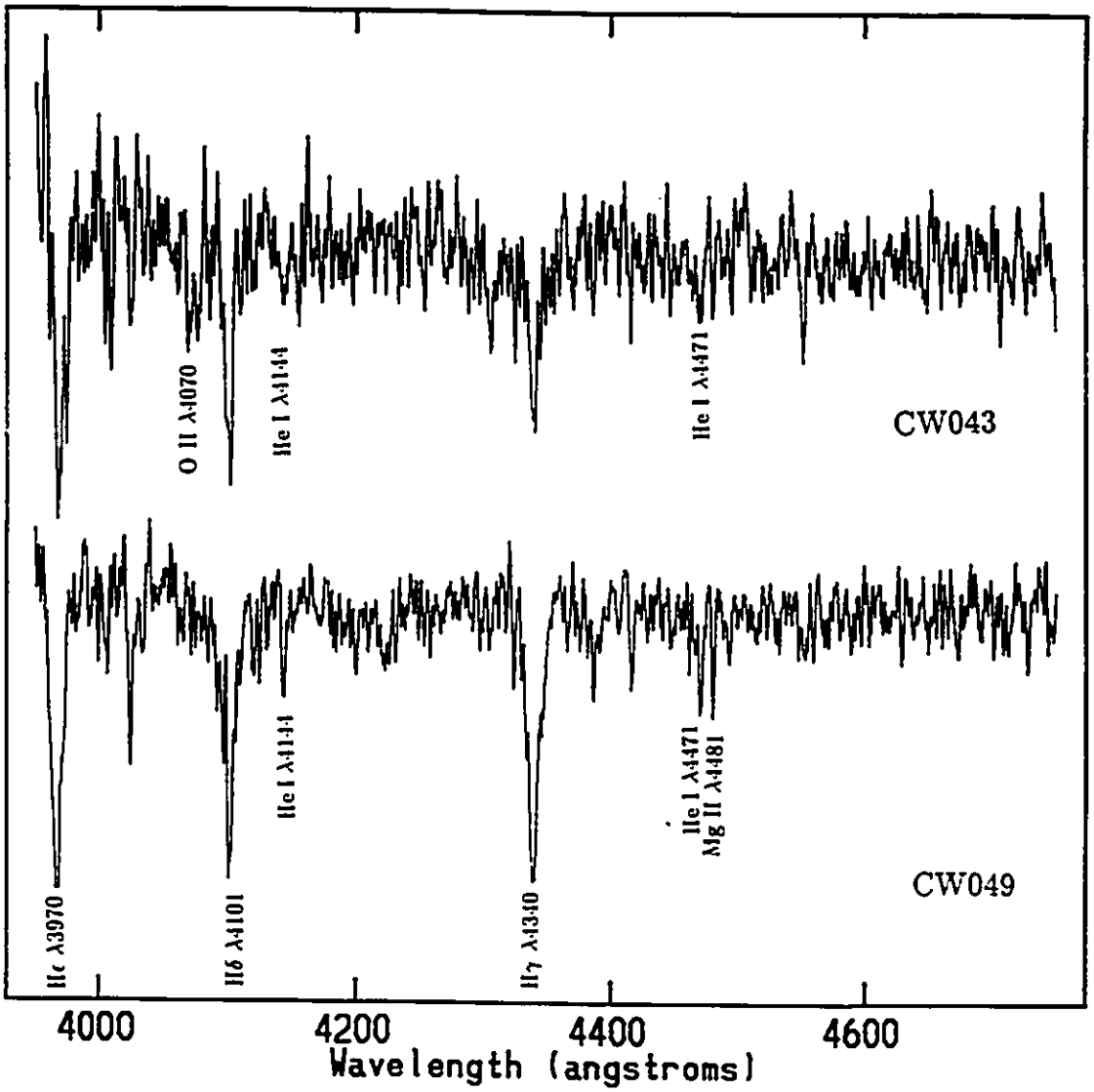

Figure 4.42: The spectra of the B type stars CW049 and CW043. The presence of Mg II λ4481 is the primary indicator of the broad classification of these stars as class B objects.

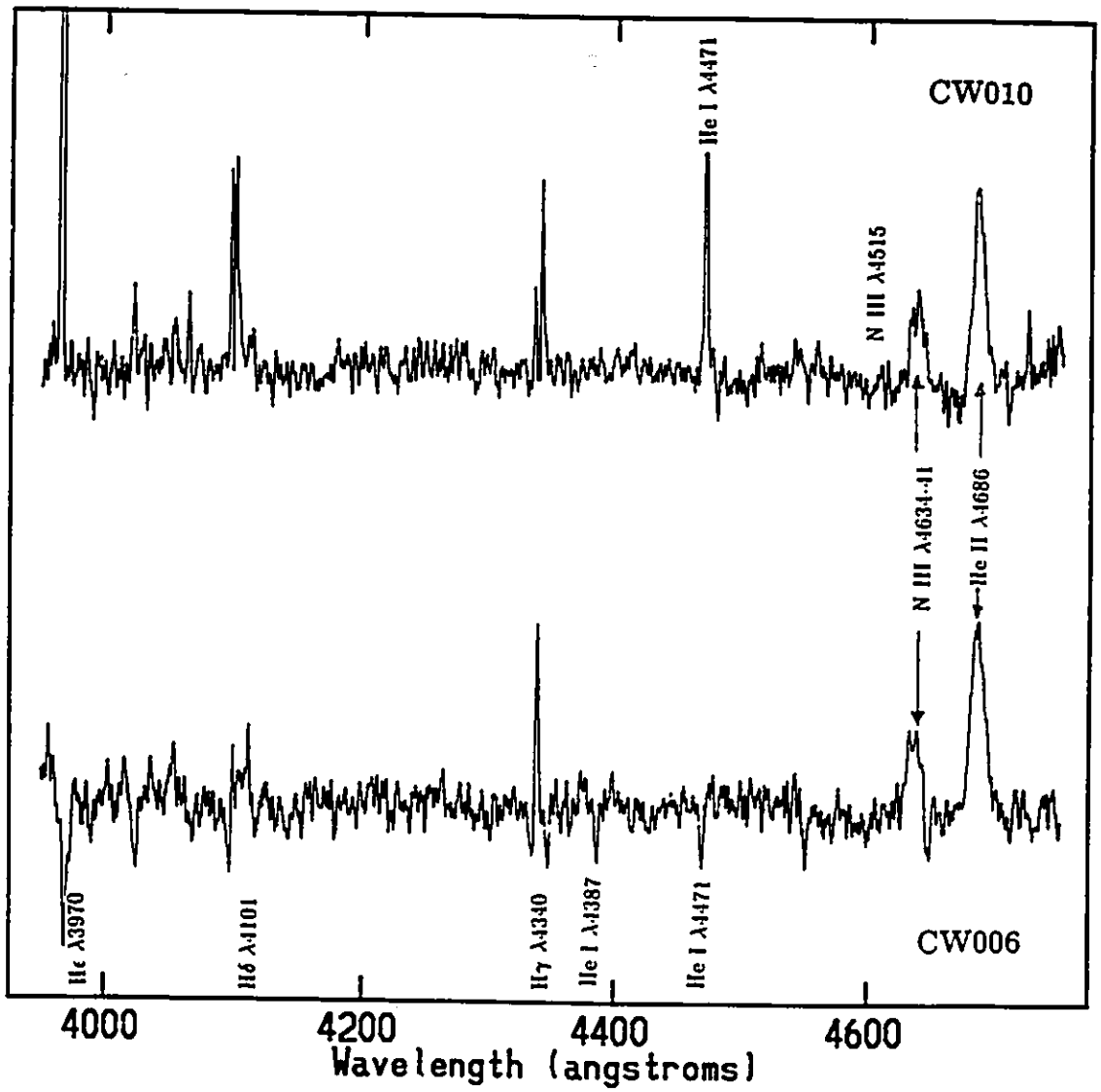

Figure 4.43: The spectra of the stars CW006 and CW010 which are classified, respectively as, WN7 and WN7 or Of+nebulosity. The strong and broad emission features at He II λ4686 and N III λ4634 are characteristic of the WN stars. The He I and He II absorption lines and the self-absorbed or emission Balmer lines in the spectrum of CW010 are suggestive of an Of type star within an HII region.

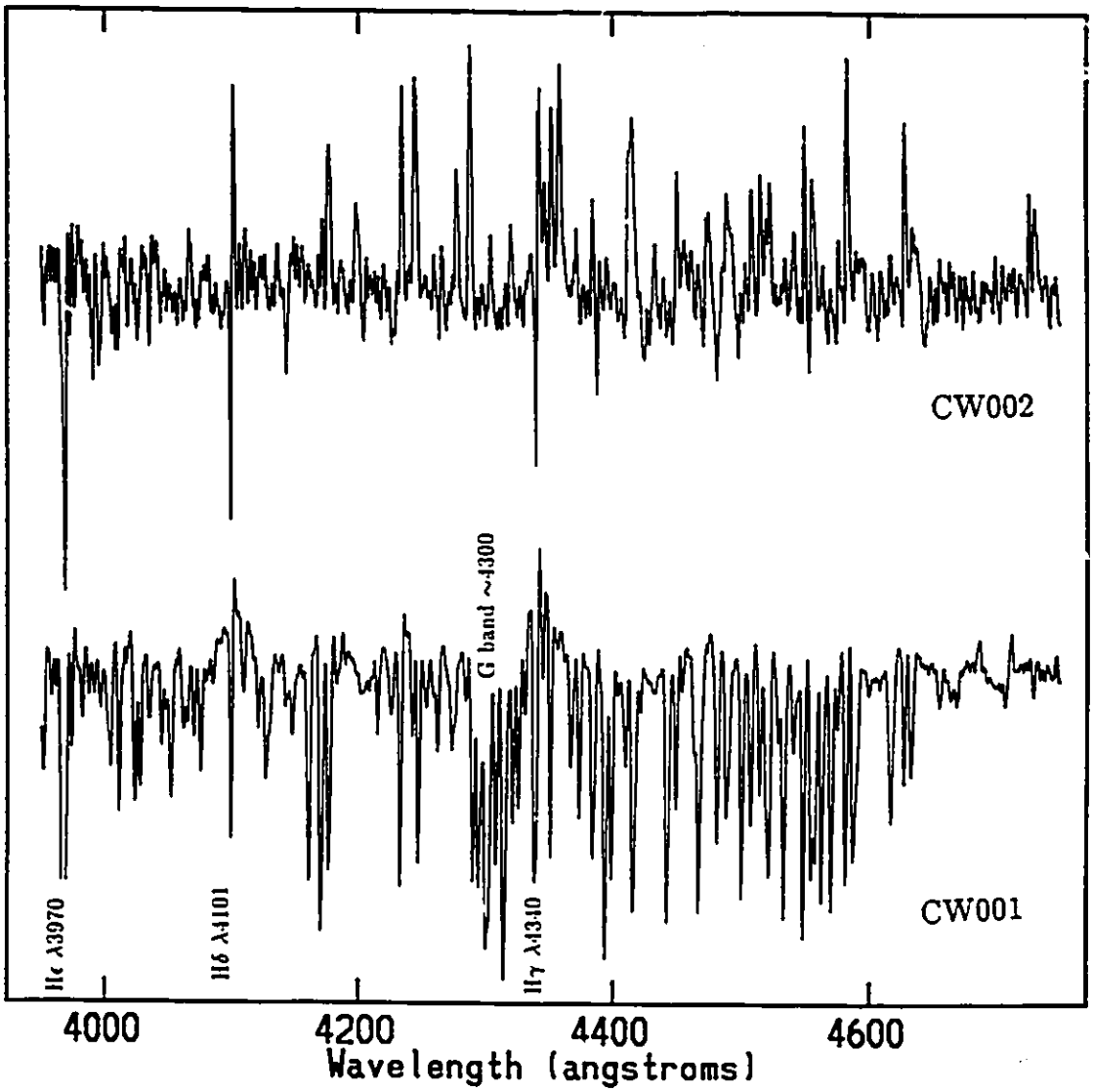

Figure 4.44: The spectra of the late type star CW001 and the potential luminous blue variable star CW002. CW001 is perhaps a G I star based on the presence of the Ca II K line at λ3968 and the broad, but rather fragmented G band $\sim$4300$\AA$. The classification of CW002 is based on the extreme brightness of the object (V=16.4) and enormous number of emission lines in the spectrum.

4.6 CONCLUSIONS

In summary, we have performed optical spectroscopy of luminous blue stars in NGC 6822 and M33 using, respectively, the 4-m CTIO telescope plus ARGUS spectrograph and the 4-m Mayall telescope at KPNO plus HYDRA spectrograph. Due to the limited S/N ratio of the data, we were able to classify only ~50% of the stars observed in NGC 6822 and ~40% of the stars observed in M33 program stars. Of the 37 NGC 6822 objects with classifiable spectra, we find 7 to most likely be Galactic foreground -A or G type stars and 2 to be WR stars. Of the 15 M33 program stars, we found 1 potential foreground G type star, 1 luminous blue variable and 2 Wolf-Rayet stars leaving only 11 O or B type stars that were identified by our investigation of this galaxy. For each individual object, we have outlined the principle spectral features used in their classification. While the small number statistics of both samples do not allow a direct determination of the high mass initial mass function and star formation rate, the individual spectra are valuable additions to existing surveys of the massive star content of Local Group galaxies. We have, in addition, used the NGC 6822 spectra to test the stellar ionization models of Panagia (1973) used in the ionization balance calculations for that galaxy (see Chapter 3).

Chapter 5

CONCLUSIONS AND FUTURE WORK

5.1 SUMMARY

Using $H\alpha$ data and stellar photometry, we have investigated the distribution of H II regions and OB stars and examined the hypothesis of ionization balance in two morphologically distinct Local Group galaxies, within the inner 1 kpc region of the late-type spiral M33 and the dwarf irregular galaxy NGC 6822. Additionally, we have obtained optical spectra of luminous blue stars in both these galaxies. While both sets of spectroscopic data have contributed towards an existing data base of individually studied massive stars within Local Group galaxies, the NGC 6822 spectra have, in addition, been used to gauge the performance of the stellar ionizing flux models applied in the ionization balance calculations. The major findings of our investigations of M33 and NGC 6822 are summarized below.

In the case of M33, we have identified three distinct components of the $H\alpha$ emission, denoted bright, halo and field, that are differentiated by their $H\alpha$ surface brightness. We find that ~50% of all stars brighter than the survey limit of V=21 and bluer than $E(B-V)\leq 0.4$ are located in the field. This finding suggests that 50%

of the main sequence lifetime of an OB star is spent outside of a classical ("bright") H II region and therefore if field OB stars escape their parent molecular clouds by destroying them, then molecular cloud lifetimes after the formation of OB stars must be shorter than $\sim 10^7$ yrs. If OB stars leave their parental molecular clouds without destroying them, then cloud lifetimes could be considerably longer.

Based on typical velocities of OB stars in molecular clouds ($\sim$3 km s^{-1}) and the average dimensions of the field regions, we find that field stars in M33 could not all have originated in and percolated out of existing bright H II regions nor a population of giant molecular clouds more massive than $0.5 \times 10^5 M_\odot$. If M33 contains molecular clouds with masses down to $\sim 10^3 M_\odot$ (a hypothesis put forward by Wilson & Scoville (1990) based on a comparison of a single dish and interferometric investigation of the molecular CO emission in M33), then it is possible that the field OB stars originated in these smaller clouds.

Comparing the observed $H\alpha$ luminosity in the surveyed inner 1 kpc region of M33 with that expected from the luminous blue stars (using the theoretical ionizing flux models of Panagia (1973) and an appropriate recombination scenario), we find that even for the most conservative estimates, the surveyed region is leaking ionizing flux and therefore *is not in ionization balance.* Over the entire surveyed region, the observed fluxes are a factor of $\sim$3-4 (Case A-Case B recombination) less than the predicted conservative estimate and $\sim$7-9 (Case A-Case B recombination) less than the predicted best estimate fluxes. While the bright ionized gas regions are closest to being ionization bounded, the field regions are definitely not: predicted fluxes are a factor of 5 larger than observed in the conservative case (assuming Case A recombination) and increase to more than a factor of 13 in the best estimate case (Case A recombination again assumed). The only situation for which the field may be

in ionization balance is if the uniform sky background is included in with the observed $H\alpha$ flux. Additionally, Case A recombination provides the best agreement between observed and predicted $H\alpha$ fluxes in the field. Investigation of an individual, isolated region containing both bright and halo emission produces comparable results: the entire region is ionizationally unbalanced by a factor of $\sim$3 and $\sim$7, for respectively, the conservative and best estimate cases.

The critical implication of the ionization balance calculation is that star formation rates calculated from the $H\alpha$ luminosity using the standard formula must under-estimate the true star formation rate. Over the entire surveyed region, the difference between the true star formation rate and that calculated from $H\alpha$ could be a factor of $\sim$3-7.

In the case of NGC 6822, we have identified four distinct components of the $H\alpha$ emission, denoted bright, halo, diffuse and field, based on the surface brightness of the gas. For comparative purposes, the dividing lines in surface brightness between the bright, halo and diffuse regions are consistent with those adopted in M33 before the correction for the [NII] emission was made.

On comparing the distribution of OB stars brighter than V=21 within the four ionized gas environments, we find that only 1/4 of the blue stars are found in the optically prominent bright and halo ionized gas regions. These results suggest that roughly 3/4 of the main sequence lifetime of an O star is spent outside of classical H II regions. The implications of this to molecular cloud lifetimes is that if OB stars destroy their parent molecular clouds while escaping their H II regions, then molecular cloud lifetimes after the formation of OB stars must be shorter than $\sim$1-3$\times10^6$ yrs. Alternatively, if the stars escape the H II regions without destroying their parent

molecular clouds, then molecular cloud lifetimes could be much longer.

A comparison of spectral classes determined from the stellar ionizing flux models of Panagia (1973) and BV photometry of luminous blue stars in NGC 6822 with those deduced from optical spectroscopy shows that the photometric classifications are biased towards earlier spectral types. This finding suggests that the theoretically predicted $H\alpha$ fluxes obtained from the Panagia models are likely to be over-estimated. In light of this, we consider all ionization balance calculations that agree to within a factor of two to be in acceptable agreement in both NGC 6822 and M33.

Application of the Panagia (1973) models to the data shows that in all four ionized gas environment, the models consistently predict more flux than observed. While the bright and diffuse regions are likely to be in ionization balance (as the predicted fluxes are, at most, a factor of 2 larger than observed), the halo region appears to be at the limit of ionization balance (as predicted fluxes differ from those observed by up to a factor of 3). The most serious loss of ionizing photons appears to be occurring in the field region: the observed and predicted $H\alpha$ fluxes differ by a factor of $\sim$6-14 (for the conservative estimate assuming Case A and B) to $\sim$8-20 (for the best estimate case assuming Case A and B). Clearly the field cannot be in a state of ionization balance. As such, these results suggest that 50% of the blue stars in NGC 6822 may be losing most of their ionizing radiation to interstellar space.

In the literature, one of the most common methods of obtaining the star formation rate of a galaxy from its $H\alpha$ luminosity uses the formula of Kennicutt (1983). This formula is based on the galaxy being ionization bounded and assumes Case B recombination is appropriate everywhere. Application of the Kennicutt formula in

NGC 6822 would underestimate the true star formation rate by ~50% due to the leakiness of the field and the use of Case A recombination in the diffuse and field regions.

Finally, comparison of the distributions of the OB stars within the ionized gas environments as well as the state of ionization balance in NGC 6822 and M33 suggests that the morphological class of the parent galaxy may be an important factor in whether or not the assumption of ionization balance holds true and therefore, in determining the star formation rate from the $H\alpha$ luminosity. It is clear from the analysis that the field region in M33 appears to be in a more serious state of ionization imbalance than NGC 6822. The surface density of OB stars, which is higher in M33, may be responsible for this difference. Specifically, since the two galaxies have comparable H I column densities, the likelihood of losing ionizing photons is increased when the stellar surface density is increased. Based on the ionization balance results, star formation rates from $H\alpha$ luminosities are less likely to reflect the true star formation rate in M33 than NGC 6822.

Optical spectroscopy of the luminous blue stars in NGC 6822 and M33 were obtained using, respectively, the 4-m CTIO telescope plus ARGUS spectrograph and the 4-m Mayall telescope at KPNO plus HYDRA spectrograph. Due to the limited signal-to-noise ratio of the data, it was possible to classify only ~50% of the stars observed in NGC 6822 and ~40% of the stars observed in M33. In all, we were able to identify 11 OB-type stars in M33 and 28 OB-type stars in NGC 6822. While the small number statistics of the two samples did not allow a direct determination of the initial mass function and star formation rate of high mass stars, the NGC 6822 spectra are useful in testing the Panagia stellar ionizing models used in ionization balance calculations. Furthermore, both sets of spectra are valuable additions to

existing surveys of the massive star content of Local Group galaxies.

5.2 FUTURE RESEARCH

In the preceding chapters we have repeatedly emphasized the importance of studying the OB star and ionized gas content of galaxies to determine, amongst other things, the star formation rate of the system. The results of our investigation of the state of ionization balance and the OB star distribution within M33 and NGC 6822 clearly underline the need to further qualify and quantify the situation in other stellar systems. In addition, our investigations have raised some new questions which, along with those that could not be satisfactorily answered in M33 and NGC 6822, remain to be addressed. Primary amongst these is the question of the qualitative effect of the morphological class of the galaxy on the state of ionization balance. In particular, the parameters that determine whether ionization balance is possible or not are yet be to satisfactorily identified and quantified. For example, although we have hypothesized that the surface density of stars may be an important factor in determining whether or not the galaxy (or region thereof) is losing ionizing photons, this hypothesis remains to be examined in greater detail. Additionally, the neutral hydrogen column density may also play a part in the ionization (im)balance. By comparing the distribution and concentration of neutral hydrogen with that of the ionized gas, the importance and relevance of this parameter may be ascertained.

An investigation of the H II regions, OB stars and the state of ionization balance in the outer portions of M33 would be very interesting. Such a study would allow us to determine if the results we have obtained within the inner 1 kpc region of M33 (in Chapter 2) are typical of the whole galaxy. This in turn would provide valu-

able information on just how serious a problem the ionization imbalance poses to star formation rates determined from $H\alpha$ luminosities over the entire galaxy. Additionally, deep HST imaging in M33 to reduce the correction for faint stars and attain a more complete sample would also allow for a more accurate estimate of the ionization (im)balance in the galaxy.

While some of the remaining questions can be addressed in M33 and NGC 6822 (*i.e.*, relevance of H I column density to the state of ionization balance), it is vital that our study be extended to other galaxies. In order to observe the effect of galaxy type on the state of ionization balance, it is necessary to increase the sample numbers. To this end, two Local Group candidate galaxies are proposed. The first system is the dwarf irregular galaxy, IC 1613 and the other is the last remaining spiral galaxy in the Local Group (outside our own and M33), the Andromeda Galaxy, M31. IC 1613 would be the ideal follow up to NGC 6822. This isolated galaxy has been the object of many investigations: OB associations have been identified and studied by Hodge (1978) and Hodge *et al.* (1991), Cepheid variables have been found by Sandage (1971), Freedman (1988b) and Carlson & Sandage (1990) and Wolf-Rayet stars have been detected by Armandroff & Massey (1991). At 0.004 $M_\odot$ yr^{-1} (Hodge 1995), the star formation rate (estimated from the $H\alpha$ luminosity of the galaxy) is closer to that of NGC 6822 than M33. From the investigation of the young stars in IC 1613 (Freedman 1988a) and OB associations (Hodge 1980), it appears that there have been at least two separate star forming episodes across the galaxy.

The spiral galaxy M31 has the highest estimated star formation rate from $H\alpha$ luminosity (6.5 $M_\odot$ yr^{-1} over the whole galaxy, Hodge 1995). While the populations of stars in M31 are believed to be similar to those in the Milky Way (Hodge 1989), the star formation histories of the two galaxies appears to be different: M31 appears to

have had a longer or more intense period of star formation in the past but currently has a lower mean star formation rate than that observed in the Galaxy. Although relatively gas-poor, the atomic, molecular and ionized gas in M31 is concentrated within a ring which is coincident with the main spiral arm of the galaxy (Kennicutt 1995; Pellet *et al.* 1978). A significant 40% of the ionized gas in M31 is detected as diffuse ionized gas (Walterbos & Braun 1994). These features, along with the fact that the distances and declinations of both galaxies allow individual high mass stars to be resolved, make M31 and IC 1613 excellent subjects for an investigation such as the one carried out in M33 and NGC 6822.

REFERENCES (CHAPTERS 1, 4 AND 5)

Abt, H.A., Meinel, A.B., Morgan, W.W. & Tapscott, J.W. 1978, An Atlas of Low-Dispersion Grating Stellar Spectra (KPNO and Yerkes Observatories)

Armandroff, T.E. & Massey. P, 1991, AJ, 102, 927

Armandroff, T.E. & Massey, P. 1985 ApJ, 291, 685.

Azzopardi, M. & Breysacher, J. 1979, A&A, 75, 120

Barden, S.C., Armandroff, T.E., Massey. P., Groves, L., Rudeen, A.C., Vaughnn, D. & Muller, G. 1992a, in Fiber Optics in Astronomy II, ASPC Series, ed. P. Gray, ASP Conference Series. (San Francisco: Brigham Young University Press)

Barden, S.C., Armandroff, T.E. & Massey, P. 1992b HYDRA USERS MANUAL, (Tuscon: NOAO)

Beals, B. 1938, AZh, 15, 225

Blitz, L. & Shu, F. 1980, ApJ, 235, 148

Bothun, G.D. 1992, AJ, 103, 104

Breysacher, J. 1981, AAS, 43, 203

Brockelhurst, M. 1971, MNRAS, 153, 471

Carlson, G. & Sandage, A. 1990, ApJ, 352, 587

Conti, P.S. & Garmany, C.D. 1983, PASP, 95, 411

Conti, P.S. & Underhill, A.B. 1988, in O Stars & Wolf-Rayet Stars, eds. Jordan S. & Thomas, R., NASA Conf. Publ. SP-497, p. 428

Courtes, G., Petit, H., Sivan, J.-P., DoDonov, S., Petit, M. 1987 A&A, 174, 28

Davidson, K., Dufour, R.J., Walborn, N.R. & Gull, T.R. 1986, ApJ, 305, 867

Davies, R.D., Elliot, K.H. & Meaburn, J. 1976, MmRAS, 81, 89

Deul, E.R. & van der Hulst, J.M. 1987, A&AS, 67, 509

Deul, E.R. & Hartog, R.H. 1990, A&A, 229, 362

Elmegreen, B.G. 1991, in The Physics of Star Formation & Early Stellar Evolution, eds. C.J. Lada & N.D. Kylafis (Dordrecht: Kluwer), p. 35

Freedman, W.L. 1988a, ApJ, 326, 691

Freedman, W.L. 1988b, AJ, 96, 1248

Henize, K.G. 1956, ApJS, 2, 315

Hester, J.J. & Kulkarni, S.R. 1990, in The Interstellar Medium in External Galaxies, eds. D. Hollenbach & H. Thronson, NASA Conf. Publ. 3084, p. 288

Heydari-Melayeri, M., Niemela, V.S. & Testor, G. 1987, A&A, 184, 300

Hodge, P.W. 1977, ApJS, 33, 69

Hodge, P.W. 1980 ApJ, 241, 125

Hodge, P.W. & Kennicutt, R.C. 1983, AJ, 88, 296

Hodge, P.W. 1989, PASP, 101, 32

Hodge, P.W., Lee, M.G. & Kennicutt, R.C. 1988, PASP, 100, 917

Hodge, P.W., Lee, M.G. & Kennicutt, R.C. 1989, PASP, 101, 32

Hodge, P.W., Smith, T., Eskridge, P., Macgillivray, H.T. & Beard, S. 1991, ApJ, 379, 621

Hodge, P.W. 1995, in The Local Group: Comparative and Global Properties, eds. A. Layden, R. C. Smith & J. Storm, (ESO: Garching), in press

Huchra, J.P. 1977, ApJ, 217, 928

Huchra, J.P., Gellar, M.J., Gallagher, J.S., Hunter, D., Hartmann, L., Fabbiano, G. & Aaronson, M. 1983, ApJ, 274, 125

Hunter, D.A. & Massey. P. 1990, AJ, 100, 1915

Hunter, D.A., Gillett, F.C., Gallagher, J.S., Rice, W.L. & Low, F.J. 1986, ApJ, 303, 171

Humphreys, R. M. 1980, ApJ 238, 65

Ingerson, T. 1988, in Fiber Optics in Astronomy, ASPC Series, ed. S. Barden, (San Francisco: Brigham Young University Press), p. 99

Ingerson, T. 1994, ARGUS-on-Line Manual, CTIO internal document

Janchek, C. & Janchek, M. 1987, The Classification of Stars, (Cambridge: Cambridge University Press)

Johnson, H.L. & Morgan, W.W. 1953, ApJ 117, 313

Kaler, J.B. 1989 Stars and their Spectra, An Introduction to the Spectral Sequence, (New York: Cambridge University Press)

Kayser, S.E. 1967, AJ, 72, 134

Kennicutt, R.C. 1983, ApJ, 272, 54

Kennicutt, R.C. 1989, ApJ, 344, 685

Kennicutt, R.C. 1990, in The Interstellar Medium in Galaxies, eds. H.A. Thronson & J.M. Shull, (Dordrecht: Kluwer), p. 405

Kennicutt, R.C. 1991, in The Magnellanic Clouds, eds. R. Haynes & D. Milne, (Dordrecht: Kluwer), p. 139

Kennicutt, R.C. 1995, in The Local Group: Comparative and Global Properties, eds. A. Layden, R. C. Smith & J. Storm, (ESO: Garching), in press

Kennicutt, R.C. & Hodge, P. 1986, ApJ, 306, 130

Kent, S.A. 1987, AJ, 94, 306

Larson, R.B. & Tinsley, B.M. 1978, ApJ, 219, 46

Lonsdale, P.C.J. & Helou, G. 1987, ApJ, 314, 88

Loret, M.-C. & Testor, G. 1984, A&A, 139, 330

Maeder, A. & Conti, P.S. 1994, ARA&A, 32, 227

Massey, P. 1993, in Massive Stars: Their Lives in the Interstellar Medium, ASPC Series, ed. J.P. Cassinelli & E.B. Chruchwell, (San Francisco: Brigham Young University Press), p. 168

Massey. P., Conti, P.S. & Armandroff, T.E. 1987, AJ, 94, 1538

Massey. P., Garmany, C.D., Silkey, M. & Degioia-Eastwood, K. 1989a, AJ, 97, 107

Massey. P., Parker, J.W. & Garmany, C.D. 1989b, AJ, 98, 1305

Massey. P., Lang, C.C., Degioia-Eastwood, K. & Garmany, C.D. 1994, ApJ, in press

McAlary, C.W., Madore, B.F., McGonegal, R., McLaren, R.A. & Welch, D.L. 1983, 273, 539

Mihalas, M. & Binney, B. 1981, Galactic Astronomy (New York: Freeman)

Miller, G.E. & Scalo, J.M. 1979, ApJS, 41, 513

Mochkovitch, M., Ichikawa, T., Tanaka, Y.D., Naki, N. & Sofue, Y. 1987, PASJ, 39, 57

Morgan, W.W., Keenan, P.C. & Kellman, E. 1943, An Atlas of Stellar Spectra (Chicago: University of Chicago Press)

Morgan, W.W. & Keenan. P.C. 1973, ARA&A, 11, 29

Morgan, W.W., Abt, H.A. & Tapscott, J.W. 1978. Revised MK Spectral Atlas for Stars Earlier Than the Sun, (KPNO and Yerkes Observatories)

Ohta, K., Tomita, A., Saito, M., Sasaki, M. & Nakai, N. 1993. PASJ, 45, L21

Osterbrock, D.E. 1989, Astrophysics of Gaseous Nebulae and Active Galactic Nuclei, (Mill Valley: University Science Books)

Parker, J.W., Garmany, C.D., Massey, P. & Walborn, N.R. 1992, AJ, 103, 1205

Pellet, A., Astier, A., Viale, A., Courtes, G., Maucherat, A., Monnet, G. & Simien, F. 1978, A&AS, 31 439.

Rand, R.J., Kulkarni, S.R. & Hester, J.J. 1990, ApJ, 352, L1

Rocca-Volmerange, B., Lequeux, J. & Marcherat-Joubert, M. 1981, A&A, 104, 177

Roberts, M.S. 1963, ARA&A, 1, 419

Sandage, A. 1971, ApJ, 166, 13

Sandage, A.R. & Humphreys, R.M. 1980, ApJL, 236, L1

Searle, L., Sargent, W.L.W. & Bagnuolo, W.G. 1973, ApJ, 179, 427

Schmidt, M. 1959, ApJ, 129, 243

Smith L.F 1968, MNRAS 138, 109

Solomon, P.M. & Sanders, D.B. 1980, in Giant Molecular Clouds in the Galaxy, eds P.M. Solomon and M.G. Edmunds (Oxford: Pergammon Press), p. 41

Sunzeff, N. 1993, ARGUS Users Manual, CTIO internal document

Thronson, H.A.J. & Telesco, C.M. 1986, ApJ, 311, 98

Thronson, H.A.J., Hunter, D.A., Telesco, C.M., Harper, D.A. & Decher, R. 1987, ApJ, 317, 180

Thronson, H.A.J., Balley, J. & Hacking, P. 1989, AJ, 97, 363

Thronson, H.A.J., Hunter, D.A., Telesco, C.M., Greenhouse, M. & Harper, D.A. 1988, ApJ, 334, 605

Tinsley, B.M. 1972, A&A, 20, 383

Tinsley, B.M. 1980, Fund. Cosmic. Phys., 5, 287

Tinsley, B.M. & Danly, L. 1980, ApJ, 242, 435

van den Bergh, S. & Humphreys, R.M. 1979, AJ, 84, 604

van der Hucht, K.A. 1992, A&ARv, 4, 123

Viallefond, F. & Goss, W.M. 1986, A&A, 154, 357

Volders, L.M.J.S. 1959, Bull. Astron. Inst. Neth. 14, 323

Walborn, N.R. & Fitzpatrick, E.L 1990, PASP, 102, 650

Walterbos, R.A.M. & Schwering, P.B.W. 1987, A&A, 180, 27

Walterbos, R.A.M. 1991, in The Interstellar Disk-Halo Connection in Galaxies, ed. H. Bloemen, (Dordrecht: Kluwer), p. 223

Walterbos, R.A.M. & Braun, R. 1994, ApJ, 431, 156

Wilcots, E.M. & Hodge, P. W. 1991, in The Magellanic Clouds, ed. R. Haynes & D. Milne, (Dordrecht: Kluwer), p. 226

Wilson, C.D. 1990. Ph.D. thesis, Caltech

Wilson, C.D. 1991, AJ, 101, 1663

Wilson, C.D. 1992a, AJ, 104, 1374

Wilson, C.D. 1992b, ApJ, 391, 144

Wilson, C.D. 1994, AJ, 434, L11

Wilson, C.D. & Scoville, N.Z. 1989, ApJ, 347, 743

Wilson, C.D. & Scoville, N.Z. 1990, ApJ, 363, 435

Wilson, C.D. & Scoville, N.Z. 1991, ApJ, 370, 184

Wilson, C.D., Scoville, N.Z. & Rice, W. 1991, AJ, 101, 1293

Wolf, C.J. & Rayet, G. 1867, Comptes Rendus Acad. Sci., 65, 292

Underhill, A.B. 1966, The Early Type Stars, (New York: Gordon & Breach)